RNA-based control of the expression of the type III secretion system of *Yersinia pseudotuberculosis*

Von der Fakultät für Lebenswissenschaften

der Technischen Universität Carolo-Wilhelmina zu Braunschweig

zur Erlangung des Grades

eines Doktors der Naturwissenschaften

(Dr. rer. nat.)

genehmigte

D i s s e r t a t i o n

von Jörn Hoßmann

aus Bützow

1. Referentin:	Professorin Dr. Petra Dersch
2. Referent:	Professor Dr. Michael Steinert
eingereicht am:	22.02.2017
mündliche Prüfung (Disputation) am:	29.06.2017

Druckjahr 2018

Vorveröffentlichungen der Dissertation

Teilergebnisse aus dieser Arbeit wurden mit Genehmigung der Fakultät für Lebenswissenschaften, vertreten durch die Mentorin der Arbeit, in folgenden Beiträgen vorab veröffentlicht:

Publikationen

Maurer CK, Fruth M, Empting M, Avrutina O, **Hoßmann J**, Nadmid S, Gorges J, Hermann J, Kazmeier U, Dersch P, Müller R and Hartmann RW: Discovery of the first small-molecule CsrA-RNA interaction inhibitors using biophysical screening technologies. *Future Med. Chem.* 8, 931–47 (2016).

Posterbeiträge

Hoßmann J, Pimenova M, Steinmann R, Opitz W, Heroven AK, Dersch P: Thermal and secretion-dependent regulation of the master regulator LcrF in *Yersinia pseudotuberculosis*. (Poster). 4th National *Yersinia* Meeting, Hamburg (2014).

Hoßmann J, Pimenova M, Steinmann R, Opitz W, Heroven AK, Dersch P: Thermal and secretion-dependent regulation of the master regulator LcrF in *Yersinia pseudotuberculosis*. (Poster). Sensory and regulatory RNAs of procaryotes meeting, Braunschweig (2015).

Hoßmann J, Pimenova M, Steinmann R, Opitz W, Heroven AK, Dersch P: Thermal and secretion-dependent regulation of the master regulator LcrF in *Yersinia pseudotuberculosis*. (Poster). 32nd Annual Meeting of NSCMID, Umea (2015).

Table of contents

List of figures

List of tables

List of abbreviations

A	adenine
APS	ammonium persulfate
ATP	adenosine triphosphate
bp	base pair
C	cytosine
Cb	carbenicillin
CDS	coding sequence
Cm	chloramphenicol
CLIP	cross-linking immunoprecipitation
Csr	carbon storage regulator
DTT	dithiothreitol
DYT	double yeast tryptone
ECM	extracellular matrix
EDTA	ethylenediaminetetraacetic acid
EMSA	electromobility shift assay
fc	fold change
G	guanine
HRP	horseradish peroxidase
IM	inner membrane
IP	immunoprecipitation
LB	lysogeny broth
Kan	kanamycin
LCR	low calcium response
MLN	mesenteric lymph node
MOPS	3-(N-morpholino)propanesulfonic acid
NaOx	disodium oxalate
ncRNA	non-coding RNA
M cells	microfold cells
NET	neutrophil extracellular trap
MS	membrane and supramembrane
OD	optical density
OM	outer membrane
ONPG	o-nitrophenyl-β-galactoside
PCR	polymerase chain reaction
PBS	phosphate-buffered saline
ps	primary CsrA binding site
ORF	open reading frame
PVDF	polyvinylidene fluoride
RBS	ribosomal binding site
rpm	rounds per minute
RBP	RNA-binding protein

RIP-Seq	RNA-binding protein immunoprecipitation sequencing
rpk	reads per kbp gene length
SD	Shine-Dalgarno
SDS-PAGE	sodium dodecyl sulfate polyacrylamide gel electrophoresis
ss	secondary CsrA binding site
Syc	specific Yop chaperone
T	thymine
T3SS	type III secretion system
T6SS	type VI secretion system
TAE	Tris-acetate EDTA buffer
TBE	Tris-borate-EDTA buffer
TEMED	tetramethylethylenediamine
Tris	trishydroxymethylaminomethane
TPR	tetratricopeptide repeats
TSS	transcriptional start site
U	uridine
UTR	untranslated region
wt	wild type
Yop	*Yersinia* outer protein
Ysc	Yop secretion

1 Introduction

As unicellular organisms, bacteria are constantly threatened by their rapidly changing environment. To thrive under such ever-changing conditions and compete with other microorganisms for resources, they are forced to sense and quickly adapt to different niches. On that account, bacteria have developed complex regulatory networks and elaborated survival strategies. Especially, pathogenic bacteria need a plethora of adaptive responses when they switch from an outside habitat to their host. Inside their host, bacteria encounter a resource rich environment, stable temperature, but they are also confronted with host responses that induce nutrient/iron depletion and the host's immune system, as well as the competing microbiota. Therefore, bacteria are forced to efficiently coordinate the expression of virulence, virulence-relevant fitness factors and colonization factors and need to decide about the right time and location of expression. Decision making and fine adjustment of these factors are regulated on every level of gene expression, in large overlapping regulatory networks [Marceau, 2005; Erhardt & Dersch, 2015; Chen *et al*., 2016].

1.1 The genus *Yersinia*

Yersinia are Gram-negative *Enterobacteriaceae*. They are rod-shaped, facultative anaerobe bacteria. As psychrophilic bacteria, they are able to grow at a temperature minimum between 1-4 °C. Nonetheless, the optimal growth temperature for *Yersinia* is between 20-30 °C [Perry *et al*., 2007].

Yersiniae are described as a highly diverse group of 18 individual species, of which three are virulent and pathogenic to humans and other mammals [McNally *et al*., 2016]. The three pathogenic yersiniae, namely *Yersinia enterocolitica*, *Yersinia pseudotuberculosis* and *Yersinia pestis* are closely related. As demonstrated by multilocus sequence typing, *Y. pseudotuberculosis* and *Y. pestis* share more than 90% DNA homology [Achtman *et al*., 1999]. Evolutionary, *Y. enterocolitica* and *Y. pseudotuberculosis* branched from their last common ancestor 50 million years ago, while *Y. pestis* and *Y. pseudotuberculosis* diverged, on an evolutionary scale just recently, 1,500 - 20,000 years ago and share an approximate DNA identity of 98% [Achtman *et al*., 1999; Prentice & Rahalison, 2007]. Although pathogenic yersiniae are genetically highly homologous, they exhibit extreme differences in virulence and pathogenicity, e.g. route of transmission and infection and the caused disease. While *Y. enterocolitica* and *Y. pseudotuberculosis* are enteropathogenic species and often cause mild

self-limiting gastroenteritis, *Y. pestis* is the causative agent of plague, a systemic disease with one of the highest mortality rates [Savin *et al*., 2014; Wren, 2003].

Both enteropathogenic species, *Y. pseudotuberculosis* and *Y. enterocolitica*, are globally widespread in the environment. They can be found in soil, water, in animals and on the surface of plants. *Y. enterocolitica* can be found in wildlife and domestic animals, especially pigs are important reservoirs for human infection [Kapperud, 1991; Bockemühl & Roggentin, 2004; Fredriksson-Ahomaa *et al*., 2006]. Although they are both able to infect a variety of animals, *Y. enterocolitica* is a widespread human pathogen, while *Y. pseudotuberculosis* only sporadically infects humans. Enteropathogenic *Yersinia* are transmitted by ingestion of contaminated food or water via the fecal-oral route. Thereby, they cause gastrointestinal diseases, called Yersiniosis. Yersiniosis describes a wide range of diseases, like enteritis, mesenteric lymphadenitis and colitis. Especially, in young children, old or immune-suppressed patients, enteropathogenic yersiniae can cause complications like reactive arthritis, erythema nodosum and bacteremia [Bottone, 1997; Galindo *et al*., 2011; Naktin & Beavis, 1999].

Y. pestis displays a complex sheltered life cycle. During the course of its evolution it gained the trait to survive and replicate inside the flea gut and also the ability to be transmitted by flea bites, but at the same time lost the ability for colonization of the intestine. This new route of transmission enabled it to bypass the gut infection phase, which the enteropathogenic *Yersinia* species share. In combination with the accumulation of new virulence factors and a complete or a partial loss of genes, *Y. pestis* exhibits a higher virulence and causes harsher diseases, but displays a reduced genomic flexibility and metabolic streamlining [McNally *et al*., 2016]. It is normally endemic in rodents and cycles, transmitted by flea bites, between its rodent reservoir and its arthropod vector. The vector-borne transmission leads to bubonic and septicemic plague and can cause a secondary, pneumonic plague. Pneumonic plague leads to a rapid, airborne transmission between humans via droplets which cause a primary pneumonic plague. A primary pneumonic plaque after airborne infection displays a very low incubation time of only 2-3 days and if untreated a 100% mortality rate [Perry & Fetherston, 1999; Prentice & Rahalison, 2007].

All pathogenic *Yersinia* species have a tropism for lymphatic tissues and carry a virulence plasmid termed pYV in *Y. enterocolitica*, pIB in *Y. pseudotuberculosis* and pCD in *Y. pestis*. This plasmid encodes a type III secretion system (T3SS), anti-inflammatory effector

molecules to overcome the host immune defense and the adhesin YadA. *Y. pestis* acquired additional plasmids that support survival in their arthropod vector, capsule formation (pFra) and dissemination from the bite site (pPCP1) [Du *et al*., 2002; Rajana *et al*., 2010; Chouikha & Hinnebusch, 2012].

1.2 Route of infection

The infection process of *Y. pseudotuberculosis* can be divided into two phases, the initial and the ongoing infection phase. *Y. pseudotuberculosis* enters the body by ingestion of contaminated food or water (initial infection phase). This phase is characterized by the invasion and colonization of the host and the expression of appropriative virulence factors. After transmigration through the intestinal barrier, *Yersinia* is threatened by the host innate immune system and expresses virulence factors required for the evasion of immune cells and the dissemination into deeper organs (ongoing infection phase) (**Fig. 1.1**).

1.2.1 Initial infection phase

The initial infection phase is characterized by the expression of early virulence factors and the passage from the outer environment through the gastrointestinal tract [Heroven *et al*., 2007]. During the initial infection phase, no host response can be measured [Handley *et al*., 2004]. The route through the gastrointestinal tract already requires a fast adaptation to stresses, like changing pH, changing oxygen levels, proteolytic enzymes and nutrient competition with other bacteria [Foster, 1999; Wallace *et al*., 2016; Spiro & Guest, 1990; Fang *et al*., 2016].

When the pathogen reaches the terminal section of the small intestine, the ileum, it utilizes the adhesion and invasion factor InvA to adhere to and finally penetrate the intestinal layer by exploiting microfold cells (M cells) (**Fig. 1.1**). These immunosurveillance cells cover the Peyer's patches - the lymphatic tissue of the intestines. Unlike enterocytes, they lack apical microvilli, have a reduced glycocalyx and are proficient for phagocytosis and transcytosis [Mabbot *et al*., 2013; Grützkau *et al*., 1990; Clark *et al*., 1998]. Invasion and colonization are further boosted by the expression of O-antigen coupled LPS and other adhesins [Uliczka *et al*., 2011; Skurnik & Toivanen, 1993].

Expression of invasin is maximally activated at temperatures below 30 °C in stationary phase. It has been suggested that expression of invasin under environmental conditions already prepares enteropathogenic yersiniae to effectively and immediately cross the intestinal barrier

[Pepe & Miller, 1993; Revell & Miller, 2000]. Invasin structurally and sequentially belongs to the intimin family and mediates interaction with M cells by β_1-integrine binding.
Interaction of integrin and invasin leads to a close binding to the target cell and in turn triggers an active uptake by the zipper mechanism. The invasin-integrin interaction induces a host cell signaling cascade that leads to rearrangements of the actin cytoskeleton and formation of filo- and lamellipodia that engulf the adhering bacterium [Dersch & Isberg, 2000; Oelschlaeger, 2001; Grassl *et al*., 2003].

1.2.2 Ongoing infection phase

The ongoing infection phase starts, after a successful invasion of the *lamina propria* and the Peyer's patches. Inside the Peyer's patches, *Yersinia* proliferates and forms necrotic microabscesses [Autenrieth & Firsching, 1996]. The ongoing infection phase is characterized by an immense influx of activated phagocytes into the site of infection, cytokine production and tissue necrosis [Autenrieth *et al*., 1993; Dube *et al*., 2003 Handley *et al*., 2004; Balada-Llasat & Mecsas, 2006]. After the invasion of the Peyer's patches, *Yersinia* starts to disseminate into deeper tissues and organs, like mesenteric lymph nodes, liver, spleen and kidneys, where the pathogen resides mostly extracellularly in microcolonies. The ongoing infection phase requires a reprogramming of the bacterial cell to survive and proliferate inside lymphatic tissues (**Fig. 1.1**) [Bengechea *et al*., 2004; Cornelis, 2006; Heesemann *et al*., 2006]. To successfully establish an infection inside lymphatic tissues, the pathogen expresses various factors encoded on its virulence plasmid pYV. This includes the adhesin YadA and the *Yersinia* outer proteins (Yops), which are directly injected into the cytosol of target cells by a T3SS [Atkinson & Williams, 2016].
YadA is a multifaceted adhesion protein present in *Y. pseudotuberculosis* and *Y. enterocolitica* that forms a fimbrial matrix on the bacterial cell envelope [Hoiczyk *et al*., 2000]. It is encoded on the virulence plasmid pYV and is transcribed at 37 °C from a σ^{70}-dependent promoter by the thermoregulated virulence master regulator LcrF. After the invasion, YadA is the predominant adhesion protein in infected tissues [Skurnik & Wolf-Watz, 1989; El Tahir & Skurnik, 2001; Hoiczyk *et al*., 2000]. The adhesin YadA mediates binding to ECM (extracellular matrix) proteins, serum complement resistance and autoagglutination. Therefore, it is essential to establish and maintain the infection [Mühlenkamp *et al*., 2015; Wren, 2003; El Tahir & Skurnik, 2001]. In *Y. pestis*, the *yadA* gene is inactivated due to a frame shift mutation. The inactivation of the *yadA* gene in

Y. pestis is thought to be due to the new transmission route. Considering its ability to efficiently bind to the ECM (in particular collagen), YadA would hinder the efficient spreading from the entry site into deeper tissues and increase susceptibility to neutrophil extracellular traps (NETs) [Casutt-Meyer *et al*., 2010; El Tahir & Skurnik, 2001]. The length of YadA and the Ysc-T3SS are well-matched, allowing efficient delivery of anti-phagocytic effector molecules by the injectisome into host cells [Mota *et al*. 2005].

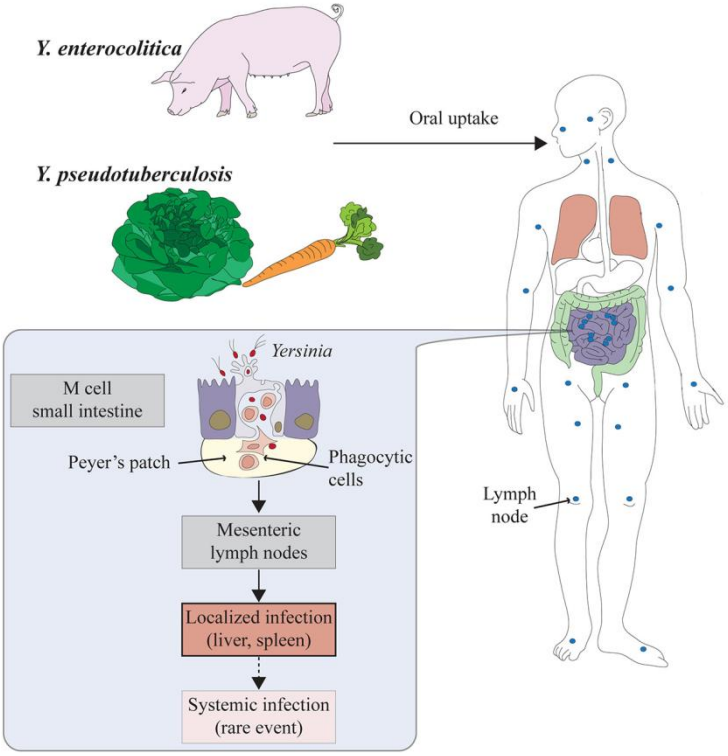

Figure 1.1: Infection route of enteropathogenic *Yersinia* species. The pathogens are ingested with contaminated food and subsequently pass the stomach and enter the small intestines. Here the bacteria pass the intestinal barrier by adhering and transmigrating through M cells. After reaching the underlying Peyers patches, they start to express virulence plasmid-encoded virulence factors like the adhesin YadA, the injectisome and anti-phagocytic effector proteins to resist the innate immune system. Starting from the Peyer's patches, the bacteria spread to the mesenteric lymph nodes and into systemic organs such as kidneys, liver and spleen. This picture is adapted from Heroven & Dersch, 2014[1]

1.2.2.1 The Ysc-Yop virulon

All pathogenic *Yersinia* species encode a complex molecular machinery for efficient host cell 'toxin' delivery. This Ysc-T3SS (Yop secretion) is encoded on the 70 kb virulence plasmid (pYV). It exhibits a syringe-like structure, called injectisome. Since the loss of the Ysc-T3SS correlates with an avirulent phenotype, its function is absolutely crucial for virulence and pathogenicity [Cornelis, 2010]. Together with the adhesin YadA, the injectisome enables adherent bacteria to inject effector molecules specifically into the target cell. The injectisome

[1] Heroven & Dersch, 2014 is licensed under the Creative Commons Attribution (CC BY) license.

creates a continuous channel between the bacterial and eukaryotic cytosol while bridging three membranes - the bacterial inner and outer membrane and the host cell membrane. Translocated effector molecules have a large repertoire of biochemical activities and modulate the function of crucial regulatory pathways in the eukaryotic cell. Subsequently, this allows the pathogen to evade the host innate immune response [Cornelis & Wolf-Watz, 1997].

Homologs of the injectisome can be found in other Gram-negative pathogens, like *Shigella flexerni*, *Salmonella* spp. and the plant pathogen *Xanthomonas* spp. [Cornelis, 2006]. The injectisome shares structural homologies with the flagellar T3SS, pointing to a common evolutionary origin [Abby & Rocha, 2012]. Similar to the flagellum, the injectisome consist of a cylindrical basal body, which anchors the complex in the IM (inner membrane) and OM (outer membrane) and harbors an export apparatus. The extracellular part forms a capped needle-like structure (**Fig. 1.1**).

The injectisome is a self-assembling multiprotein complex that consists of multiple copies of 29 individual structural proteins (Ysc proteins). The basal body is assembled into two double rings and an inner rod that forms a channel for protein export [Marlovits *et al*., 2004]. The O-ring anchors the T3SS inside the OM and the peptidoglycan layer and is formed by a 15mer of secretin (YscC). Thereby, YscC forms two distinct rings inside the OM and a neck-like structure embedded into the periplasmatic peptidoglycan layer, which connects to the MS-ring. The MS-ring (membrane and supramembrane) is located in the IM and consists of a membrane-anchored layer of YscD and YscJ 24mers [Schraidt & Marlovits, 2011]. The assembled cytosolic C-ring consists of a YscQ 22mer and accessory proteins (YscKLO). It functions as a sorting platform involved in cargo handling. Central for its function is the ATPase activity of the YscN protein. YscN is an AAA^{+}-type ATPase, which catalyzes substrate unfolding and chaperone removal of T3SS substrates [Akeda & Galán, 2005; Notti & Stebbins, 2016]. Recently, the non-flagellar C-ring was demonstrated to be highly dynamic, which explains the struggle to crystallize a fully assembled C-ring. The C-ring is composed of a YscQ 22mer cycling between a cytosolic and docked pool. This cycle is regulated by ATPase activity and secretion status [Diepold *et al*., 2015]. The inner basal body is formed by YscRSTUV proteins, which assemble the export apparatus. The rod (YscI) and the extracellular needle (YscF) form a continuous channel build from homomultimers spanning the cytosol and the extracellular milieu. The needle tip is capped by a 5mer of scaffold protein LcrV [Broz *et al*., 2007]. The oligomerization of the LcrV needle cap is considered as a final checkpoint in injectisome assembly. Secretion of structural components is stopped and the

secretion machinery remains in a standby mode until needed. Upon cell contact, the injectisome is activated to secrete the hydrophobic translocator proteins (YopBD). During this process, the hydrophilic translocator LcrV functions as an assembly platform for YopB and YopD to induce pore formation in the eukaryotic cell membrane (**Fig. 1.2**) [Cornelis, 2002; Diepold & Armitage, 2015].

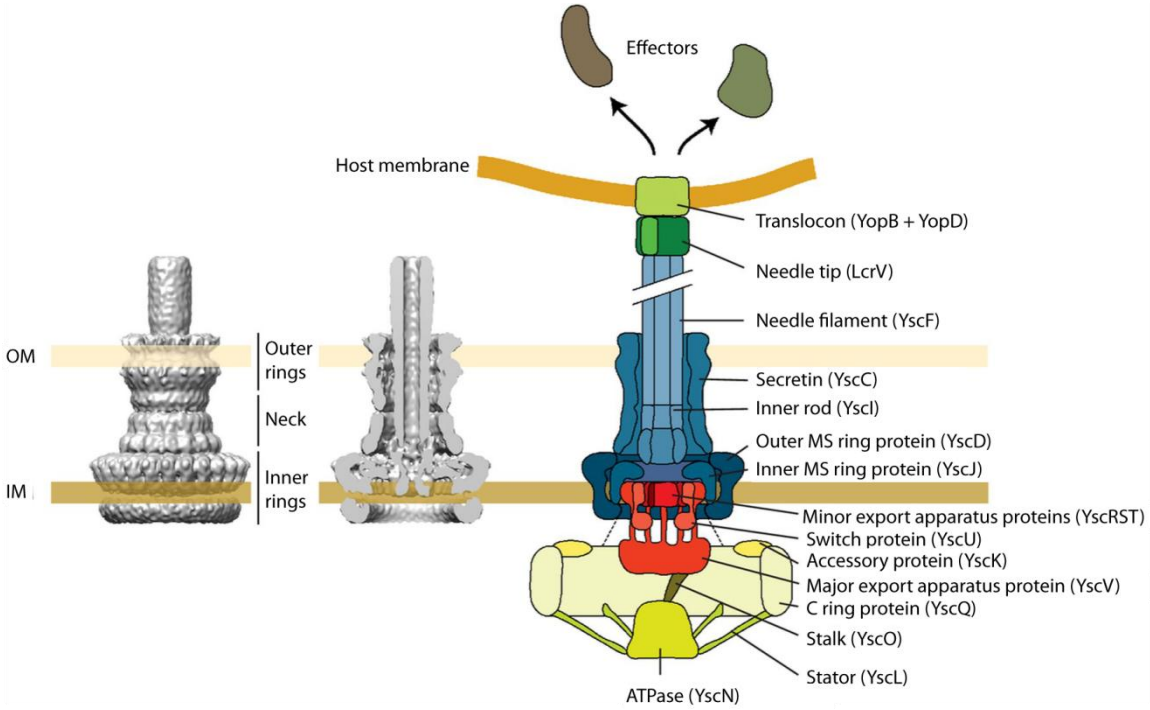

Figure 1.2: Overview of the injectisome and its components. Left and middle panel show a 3D reconstruction of the needle complex from cryo-electron microscopic data in a side (left) and cut (middle) view. The left panel shows an overview of the injectisome and its structural components. The injectisome consists of the C-ring (yellow), the export apparatus (red), the MS-ring in dark blue, the O-ring and needle components (light blue) and the needle tip and the translocon (green). This figure is adapted from Diepold & Wagner, 2014[2].

Macrophages can internalize *Yersinia* cells within one minute. Considering this, a fast response is needed to save the bacterium. By rapid injection of Yop effector molecules, phagocytosis can be blocked. The arsenal of antiphagocytic effector molecules comprises six different Yops (YopEHJMT and YpkA). A set of the Yop effectors (YpkA, YopE, YopH, YopT) inhibit phagocytosis by disrupting the cytoskeleton (YpkA, YopEHT), suppress the production of proinflammatory cytokines and chemokines (YopEHM) and also induce apoptosis (YopM). All Yops possess enzymatic activities that mimic and hijack cellular signaling pathways (**Fig. 1.3)** [Cornelis, 2002; Navarro *et al*., 2005].

[2] Permitted for use in a doctoral thesis by the Federation of European Microbiological Societies; Diepold & Wagner, 2014, Copyright: © 2014 Federation of European Microbiological Societies.

Yersinia protein kinase A or **YpkA** (YopO in *Y. enterocolitica*) displays serine/threonine kinase and guanine nucleotide dissociation-like inhibitor (GDI) activities that disrupt the actin cytoskeleton. With these enzymatic activities, YpkA targets the Rho GTPase activation status of RhoA and Rac1. The Ser/Thr kinase activity inhibits the activity of Rho activators, like WASP, WIP or cofilin by phosphorylation. The GDI domain directly binds to RhoA or Rac1 and interferes with the nucleotide exchange of GDP to GTP, which in turn also blocks reactivation [Barz *et al*., 2000; Juris *et al*., 2000; Navaro *et al*., 2007].

YopE is a GTPase-activating protein (GAP). It is involved in the inactivation of Rho GTPases, like RhoA, RhoG, Rac1, Rac2 and Cdc42, by increasing GTP hydrolysis. Similar to YpkA this leads to cytoskeleton disruption and as a consequence to inhibition of phagocytosis. Interestingly, the GAP activity also inhibits maturation of caspase-1, caspase-1-mediated macrophage responses and IL-18 maturation [Schotte *et al*., 2004].

The cysteine protease **YopT** is an inhibitor of Rho-GTPases. It post-translationally cleaves modified (cysteine prenylated) Rho-GTPases (RhoA, Rac1, Cdc42). This leads to Rho-GTPase release from the cellular membrane. As a consequence, the actin cytoskeleton is disrupted, which induces rounding of the host cell, inhibits the formation of the actin-rich phagocytotic cup and reduces chemotaxis. Intriguingly, YopT also interferes with the NFκB signaling pathway [Shao *et al*., 2001; Aepfelbacher *et al*., 2003; Schmidt, 2010].

YopH is a protein tyrosine phosphatase that specifically targets and dephosphorylates focal adhesion proteins, like focal adhesion kinase (Fak), paxillin or $p130^{Cas}$. By this mechanism YopH disrupts focal contacts and stress fiber, preventing phagocytosis by macrophages and neutrophils. Additionally, YopH suppresses the oxidative burst in macrophages and reduces Ca^{++} signaling in neutrophils. Furthermore, it induces T-cell apoptosis, suppress B- and T-cell activation and inhibits chemokine production in macrophages. In combination with all these immune-modulatory effects, YopH is the most potent effector molecule and especially needed for evasion of the early innate immune response [Aepfelbacher *et al*., 2007; Black *et al*., 2000; Fahlgren *et al*., 2009].

YopJ (YopP in *Y. enterocolitica*) is a multifunction protein. It possesses acyl transferase, cysteine protease and deubiquitinase activity. These functions especially interfere with the MAPK and NFκB pathways. Moreover, it induces cell death in macrophages [Mills *et al*., 1997; Orth, 2002].

YopM is a leucine-rich repeat protein and the only effector that is secreted into the extracellular milieu. It can enter host cells either by a T3SS-mediated injection or a direct penetration of the cell membrane. Intracellular YopM targets RSK and PRK isoforms and

caspase-1 to inhibit cytokine production and induce apoptosis [Rüter *et al*., 2010; Höfling *et al*., 2015]. [Chung *et al*., 2016] A recent study demonstrated, YopM recruits the PRK1/2 kinases to phosphorylate and thereby inactivate pyrin. This mechanism prevents the YopE- and YopT-triggered activation of the pyrin inflammasome and promotes virulence [Schoberle *et al*., 2016].

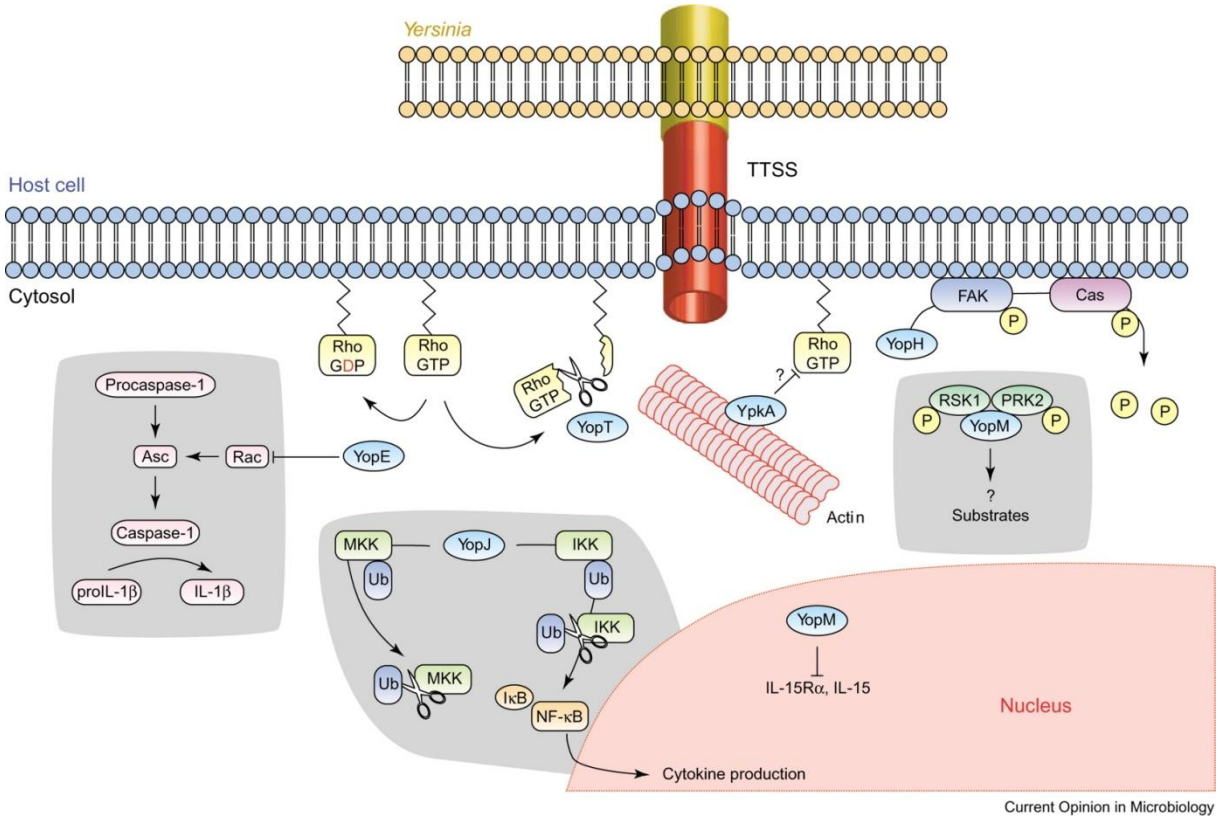

Figure 1.3: Overview of *Yersinia* effector proteins and their targets. Pathogenic yersiniae inject anti-phagocytotic effector proteins into the cytosol of host cells modulating multiple eukaryotic signaling pathways. YpkA, YopH, YopT and YopE disrupt the cytoskeleton. **YpkA** inhibits the nucleotide exchange of Rho GTPases, needed for actin polymerization, thereby inhibiting reactivation. Similarly, **YopT** interferes with the membrane localization of Rho GTPases. **YopE** deactivates Rho GTPases by increasing the GTP hydrolyzes rate. **YopH** disturbs focal adhesions by a phosphorylation and inactivation of central focal adhesions complex components. All these cytoskeleton-interfering effector proteins cooperate in the prevention phagocytosis. The remaining effector proteins block cytokine production and/or facilitate apoptosis. **YopJ** blocks cytokine production by interfering with the NFκB and MAPK pathways. **YopM** targets RSK1/PRK2 kinases and caspase I to inhibit cytokine production and induce apoptosis. This figure is derived from Navarro *et al*., 2005[3].

The export of effector proteins and assembly of the injectisome is strictly ordered and tightly regulated. After assembly of a functional injectisome, a target switch of the export apparatus from structural components to translocator and effector proteins occurs. Translocator and effector proteins are bound by Syc (specific Yop chaperone) proteins (e.g. SycEHTN and LcrH/SycD), which are needed for solubilization and export of their cognate binding partner.

[3] Reprinted from Current opinion in microbiology, 8/1, Navarro L, Alto N, Dixon JE, Functions of the Yersinia effector proteins in inhibiting host immune responses, 465-477, Copyright (2005), with permission from Elsevier.

These chaperones are subdivided, based on their fold, into class I chaperones (SycEHO) and class II chaperones (SycD/LcrH). Until now, four class I chaperone/effector pairs have been found - SycE/YopE, SycH/YopH, SycO/YpkA (YopO) and SycT/YopT. Additionally, the class II chaperone LcrH (SycD) binds the two translocator proteins YopD and YopB. Moreover, the chaperone SycH also binds regulator LcrQ. The gatekeeper protein YopN is only functional when bound by SycN and YscB [Akeda & Galán, 2005; Page & Parsot, 2002; Stebbins & Gallan, 2001].

The role of the Ysc-Yop-T3SS as a microsyringe that directly delivers effector molecules into target cells, is controversially discussed at the moment. As demonstrated by Akopyan *et al*., effector molecules are secreted into the supernatant prior to cell contact and localize to the bacterial cell envelope [Akopyan *et al*., 2011]. Deletions in the N-terminal domain of YopH also revealed the presence of two separate domains for secretion and translocation. Deletion of the secretion domain prohibited effector secretion, although when cells were coated with these secretion-defective YopH proteins, translocation into target cells still took place [Akopyan *et al*., 2011]. *Vice versa*, deletion of the translocation domain still allowed secretion into the supernatant, although these effector proteins were translocation-incompetent. Considering this, a two-step model was proposed, in which secretion and translocation are uncoupled. Effectors and translocators coat the bacterial cell prior to cell contact and function together in a binary AB-toxin-like delivery mechanism [Akopyan *et al*., 2011; Edgren *et al*., 2012; Pilar & Coombes, 2011].

1.3 Regulation of Type III secretion

In vitro, virulence genes of the *ysc-yop* and *yadA* regulon are strongly induced at 37 °C during the late exponential growth phase. When cultures are shifted from 25 °C to 37 °C expression of T3SS genes is activated and injectisomes assembly starts. Upon calcium depletion, transcription of T3SS-associated genes is massively induced, enormous amounts of Yops are secreted into the supernatant and a growth arrest occurs. This phenotype is also known as the low calcium response (LCR) [Sample *et al*., 1989; Straley *et al*., 1993]. *In vivo*, transcription of T3SS-associated genes encoded on the pYV plasmid is triggered at 37 °C by cell contact, which causes secretion of effector proteins [Hakansson *et al*.; 1996, Pettersson *et al*., 1996].

1.3.1 The virulence master regulator LcrF

Expression of all Ysc-Yop T3SS genes depends on the presence of the transcriptional master regulator LcrF. LcrF is a DNA binding protein that belongs to the family of AraC-type transcriptional regulators. The DNA-binding activity is conferred by two conserved helix-turn-helix motifs [Gallegos *et al*., 1997]. The N-terminal domain of AraC-like proteins contributes to the dimerization and binding of cofactors [Schleif, 2010]. Although LcrF forms dimers in solution, no cofactor binding has been described. LcrF activates pYV-encoded T3SS genes by binding to a TTTTaGYcTgTat DNA motif in the vicinity of the respective promoter regions [Wattiau & Cornelis, 1994]. Recently, it was demonstrated that LcrF and its homolog ExsA from *Pseudomonas aeruginosa* recognize the consensus sequence AaAAAnwnMygrCynnnmYTGyaAk (M: A or C; W: A or T; Y: C or T; R: A or G; K: G or T) [Brutinel *et al*., 2008; King *et al*., 2013].

LcrF is encoded on the bicistronic *yscW-lcrF* operon and expressed from the σ^{70}-dependent P_{yscW} promoter. The *yscW* gene (*virG* in *Y. enterocolitica*) encodes the lipoprotein YscW that functions as a pilotin for YscC [Burghout *et al*., 2004; Schwiesow *et al*., 2015; Yother *et al*., 1986].

Expression of *lcrF* is repressed at moderate temperature (25 °C), activated at 37 °C and even further triggered under low calcium conditions (secretion condition). This strict thermoregulation ensures expression of the T3SS regulon only inside the warm-blooded host. Thermoregulation is controlled on multiple layers of gene expression. One player is the *Yersinia* modulator A (YmoA). YmoA is a small, nucleoid-associated protein, homologous to the *E. coli* Hha protein. It is known to influence DNA supercoiling and gene expression. Binding to DNA occurs via heterocomplex formation of YmoA with the nucleoid structuring protein H-NS [Balsalobre *et al*., 1996; Madrid *et al*., 2006; Nieto *et al*., 2002]. The H-NS-YmoA heterocomplex represses T3SS expression at moderate temperatures (15-30 °C). By binding to a sequence downstream of the P_{yscW} transcriptional start site (TSS) [Böhme *et al*., 2012; Schwiesow *et al*., 2015]. At 37 °C, repression of *lcrF* is diminished as YmoA is degraded in a ClpXP- and Lon protease-dependent manner (**Fig. 1.4**) [Jackson *et al*., 2004].

Thermoregulation of *lcrF* is also controlled on the post-transcriptional level, independent of the YmoA-mediated transcriptional thermocontrol. Deletion of *ymoA* does not fully derepress *lcrF* transcription at moderate temperature and thermosensitivity of the T3SS regulon is maintained, even when *lcrF* is constantly transcribed [Böhme *et al*., 2012; Hoe *et al*., 1992; Hoe & Goguen, 1993]. The intergenic region between the *yscW* and the *lcrF* gene folds into

two hairpin structures - hairpin 1 and hairpin 2. Hairpin 2 contains the ribosomal binding site (RBS), as well as a thermolabile four uridine ('four U') motif. At moderate temperatures, the 'four U' motif incompletely base-pairs with the AGGA motif of the RBS and prohibits translation by blocking access of the 30S ribosome to the RBS. With increasing temperatures, the interaction of the 'four U' motif with the RBS is gradually disturbed and finally permits *lcrF* translation at 37 °C (**Fig. 1.4**) [Böhme *et al*., 2012; Hoe & Goguen, 1993; Waldminghaus *et al*., 2007; Kortmann & Narberhaus, 2012].

Other 'four U' motifs are located in the 5'-UTR of heat shock and virulence genes like in the *Salmonella enterica agsA* gene or in the *Vibrio cholera toxT* gene, where they function as an RNA thermometer [Weber *et al*., 2014; Kortmann & Narberhaus, 2012].

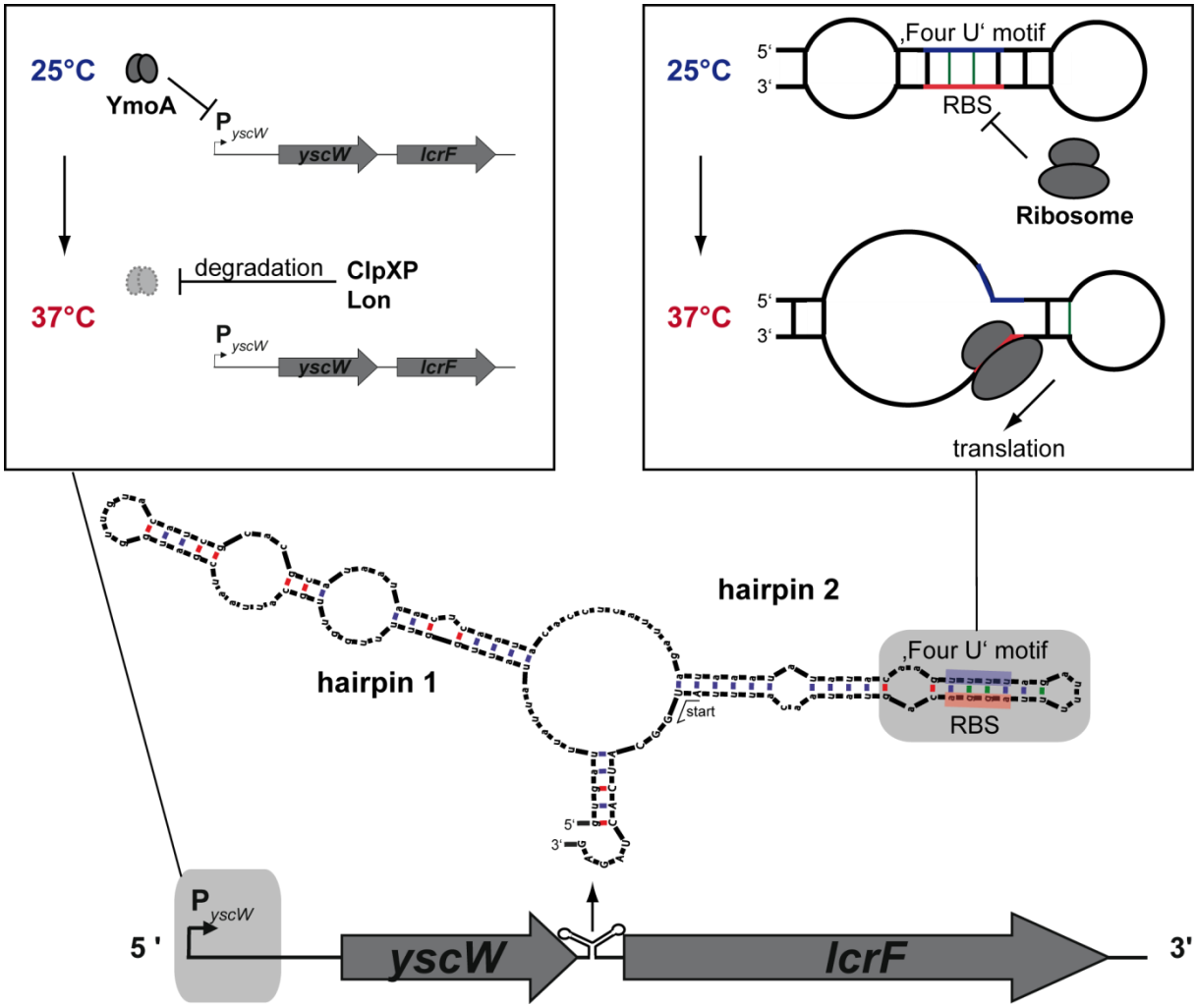

Figure 1.4: Expression of *lcrF* is thermoregulated on the transcriptional and post-transcriptional level. The transcriptional thermoregulation is mediated by YmoA. At 25 °C, it interacts with promoter P_{yscW} and blocks transcription, while at 37 °C YmoA is degraded by the Lon and ClpXP proteases, which results in a derepression of transcription of *yscW-lcrF* (upper left panel). The post-transcriptional thermoregulation is mediated by a thermolabile element ('four U' motif) in the 5'-UTR of the *lcrF* mRNA. At 25 °C, the 'four U' motif (blue) base pairs with the RBS (red) and blocks ribosomal access. At 37 °C, the thermometer melts open and allows the translational initiation (upper right panel).

1.3.2 Yop-dependent regulation of the injectisome

The expression of *yop* genes and other T3SS-associated genes is regulated in a negative feedback loop, independent of other regulatory processes. This negative feedback loop functions on the post-transcriptional level with the involvement of at least four proteins: the minor translocator YopD, its cognate chaperone LcrH, LcrQ which possesses a YopH-homolog domain and the YopH chaperone SycH. The interplay of these proteins prevents an uncontrolled overproduction of Yops and other T3SS-associated proteins under non-secretion conditions (high calcium concentration or in absence of cell contact) [Cambronne & Schneewind, 2004; Kopaskie *et al*., 2013].

YopD is a multifaceted protein with a molecular weight of 33 kDa. Although homologs in many injectisome encoding bacteria can be found, its full structure has not yet been resolved. Important structural features are its N-terminal coiled-coil domain, a hydrophobic and an amphipathic α-helix. Two additional regions are crucial for binding of its chaperone LcrH - the N-terminal hydrophobic domain and the amphipathic domain on the C-terminus [Costa *et al*., 2013; Francis *et al*., 2000; Olsson *et al*., 2004]. YopD has different functions, depending on its localization. Extracellular YopD acts as a minor translocator. Together with the major translocator YopB, it confers pore formation in the cell membrane of eukaryotic cells. In this process, it assists in the pore assembly and modifies pore size. A *yopD* mutant is defective in pore formation, while mutated YopD, missing its transmembrane (TM) domain, produces smaller pores in macrophages [Kwuan *et al*., 2013; Montagner *et al*., 2011; Neyt & Cornelis, 1999]. Intracellular YopD, together with its cognate chaperone LcrH, possesses RNA-binding capabilities and functions as a post-transcriptional repressor of *yop* genes. Therefore, it plays an important role in the LCR of yersiniae [Olsson *et al*., 2004; Francis *et al*., 2001; Anderson *et al*., 2002]. Upon calcium depletion, YopD is secreted into the supernatant, massively triggering Yop synthesis and inducing growth restriction. Additionally, a *yopD* mutant displays a thermosensitive phenotype, as *yop* expression is deregulated and massively activated at 37 °C. Indicating that the interaction of YopD with its cognate chaperone LcrH (SycD in *Y. enterocolitica*) is strictly required for its regulatory function. Deletion of *lcrH* destabilizes YopD [Francis *et al*., 2001]. The YopD/LcrH-dependent feedback regulation of *yop* genes requires AU-rich sequences in the leader transcript of target mRNAs, similar to the LcrQ-dependent regulation [Chen & Anderson, 2011; Anderson *et al*., 2002; Cambronne *et al*., 2002]. However, an exchange of these AU-rich elements does not change binding capabilities of YopD, indicating that further factors are necessary for binding and regulation

[Chen & Anderson, 2011]. Also, binding of YopD to its target transcripts results in a destabilization and translational repression [Anderson *et al*., 2002]. Kopaskie and colleagues could demonstrate that YopD associates with the 30S ribosomal subunit and this interaction prevents assembly of the 70S ribosome. Fully assembled ribosomes are resistant to YopD binding [Kopaskie *et al*., 2013].

LcrH acts as a chaperone of both translocator proteins YopD and YopB, classifying it as a T3SS class II chaperone. Like other T3SS chaperones, it has a low molecular weight, an acidic pI and a C-terminal hydrophobic helix. It displays an all α-helical fold, composed of three tetratricopeptide repeats (TPR). These TPR motifs can form elongated structures conferred by their helix-turn-helix conformation. Class II chaperones generally form homodimers. Moreover, the C-terminus has a quite loose fold, supporting the idea of a 'fly-casting' binding mechanism. In this model, the unfolded terminus binds at first loosely to its cognate partner, in turn increasing the binding strength. At the moment it is still controversially discussed whether LcrH dimers are loaded with one or more translocator proteins (**Fig. 1.4**) [Page & Parsot, 2002; Singh *et al*., 2013].

Figure 1.5: Crystal structure of the SycD-YopD complex. Representation of *Y. enterocolitica* chaperone dimer SycD (LcrH) with a bound peptide of translocator YopD. SycD possesses an all α-helical fold comprised of three tandem tetratricopeptide repeats. The extended YopD peptide binds the concave face of the TPR domain. The SycD chains are colored in red and blue. The YopD peptide is colored in purple. The picture is derived from Singh *et al*., 2013[4]

[4] This figure was originally published in Journal of Biological Chemistry. Singh, S. K., Boyle, a. L. & Main, E. R. G. LcrH, a class II chaperone from the Type Three Secretion System, has a highly flexible native structure. *J. Biol. Chem.* (2013); 288: 4048–4055. © the American Society for Biochemistry and Molecular Biology

Another LCR-associated regulator playing a major role in the negative feedback loop is **LcrQ**. LcrQ is a 12 kDa protein with homologies to the N-terminus of YopH [Rimpiläinen *et al*., 1992]. In *Y. enterocolitica* two *lcrQ* homologs, namely *yscM1* and *yscM2*, are encoded on the virulence plasmid. As demonstrated in *Y. enterocolitica*, the YscM1/2-dependent post-transcriptional *yop* genes repression targets the 5'-UTR of target genes, similar to YopD/LcrH [Cambronne *et al*., 2002]. The YopH chaperone, SycH, can bind to LcrQ, due to homologies to the N-terminus of YopH. LcrQ-dependent repression is released upon secretion of LcrQ or binding by the YopH chaperone SycH [Pettersson *et al*., 1996; Wulff-Strobel *et al*., 2002]. Cambronne and colleagues demonstrated that a short AUAAA sequence in the 5'-UTR of *yop* genes is involved in the LcrQ-dependent repression [Cambronne & Schneewind, 2002; Cambronne *et al*., 2004].

1.3.3 The Carbon storage system

The carbon storage regulator (Csr) system is a well-studied global regulatory system found in many Gram-negative bacteria. The Csr system is involved in regulation of various virulence factors, quorum sensing, carbon metabolism, peptide uptake and biofilm formation. In *Y. pseudotuberculosis*, it consists of the RNA-binding protein (RBP) CsrA and two regulatory, non-coding RNAs, CsrB and CsrC [Heroven *et al*., 2012; Vakulskas *et al*., 2015].
CsrA is a small 9 kDa protein that functions as a dimer. The monomer folds into five consecutive, antiparallel β-strands (β1-5) and a C-terminal winged α-helix. Upon dimerization, a sandwich of intertwined β-strand is formed. The β1 and β5 strand confer RNA-binding activity by a single-stranded RNA binding motif (KH motif). Because of this architecture, the RNA-binding domains lie on opposing sides of the dimer, which enables binding of two neighboring RNA binding sites on the same RNA molecule (**Fig. 1.6**) [Gutiérrez *et al*., 2005; Mercante *et al*., 2006; Rife *et al*., 2005].

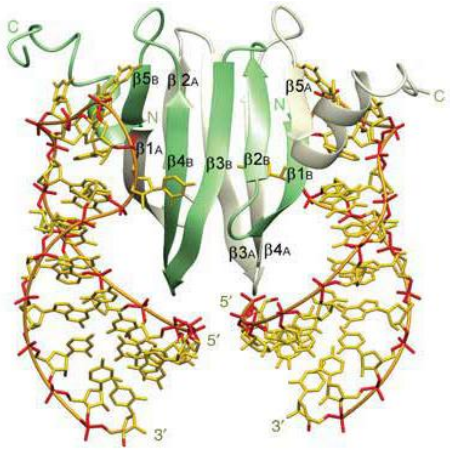

Figure 1.6: Structure of the CsrA-RNA complex. Representation of a dimer of the CsrA-homolog RsmE (green/gray) in complex with two RNA stem-loops structures (yellow). The CsrA dimer contains two RNA-binding domains allowing cooperative binding of two different RNA sites. The picture is adapted from Schubert *et al*., 2007[5].

The GGA sequence motif is the most conserved binding elements for CsrA [Dubey *et al*., 2005]. Since GGA motifs are part of the RBS and found in many 5'-UTRs of bacterial mRNAs, further binding motifs are needed to facilitate specificity in target RNA-binding. Binding motifs are especially recognized when exposed on a single stranded hairpin structure. Further comparative studies lead to the classification of high affinity, primary (A(N)GGA) and low affinity, secondary binding sites (AGAGA, YGGGA, CTGGA) [Baker *et al*., 2002; Wang *et al*., 2005; Yankhin *et al*., 2011]. Furthermore, neighboring binding sites need a proper spacing of 10-63 nt for efficient binding. A smaller spacing is unlikely because of intramolecular, sterical hindrance by the dimer [Kulkarni *et al*., 2014].

Most direct targets of the CsrA protein are repressed by its presence. Repression depends on binding to multiple sites in the 5'-UTR or the first codons of target transcripts, while one binding site needs to overlap the SD. By this mechanism, CsrA competes with the 30S ribosomal subunit for binding of the SD which in turn inhibits translation initiation. As a secondary effect, this often leads to fast RNA decay, since ribosome binding protects RNAs from degradation by RNases (**Fig. 1.7**) [Deneke *et al*., 2013; Romeo *et al*., 2012]. Until now CsrA-dependent activation of gene expression was only demonstrated for the flagellar master regulator *flhDC*. Here, CsrA binding confers protection from RNase E-mediated cleavage and subsequent degradation [Yakhnin *et al*., 2013].

A tight regulation of the Csr system is needed due to the global effect on the bacterial fitness. The activity of CsrA is finely adjusted by the action of the two non-coding RNAs CsrB and CsrC. These non-coding RNAs are highly structured and harbor multiple binding motifs

[5] Adapted and reprinted by permission from Macmillan Publishers Ltd: Nature Structural & Molecular Biology (Schubert *et al*., 2007)), copyright © 2007.

exposed on hairpin loops, allowing binding of multiple CsrA molecules. Thereby, they function as 'molecular sponges' that fine-tune the pool of active CsrA proteins [Babitzke & Romeo, 2007; Liu *et al*., 1997]. The amount of CsrB/C is indirectly regulated by CsrA, as binding to the Csr-type RNAs stabilizes both non-coding RNAs [Böhme, PhD thesis; Heroven *et al*., 2012]. Furthermore, both RNAs are counter-regulated in *Yersinia*, as upregulation of one RNA downregulates its counterpart [Fortune *et al*., 2005; Heroven *et al*., 2012]. By this means, they exhibit a compensatory regulation (**Fig. 1.7**) [Heroven *et al*., 2008]. In *E. coli*, RNA turnover of CsrB/C is controlled by the regulator protein CsrD. CsrD triggers RNase E-dependent degradation of CsrB/C, increasing CsrA availability [Suzuki *et al*., 2006; Romeo *et al*., 2012]. In Gram-positive bacteria, like *Bacillus subtilis*, a CsrB/C-type-independent regulation evolved, as homologs of these ncRNAs are completely missing. Instead, CsrA-mediated repression of motility is adjusted by direct protein-protein interactions with the alternative flagellar chaperone FliW, which is not present in *Enterobacteriaceae*. During assembly of the flagellar T3SS when high amounts of unbound cytosolic FliW are present, FliW directly binds CsrA and inhibits binding of target RNAs [Mukherjee *et al*., 2011; Mukherjee *et al* 2016].

Besides the sequestration mechanism, the pool of CsrA is precisely regulated in an autoregulatory feedforward loop. In *E. coli*, *csrA* is transcribed from five promoters that are either σ^{70}- or σ^{S}-dependent. Autoregulation of CsrA is very complex. Transcription from the σ^{S}-dependent P3 promoter is indirectly activated by the presence of CsrA. The 5'-UTR of the *csrA* transcript harbors four CsrA binding sites and is directly targeted by the CsrA protein, leading to a translational repression. As translational inhibition can be rapidly induced, this leads to an efficient shut-down of CsrA production when a critical level is reached [Yakhnin *et al*., 2011; Vakulskas *et al*., 2015].

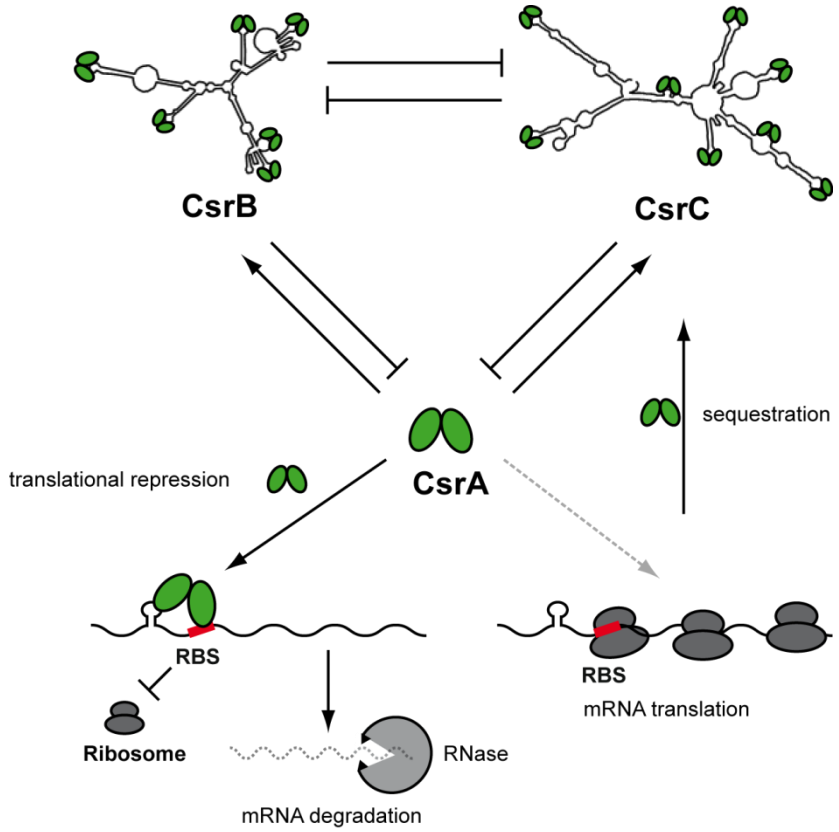

Figure 1.7: Mechanism of action of the Csr system. The Csr system consists of the RNA-binding protein CsrA and the non-coding RNAs CsrB/C. CsrB/C are counter-regulated and are stabilized by binding of CsrA. Both non-coding RNAs harbor multiple CsrA-binding motifs and function as a 'molecular sponge' for CsrA, reducing the overall CsrA activity. Dimeric CsrA binds to the 'GGA' core motifs of target mRNAs in the vicinity of and overlapping with the ribosomal binding site, thereby denying translational initiation and/or destabilizing the transcript. As CsrA has a high binding affinity to CsrB/C, high amounts of CsrB/C sequester CsrA from target mRNAs, allowing ribosomal access and mRNA translation.

1.3.4 The RNA degradosome

The RNA degradosome is a central player in the control of protein synthesis and many other regulatory processes. It ensures the control of RNA homeostasis and facilitates a rapid adaptation to environmental changes. A lot of these adaptations are conferred by the RNA degradosome, a multiprotein complex that controls RNA processing, dynamics and stability. The RNA degradosome is best studied in *E. coli*. It consists of the endoribonuclease RNaseE, the polynucleotide phosphorylase PNPase, the glycolytic enolase Eno and the RNA helicase RhlB (**Fig 1.8**) [Bandyra *et al*., 2013].

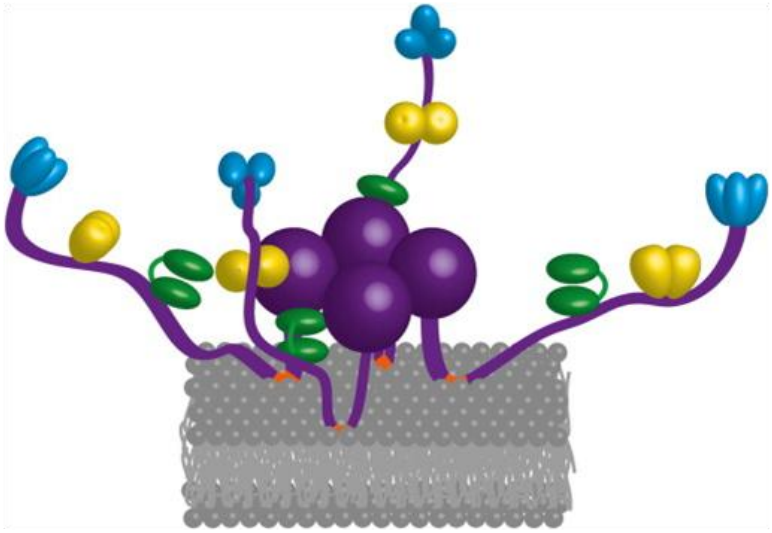

Figure 1.8: Schematic representation of the RNA degradosome complex. RNase E (purple) multimerizes and associates with the cytoplasmic membrane. The N-terminal half of RNase E (purple sphere) folds into a globular structure and contains the endoribonucleolytic catalytic core. The C-terminal half of RNase E confers membrane association and functions as an assembly platform for RNA helicase RhlB (green), enolase (yellow) and exoribonuclease PNPase (blue). Target RNAs are initially cleaved by RNase E and digested into nucleotides by PNPase, while secondary structures are unwinded by RhlB. The picture is adapted from Bandyra *et al*., 2013[6]

The endonuclease **RNase E**, encoded by the *rne* gene, is a large homotetrameric complex. Its N-terminus harbors the well conserved endoribonucleolytic site and an arginine-rich RNA-binding domain. The N-terminus can be divided into smaller subdomains, briefly S1-, RNase H- and DNase I-like domains. The RNase H subdomain has structural functions and misses catalytic activity. The S1 subdomain recognizes and binds the 5'-end of monophosphorylated RNAs. The DNase I-like subdomain confers enzymatic activity. The endonuclease active site is located in a shallow groove and confers binding with low sequence specificity. However, the AU sequence specificity most probably reflects the fitting of single-stranded RNA into the groove. In summary, RNase E can cleave far from the 5'-end but has a preference for 5'-monophosphorylated RNAs [Callaghan *et al*., 2005; Katarzyna *et al*., 2013; Mackie, 1998].

The C-terminus is less well conserved and contains helices for membrane localization, RNA-binding sites and the assembly site for other components of the degradosome [McDowall & Cohen, 1996; Khemici *et al*., 2008]. The C-terminal half of RNase E also seems to interact with other non-degradosome components, like Hfq, the ribosomal polyA-binding protein S1 and RNase E inhibitor proteins [Feng *et al*., 2001; Morita *et al*., 2005]. The importance of RNase E as an assembly platform for other degradosome players becomes especially evident in the degradation mechanism. RNase E functions as the decay initiator by undertaking the initial cleavage of substrate RNAs. Following this, RNA helicases RhlB unfolds the RNA and

[6] Bandyra *et al.,* 2013 is licensed under the Creative Commons Attribution (CC BY 3.0) license. https://creativecommons.org/licenses/by/3.0/

PNPase digests the remaining fragments into nucleotides (**Fig. 1.8**) [Carpousis, 2007; Hui *et al*., 2014].

PNPase is a homotrimeric exoribonuclease that catalyzes the phosphorolytic 3'- to 5'-end degradation of RNAs. However, PNPase can also reverse this reaction and function as a template-independent polynucleotide polymerase [Andrade *et al*., 2009; Mohanty & Kushner, 2000]. Each protomer contains two ribonucleolytic PH domains and two RNA-binding S1 domains. The PH domains are arranged in a small channel allowing entrance only to unfolded single-stranded RNAs [Shi *et al*., 2008; Symmons *et al*., 2000]. PNPase requires the interaction with RNA helicase RhlB for this process. This interaction can be direct and independent of the scaffold protein RNase E [Gunn-Guang *et al*., 2002; Lin & Lin-Shao; 2005]. Surprisingly, besides its role in RNA degradation, *in vitro*, PNPase together with the RNA chaperone Hfq was shown to protect certain sRNAs [Bandyra *et al*., 2016].
Interestingly, PNPase and the Csr system control their expression mutually. In *E. coli*, PNPase is involved in the CsrD-dependent degradation of CsrB/C and CsrA is involved in the autoregulation of *pnp* [Vakulskas *et al*., 2016; Leng *et al*., 2016; Suzuki *et al*., 2006]. Autoregulation of *pnp* is complex and involves CsrA binding and multiple nucleolytic cleavages. The leader transcript of *pnp* folds into multiple hairpin loops and contains two CsrA binding sites. The first one overlaps with the RBS and the second one is inaccessibly sequestered in a double-stranded stem-loop structure. Initially, the endoribonuclease RNase III cleaves the CsrA binding site-containing, double-stranded stem-loop structure. PNPase exonucleolytically degrades the 5'-fragment and liberates the CsrA binding site. Now, CsrA can access both binding sites and induces translational repression of *pnp* [Park *et al*., 2015; Condon, 2015; Robert-Le Meur *et al*., 1994].
In *Yersinia*, both major degradosomal RNases, RNase E and PNPase, are post-transcriptional regulators of the Ysc-Yop T3SS. A dominant negative RNase E mutant is unable to secrete effector molecules, although intracellular effector levels are unchanged [Yang *et al*., 2008]. Similarly, PNPase is also crucial for the secretion of effector proteins. Surprisingly, only the RNA-binding domain, but not the catalytic activity of PNPase is needed for this process [Rosenzweig *et al*., 2005; Rosenzweig *et al*., 2007].

RhlB is a DEAD-box RNA helicase playing a crucial role in RNA degradation. Proteins of the DEAD-box family share a structurally conserved ATPase domain containing a Walker II motif, which harbors the D-E-A-D amino sequence. This DEAD-box domain hydrolyzes ATP

to power the unwinding of structured RNAs. A RecA-like tandem-repeat structurally resembles the catalytic core. These domains support ATP and RNA binding and catalysis [Caruthers & McKay, 2002; Cordin *et al*., 2006; Lindner *et al*., 1989]. The C-terminal RecA-like domain also confers RNase E and PNPase interaction. The interaction with RNase E is boosted by the helicase activity of RhlB, which has a 5'-to 3'-directionality. In contrast, PNPase acts from the 3'- to 5'-end. Because of this, RhlB can rescue PNPase proteins that are stalled in hairpin structures. [Chandran *et al*., 2007; Liou *et al*., 2002; Tseng *et al*., 2015].

Enolase is a glycolytic protein that is only loosely connected to the degradosome. It is associated with the glycolysis cycle and reversibly catalyzes the dehydration of 2-phosphoglycerate to phosphoenolpyruvate. Although enolase does not bind RNA, up to 10% of enolase proteins are in complex with the RNA degradosome. Its role in the degradosome is still unclear, but it seems to link the energetic state of the cell to mRNA degradation [Carpousis, 2007; Chandran & Luisi, 2006; Py *et al*., 1996; Morita *et al*., 2004].

The so far identified factors involved in the regulation of late virulence are summarized in **Fig. 1.9**.

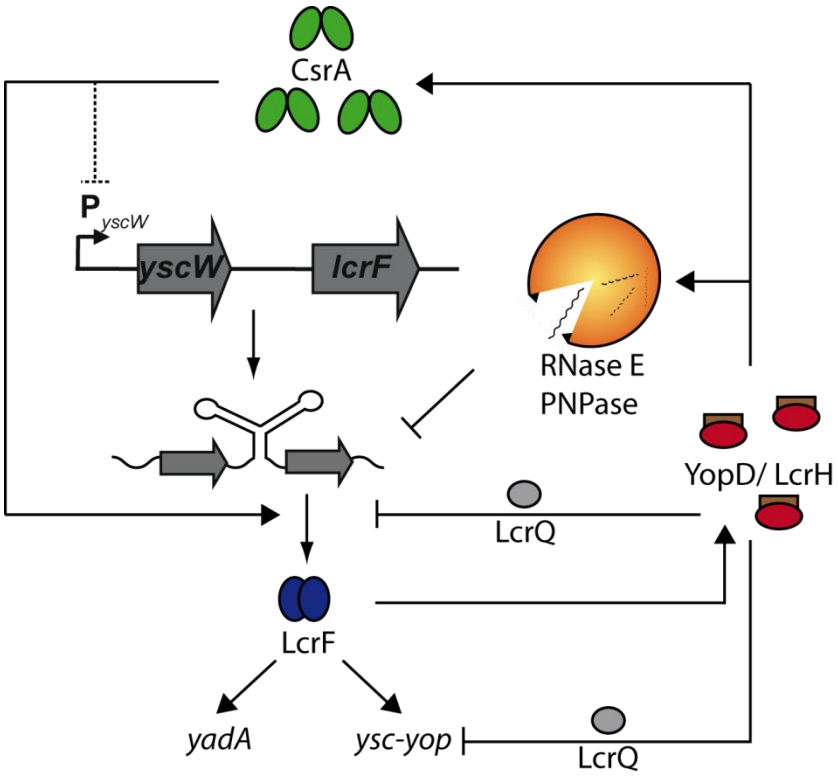

Figure 1.9: Working model of late virulence regulation in *Y. pseudotuberculosis*. The figure summarizes known relations between the components of the late virulence regulatory network. Expression of the late virulence master regulator *lcrF* is mainly controlled by the RNA-binding proteins CsrA and YopD/LcrH and degradosomal proteins (PNPase and RNase E). Positive effects (arrow-headed line) and negative (bar-headed line) effects are indicated.

1.4 Aim of the study

This study is focused on the molecular mechanism of the RNA-binding proteins YopD and CsrA in the regulation of late virulence genes in *Y. pseudotuberculosis*. Enteropathogenic *Yersinia* species need to coordinate the expression of their Ysc-Yop T3SS for survival and evasion from the innate immune response. The main hub for signal integration into the late virulence regulon is the transcriptional activator LcrF. Preliminary data revealed that *lcrF* expression is regulated by the action of two RNA-binding proteins [Steinmann, PhD thesis; Opitz, PhD thesis]. YopD, a bifunctional regulator with RNA-binding capabilities which also represses *lcrF* expression in a negative feedback loop under non-secretion conditions. CsrA, a central global-acting RNA-binding protein, which is involved in repression and activation of *lcrF* expression. Recent findings revealed that *csrA* expression is activated by YopD via an unknown mechanism. Through this mechanism, *lcrF* is regulated in a negative feedforward loop. As CsrA is also a central mediator in the regulation of many other stress adaptation and virulence systems, this connects the status of the Ysc-Yop T3SS to other regulatory modules. To analyze the underlying molecular mechanism of this negative feedforward loop, RNA-binding regions of YopD and CsrA and the underlying regulatory networks should be identified and characterized. Moreover, to get a deeper understanding of CsrA's role in *Yersinia* virulence, new direct CsrA targets should be identified.

2 Material and Methods

2.1 Materials

2.1.1 Chemicals and buffers

All chemicals used in this study were purchased from Merck, NEB, Fisher Scientific, Roth, Pierce, Qiagen, Sigma-Aldrich, T. H. Geyer, PerkinElmer, Invitrogen, Fermentas, Difco, BD Bioscience or Applichem, if not stated otherwise. The content of all buffers and solutions used in this study is described in the chapter of the corresponding method.

2.1.2 Enzymes, Kits and Antibodies

All enzymes, kits and antibodies with their manufacturers, which were used in this study, are listed in **Table 2.1**, **2.2** and **2.3**, respectively.

Table 2.1 Enzymes

Enzyme	Manufacturer
Benzonase	Merck
Mango *Tag*™ DNA Polymerase	Bioline
Phusion® High-Fidelity DNA Polymerase	New England Biolabs (NEB)
Restriction enzymes	NEB
Taq Polymerase	NEB
T4 DNA Ligase	NEB
T4 RNA Ligase I	NEB

Table 2.2: Kits

Kit	Manufacturer
Chemiluminescent Nucleic Acid Detection Module	Thermo Fisher Scientific
DIG luminescent detection	Roche
Mango Mix™	Bioline
QIAquick™ PCR Purification	Quiagen
QIAquick™ Plasmid Midiprep	Quiagen
QIAquick™ PCR Miniprep	Quiagen
SensiFast™ SYBR® No-ROX	Bioline
SV Total RNA Isolation	Promega
TranscriptAid™ High Yield	Fermentas

Table 2.3: Antibodies

Antibody (dilution)	Manufacturer
Primary antibody	
Anti-CsrA (1:5.000)	Davids Biotechnology
Anti-H-NS (1:150.000)	Davids Biotechnology
Anti-LcrH (1:1.000)	Davids Biotechnology
Anti-YopD (1:2.500 - 1:10.000)	Davids Biotechnology
Secondary antibody	
Anti-rabbit Immunoglobulin HRP conjugate	Cell Signaling

2.1.3 Organisms

2.1.3.1 *Escherichia coli* strains

All strains used in this study are listed in **table 2.4**.

Table 2.4: *Escherichia coli* strains

Strain	Description	Reference
DH10β	F$^-$ *mcrA* Δ(*mrr-hsd*RMS-*mcr*BC) Φ80d*lacZ*ΔM15 Δ*lac*X74 *end*A1 *rec*A1 *deo*R Δ(*ara*,*leu*)7697 *ara*D139 *galU galK nupG rpsL* λ$^-$	Casadaban & Cohen, 1980
BL21(DE3)	F- *gal met r-m- lon hsdS* λLysp*lac*UV5-T7 gene1p*lacI*^{q} *lacI*	Studier & Moffatt, 1986
S17-1λpir	*recA*, *thi*, *pro*, *hsdR*$^-$M$^+$ (RP4-2 Tc::Mu-Km::Tn7), λpir	Simon *et al*., 1983

2.1.3.2 *Yersinia pseudotuberculosis* strains

All strains used in during this study are listed in **table 2.5**.

Table 2.5: *Yersinia pseudotuberculosis* strains

Strain	Description	Reference
YPIII	pIB1, wild-type	Bölin *et al*., 1982
YP53	YPIII, pIB1, Δ*csrA*, Kan^R	Heroven *et al*., 2008
YP63	YPIII, pIB1, Δ*clpP*, Kan^R	A.-K. Heroven
YP67	YPIII, pIB1, Δ*lon*, Amp^R	A.-K. Heroven
YP79	YP69 (Δ*csrB*), pIB, Δ*csrC*	Heroven *et al*., 2012
YP83	YPIII, pIB1, *lcrF*(GUU-30/-28AAA)	R. Steinmann

YP84	YPIII, pIB1, *lcrF*(UU-28/-27CC)	R. Steinmann
YP91	YPIII, pIB1, Δ*yopD*	R. Steinmann
YP92	YPIII, pIB1, Δ*lcrH*	R. Steinmann
YP145	YP53, pIB1, Δ*csrA* Δ*yopD*, Kan^R	R. Steinmann
YP183	YP92 (Δ*lcrH*), pIB1, Δ*yopD*	This study
YP326	YPIII (Δ*hslV)*	This study
YP327	YPIII (Δ*ftsH)*	This study

2.1.4 Plasmids

All plasmids used in this study are listed in **table 2.6**. All constructed plasmids were sequenced by the in-house facility (GMAK). All gene coordinates are indicated relative to their translational start site.

Table 2.6: Plasmids

Plasmid	Description	Reference
pACYC184	Expression vector, ori p15a, Tet^R, Cm^R	Chang & Cohen, 1978
pAKH3	Mutagenesis vector, ori R6K, *sacB*, Amp^R	Heroven *et al.*, 2012
pAKH56	pACYC184, P_{csrA}-*csrA*$^+$ (-518/+183), Cm^R	A. K. Heroven
pAKH172	pET28a, *csrA*$^+$, Kan^R	A. K. Heroven
pBAD33	Expression vector, P_{araC}, *araO2*, *araC*, ori p15a, Cm^R,	Guzman *et al*., 1995
pDM4	Mutagenesis vector, ori R6K, *sacB*, Cm^R	Milton *et al*., 1996
pET28a	Expression vector, ori 3286, Kan^R	Novagen
pFU50	*dsRed2*, P_{lac}, ori 29807, Kan^R	F. Uliczka
pHSG576	Expression vector, ori pSC101, Cm^R	Takeshita *et al.* 1987
pJH4	pKB63, *csrA'-'lacZ* (-298/+17), Amp^R	This study
pJH5	pKB63, *csrA'-'lacZ* (-249/+17), Amp^R	This study
pJH6	pKB63, *csrA'-'lacZ* (-121/+17), Amp^R	This study
pJH10	pKB63, *csrA'-'lacZ* (-83/+17), Amp^R	This study
pJH12	pET28a, *yopD*$^+$, *lcrH*$^+$, Kan^R	This study
pJH25	pBAD33, *araC*(-22/0)::*csrA*$^+$(+1/+186), Cm^R	This study
pJH27	pKB63, P_{tet}:*csrA'-'lacZ* (-70/+17), Amp^R	This study
pJH30	pAKH3, Δ*hslV*, Amp^R	This study
pJH33	pAKH3, Δ*ftsH*, Amp^R	This study
pJH35	pHSG576, P_{csrA}::*csrA*:3xFLAG$^+$ (-298/+183), Cm^R	This study
pJH36	pKB63, P*yopD'-'lacZ*(-3314/+20), Amp^R	This study
pJH38	pKB63, P*yopD'-'lacZ*(-1224/+20), Amp^R	This study
pJH48	pKB63, *csrA'-'lacZ* (-298/+17, Δ-89/-51), Amp^R	This study
pJH49	pKB63, *csrA'-'lacZ* (-298/+17, Δ-89/-33), Amp^R	This study

pKB60	pHSG576, *csrA* (-518/+186), Cm^R	K. Böhme
pKB63	*csrA'-'lacZ* (-1071/+17), ori SC101, Amp^R	K. Böhme
pRS1	pFU50, ori 29807, Cm^R	R. Steinmann
pRS2	pRS1, *yopD*$^+$, Cm^R	R. Steinmann
pRS3	pRS1, *lcrH*$^+$, Cm^R	R. Steinmann
pRS5	pRS1, *lcrH-yopBD*$^+$, Cm^R	R. Steinmann
pRS15	pRS1, ori p15A, Cm^R	R. Steinmann
pRS16	pRS2, ori p15A, *yopD*$^+$, Cm^R	R. Steinmann
pRS17	pRS3, ori p15A, *lcrH*$^+$, Cm^R	R. Steinmann
pRS34	pDM4, Δ*yopD*, Cm^R	R. Steinmann
pRS42	pDM4; *yscW-lcrF*(GUU-30/-27AAA)*, Cm^R	R. Steinmann
pRS43	pDM4; *yscW-lcrF*(UU-28/-27CC)*, Cm^R	R. Steinmann
pRS45	pDM4; *yscW-lcrF*(Δhairpin 1 -44/-25)*, Cm^R	R. Steinmann
pRS46	pDM4; *yscW-lcrF*(Δhairpin 2 -111/-57)*, Cm^R	R. Steinmann

*... relative to translational start site of *lcrF*

2.1.5 Oligonucleotides

The oligonucleotides used for cloning and mutagenesis were purchased from Metabion and are listed in **table 2.7**. The corresponding restriction sites are underlined.

Table 2.7: Oligonucleotides

Oligonucleotide	Sequence (5'-- 3')	Restriction site
II275	GGGGCCCTGCAGCGAGTCAGAATAAGCATTCTTTG	*Pst*I
III645	GGGCGCACTAGTTCAGACAACACCAAAAGCG	*Spe*I
III647	GGGCGCCTCGAGTCATCATGGGTTATCAACGCAC	*Xho*I
IV436	GGGGCCGAATTCGCCAGCGGCATTAG	*Eco*RI
IV437	GGGGCCGAATTCGTAATCATCTATTAAATCAACACGC	*Eco*RI
IV438	GGGGCCGAATTCGGACTCGACCAAGCTACTTAC	*Eco*RI
IV706	GGGCGCCATATGACAATAAATATCAAGACAGAC	*Nde*I
IV707	GGGGCCGAATTCTGGCTTACGTTTTCACGGTG	*Eco*RI
IV708	GGGCGCACTAGTGTGATGCAACGTCTGCTAGATG	*Spe*I
V511	GGGCGCGTCGACCTGCTTCAAAATCAGTAAGTC	*Sal*I
V873	GCGGGAGCTCGTTCAGCGGTAACCATCAAAC	*Sac*I
V876	CCGCGAGCTCCTTTATCATCCAGTTGGCCTTC	*Sac*I
VI009	GCGGGAGCTCGCGATAAATATGTAATTCAGGCAC	*Sac*I
VI012	CCGCGAGCTCGCAACACAGCGTTCAATATG	*Sac*I
VI069	AATTATGCAGTGCGTTAATTACGTCACGGCGTACACTTACAATTG	
VI070	CAATTGTAAGTGTACGCCGTGACGTAATTAACGCACTGCATAATT	
VI071	GATGCCAACAGCTAGTTGATGTCACTCAAGGGATTAACCTC	

VI072	GAGGTTAATCCCTTGAGTGACATCAACTAGCTGTTGGCATC	
VI073	GCGGGGATCCGCCAGCGGCATTAG	*Bam*HI
VI074	GCGGGTCGACCGCTGCTTCAAAATCAC	*Sal*I
VI182	GGCGAATTCATGAGTGCGTTGATAACCC	*Eco*RI
VI184	GCCCTGCAGGTCTTGATATTTATTGTCATGGTTATTC	*Pst*I
VI185	GGCGAATTCGATCGTGCTTATCCAACGAG	*Eco*RI
VI419	GGTCTCTCTGTTTCCCCGCCTCATATAAAATGTAAGTAGC	
VI420	GCTACTTACATTTTATATGAGGCGGGGAAACAGAGAGACC	
VI421	GAAAAATTAAAAGAGTCGGGTCATATAAAATGTAAGTAGC	
VI422	GCTACTTACATTTTATATGACCCGACTCTTTTAATTTTTC	

2.1.6 Media and Antibiotics

All media used were prepared with ddH_2O and sterilized by autoclaving, if not indicated otherwise. The Media used are listed in **table 2.8**. For solid media 15 g/L of agar (Difco, USA) were added to liquid media. For selective media, antibiotics were added to a final concentration as listed in **table 2.9**. Antibiotics were prepared as stock solutions in the indicated solvents and filter sterilized afterward.

Table 2.8: Media

Media	Composition
BHI (Brain-Heart Infusion)	37 g/L BHI (BD Biosciences, USA)
DYT (Double Yeast Tryptone, complex medium) [Miller, 1992]	10 g/L yeast extract, 5 g/l NaCl, 16 g/L tryptone
LB broth (Lysogeny Broth Medium) [Sambrook *et al*., 1989]	5 g/L yeast extract, 5 g/L NaCl, 10 g/L tryptone

Table 2.9: Antibiotics

Antibiotic	Composition	Final concentration
Carbenicillin (Cb)	100 mg/mL in H_2O (Roth, Germany)	100 µg/mL
Chloramphenicol (Cm)	30 mg/mL in 70% EtOH (Roth, Germany)	30 µg/mL
Kanamycin (Kan)	50 mg/mL in H_2O (Merck, Germany)	50 µg/mL
Rifampicin	20-30 mg/mL in methanol (Merck, Germany)	1 mg/mL
Spectinomycin	50 mg//mL in H_2O (Roth, Germany)	50 µg/mL

2.2 Methods

2.2.1 General microbial methods

2.2.1.1 Cultivation of bacterial cells

Escherichia coli and *Yersinia pseudotuberculosis* cells were cultivated in liquid or solid media at 25 °C or 37 °C under aerobic conditions. Liquid cultures were grown in a Multitron Standard incubation shaker (Infors HT, Switzerland) at 200 rpm in reaction tubes or Erlenmeyer flasks. Bacteria on solid media were cultivated in a Heraeus B 6200 microbiological incubator (Thermo Scientific, USA).

2.2.1.2 Storage of bacterial strains

For short periods bacterial strains were stored on LB agar plates at 4 °C. For mid or long term storage glycerol stocks were prepared from LB overnight cultures and stored in screw-top tubes at -80 °C. For glycerol stocks, 1.25 mL of bacterial cultures were mixed with 0.75 mL 80% (v/v) glycerol.

2.2.1.3 Determination of bacterial cell density

Bacterial cell density was determined photometrically by measuring the optical density at a wavelength of 600 nm (OD_{600}) with the Ultrospec 3100 pro spectrophotometer (Amersham Biosciences, USA).

2.2.1.4 Chemically competent *E. coli* strains

Chemically competent *E. coli* strains, used for heat shock transformation, were prepared by the rubidium chloride method. Therefore, 100 mL LB medium supplemented with 20 mM $MgSO_4$ was inoculated 1:100 with a 37 °C *E. coli* overnight culture. Cells were cultivated to exponential phase for 3-5 h at 37 °C and harvested by centrifugation for 5 min at 3743 x g and 4 °C in a 3-18K centrifuge (Sigma, UK). Pellets were washed in 40 mL of ice-cold, sterile TFB1 buffer and incubated for 10 min on ice. Afterward, cells were pelleted again at 3743 x g, 4 °C and 5 min. The pellet was resuspended in 4 mL ice-cold, sterile TFB2 buffer and incubated on ice for 15-60 min. Finally, chemically competent cells were directly used in 100 µL aliquots or stored at -20 °C for up to 6 months.

TFB1 buffer: 30 mM potassium acetate, 10 mM $CaCl_2$, 50 mM $MnCl_2$, 100 mM RbCl, 15% (v/v) glycerol, pH 5.8
TFB2 buffer: 10 mM MOPS, 75 mM $CaCl_2$, 10 mM RbCl, 15% (v/v) glycerol, pH 6.5

2.2.1.5 Electrocompetent *Y. pseudotuberculosis* strains

For transformation by electroporation, electrocompetent *Y. pseudotuberculosis* strains were needed. A 25 °C LB overnight culture was used for a 1:50 inoculation of 20 mL BHI medium. The culture was grown to exponential phase for 3 h at 25 °C to an OD_{600} of 0.5 to 0.8 and harvested by centrifugation for 5 min at 3743 x g and 4 °C in a 3-18K centrifuge (Sigma, UK). The pellet was resuspended in 2 mL ice-cold transformation buffer and transferred to a new 2 mL microtube. Cells were harvested in a pre-cooled 5417R microcentrifuge (Eppendorf, Germany) at 6797 x g, 4 °C for 3 min. After two additional washing steps with 2 mL Transformation buffer, the pellet was resuspended in 200 µL Transformation buffer. Finally, 40 µL aliquots were directly used for electroporation.

Transformation buffer: 272 mM sucrose, 15% (v/v) glycerol, sterile filtrated

2.2.1.6 Transformation by heat shock of *E. coli*

For routine transformation of *E. coli* cells with plasmid DNA or ligation products, DNA was introduced by heat shock into chemically competent *E. coli* strains, like BL21(DE3) or DH10β [Pope & Kent, 1996]. For that, a 100 µL aliquot of chemically competent cells was thawed on ice and 100 ng of plasmid DNA or 10 µL of ligation product was added and incubated on ice for 5 min. Afterward, a one-minute heat-shock at 42 °C was applied. Cells were immediately cold-shocked on ice for 2 minutes. Additionally, 1 mL of ice-cold BHI medium was added and bacteria were incubated at 37 °C and 1,000 rpm for at least 30 min for phenotypic expression of the resistance marker. Subsequently, bacteria were pelleted for 3 min at room temperature and 8,000 rpm in a microcentrifuge. The supernatant was discarded and the pellet was resuspended in 100 µL LB medium and plated on the appropriate LB agar selection plate with the corresponding antibiotic. Bacteria were grown overnight at 37 °C in an incubator.

2.2.1.7 Transformation of *Y. pseudotuberculosis* by electroporation

Plasmid DNA is introduced into *Y. pseudotuberculosis* via electroporation. To do so, a high power electrical pulse was applied to electrocompetent cells to increase the permeability of the cell membrane.

An aliquot of electrocompetent cells was thawed on ice and 100 ng of plasmid DNA were added. The bacteria-DNA mixture was pipetted into pre-chilled electro cuvettes. The electro cuvette was put into a Gene Pulser™ electroporator and the bacteria-DNA mixture was exposed to a high voltage electrical pulse with the following parameters:

Voltage	2500 V
Resistance	200 Ω
Capacity	25 µF
Time constant	5 ms

The electroporated cells were directly mixed with 1 mL pre-chilled BHI medium and incubated for a minimum of 2 h at 25 °C and 1,000 rpm for phenotypic expression of the resistance marker. The cells were pelleted in a microcentrifuge for 3 min at 8,000 rpm at room temperature. The supernatant was decanted, bacteria were resuspended in 100 µL LB liquid medium and plated on LB agar plates containing appropriate antibiotics for phenotypic selection. Finally, bacteria were grown at 25 °C for two days or as long as required.

2.2.1.8 Mutagenesis of *Y. pseudotuberculosis*

Mutagenesis of *Y. pseudotuberculosis* was performed by chromosomal integration of a suicide plasmid by homologous recombination. The suicide plasmid was transferred via conjugation-competent *E. coli* S17-λpir into target *Yersinia* cells. Therefore, overnight cultures of the target *Y. pseudotuberculosis* strain and *E. coli* S17-λpir harboring the suicide plasmid with an R6K ori were grown at 25 °C or 37 °C, respectively. To remove traces of antibiotics, 300 µL of *E. coli* cells were centrifuged for 3 min, 2780 x g and room temperature and washed twice in LB medium. Subsequently, the *E. coli* cell pellet was resuspended in 900 µL of *Y. pseudotuberculosis* overnight culture, centrifuged and resuspended in 100 µL LB medium. A sterile filter membrane (0.22 µm pore size) was placed on an LB agar plate and the bacterial suspension was spread on the filter membrane and incubated for 6 to 12 h at 25 °C. Subsequently, the filter membrane was placed in a sterile 50 mL reaction tube and bacteria were washed off the membrane by mixing in 1 mL sterile 1 x PBS. Then, the cell suspension

was pelleted by centrifugation, washed in 1 x PBS and plated on *Yersinia* selective solid media plates, supplemented with appropriate antibiotics. Bacteria were then incubated for 2 days at 25 °C. Only those *Y. pseudotuberculosis* cells that stably integrated the mutagenesis plasmid into their genome were able to grow. Following this, bacteria were transferred to LB solid plates supplemented with 10% (w/v) sucrose. The suicide vector harbors the *sacB* marker gene, encoding levansucrase. In Gram-negative bacteria, the presence of sucrose expression of *sacB* leads to the accumulation of toxic levans in the periplasm [Reyrat *et al*., 1998]. Therefore, only bacteria that lost the *sacB*-harboring vector backbone are selected. Finally, fast growing colonies were analyzed by colony PCR for deletion of the target locus. *Y. pseudotuberculosis* strain YP183 was constructed from YP92 with the mutagenesis vector pRS34. Strain YP326 and YP327 were both constructed from YPIII with the suicide plasmids pJH30 and pJH33, respectively (see chapter 2.2.2.6.4).

2.2.2 Molecular biological methods

2.2.2.1 Determination of nucleic acid concentration and purity

Nucleic acid concentration and purity were determined by absorbance measurement utilizing a NanoDrop™ ND-1000 UV spectrometer (Thermo Scientific, USA). The nucleic acid concentration was measured by their absorbance at λ = 260 nm. An absorption of A_{260} = 1.0 corresponds to an RNA concentration of 40 µg/µL. The ratio of A_{260} and A_{280} was used to assess the nucleic acid purity. A ratio of ~1.8 or ~2.0 is defined as pure DNA or RNA, respectively. The ratio of A_{260} to A_{230} was used as a secondary parameter for evaluation of nucleic acid purity. Values between 2.0 and 2.2 could be considered as pure DNA/RNA. Lower values indicate contaminants that absorb at A_{230}, such as phenol.

2.2.2.2 Polymerase chain reaction (PCR)

Polymerase chain reaction is a powerful tool to specifically amplify linear DNA fragments for cloning and gene analysis [Saiki *et al*., 1988]. By using specific flanking oligonucleotides (primer) a thermostable DNA-dependent DNA polymerase amplifies double stranded DNA regions in changing thermocycles. Thereby, the PCR proceeds in cycles of three repeating steps: double-stranded DNA (dsDNA) is denatured at 95 °C, primer specifically anneal to the single-stranded DNA template at 50-62°C and complementary single stranded DNA is synthesized at 72 °C. The annealing temperature depends on primer length and its GC content

and was calculated by ApE plasmid editor software (M. Wayne Davis). The elongation time depends on the fragment length to be synthesized and on the synthesis rate of the used DNA polymerase.

When high fidelity in DNA synthesis was needed, e.g. for amplification of cloning inserts, the Phusion® High-Fidelity DNA polymerase (Thermo Scientific, USA) was used. This polymerase harbors a 3'-5' exonuclease proofreading activity, resulting in low error rates. The MangoMix™ (Bioline, Germany) containing the MangoTaq™ DNA polymerase (Bioline, Germany) was taken for control colony PCR to check for positive clones. Phusion polymerase PCR reactions were carried out in a volume of 50 µL, whereas colony PCRs were prepared in aliquots of 15 µL according to the manufacturer's instructions). For colony PCR, a single colony was picked with a sterile pipette tip and mixed directly into the PCR reaction mixture (*E. coli*). To screen for *Yersinia* mutants, a single colony was mixed into 10 µL of sterile ddH_2O and boiled for 10 min at 95°C. 1 µL of lysed bacterial cells was added to the PCR mix. All PCRs were amplified in the T3,000 Thermocycler (Peqlab, Germany) or the Mastercycler EP S gradient cycler (Eppendorf, Germany).

2.2.2.3 Isolation of plasmid DNA

Depending on the plasmid copy number 5-10 mL LB overnight culture was used for plasmid preparation. For rapid and low-scale extraction of plasmid DNA the QIAprep® Miniprep kit (QIAGEN, Germany) was utilized according to the manufacturer's instructions).

2.2.2.4 Gel extraction and purification of DNA

DNA Purification and extraction from agarose gels for further application was performed with the QIAquick® PCR purification kit or QIAquick® Gel extraction kit (QIAGEN, Germany) according to the manufacturer's recommendations. Therefore, DNA fragments of interest were separated by agarose gel electrophoresis (AGE), stained with ethidium bromide, visualized and isolated under UV light (λ = 315 nm). Small DNA fragments less than 100 nucleotides were purified using the NucleoSpin® Gel and PCR Clean-up kit (Macherey-Nagel, Germany). The DNA was routinely eluted in 50 µL ddH_2O.

2.2.2.5 Agarose gel electrophoresis for separation of DNA fragments

Separation of DNA molecules was carried out by agarose gel electrophoresis (AGE). When power is applied, the negatively charged DNA molecules transmigrate through an agarose gel matrix towards the anode. During this process, DNA molecules are separated depending on their size and conformation. In this work 0.8% (w/v) agarose gels in 1 x TAE buffer were used for gel extraction after plasmid digestion and to check PCR fragments for integrity and correct size. For DNA fragments smaller than 100 nucleotides 2.5% (w/v) agarose gels were used. Separation was done in a gel electrophoresis chamber (Peqlab, Germany) in 1 x TAE buffer for 45 min at 120 V. To determine the fragment size, 3 µL of GeneRuler DNA Ladder Mix (Thermo scientific, USA) was used. Before applying, the samples were diluted in 6 x DNA Gel Loading Dye (Thermo Scientific, USA). To visualize DNA fragments, agarose gels were stained in an ethidium bromide bath (1 µg/mL in ddH_2O) for 15 min and documented with a GelDoc™ XR+ (Bio-Rad, USA) at a wavelength of 302 nm.

TAE buffer: 40 mM TRIS acetate (pH 8.0); 1 mM EDTA (pH 8.0)

2.2.2.6 Cloning techniques

2.2.2.6.1 Restriction digest

Targeted cleavage of DNA molecules to determine the size or insertion of a specific DNA fragment into a specific vector site was carried out by restriction digestion. In this study type II restriction endonucleases (NEB, USA) that recognize and cleave specific palindromic 4-8 nucleotide long sequences were used. These nucleases produce blunt or sticky ends (5'-single stranded sequence). For simultaneous digestion with two restriction enzymes the suitable reaction buffer was chosen according to the manufacturer's instructions). The reaction was incubated for 2 h at 37 °C and subsequently separated by AGE or purified by PCR purification.

Restriction digest reaction (50 µL)

DNA (0.1-2.0 µg)	x µL
Reaction buffer (10x)	5 µL
Reaction enzyme 1 (1U/µL)	1 µL
Reaction enzyme 2 (1U/µL)	1 µL
ddH_2O	x µL

2.2.2.6.2 Dephosphorylation of plasmid DNA

After restriction digestion, 5'-phosphates were removed by dephosphorylation using the Antarctic Phosphatase (NEB, USA), to prevent recirculation of linearized plasmid DNA. After isolation of a cleaved cloning vector by gel extraction, appropriate amounts of 10 x Antarctic Phosphatase Reaction buffer and 1 µL Antarctic Phosphatase were added and incubated for 30 min at 37 °C. The reaction was heat inactivated at 70 °C for 5 min and used for ligation.

2.2.2.6.3 Ligation

Insertion of DNA fragments into a linear, dephosphorylated cloning vector was done by ligation with T4 DNA ligase (Promega, USA). T4 DNA ligase catalyzes ligation of DNA strands by forming a phosphodiester bond. To increase the ligation rate, ligation reactions were carried out in two reactions with a 1:1 and 1:6 vector-to-insert ratio (v/v). Additionally, to examine the religation rate of the cloning vector ddH_2O instead of insert DNA was used. The reaction was incubated for 2 h at room temperature or overnight at 18 °C. Afterward, the ligation reaction was transformed by heat shock into chemically competent *E. coli* DH10β and plated onto LB agar plates supplemented with the corresponding antibiotics. Clones carrying the respective antibiotics resistance marker were picked and checked by colony PCR. Therefore, insert- and plasmid-specific primer were used to check for proper insertion and orientation of the insert fragment. Finally, plasmid DNA was prepared from positive clones and sequenced by the HZI in-house sequencing facility.

Ligation reaction (10 µL)

Ligase buffer (10x)	1 µL
Vector DNA	1 µL or 3.5 µL
Insert DNA	6 µL or 3.5 µL
ATP (10 mM)	1 µL
T4 DNA Ligase	1 µL

2.2.2.6.4 Construction of plasmids

The *csrA-lacZ* reporter fusion plasmids **pJH4**, **pJH5**, **pJH6**, **pJH10** and **pJH27** were all constructed by amplification of *csrA* upstream fragments from chromosomal DNA of the *Y. pseudotuberculosis* strain YPIII. The resulting fragment and vector pKB63 were digested with

*Eco*RI and *Pst*I and ligated. The following primer combinations were used to amplify the inserts: IV436/II275 (pJH4), IV437/II275 (pJH5), IV438/II275 (pJH6), IV707/II275 (pJH10) and V835/II275 (pJH27). The forward primer for the construction of pJH27 encodes the tetracycline promoter (P_{tet}) at its 5'-end.

The *lacZ* reporter plasmids **pJH36** and **pJH39** were created by amplification of a *yopD* upstream fragment with primer pair VI185/VI184 and VI182/VI184, respectively. The inserts and pKB63 were digested with *Eco*RI and *Pst*I and ligated.

The YopD/LcrH overexpression plasmid **pJH12** was constructed by amplification of the *yopD* gene with primer pair IV706 and III644 and the *lcrH* gene with primer pair IV708 and III647 from DNA of the virulence plasmid of YPIII. The *yopD* fragment was cut with *Nde*I/*Spe*I and the *lcrH* gene fragment was digested with *Spe*I/*Xho*I. Both fragments were ligated into the *Nde*I/*Xho*I sites of plasmid pET28a.

The complementation plasmid **pJH25** was constructed by amplifying the *csrA* gene with primer pairs V821 and V511. To create a CsrA-independent, inducible *csrA* complementation vector, the *csrA* gene was fused to the 5'-UTR of the *araC* gene of *E. coli* K12. The *araC* upstream region was introduced by forward primer V821 containing the corresponding sequence at its 5' end. The resulting fragment was digested with *Xba*I and *Sal*I and ligated into the *Xba*I/*Sal*I site of pBAD33.

Mutagenesis plasmids **pJH30** and **pJH33** were used for a markerless deletion of the *hslV* and *ftsH* gene by homologous recombination. To create a markerless deletion, an insert containing the upstream and downstream regions, without the target gene's coding sequence, was created by three step PCR. First, two 500 nt fragments of the up- or downstream region of the target gene were amplified by PCR from chromosomal DNA of YPIII. Thereby, the reverse primer of the upstream fragment and the forward primer of the downstream fragment contained a 20 nt long homologous sequence to the down- or upstream fragment. Next, both fragments were used as DNA templates for the final amplification of the full-length insert using the forward primer of the upstream fragment and the reverse primer of the downstream fragment. The full-length fragment was digested with *Sac*I and ligated into the *Sac*I site of pAKH3. The upstream fragment of pJH30 was amplified with primers V873/VI069 and the downstream fragment using primer pair VI070/V876. The full-length product was amplified with primer pair V873/V876. The up- and downstream fragments for construction of pJH33 were amplified with primer pairs VI009/VI072 and VI073/VI012, respectively. The final full-length fragment was amplified by PCR using primers VI009/VI012.

The *csrA*-3xFLAG expression vector **pJH35** was constructed by ligating the PCR product of primer combination VI073/VI074 amplified from chromosomal DNA of strain YPIII into the *Bam*HI/*Sal*I site of pKB60. To create a C-terminally 3xFLAG tagged CsrA variant, the 3xFLAG epitope was introduced by reverse primer VI074.

The *csrA-lacZ* reporter plasmids **pJH48** and **pJH49**, harboring deletions in the *csrA* upstream region were all constructed using plasmid pKB63 as a backbone. Deletions were introduced by three step PCR from genomic DNA of strain YPIII as described for pJH30 and pJH33. To do so, the up- and downstream regions of the deletion site were amplified by PCR. Both fragments contained overlapping homologous regions at their 3' or 5' end. These homologous regions allowed the amplification of a third full-length fragment containing a markerless deletion in the 5'-UTR of the *csrA* gene. To create plasmid **pJH48**, the upstream fragment was amplified by PCR with primer IV436 and VI419 and the downstream fragment was amplified utilizing primer VI420 and II275 using chromosomal DNA of *Y. pseudotuberculosis* strain YPIII as a template. To create the final full-length fragment, the up- and downstream fragment functioned as a template for a third PCR with the primer combination IV436/II275. The digested inserts were ligated into the *Eco*RI/*Pst*I site of pKB63. The same procedure was used for the construction of **pJH49**. The PCR products of primer combination IV436/IV421 (upstream fragment) and of VI422/II275 (downstream fragment) were used as a template for the final full-length fragment (IV436/II275).

2.2.2.7 Isolation of total RNA from *Y. pseudotuberculosis*

The SV total RNA isolation kit (Promega, USA) was applied for quick isolation of total RNA from *Y. pseudotuberculosis*. To do so, bacterial cultures were grown under the desired conditions. Two mL of the culture was transferred to a 2 mL reaction tube and harvested by centrifugation (18,000 x g, 5 min, 4 °C). After removal of the supernatant, total RNA was extracted according to the manufacturer's instruction. Finally, RNA concentration was photometrically measured using the NanoDrop™ ND-1000 UV spectrometer (Thermo Scientific, USA). Samples were stored at -20 °C.

2.2.2.8 Phenol-chloroform extraction of RNAs

Removal of contaminating proteins and lipids is crucial for downstream applications (e.g. biotinylation or RNA electromobility shift assay) of *in vitro* transcribed or biotinylated RNAs. For extraction of RNAs, samples were filled up to a volume of 150 µL with RNase-free

ddH_2O, 400 µL CPI was added and mixed vigorously. Separation of phases was done by centrifugation for 5 min at full speed. The nucleic acid rich aqueous phase was transferred to a new test tube. Then, 405 µL of ice-cold absolute ethanol and 45 µL of 3 M sodium acetate (pH 4.5) were added and the samples were mixed thoroughly. To visualize precipitated nucleic acids, 2 µL glycogen (RNase and DNase free) was added. The RNA was precipitated at -20 °C for at least 2 h or overnight. After centrifugation 18,000 x g and 4 °C for 30 min the supernatant was carefully removed using a pipette and the pellet was washed with 500 µL 70% ethanol. Again, samples were centrifuged 18,000 x g for 15 min at 4 °C, the supernatant was carefully removed and the pellet was air dried and resuspended in 20-50 µL of TE buffer. RNA concentration was determined with the NanoDrop™ ND-1000 UV spectrometer (Thermo Scientific, USA) and samples were stored at -20 °C.

TE buffer: 10 mM Tris-HCl (pH 8.0), 1 mM EDTA

2.2.2.9 Hot Phenol RNA extraction

The isolation of high yield and high-quality RNA for critical downstream applications, like RNA-sequencing, was carried out by hot phenol extraction. For this purpose, bacterial pellets were resuspended in 250 µL RNA resuspension buffer and transferred into 2 mL safe-lock tubes. After addition of 250 µL RNA lysis buffer, samples were inverted five times and incubated for 90 s at 65 °C to ensure a rapid and complete cell lysis. The cell lysate was then supplied with 500 µL pre-heated aqua phenol (65°C), incubated for 3 min at 65 °C and snap frozen in liquid nitrogen for at least 30 s. Samples were centrifuged for 10 min at 18,000 x g at room temperature and the aqueous phase was transferred to a fresh 2 mL safe-lock tube. To prevent rupture of reaction tubes due to too rapid thawing during centrifugation, samples were pre-thawed for 1 min at room temperature before centrifugation. This process was repeated twice. The supernatant was mixed with 300 µL chloroform-isoamyl alcohol (24:1) in a 1.5 mL tube, mixed vigorously for at least 30 s and centrifuged (3 min, 18,000 x g, room temperature). The aqueous phase was transferred to a new reaction tube and the step was repeated once more. Finally, the RNA in the aqueous phase was precipitated with 1/10 volume 3 M NaOAc pH 4.5, 2.5 volumes of absolute ethanol and 2 µL of glycogen overnight at -20 °C. The precipitate was collected by centrifugation for 30 min at 18,000 x g and 4 °C. The ethanol was removed and the pellet was washed in 500 µL ice-cold 70% ethanol and centrifuged (15 min, 18,000 x g, 4 °C). Finally, ethanol was removed completely by pipetting,

the pellet was air-dried and resuspended in TE buffer. RNA concentration and quality were assessed with the NanoDrop™ ND-1000 UV spectrometer (Thermo Scientific, USA).

RNA resuspension buffer: 0.3 M Sucrose in 0.01 M NaOAc (pH 4.5)
RNA lysis buffer: 2% SDS in 0.01 M NaOAc (pH 4.5)

2.2.2.10 Agarose gel electrophoresis of RNA

Denaturing agarose gel electrophoresis was carried out to separate total RNA for control of RNA integrity and for the detection of specific RNAs by northern blot analysis. Thereby, the negatively charged RNA is separated depending on the molecular weight as it migrates through an agarose gel matrix in an electrical field. A 1.2% agarose gel in 1 x MOPS buffer was used for RNA separation. For this purpose, 5-60 µg total RNA was mixed with RNA loading buffer, heated for 10 min at 70 °C and incubated on ice for at least three minutes. The denatured RNA samples were loaded on a MOPS agarose gel and separated for 1 h at 120 V. The ethidium bromide in the loading buffer ensured the detection of 16 S and 23 S ribosomal RNAs as a loading control. Ribosomal RNAs were visualized with a GelDoc™ XR+ (Bio-Rad, USA) at a wavelength of 302 nm. For identification of specific RNAs, the gel was further used for northern blotting.

MOPS (20 x): 200 mM MOPS; 50 mM sodium acetate; 10 mM EDTA
RNA loading buffer (5 x): 2.7% formaldehyde; 0.1 mg/mL ethidium bromide; 4 mM EDTA; 0.03% bromphenol blue; 20% glycerol in 4 x MOPS

2.2.2.11 Northern blot analysis

Detection of specific RNAs, e.g. for gene expression analysis, was carried out by northern blotting. After RNA separation by agarose gel electrophoresis, the RNA was transferred to a 0.45 µm Nytran® N nylon blotting membrane (GE Healthcare, Germany) with a vacuum blotter (vacuum blotter Model 785 and vacuum regulator; Bio-Rad, USA) at 5 bar for 1.5 h in 10 x SSC buffer, according to the manufacturer's instructions). The transferred RNA was cross-linked to the membrane with UV light for 3 min in a Stratalinker UV crosslinker (Agilent Technologies, USA).

Specific RNAs were then identified by hybridization with DIG-labeled DNA probes and detected by utilizing the DIG luminescent detection kit (Roche, Switzerland) according to the manufacturer's instructions. For this purpose, cross-linked blots were prehybridized in

hybridization buffer for 1 h at 42 °C in an OV2 mini-hybridization oven (Biometra, Germany). Hybridization of DIG-labeled probes and target RNAs occurred overnight at 42 °C in hybridization buffer. Before use, 5 µL of DNA probes were diluted in 100 µL ddH_2O, denatured twice for 10 min at 95 °C and incubated on ice for 5 min after each heating step. All probes used in this study were amplified by PCR with a 10 x DIG DNA labeling Mix (Roche, Switzerland) instead of the standard dNTP mix. Their corresponding primer pairs are listed in **table 2.10**.

Table 2.10: DNA probes used for mRNA detection

probe	primer pair
csrA	V004/V005
lcrF	I214/I303

The next day, the membrane was washed twice in washing buffer I for 5 min and two times in washing buffer II for 15 min at 68 °C in a hybridization oven. The membrane was blocked in CDP* blocking buffer for 30 min. Incubation with anti-DIG AP-conjugates (Sigma, UK) diluted 1:6,000 in CDP* blocking buffer was carried out for 1 h. Blots were washed twice in CDP* washing buffer for 15 min and equilibrated for 5 min in CDP* detection buffer. The blot was developed with CDP* diluted 1:100 in detection buffer for 5 min. The chemiluminescent signal could be documented either by utilizing the ChemiDoc XR+ System for high abundant RNAs or otherwise using a CL-XPosure X-ray film (Thermo Scientific, USA).

SSC (20 x): 0.3 M trisodium citrate; 3 M NaCl
Washing buffer I (1 x): 2 x SSC; 2% SDS
Washing buffer II (1 x): 0.1 x SSC; 0.1% SDS
CDP* maleic acid buffer: 0.1 M maleic acid; 0.15 M NaCl; pH 7.5
CDP* blocking buffer: 10% (w/v) blocking reagent in CDP* maleic acid buffer
CDP* washing buffer: 0.1 M maleic acid; 0.15 M NaCl; 0.3% TWEEN-20; pH 7.5
CDP* detection buffer: 0.1 M Tris-HCl; 0.1 M NaCl; pH 9.5

2.2.2.12 RNA stability assay

To determine the stability of mRNA transcripts, an RNA stability assay was performed. For this purpose, synthesis of new RNAs was stopped, by the addition of rifampicin that blocks the activity of the bacterial DNA-dependent RNA polymerase. As a result, the stability of

target RNAs can be monitored and analyzed by addressing differences in mRNA levels over time using northern blot analysis.

The corresponding *Yersinia* strains were grown in 100 mL Erlenmeyer flasks with 20-30 mL LB medium and if necessary with the corresponding antibiotics, for 2 h at 25 °C followed by a shift to 37 °C for 4 h. Transcription was stopped by addition of 1 mL rifampicin to a final concentration of 1 mg/mL (Serva, Germany). Generally, 1.8 mL of the culture was taken and added to 0.2 mL stop solution at appropriate time points. Samples were mixed well by inverting and snap frozen in liquid nitrogen. Total RNA was isolated, quantified and analyzed by northern blotting as described previously.

To determine mRNA half-life, target transcripts and ribosomal RNAs were quantified using the ImageJ image processing software [Schneider *et al*., 2012]. The mRNA quantity at time point zero of each strain was taken as a reference. The ratio of mRNA to 16 S and 23 S ribosomal RNAs of each sample was calculated relative to the reference. The half-life of the respective transcript was calculated as described below. The decaying constant λ was calculated as the absolute value of the exponential regression coefficient.

$$t\left(\frac{1}{2}\right) = \frac{\ln(2)}{\lambda}$$

$t_{(1/2)}$ - transcript half-life

λ - decaying constant

Stop solution: 10% (v/v) aqua phenol in absolute ethanol

2.2.2.13 Quantitative real-time PCR

Fast and sensitive analysis of transcript levels was done by quantitative real-time reverse transcription PCR. For this purpose, the RNA was reverse transcribed to complementary DNA (cDNA) by a reverse transcriptase. The resulting cDNA was used as a template for PCR amplification. The accumulation of dsDNA can be quantified by measuring the emission of the incorporated fluorescent dye SYBR Green I. The resulting SYBR Green-dsDNA complex can by quantified by excitation at λ = 497 nm and measuring the emission of green light at λ = 520 nm [Bustin *et al*., 2005].

Total RNA was isolated using the SV total RNA isolation kit (Promega, USA). Residual DNA was removed by TURBO™ DNase (Thermo Scientific, USA) treatment according to the manufacturer's instructions). Samples were diluted to a concentration of 10 ng/µL and the

respective RNAs were analyzed with corresponding primer pairs as listed in **table 2.11** The *sopB* gene was used as a reference. Quantitative real-time PCR was performed utilizing the SensiFAST™ SYBR® No-ROX kit (Bioline, Germany). Therefore, a master mix was prepared with a final volume of 12.5 µL per reaction. For each primer pair a non-template control, replacing the RNA template with RNase-free ddH_2O was used. For each RNA sample a no reverse transcription control, containing RNase-free ddH_2O instead of reverse transcriptase was used.

Example of a one reaction master mix:

2 x SensiFAST SYBR No-ROX Mix	6.25 µL
Forward primer (10 µM)	0.5 µL
µL Reverse primer (10 µM)	0.5 µL
Reverse transcriptase	0.125 µL
RiboSafe RNase inhibitor	0.25 µL
RNase-free ddH_2O	2.375 µL

A volume of 10 µL master mix reaction was pipetted into 0.1 mL strip tubes and 2.5 µL of RNA sample (10 ng/µL) were added. All reactions were kept in a pre-cooled steel block. Reverse transcription and the following qPCR reaction were done in a Rotor-Gene Q lightcycler with a 3-step cycling program.

1. Reverse transcription

1 x 45 °C for 20 min

2. PCR initial activation step

1 x 95 °C for 5 min

3. 3-step cycling (40 cycles)

Denaturation	95 °C for 10 s
Annealing	60 °C for 20 s
Elongation	72 °C for 10 s
Final Elongation	72 °C for 10 min

A melt profile analysis with a temperature ramp from 58 °C to 99 °C was done to check product specificity. Relative expression was calculated using the Rotor Gene Q Series Software by determination of the crossing point (CP) after setting a threshold of 0.015. The CP is defined as "the point at which fluorescence rises appreciably above the background

fluorescence" [Pfaffl, 2001]. Assuming a primer efficiency of 2, relative expression was calculated according to the Pfaffl's formula.

$$ratio = \frac{2^{\Delta CP(target)}}{2^{\Delta CP(reference)}}$$

$$\Delta CP = CP(control) - CP(sample)$$

Table 2.11: Oligonucleotides used in qRT-PCR

Oligonucleotide	Sequence (5' -> 3')	Function
III393	CCGACGTAAAGCCGCGATAC	*sopB* (fw)
III394	CCTCGTTCATAAGCACTCGTC	*sopB* (rev)
IV529	CGCGACTCAGCAAGAAGAG	*rne* (fw)
IV530	GCCGATGTCTGGGCGCAG	*rne* (rev)
IV931	CGCCCAGACGCGCTTCGGCC	*pnp* (rev)
IV946	GTTGGGCGCGGTCGTCTTCGG	*pnp* (fw)
VI165	GGCCGTTTAATCGATTACGCGAAAC	*rhlB* (fw)
VI166	GCCAATTCACGTACCCGATACGAG	*rhlB* (rev)
VI167	CCGCCGTGTATTAGCCAAATTACC	*rhlE* (fw)
VI168	CGCTTTGGGCGATCTGCTCTG	*rhlE* (rev)
VI173	GCCTGAACACGGCTGTTGGTG	*eno* (fw)
VI174	GGCTTTGTTACCTTCGCCAGC	*eno* (rev)

2.2.2.14 *In vitro* transcription of RNAs

To obtain defined RNAs for RNA electromobility shift analyses (RNA-EMSA), RNAs were transcribed *in vitro* according to the TranscriptAid T7 High Yield Transcription Kit (Thermo Scientific, USA) user handbook. Double-stranded DNA templates were amplified from chromosomal DNA of strain YPIII by PCR with specific primer pairs for the desired region. PCR templates for 5'-*lcrF* mutants were amplified from plasmid DNA pRS42 (open mutation: GUU-30/-27AAA), pRS43 (closed mutation: UU-28/-27CC), pRS45 (Δhairpin 1) or pRS46 (Δhairpin 2). For this purpose, the respective forward primer encoded the T7 promoter to allow transcription by the T7 DNA-dependent RNA polymerase. All primers used to generate the T7 promoter containing DNA template are listed in **table 2.12**. Obtained PCR fragments were purified using the NucleoSpin® Gel and PCR Clean-up kit (Macherey-Nagel, Germany). This kit allowed purification of very small DNA fragments (down to 50 bp). *In vitro* transcription was carried out at 37 °C for 2 h or overnight in a 20 µL reaction mix with 6 µL template DNA according to the manufacturer's recommendation. Subsequently, the

DNA template was digested with 2 µL DNaseI for 15 min at 37 °C. DNaseI was then inactivated by addition of 2 µL of 0.5 M EDTA at 65 °C for 10 min. Finally, RNA was purified by phenol-chloroform extraction.

Table 2.12: Oligonucleotides used for *in vitro* transcription

Oligonucleotide	Sequence (5' -> 3')	Function
V830	GGGCGCGTAATACGACTCACTATAGCTTACATTTTATATGAATGTAATGGC	*csrA*(-105)_fw
V066	GGGCGCGTAATACGACTCACTATAGGAATGTAATGGCTTACGTTTTC	*csrA*(-91)_fw
V832	GGGCGCGTAATACGACTCACTATAGCACGGTGTATGATGGATAATG	*csrA*(-70)_fw
VI386	GCGCGTAATACGACTCACTATAGGGCGGGGAAACAGAGAG	*csrA*(-50)_fw
V708	GGGCGCGTAATACGACTCACTATAGAACAGAGAGACCCGACTC	*csrA*(-42)_fw
V631	GTTTCCCCGCCATTATCC	*csrA*(-39)_rev
III731	GAATAAGCATTCTTTGCTCC	*csrA*(+10)_rev
I514	GGGCGCGTAATACGACTCACTATAGGCACTCTATTATTATCCAGAC	*hns*(-55)_fw
V700	GGGCGCGTAATACGACTCACTATAGCAACAATACCGTGAAATGC	*hns*(+175)_fw
I515	GCAGTTCATTTGGATCAATAC	*hns*(+226)_rev
VI525	GGCTAATACGACTCACTATAGTACCTGAAGGGGAATGGGAG	*glgC*(-125)_fw
VI526	AGTCTGTACTTTCAAACCTC	*glgC*(+25)_rev
V730	GGGCGCGTAATACGACTCACTATAGGGGAATGGGTTGTTATTTTAC	*yscW*(-107)_fw
III733	CGACTCACGCCAGTCCC	*yscW*(+8)_rev
V731	GGGCGCGTAATACGACTCACTATAGGGTGATTTATTATATTGGTTTTGGTTG	*lcrF*(-123)_fw
V732	CTCTAGTGATGCCATAAATGTTATAC	*lcrF*(+15)_rev
I404	TTTGAA TTCGCCATCTTGTGAATGCTCAAC	*lcrF*(+75)_rev
V733	GGGCGCGTAATACGACTCACTATAGGCTAAAATAGCAACCACAGGC	*yscA*(-101)_fw
V734	CCATTGAATCTTCACAATCTAATCCCG	*yscA*(-1)_rev

* T7 primer underlined

2.2.2.15 3'-Biotinylation of RNAs

The RNA fragments for RNA electromobility shift assays (RNA-EMSAs) were labeled at their 3'-ends with biotin. To do so, biotin-labeled cytosine (pCp-Biotin) was ligated to the 3'-end of *in vitro* transcribed RNAs. For a biotinylation reaction, 1 µg of purified transcript was denatured at 70 °C for 10 minutes and immediately put on ice. Before usage, all reagents were thawed on ice, besides PEG-8,000 which was pre-warmed at 37 °C until the volume was fluid, and DMSO, which was thawed at room temperature.

Biotin labeling of 1 µg linearized RNA was performed in a volume of 20 µL in 1 x T4 RNA ligase buffer, 1 mM ATP, 10% (w/v) DMSO, 1 µM pCp-Biotin (Jena Bioscience, Germany), 15% (w/v) PEG-8,000 and 1 µL T4 ssRNA ligase 1 (20 units; NEB, USA). The reaction was

carried out at 18 °C for 2 h or overnight. Afterward, the labeled RNA was purified by phenol-chloroform extraction and RNA concentration was measured using the NanoDrop™ ND-1000 UV spectrometer (Thermo Scientific, USA). Northern blotting of 20 fmol RNA and subsequent detection with the Chemiluminescent Nucleic Acid Detection Module (Thermo Scientific, USA) was carried out to analyze the labeling efficiency and RNA integrity.

2.2.2.16 Detection of Biotin-labeled RNAs

For detection of biotinylated nucleic acids, the Chemiluminescent Nucleic Acid Detection Module (Thermo Scientific) and supplied buffers were used. All incubation steps were carried out in 50 mL Falcon tubes on a tube roller. Since only small volumes of buffer were used, it was crucial to remove all remaining buffer volumes by pipetting. Before usage, an aliquot of 5 mL 1 x blocking buffer and 4 x wash buffer was pre-warmed in a water bath (37-50 °C) until precipitates were resolubilized. UV-cross-linked membranes were blocked for 15 min in 5 mL blocking solution. Afterward stabilized Streptavidin-HRP conjugates were added in a dilution of 1:300. The membrane was washed four times for 5 min in 5 mL of 1 x wash buffer and equilibrated in 5 mL substrate equilibration buffer. Finally, the membranes were wrapped in a foil and developed by incubation for 5 min in 1 mL Chemiluminescent Substrate Working Solution (500 µL Luminol/Enhancer Solution and 500 µL Stable Peroxide Solution). Detected RNAs were documented utilizing the ChemiDoc™ XRS+ (Bio-Rad, USA) imaging system.

2.2.2.17 RNA electromobility shift assay (RNA-EMSA)

Electromobility shift assays are a valuable tool to study RNA binding capabilities of a protein to a specific target RNA. For this purpose, increasing amounts of the protein were incubated with biotin-labeled target RNAs. Migration of RNA-protein complexes through a gel matrix is retarded for high molecular complexes in comparison to free RNAs. Leading to the appearance of a shifted RNA. To evaluate RNA binding capabilities of a protein, the protein was purified as described in section 2.2.3.5 and dialyzed against 1 x band shift buffer. Visible protein precipitates were removed by centrifugation (18,000 x g, 4 °C, 5 min) and protein concentration was evaluated by a Bradford assay (Thermo Fisher Scientific). If not mentioned otherwise, all reaction steps were performed on ice. Prior to the binding reaction, RNAs were diluted in 1 x band shift buffer, incubated for 10 min at 70 °C for RNA linearization and immediately cooled on ice. For a 10 µL binding reaction, 20 fmol of each control and target RNA and 0-10,000 fmol of protein were incubated for 20 min on ice. This corresponded to

2 nM of each RNA and 0-1,000 nM protein. In the next step, the samples were electrophoretically separated in a native 5-8% TBE polyacrylamide gel (1,5 mm spacer, 10 wells) and successively transferred by semi-dry blotting to a positively charged nylon membrane (Roche, Switzerland). For this, the gel is placed on top of the membrane and sandwiched between a pair of Whatman paper. The transfer took place in 1 x TBE for 30 min at 20 V with a Trans-Blot® SD Semi-Dry Transfer Cell (Biorad, Germany). RNAs were cross-linked to the membrane in a Stratalinker® UV-Crosslinker (Stratagene, USA) with 120,000 µJ or for 3 min. Finally, biotinylated RNAs were detected as described in section 2.2.2.16.

Table 2.13: 7% TBE-polyacrylamide gel

Component	Volume
10 x TBE	1 mL
40% (w/v) Polyacrylamide	1.75 mL
10% APS	100 µL
TEMED	10 µL
ddH_2O (RNase-free)	7.25 mL

Protocol for a 1.5 mm spacer plate

1 x bandshift buffer (YopD/LcrH): 20 mM Na_2HPO_4/NaH_2PO_4 (pH 8.0), 100 mM KCl, 5% (w/v) glycerol, 2 mM DTT

1 x bandshift buffer (CsrA): 20 mM HEPES (pH 7.6), 100 mM KCl, 5% (w/v) glycerol, 2 mM DTT

2.2.2.18 CsrA-RIP-Seq

Identification of potential RNA binding partners of CsrA was performed by RNA-binding protein immune precipitation followed by high-throughput sequencing (RIP-Seq). The *Y. pseudotuberculosis* wild-type strain YPIII was transformed with plasmid pJH35 encoding a 3xFLAG-tagged CsrA protein variant or the empty vector control pHSG576. The strains were cultivated in 500 mL LB_{BD} supplemented with chloramphenicol for 2 h at 25 °C, followed by a 4 h temperature shift to 37 °C. Cells were harvested by centrifugation in an SLA-3000 rotor (10 min, 6.000 rpm, 4 °C). Pellets were stored at -40 °C until use.

The cell pellet was thawed on ice and resuspended in 6 mL ice-cold PBS and lysed by four passages through a French Press cell at 18.000 psi. The lysate was cleared by centrifugation (30 min, 18.000 x g, 4 °C). The resulting supernatant was normalized corresponding to their cultures OD_{600} by the addition of ice-cold PBS to ensure an equal concentration of cellular

contents. 1.5 mL of normalized cleared supernatants were used for the IP experiment (immune precipitation).

100 µL of Anti-FLAG® Magnetic Beads (Sigma, UK) were washed three times in 1 mL PBS before usage. 1.5 mL of normalized cleared supernatant were added and incubated for 1 h on a tube roller at 4 °C. The supernatant was removed and the beads were washed five times with ice-cold PBS. Finally, beads were used for RNA extraction by the hot phenol method. To evaluate the quality of the IP experiment, 0.5 OD equivalents of the supernatant, flow through, wash fraction and beads (elution fraction) were collected. Samples were prepared and separated by SDS-PAGE and subsequently stained with Coomassie. According to the hot phenol protocol, beads were resuspended in 250 µL resuspension and lysis buffer. Residual DNA traces were removed by TURBO™ DNase (Thermo Scientific, USA) treatment according to the manufacturer's instructions). To ensure high quality of RNA samples for RNA-Seq, RNA integrity was analyzed by the Agilent BioAnalyzer 2100 electrophoresis system. Library preparation of RNA samples was performed with the ScriptSeq RNA-Seq Library Preparation Kit (Illumina, USA). High-throughput sequencing was performed using the Genome Analyzer IIx (Illumina, USA). Analysis of RNA integrity and RNA-sequencing experiment were performed by the in-house gene analytic facility (GMAK). Quality control, sequencing adapter clipping and quality trimming of the output sequence were performed utilizing the fastqc [Andrews, 2010] and fastq-mcf tools [Aronesty, 2011]. The sequencing output quality was analyzed using FastQC (Babraham Bioinformatics). All sequenced libraries were mapped to the YPIII chromosome (NC_010465) and the pIB virulence plasmid (NC_006153) with Bowtie2 (ver. 2.1.0) using the default parameters. The resulting BAM files were filtered for unique mapped reads with SAM tools, which were used for downstream analysis [Li *et al*., 2009].

2.2.2.19 Measurement of promoter activity using β-galactosidase reporter fusions

Measurements of transcriptional or post-transcriptional gene expression using gene fusions to *lacZ* were performed by β-galactosidase activity assay. To do so, the promoter region of the respective target gene including the 5'-UTR and the first codons is fused to the *lacZ* reporter gene (translational fusion). When the corresponding promoter or upstream region is activated, the *lacZ* gene coding for the β-galactosidase enzyme is expressed and its activity can be measured. This assay is based on the enzymatic activity of β-galactosidase, which cleaves galactose to glucose and lactose. The artificial, colorless substrate ortho-nitrophenyl-β-D-

galactopyranoside (ONPG) is also recognized and cleaved to galactose and the yellow colored ortho-nitrophenyl, whose absorption can be photometrically measured at λ = 415 nm.

For this assay, 5 mL bacterial cultures were grown under desired conditions and the optical density was measured at λ = 600 nm (OD_{600}). Typically, over day cultures were grown for 2 h at 25 °C and shifted to 37 °C for 4 h. The OD_{600} of these cultures was adjusted to a final OD_{600} of 0.1 to 0.9. Typically, 1 mL of a 1:10, or for strains with a growth defect a 1:5 dilution, was measured. 200 µL of the diluted culture was lysed for 10 min by addition of 50 µL 20% SDS and 100 µL chloroform. Afterward, 1.8 mL Z-buffer was added. The reaction was started by addition of 400 µL ONPG and the time was measured until the solution turned yellow. The reaction was stopped by addition of 1 mL 1 M $NaCO_3$. 200 µL of the reaction were finally photometrically measured with a Sunrise™ microplate reader (Tecan, Switzerland) at λ = 415 nm, corresponding to the β-galactosidase activity and at λ = 655 nm corresponding to the bacterial background. The β-galactosidase activity could be calculated by the following formula.

$$activity = \frac{OD(415nm) * 6.75}{OD(600nm) * V * t}$$

t - time [min]

V - volume [mL]

OD - optical density measured at indicated wavelength

5 x Z-buffer: 300 mM Na_2HPO_4; 100 mM NaH_2PO_4; 50 mM KCl; 5 mM $MgSO_4$

2.2.3 Protein biochemical methods

2.2.3.1 Measurement of protein concentration (Bradford assay)

Quantification of protein concentration was carried out by Bradford Assay (Bradford, 1976). The principle is based on the formation of a protein-dye complex. In this work, Coomassie Brilliant Blue G250 was used, which specifically binds to unpolar and cationic side chains and thereby stabilizes the blue anionic form of the Coomassie dye. Since the absorption maximum of the blue Coomassie form is at λ = 595 nm, measurement of absorption at this wavelength was used for protein quantification. For this purpose, 5 µL of protein solution and 250 µL of Bradford reagent were incubated for 5 min at room temperature in a 96-well microplate. Samples were photometrically measured in a Sunrise™ microplate absorbance

reader (Tecan, Switzerland). After determining the extinction of a BSA equilibration curve (25-1000 ng/µL), the protein concentration was calculated.

2.2.3.2 SDS-polyacrylamide gel electrophoresis (SDS-PAGE)

Separation of proteins based on their size was carried out by denaturing SDS polyacrylamide gel electrophoresis (SDS-PAGE) [Laemmli, 1970]. Unfolded and negatively charged proteins are separated, powered by an applied electrical field, as they migrated through a discontinuous polyacrylamide gel matrix. Since proteins were unfolded, denatured and negatively charged by boiling in a denaturing buffer containing SDS, they are separated solely by their molecular weight, independent of their net charge and conformation.

During this work, SDS-PAGE was carried out as vertical electrophoresis in Mini-PROTEAN® tetra cells system (Bio-Rad, USA). For proteins larger than 15 kDa, Laemmli polyacrylamide gels with a 5% stacking gel and depending on molecular weight of the target protein, a 12% or 15% resolving gel were used.

Table 2.14: SDS glycine polyacrylamide gel

Component	Resolving gel (5%)	Separating gel (12%)	Separating gel (15%)
Upper buffer	2.5 mL	-	-
Lower buffer	-	2.5 mL	2.5 mL
30% (w/v) Polyacrylamide	1.1 mL	4.0 mL	5 mL
ddH_2O	6.5 mL	3.5 mL	2.5 mL
APS (10% w/v)	50 µL	50 µL	50 µL
TEMED	10 µL	10 µL	10 µL

Upper buffer (4 x): 1.5 M Tris-HCl pH 8.8; 4% SDS

Lower buffer (4 x): 0.5 M Tris-HCl pH 6.8; 4% SDS

SDS running buffer (10 x): 33 mM Tris-HCl pH 8.3; 192 mM glycine; 0.1% SDS

For proteins smaller than 15 kDa, such as CsrA, SDS tricine polyacrylamide gels with a 15% separating gel were used [Schägger, 2006].

Table 2.15: SDS tricine polyacrylamide gel

Component	Resolving gel (5%)	Separating gel (15%)
3 x gel buffer	3.1 mL	5.0 mL
30% (w/v) Polyacrylamide	1.1 mL	7.5 mL
ddH_2O	7.6 mL	1.5 mL
Glycerol	-	1.5 mL
APS (10% w/v)	150 µL	150 µL
TEMED	15 µL	15 µL

Gel buffer (3 x): 3 M Tris-HCl, pH 8.45; 0,3% SDS

Anode buffer (10 x): 1 M Tris; 225 mM HCl

Cathode buffer (10 x): 1 M Tris; 1 M tricine; 1% SDS

SDS sample buffer (3 x): 240 mM Tris-HCl pH 6.8; 8% SDS; 40% Glycerol; 12% DTT; 0.02% bromphenol blue

2.2.3.3 Coomassie staining of proteins after SDS-PAGE

Visualization of proteins after separation by SDS-PAGE was carried out by staining with Coomassie Brilliant Blue. For this purpose, gels were incubated in Coomassie stain on a shaker until the gels are completely stained in blue. Afterward, the staining solution was removed and gels were washed several times in water until protein bands were visible and the background was sufficiently destained. The staining solution could be reused several times. The staining and washing process was accelerated by heating of the gel in staining solution or ddH_2O in a microwave oven.

Coomassie stain: 0.05% (w/v) Coomassie Brilliant Blue G250; 20% (v/v) isopropanol; 10% (v/v) acetic acid

2.2.3.4 Western blot and immune detection

Identification of specific proteins was carried out by western blotting following immune detection. (Towbin *et al*., 1979). After separation of protein samples by SDS-PAGE, proteins were electrophoretically transferred and thereby immobilized on a hydrophobic Immobilon®-P PVDF membrane (Sigma, UK). For this purpose, the PVDF membrane was activated in 100% methanol and presoaked, together with two pieces of Whatman paper 17 Chr (Neolab, Germany) and the polyacrylamide gel. The gel was topped by the membrane and sandwiched between the Whatman paper and foam pads. The transfer was performed in the Mini Trans-

Blot® cell system (Bio-Rad, USA). To do so, the sandwich was placed in the Mini Trans-Blot® cell, the gel facing the cathode and the membrane facing the anode. The tank was filled with transblot buffer and the transfer took place for 1 h at 100 V. Following transfer, the membrane was blocked in TBST-M for at least 15 min at room temperature or overnight at 4 °C on a shaker. Afterward the primary antibody was added (concentration listed in **table 2.3**) and the membrane was incubated for 1 h at room temperature or overnight at 4 °C. Routinely, incubation with antibody solution was done in 15 mL solution on a shaker or in 5 mL solution in a 50 mL Falcon tube on a roller. After removal of the antibody solution, the blot was rinsed twice with a small volume of 1 x TBST and washed three times for 10 min in TBST. The membrane was incubated for at least 1 h with a secondary antibody in TBST-M. Depending on the primary antibody used, goat anti-mouse horseradish peroxidase (HRP) conjugates or goat anti-rabbit HRP conjugates were used at a 1:8,000 dilution. After removal of the antibody solution, the blot was rinsed and washed as stated above and target proteins were detected by chemiluminescence utilizing the Western Lightening ECL II kit (Perkin Elmer, USA) and documented using the ChemiDoc XR+ System (Bio-Rad, USA).

Transblot buffer (1 x):	25 mM Tris; 192 mM glycine; 20% methanol (v/v)
TBST (10 x):	20 mM Tris-HCl, pH 7.5; 150 mM NaCl; 0.05% (v/v) TWEEN-20
TBST-M (1 x):	5% (w/v) in 1 x TBST

2.2.3.5 Expression and purification of recombinant proteins

For the study of protein-RNA interactions in RNA electromobility shift assays (RNA-EMSA), CsrA was expressed with a C-terminal His_6 epitope from pAKH172. His_6-YopD and LcrH were expressed from pJH12. For this purpose, pAKH172 or pJH12 were transformed into chemically competent *E. coli* BL21(DE3) by heat shock. For protein expression, cells were grown to an OD_{600} of ~0.5 in 500 mL DYT supplemented with kanamycin. Subsequently, protein expression was induced by addition of 1 mM IPTG for 5 h at 18 °C. Cells were harvested by centrifugation for 10 min at 6,000 rpm and 4 °C in an SLA-3000 rotor. The cell pellet was stored at -20 °C.

The cell pellet was resuspended in 10 mL CsrA lysis buffer supplemented with 20 mM imidazole and cOmplete™ EDTA-free protease inhibitor cocktail (Roche, Switzerland). Cells were lysed by four passages through a French Press cell disruptor (G. Heinemann, Germany) at 18,000 psi. To remove cell debris, lysates were cleared by centrifugation (30 min at 18,000 x g and 4 °C) and sterile filtered with a 0.2 µm syringe sterile filter. CsrA-His_6 was

then purified by Ni-NTA affinity chromatography utilizing a 1 mL HisTrap FF Crude column in a ÄKTApurifier (GE Healthcare, Germany) according to the manufacturer's instructions). Prior usage all buffers were sterile filtered, degassed and pre-cooled to 4 °C.

Bound protein was eluted from the column by applying an imidazole gradient from 0 to 500 mM over 20 column volumes in 1 mL fractions. Fractions were tested for protein content photometrically by their absorption at 260 nm. Since protein detection at 260 nm is based on the absorption of aromatic amino acid side chains and CsrA does not contain any tryptophan, absorption of peptide bonds was determined at 230 nm. Fractions with a peak at 230 nm (protein containing) were analyzed for purity and protein content by SDS-PAGE and Coomassie stain. The fraction with the highest protein content was dialyzed overnight at 4 °C in 1000 x volumes of dialysis buffer. Dialyzed proteins were then stored at -20 °C [Maurer, *et al*. 2016].

His-YopD/LcrH complexes were purified by flow-through Ni-NTA affinity chromatography with a bed volume of 0.5 mL Protino Ni-NTA agarose (Macherey & Nagel, Germany). Prior to use, the column was washed with 10 mL ddH_2O to remove traces of the ethanol containing storage solution and equilibrated with 10 mL YopD lysis buffer supplemented with 20 mM imidazole. Subsequently, 10 mL lysates were loaded on the column and run by gravity flow. Subsequently, the column was washed two times with 10 mL of YopD lysis buffer supplemented with 50 mM imidazole. Bound protein was eluted by adding six bed volumes of YopD lysis buffer supplemented with 250 mM imidazole. To analyze the quality of the purification efficiency, fractions of the supernatant, flow through, wash and elution fractions were analyzed by SDS-PAGE and Coomassie staining. The fraction with the highest purity and an equal ratio of YopD to LcrH were dialyzed overnight in YopD dialysis buffer and stored at 4 °C. The column could be reused after removing residual bound protein by eluting with 10 x column volumes of YopD lysis buffer with 250 mM Imidazole. The columns were then equilibrated in 20% ethanol and were stored at 4 °C.

CsrA lysis buffer:	50 mM HEPES (pH 7.6), 150 mM NaCl
CsrA dialysis buffer:	50 mM HEPES (pH 7.6), 150 mM KCl, 2 mM DTT, 5% glycerol
YopD lysis buffer:	50 mM Na_2HPO_4/NaH_2PO_4, pH 8.0; 150 mM NaCl
YopD dialysis buffer:	50 mM Na_2HPO_4/NaH_2PO_4, pH 8.0; 150 mM KCl; 2 mM DTT; 5% glycerol

2.2.3.6 Protein stability assay

Analysis of protein stability was carried out by an *in vivo* protein degradation assay. Therefore, over day cultures of *Y. pseudotuberculosis* were grown under desired conditions. Subsequently, protein synthesis was stopped by antibiotics and samples were taken. To ensure a complete shutdown of protein synthesis spectinomycin and chloramphenicol (Roth, Germany) were added to a final concentration of 0.5 mg/mL, corresponding to time point zero. Typically, 2 mL of the culture were taken at appropriate time points and pelleted in a pre-cooled centrifuge. Additionally, bacterial cell density was measured to check growth arrest and stop of translation. The cell pellet was resuspended in 1 x SDS loading buffer to a concentration of 1 OD_{600} equivalents and boiled for 5 min at 95 °C. Protein samples were then stored at -20 °C until they were analyzed by western blotting.

2.2.4 Bioinformatic methods

2.2.4.1 CsrA target prediction with CSRA_TARGET_PREDICTER

Prediction of potential CsrA target RNAs was done by a self-written Python script, based on an algorithm outlined by Kulkarni and colleagues [Kulkarni *et al*., 2014]. Upstream sequence of annotated coding genes, spanning the region from -150 to +60 relative to the annotated start codon were extracted with a self-written Python script. FASTA sequence files and annotation tables of coding genes were obtained from the PATRIC bacterial bioinformatics database [Wattam *et al*., 2013]. For this analysis, upstream sequences of monocistronic and polycistronic genes of *E. coli* K12 MG1655 (NC_000913) and *Y. pseudotuberculosis* YPIII (NC_10465) were extracted. These sequences were then analyzed by CSRA_TARGET_PREDICTER. The corresponding flowchart is depicted in **figure 3.21A**. Subsequently, from all input sequences non-overlapping primary and secondary sites were located and counted. Primary sites were defined as A(N)GGA motifs (AAGGA, ACGGA, AGGGA, ATGGA, AGGA), while secondary sites were defined as AGAGA, CTGGA, CGGGA and TGGGA. In a first step, sequences with a primary site in the vicinity to the Shine-Dalgarno (SD) sequence were chosen. The region in the vicinity to the SD was defined according to Kulkarni and colleagues as the region from -30 to +5 nt relative to the start codon. Then the total number of binding sites (primary or secondary sites) in the whole sequence were counted and only sequences with a total number of at least three primary or secondary sites were selected. Since CsrA binds secondary binding sites with a low affinity, additional binding sites need to be in close vicinity. For that reason, only secondary sites were

considered whose maximal distance to the next binding site (primary or secondary) was less or equal than 10 nt [Kulkarni *et al*., 2014]. From these sequences, only the ones were chosen, which contained at least three primary sites or two primary site and two or more secondary sites. Finally, the distance between consecutive motifs was determined and all remaining sequences with at least two neighboring sites with a distance of 10 to 60 nt were considered as putative direct CsrA targets.

For the comparison of predicted CsrA targets in *E. coli* and *Y. pseudotuberculosis*, the protein sequence of all annotated ORFs were extracted and aligned using the protein-protein BLASTP command line tool (Protein-Protein BLAST 2.3.0+) with an e-value threshold (≤ 0.001) [Camacho *et al*., 2009]. For the analysis of differences in the CsrA binding motif distribution of assigned genes, the upstream region (-150 to +60 relative to the translational start site) of these genes was aligned utilizing the ClustalO command line tool (Clustal Omega 1.2.1) with default settings [Sievers *et al*., 2011].

3 Results

After assembly of the injectisome, it remains in a stand-by mode until secretion is triggered by host cell contact. Under these conditions, T3SS gene expression needs to be shut-down to not overstrain the protein quality control system and the energetic homeostasis of the bacterial cell. To accomplish this, *Yersinia* developed a sophisticated feedback mechanism that represses T3SS genes until cell contact takes place and secretion is triggered. This state is monitored and controlled by the translocator and RNA-binding protein YopD, which acts as a general *yop* gene repressor. Additionally, the status of the Ysc-Yop T3SS is linked to the central Csr system. It could be shown that the RNA-binding protein CsrA, together with YopD, represses expression of the T3SS master regulator LcrF. First experiments also demonstrated that YopD activates *csrA* expression in the absence of host cell contact [Opitz, PhD thesis; Steinmann, PhD thesis]. The present study investigates the underlying mechanism of the two RNA-binding proteins CsrA and YopD controlling T3SS expression.

3.1 YopD activates *csrA* expression

The global acting RNA-binding protein CsrA is involved in the regulation of a plethora of cellular processes, such as motility or biofilm formation [Heroven *et al*., 2012]. CsrA is also linked to the regulation of the Ysc-Yop T3SS in *Y. pseudotuberculosis* and controlled by the translocator protein YopD [Steinmann, PhD thesis].

In a previous study, it could be demonstrated that a deletion of *yopD* reduces *csrA* mRNA levels [Steinmann, PhD thesis]. To further assess the principle of YopD-dependent *csrA* regulation and to identify the YopD-dependent regulatory region in the *csrA* locus, translational *csrA'-'lacZ* reporter fusions carrying continuous deletions of the 5'-end of varying lengths were tested for YopD dependency. So far, the promoter structure of the *Y. pseudotuberculosis csrA* gene locus is unknown. In *E. coli*, the *csrA* regulatory region is well described and contains five different promoters (see **Fig. 3.1A**) [Yakhnin *et al*., 2011]. Therefore, the *csrA* upstream region of *Y. pseudotuberculosis* and *E. coli* were compared using a Clustal Omega alignment analysis (**Fig. S1**). In *E. coli*, promoters P1/2 are located at the 3'-end of the *alaS* gene. The corresponding region (fragment F2) is poorly conserved (>50%) in *Y. pseudotuberculosis*. Promoter P3 of *E. coli* is located in the intergenic region of the *alaS* and the *csrA* gene. This region (fragment F3) is only lowly conserved (>50%).

Promoters P4/5 are located downstream of P3 and are well conserved (84%) in *Y. pseudotuberculosis* (fragment F4/5) (see **Fig. 3.1**).

A manual analysis of RNA-Seq data verified the existence of two promoters with homology to the *E. coli* promoters P3 and P5 [Nuss *et al*., 2015]. The *E. coli* promoters P1/2/4 might be as well present in *Y. pseudotuberculosis*, but are only active under unidentified conditions. For this reason, the *E. coli* promoter nomenclature (P1-5) will be used in this study.

To identify regions essential for *csrA* expression and to analyze the influence of YopD on the *csrA* upstream region, *csrA*'-'*lacZ* fusions were designed harboring different parts of the *csrA* upstream region, e.g. region -1071 to +17 nt (pKB63), region -298 to +17 nt (pJH4), region -249 to +17 nt (pJH5), region -121 to +17 nt (pJH5) and region -83 to +17 nt (pJH10) (**Fig. 3.1A**).

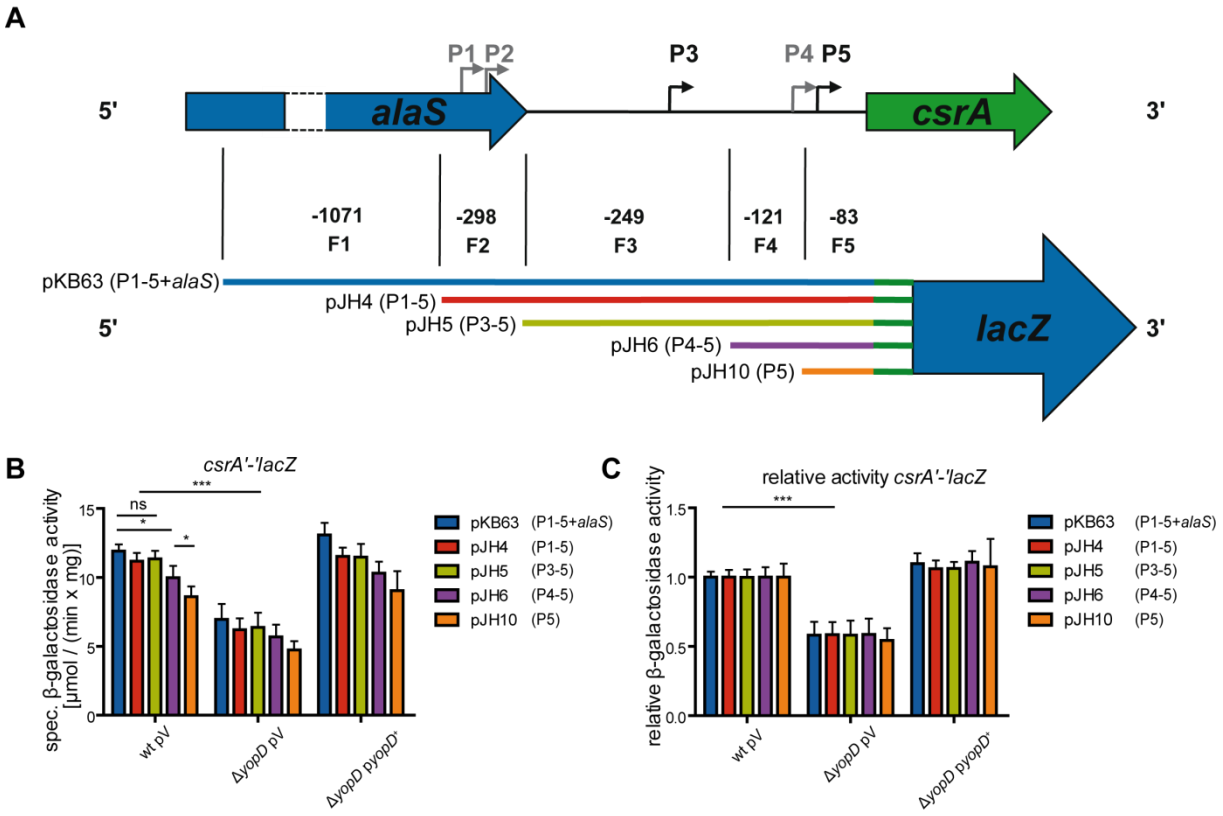

Figure 3.1: Analysis of YopD-dependent regulation of essential promoter regions of *csrA*. (**A**) Schematic presentation of the *alaS-csrA* gene locus of *Y. pseudotuberculosis* showing the different promoters as described in *E. coli* (broken arrows, P1-P5). Promoters identified only in *E. coli* are depicted in gray. Promoters identified both in *Y. pseudotuberculosis* [Nuss, unpublished data] and *E. coli* [Yakhnin *et al*., 2011] are depicted in black. A schematic presentation of the translational *csrA*'-'*lacZ* deletion constructs and upstream regions (fragment F1-5), encoding the different putative promoters, is depicted below. (**B**) The YopD-dependent expression of translational *csrA*'-'*lacZ* reporter fusions was monitored in the *Y. pseudotuberculosis* wild-type (YPIII) and the *yopD* mutant (YP91) strain. Strains were transformed with the empty vector (pV; pRS15) or complemented with its *yopD*$^+$ derivate pRS16 (p*yopD*$^+$) and different *csrA*'-'*lacZ* deletion constructs (pKB63 (blue), pJH4 (red), pJH5 (green), pJH6 (purple) or pJH10 (orange)). The specific β-galactosidase activity [µmol/(min*mg)] was measured after the strains were grown in LB medium for 2 h at 25 °C following a shift to 37 °C for 4 h. The data represent the mean +/- the standard deviation of 3 biological and 3 technical replicates. The data were analyzed by a paired Student's t-test to compare differences in promoter activity in the wild-type with * - P < 0.05; ** - P < 0.005; *** - P < 0.001; ns - not significant). (**C**) To compare the overall YopD-dependency of the different *csrA*'-'*lacZ* deletion constructs, the specific β-galactosidase activity of the respective *csrA*'-'*lacZ* fusion was normalized to the corresponding wild-type. The data were analyzed by an unpaired t-test.

The different *csrA'-'lacZ* fusion constructs were transformed into the *Y. pseudotuberculosis* wild-type (YPIII) and a *yopD* mutant (YP91) strain. The *yopD* mutant was additionally complemented with a *yopD*$^{+}$ plasmid. The bacteria were grown in overnight cultures for 2 h at 25 °C and shifted to 37 °C for 4 h to induce expression of the Ysc-Yop T3SS (T3SS-inducing conditions). Neither deletion of the most upstream region encompassing the *alaS* gene (fragment 1) nor the deletion of sequence -298 to -249 nt (fragment 2) affected the *csrA'-'lacZ* activity. This might indicate that in *Y. pseudotuberculosis* these segments do not include promoters P1 and P2 or these promoters are not expressed under the used conditions. Additionally, the deletion of the region -249 to -121 nt (fragment F3), containing promoter P3 (pJH6) slightly but significantly reduced the β-galactosidase activity. The lowest expression was observed for fragment F5, containing only the well-conserved promoter P5 (**Fig. 3.1B**). This indicates that expression of *csrA* in *Y. pseudotuberculosis* is mainly controlled by the region containing promoters P3, P4 and P5. Thereby, *Yersinia* promoter P5 seems to be the most induced promoter under T3SS-inducing conditions. Deletion of *yopD* led to a decrease of 50% β-galactosidase activity, irrespective of the length of the different promoter regions. This effect could be compensated by the ectopic expression of *yopD* (**Fig. 3.1C**). This indicates that the YopD influence does not depend on segments of the *csrA* promoter region that are located upstream of position -83 nt relative to the translational start site (**Fig. 3.1**).

3.2 YopD binds the *csrA* leader transcript close to promoter P4/5

Previously, it has been shown that YopD together with its chaperone LcrH bind to RNA to suppress target gene expression [Chen & Anderson, 2011]. To test if the activation of *csrA* expression is a result of direct binding of YopD to the *csrA* 5'-UTR, the interaction of *csrA* mRNA and YopD was tested in an RNA electromobility shift assay (RNA-EMSA). As YopD is only stable when its cognate chaperone LcrH is present, N-terminally His-tagged YopD and LcrH were cloned in tandem. Both were overexpressed in *E. coli* and the His-YopD/LcrH complex was co-purified by Ni-NTA affinity chromatography (**Fig 3.2B**). A biotinylated 5'-*csrA* RNA fragment, spanning the region from the -35 region of promoter P4 to the first three codons (-91 to +10 nt), was incubated with increasing amounts of purified YopD/LcrH complexes. A specific shift of the *csrA* RNA fragment was detected, but not of the control fragment, encompassing a part of the coding region of *hns* (+175/+226) (**Fig. 3.2A+C**). To specify the YopD interaction site in the 5'-UTR of *csrA*, YopD RNA-EMSAs were carried

out, whereby the *csrA* 5'-UTR fragment (-105/+10) was shortened from the 5'-end by 20 nt (-70/+10 or -50/+10) (**Fig. 3.3A**). Upon adding YopD/LcrH complexes to the target RNA fragments, all fragments, but the shortest (-50/+10) formed a high molecular weight complex. The shortest fragment was not bound. This indicates the YopD binding region is close to position -50 relative to the translational start site (**Fig. 3.2D-G**). The affinity to the targets was strongly dependent on the integrity of the YopD/LcrH complex as seen when comparing **Fig. 3.2DE** and **Fig. 3.2FG**. The affinity depended mostly on LcrH in the samples and resulted in differences in the protein concentration required for YopD binding in different protein fractions. Also, the ratio of YopD to LcrH was important because lower amounts of LcrH in the fraction led to an affinity decrease (data not shown), demonstrating that LcrH is needed for RNA-binding activity of YopD (see also **chapter 3.4**).

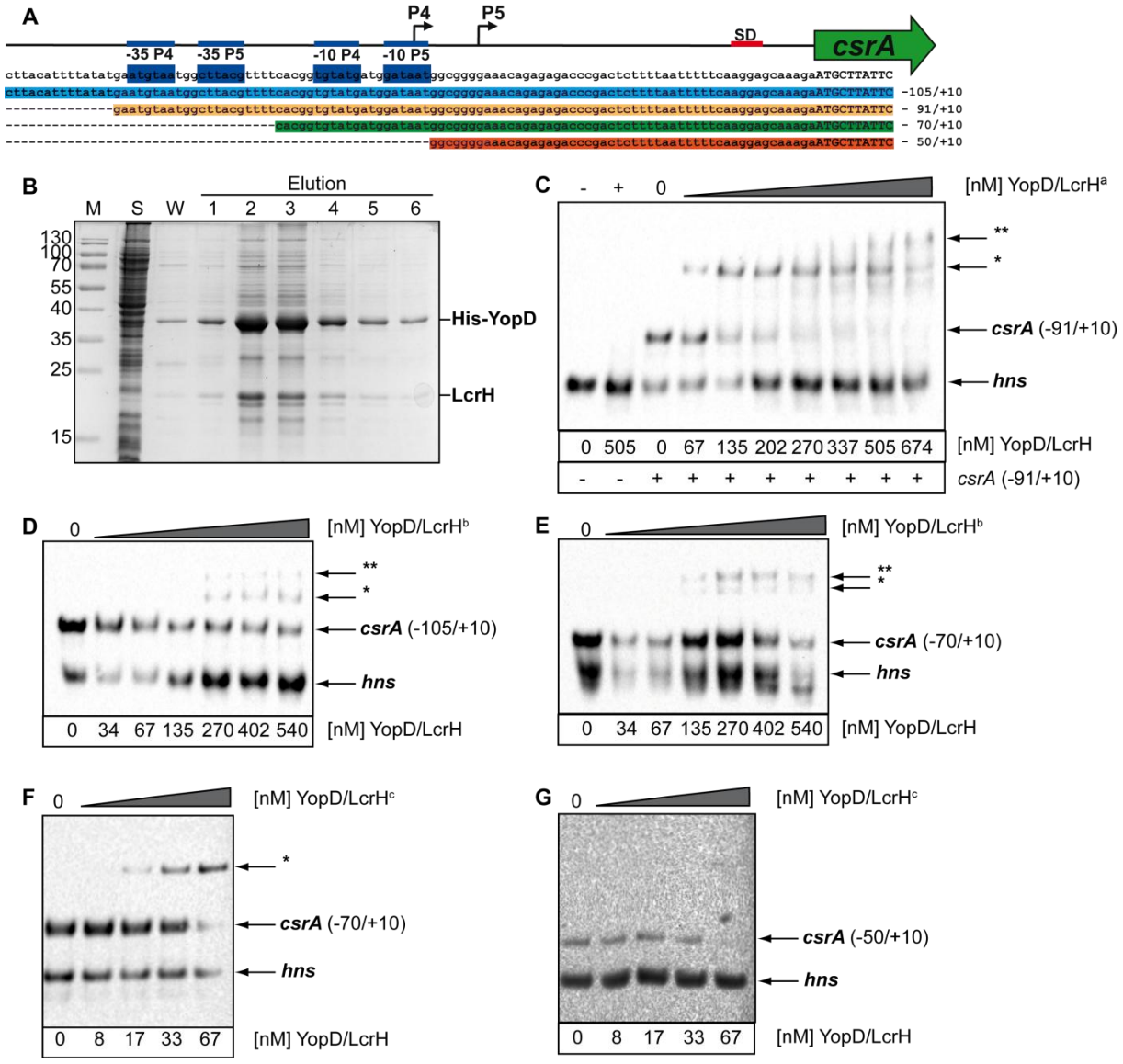

Figure 3.2: YopD/LcrH interacts with the *csrA* 5'-UTR in the vicinity to promoters P4/P5. (**A**) Schematic presentation of the *csrA* gene locus of *Y. pseudotuberculosis* showing the transcriptional start sites (TSS; broken arrows), the -35 and -10

boxes (blue box), the Shine-Dalgarno sequence (SD; red box) and parts of the *csrA* gene (green arrow). The *in vitro* transcribed RNA fragments used in RNA-EMSA are depicted below. The region of the RNA fragments is indicated relative to the translational start site. (**B**) Coomassie blue-stained SDS-PAGE of Ni-NTA affinity chromatography purified His_6-YopD/LcrH complexes. Supernatant (S); wash fraction (W); eluate fraction (E1-6). (**C-G**) Binding of YopD/LcrH complexes to the *csrA* leader transcript was analyzed by RNA-EMSAs. Parts of the *csrA* 5'-UTR and the *hns* control fragment were *in vitro* transcribed and biotin-labeled. 2 nM of the resulting *csrA* and the *hns* control fragment were incubated with increasing concentrations of purified YopD/LcrH complexes, separated onto a native 7% TBE-PAA gel and the biotin-labeled RNAs were visualized after transfer to a nitrocellulose membrane. Higher molecular bands, as a result of YopD/LcrH-RNA binding, are indicated with asterisks. Different YopD/LcrH fractions are marked ($YopD/LcrH^{a-c}$).

3.3 YopD binds to the *csrA* 5'-UTR-independent of an AU-rich element

Alignment analyses of YopD repressed genes led to the assumption that an AT-rich element can be found in the vicinity to the ribosomal binding site (RBS), which is involved in the YopD-dependent regulation [Chen & Anderson, 2011]. A similar element is present close to the RBS of *csrA* between position -24 to -14 upstream of the ATG (**Fig. 3.3A**). To investigate the role of this element in RNA binding of YopD and to further narrow down the binding region, 50 nt long, overlapping RNA fragments were tested in gel shift experiments. The fragment encompassing the region from position -105 to -60 and -42 to +10 were not bound by YopD/LcrH even at high concentrations and independent of the AT-rich element. Binding only occurred with the RNA fragment spanning from position -91 to -39 (**Fig 3.3B)**. This demonstrates that the YopD binding region is located close to the transcriptional start site and the -10 regions of promoters P4 and P5. In contrast to YopD-repressed genes, the AT-rich region in the *csrA* leader transcript does not influence binding of YopD/LcrH.

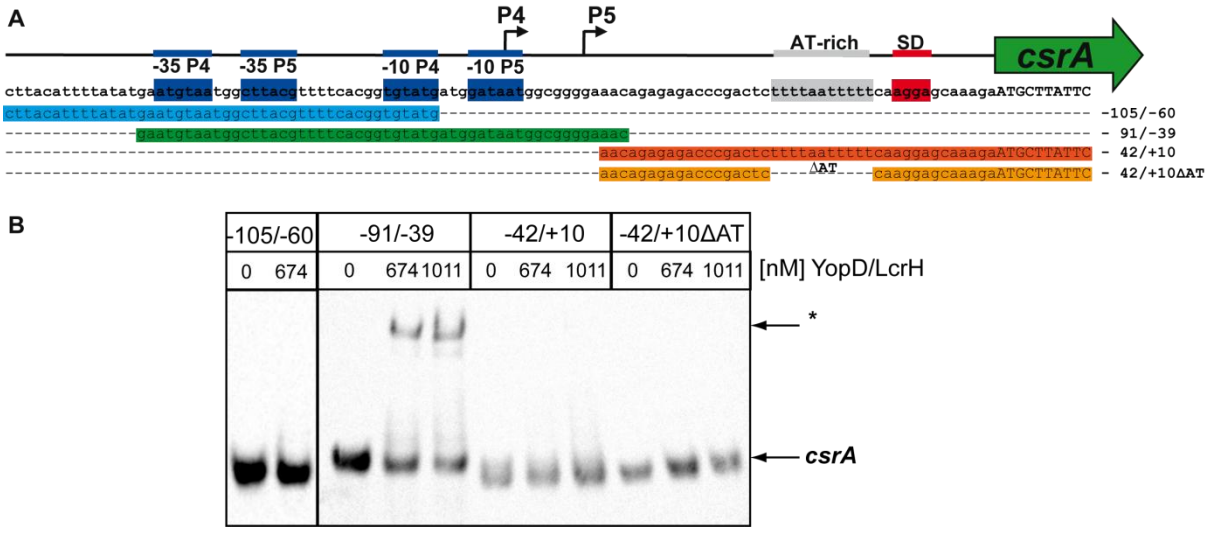

Figure 3.3: An AT-rich element in the *csrA* 5'-UTR is not required for YopD/LcrH binding. (**A**) Schematic presentation of the *csrA* gene locus of *Y. pseudotuberculosis* showing the transcriptional start sites (TSS; broken arrows), the -35 and -10 boxes (blue box), the Shine-Dalgarno sequence (SD; red box), an AT-rich element (gray box) and parts of the *csrA* gene (green arrow). The *in vitro* transcribed RNA fragments used in RNA-EMSA are depicted below. The region of the RNA

fragments is indicated relative to the translational start site. (**B**) Binding of YopD/LcrH complexes to the *csrA* leader transcript was analyzed by RNA-EMSAs. Parts of the *csrA* 5'-UTR were *in vitro* transcribed and biotin-labeled. 2 nM of the resulting *csrA* fragment was incubated with increasing concentrations of purified YopD/LcrH complexes, separated onto a native 5% TBE-PAA gel and the biotin-labeled RNAs were visualized after transfer onto a nitrocellulose membrane. Higher molecular bands, as a result of YopD/LcrH-RNA binding, are indicated with asterisks.

3.4 LcrH alone does not confer CsrA activation

In the Gram-positive soil bacterium, *B. subtilis*, the function of *csrA* is dependent on the loading status of a flagellar T3SS chaperone and therefore on the secretion status of the flagellar T3SS. The flagellin protein Hag is intracellularly protected by its chaperones FliS and FliW. When the flagellar filament is assembled and Hag gets secreted, FliW remains in the cytosol. Free FliW binds to CsrA, thus preventing CsrA from the repression of *hag* translation [Mukherjee *et al*., 2011]. As well in *Y. pseudotuberculosis*, regulation of *csrA* is dependent on the secretion status of the cell. In a *yopD* mutant or when secretion is triggered by calcium depletion, *csrA* gene expression is repressed [Steinmann, PhD thesis]. In order to test whether YopD or LcrH alone are able to affect CsrA expression, synthesis of CsrA in the *yopD*, *lcrH* and *yopD*/*lcrH* double mutant and in mutants complemented with either a $yopD^+$ or a $lcrH^+$ plasmid were analyzed by western blot analysis under T3SS-inducing conditions. Deletion of *yopD* as well as of *lcrH* strongly decreased CsrA protein amounts within the bacterial cell (**Fig. 3.4A**). Furthermore, in a *yopD*/*lcrH* background expression of *lcrH* or *yopD* alone could not restore CsrA to wild-type levels. This demonstrates that both proteins, YopD and LcrH, contribute to CsrA synthesis. Low CsrA levels in the *lcrH* mutant are most likely caused by the absence of LcrH which indirectly affects YopD protein levels. As shown in **Fig 3.4A**, the absence of LcrH results in low levels of YopD and supports previous studies showing that loss of *lcrH* inhibits YopD synthesis [Wattiau *et al*., 1994]. Furthermore, binding of LcrH alone to the *csrA* 5'-UTR RNA fragment is rather unspecific as no specific RNA-protein complex band is detectable even at very high LcrH concentrations (**Fig. 3.4B**). Interestingly, YopD also influences LcrH protein levels, as deletion of *yopD* strongly increases LcrH levels (**Fig. 3.4A**).

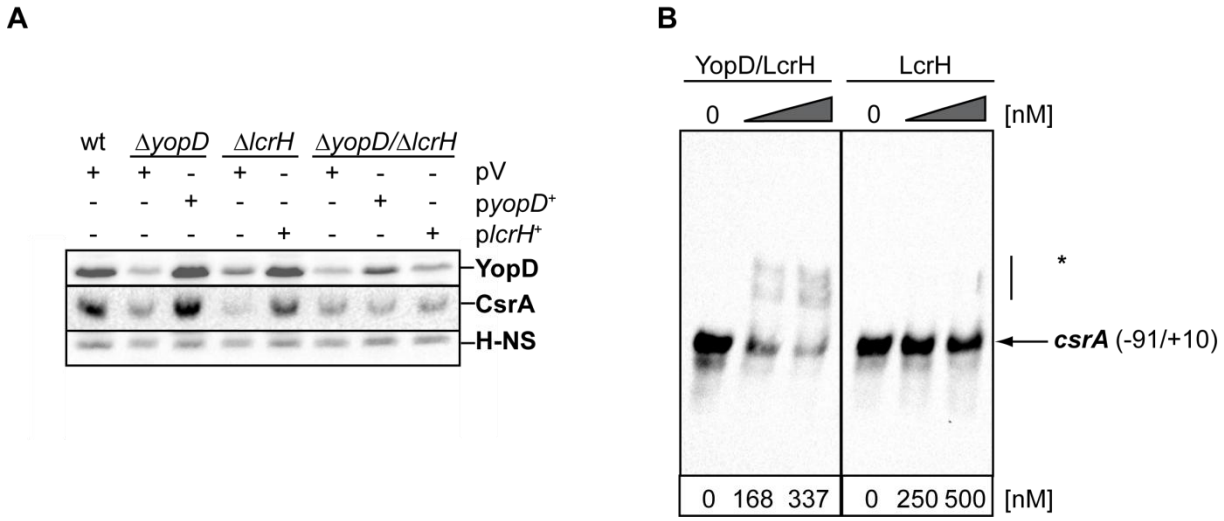

Figure 3.4: Role of the chaperone LcrH in the regulation of *csrA* expression. (**A**) The wild-type (YPIII) and the *yopD* (YP91) mutant, the *lcrH* mutant (YP92) and the *yopD*/*lcrH* mutant (YP183) strain were transformed with either the empty vector (pV; pRS1) or complemented with its derivate pRS2 (p*yopD*$^+$) or pRS3 (p*lcrH*$^+$). Strains were grown in LB medium for 2 h at 25 °C with a subsequent shift to 37 °C for 4 h. The CsrA, YopD and LcrH protein content was analyzed by western blot analysis (WB). An equivalent of OD_{600} = 1 was prepared for SDS-PAGE and a subsequent western blot analysis with polyclonal α-CsrA, α-YopD and α-H-NS rabbit sera. The H-NS band served as a loading control. A lower molecular weight LcrH degradation product is marked (LcrH*). (**B**) Binding of YopD/LcrH complexes or LcrH alone to the *csrA* leader transcript was analyzed by RNA-EMSAs. Parts of the *csrA* 5'-UTR was *in vitro* transcribed and biotin-labeled. 2 nM of the resulting *csrA* was incubated with increasing concentrations of purified YopD/LcrH complexes, separated onto a native 5% TBE-PAA gel and the biotin-labeled RNAs were visualized after transfer to a nitrocellulose membrane. Higher molecular bands, as a result of protein-RNA binding, are indicated with asterisks. The region of the *csrA* RNA fragment is indicated relative to the translational start site.

3.5 Deletion of the putative YopD binding region does not fully remove YopD-dependent regulation of *csrA*

RNA binding studies revealed a putative YopD binding site in the *csrA* locus to a region close to the -10 regions and the transcriptional start sites of promoter P4 and P5. To test if deletion of the putative binding region eliminates the YopD dependency of *csrA*, two deletions were introduced within the translational *csrA*'-'*lacZ* reporter fusion plasmid (pJH4) encoding the entire *csrA* upstream region with all putative promoter sites. The first deletion spanned a region including the -35 and -10 region of promoters P4 and P5 (pJH48), while the second deletion additionally excluded the TSS of P4 and P5 (pJH49) (**Fig. 3.5A**). Deletion of promoters P4 and P5 reduced the *csrA*'-'*lacZ* activity in the wild-type strain YPIII under T3SS-inducing conditions by 70%. This confirms the previous observation that the putative promoters P1 and P2, as well as promoter P3, are barely expressed (see **Fig. 3.1**) whereas promoters P4+5 seem to be the main drivers of *csrA* transcription under this growth condition. An additional deletion of the P4/5 TSS region decreased the LacZ activity by 90% in comparison to the full-length reference reporter construct pJH4. This could indicate that a regulatory element is located in this region (**Fig. 3.5B**). Deletion of the putative YopD/LcrH

binding site did not completely abolish the YopD-dependent regulation in the pJH48 and the pJH49 *csrA'-'lacZ* reporter plasmids. However, a comparison of the relative β-galactosidase activity of the different *csrA'-'lacZ* reporter plasmids revealed that the deleted region in the mutated reporter plasmid pJH48 and pJH49 might be involved in YopD-dependent regulation. Expression of the mutated reporter plasmids pJH48 and pJH49 were less reduced in the *yopD* mutant (65% and 74%) than in the wild-type reporter construct pJH4 (45%) (**Fig. 3.5C**). According to these data, the deletion of the putative YopD binding site, as defined in RNA binding studies, does not completely abolish YopD-dependent regulation of *csrA* indicating an additional factor is involved in *csrA* regulation.

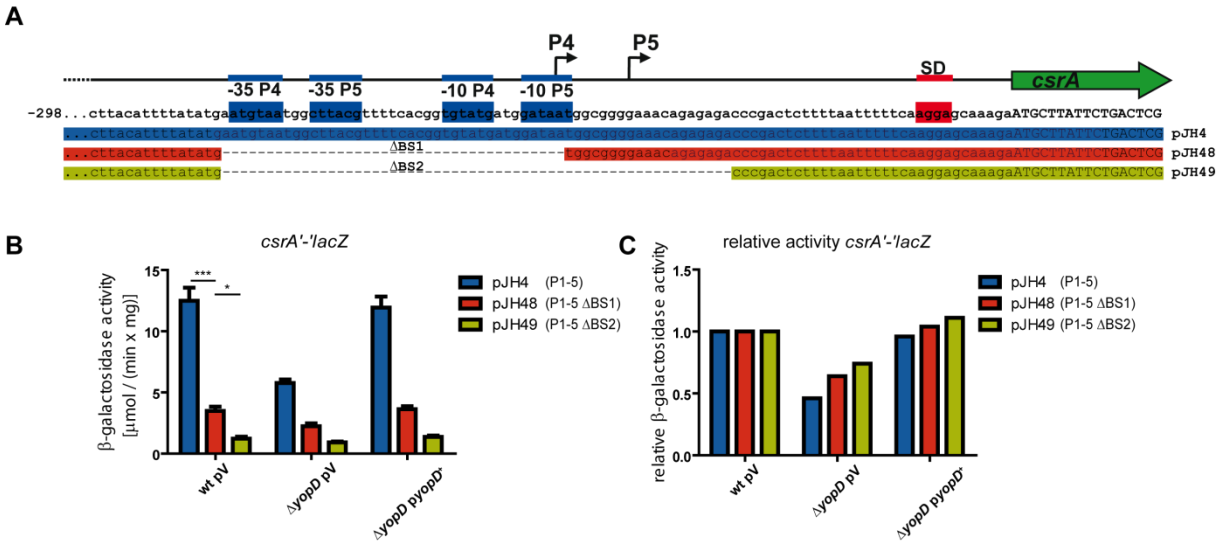

Figure 3.5: Deletion of the putative YopD binding region does not fully abolish YopD-dependent *csrA* regulation. (**A**) Schematic presentation of the *csrA* gene locus of *Y. pseudotuberculosis* showing the transcriptional start sites (TSS; broken arrows), the -35 and -10 boxes (blue box), the Shine-Dalgarno sequence (SD; red box) and parts of the *csrA* gene (green arrow). A schematic presentation of the downstream sequence of the translational *csrA'-'lacZ* constructs containing the whole *csrA* regulatory upstream region (pJH4) or mutated reporter constructs (pJH48 and pJH49) with a deletion in the putative YopD binding region (ΔBS1 and ΔBS2) is depicted below. (**B**) The YopD-dependent expression of translational *csrA'-'lacZ* reporter fusions was monitored in *Y. pseudotuberculosis* wild-type (YPIII) and the *yopD* mutant (YP91) strain. Strains were transformed with the empty vector (pV; pRS15) or complemented with its derivate pRS16 (p*yopD*$^{+}$) and different *csrA'-'lacZ* reporter constructs (pJH4 (blue), pJH48 (red) or pJH49 (green)). The specific β-galactosidase activity [µmol/(min*mg)] was measured after the strains were grown in LB medium for 2 h at 25 °C following a shift to 37 °C for 4 h. The data represent the mean +/- the standard deviation of 3 biological and 3 technical replicates. The data were analyzed by a paired Student's t-test to compare differences in promoter activity in the wild-type with * - P < 0.05; ** - P < 0.005; *** - P < 0.001; ns - not significant). (**C**) To compare the overall YopD-dependency of the different *csrA'-'lacZ* deletion constructs, the specific β-galactosidase activity of the respective *csrA'-'lacZ* fusion was normalized to the corresponding wild-type.

3.6 CsrA directly binds to its leader transcript

Previous results indicated the presence of an additional regulator binding the region between promoters P4 and P5. Analysis of the well conserved upstream region of *csrA* revealed at least two high-affinity binding motifs for CsrA (ANGGA). One of these binding sites overlap with the ribosomal binding site, another one is located between the -10 regions of promoters P4

and P5. Two additional putative low-affinity binding sites (AGAGA, GGGGA) are located between these two high-affinity binding sites. These binding sites are also present in the *E. coli csrA* upstream region and are directly bound by CsrA [Kulkarni *et al*., 2014; Yakhnin *et al*., 2011]. This led to the question whether CsrA could be the missing regulator binding to the same upstream region as YopD/LcrH. To analyze binding of CsrA to its 5'-UTR, two transcripts were tested for CsrA binding in RNA gel shift assays. The first RNA transcript contained both primary binding sites and both putative secondary binding sites (-70/+10), while the second transcript was truncated from the 5'-end and missed the 5'-primary binding motif (-50/+10) (**Fig. 3.6A**). The respective transcripts were incubated with increasing amounts of C-terminally His-tagged CsrA protein. RNA-EMSAs with the longer transcript led to the formation of two high molecular weight RNA-CsrA complexes. At low CsrA concentrations, a small RNA-CsrA complex appeared, while at the highest protein concentration a larger high-molecular RNA-CsrA complex was formed, indicating that multiple CsrA molecules interacted with the RNA fragment (**Fig. 3.6B**). The shorter transcript (-50 to +10) was not bound by the CsrA protein (**Fig. 3.6C**). Interestingly, the absence of the upstream primary binding site eliminated the specific binding by CsrA demonstrating the importance of both ANGGA motifs for effective, high affine binding of CsrA to its transcript. Furthermore, both putative secondary binding sites do not seem to play role in CsrA-*csrA* binding.

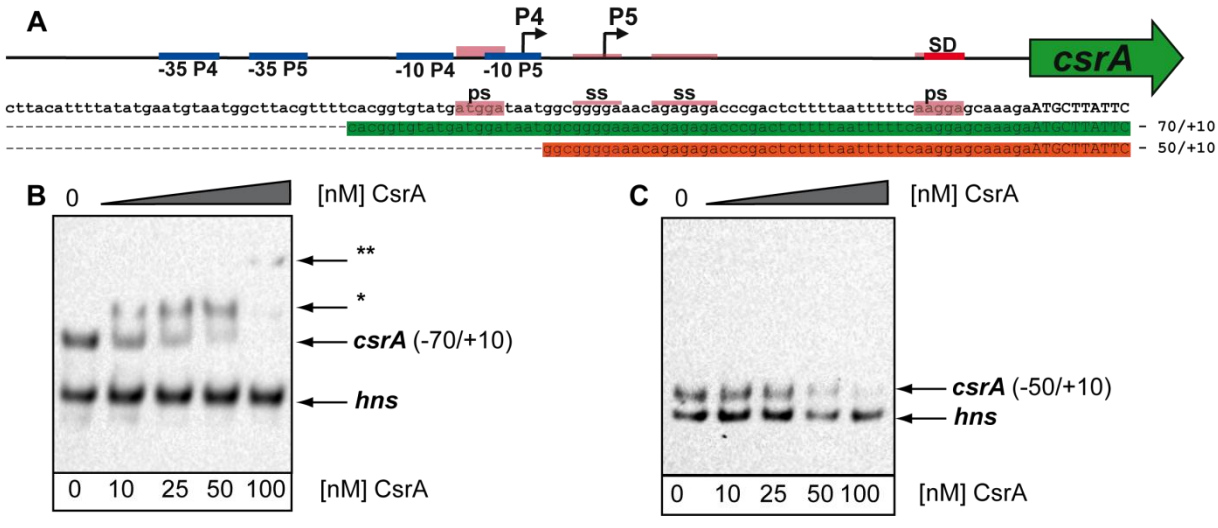

Figure 3.6: CsrA interacts with its leader transcript. (**A**) Schematic presentation of the *csrA* gene locus of *Y. pseudotuberculosis* showing the transcriptional start sites (TSS; broken arrows), the -35 and -10 boxes (blue box), the CsrA binding sites (light red box; ps - primary high affinity binding site; ss - secondary low affinity binding site), the Shine-Dalgarno sequence (SD; red box) and parts of the *csrA* gene (green arrow). The *in vitro* transcribed RNA fragments used in RNA-EMSA are depicted below. The region of the RNA fragments is indicated relative to the translational start site. (**B-C**) Binding of CsrA to the *csrA* leader transcript was analyzed by RNA-EMSAs. Parts of the *csrA* 5'-UTR and the *hns* control fragment were *in vitro* transcribed and biotin-labeled. 2 nM of the resulting *csrA* and the *hns* control fragment were incubated with increasing concentrations of CsrA, separated onto a native 7% TBE-PAA gel and the biotin-labeled RNAs were

visualized after transfer to a nitrocellulose membrane. Higher molecular bands, as a result of CsrA-RNA binding, are indicated with asterisks.

3.7 Complex autoregulation of *csrA* in *Y. pseudotuberculosis*

Autoregulation of *csrA* expression in *E. coli* occurs by a complex autoregulatory mechanism, including indirect activation of its own transcription and a direct repression of translation [Yakhnin *et al*., 2011]. To further analyze the CsrA-dependent *csrA* regulation in *Y. pseudotuberculosis*, expression of a translational *csrA'-'lacZ* fusion in which the first 70 nt upstream of the start codon were fused under the control of the constitutive *tet* promoter (pJH27), was investigated in the absence of *csrA* and in the presence of an arabinose-inducible *csrA*+ plasmid (pJH25) (**Fig. 3.7AB**). Deletion of *csrA* did not affect the reporter activity. However, high levels of CsrA strongly repressed *csrA'-'lacZ* activity (**Fig. 3.7B**). This strongly suggests, that similar to *E. coli*, binding of CsrA of *Y. pseudotuberculosis* to the region in proximity of promoters P4/5 led to translational repression of *csrA*. Expression of a *csrA'-'lacZ* construct, encoding the entire 5'-region of *csrA* (P1-5), was slightly but significantly down-regulated in the *csrA* mutant. This indicates a positive transcriptional autoregulation of the *csrA* locus. Complementation of the *csrA* mutant with a P_{BAD}::*csrA* construct could not fully restore wild-type levels. This could be explained by the observed repressive effect of CsrA on its own translation. (**Fig. 3.7C**). To further investigate the effect of CsrA on its own transcription, expression of a translational *csrA'-'lacZ* fusion in which promoters P4 and P5 (pJH48) and thus the repressive CsrA binding site was deleted was analyzed. The absence of *csrA* resulted in a reduced *csrA'-'lacZ* expression. Complementation of *csrA* with the P_{BAD}::*csrA* construct led to an induction of *csrA'-'lacZ* reporter gene activity above the wild-type level (**Fig. 3.7D**). As the binding motif needed for autorepression was deleted, high CsrA protein levels could not inhibit *csrA* expression as observed in the full-length construct. In summary, this demonstrated *csrA* is autoregulated in a direct negative and a positive indirect manner ensuring a tightly controlled expression of *csrA*. Since no additional CsrA binding sites are located upstream of promoters P4 and P5 the positive autoregulation is most probably mediated indirectly on the transcriptional level as described for *E. coli* (Yakhnin *et al*., 2011).

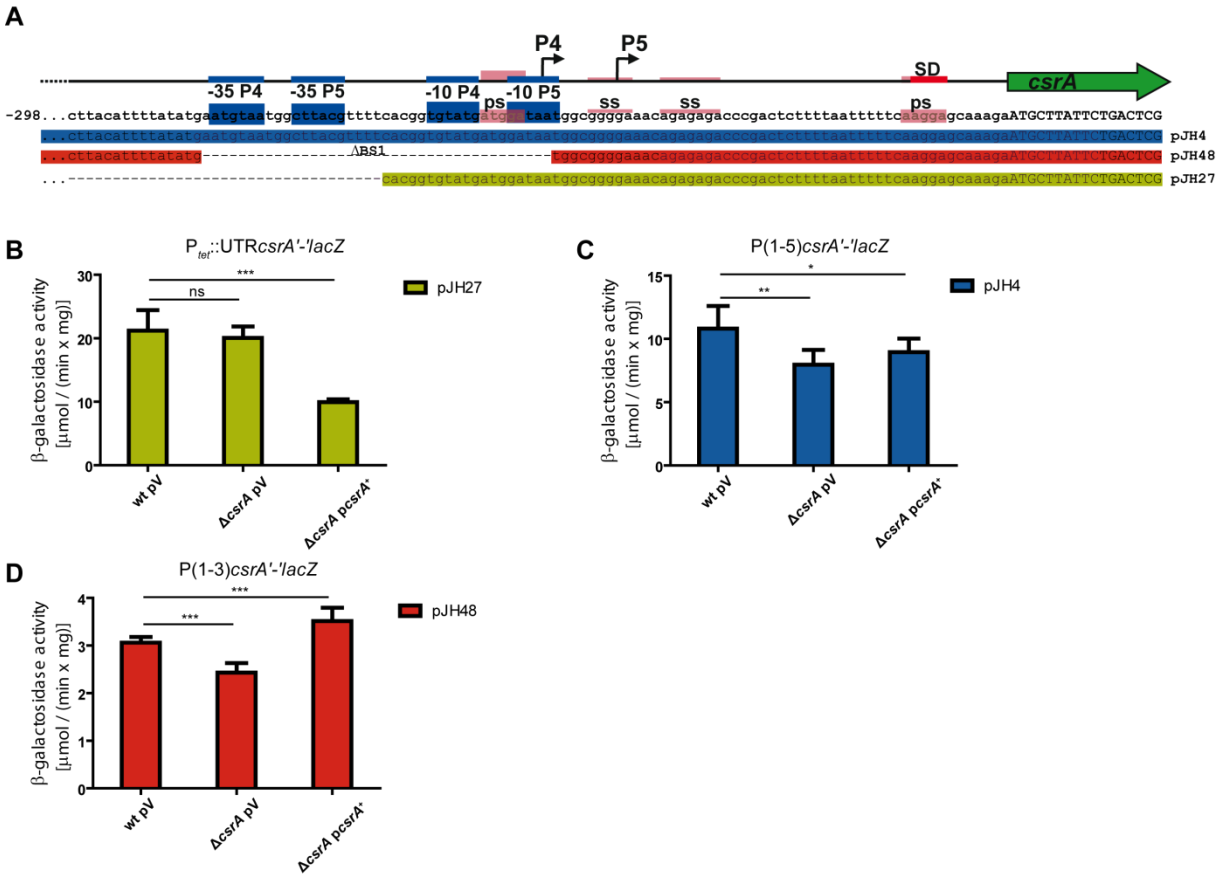

Figure 3.7: Autoregulation of *csrA*. (**A**) Schematic presentation of the *csrA* gene locus of *Y. pseudotuberculosis* showing the transcriptional start sites (TSS; broken arrows), the -35 and -10 boxes (blue box), CsrA binding sites (light red box; ps - primary high affinity binding site; ss - secondary low affinity binding site), the Shine-Dalgarno sequence (SD; red box) and parts of the *csrA* gene (green arrow). A schematic presentation of the translational *csrA*'-'*lacZ* constructs containing the whole *csrA* regulatory upstream region (pJH4, blue), mutated reporter constructs (pJH48, red) with a deletion in the putative YopD binding region (ΔBS1) or a translational *csrA*'-'*lacZ* reporter construct encoding the *csrA* upstream region under the control of a constitutive P_{tet} promoter (pJH27, green) is depicted below. (**B**-**D**) The CsrA-dependent expression of translational *csrA*'-'*lacZ* reporter fusions was monitored in *Y. pseudotuberculosis* wild-type (YPIII) and the *csrA* mutant (YP53) strain. Strains were transformed with the empty vector (pV; pBAD33) or complemented with its derivate pJH25 (p*csrA*$^+$) and different *csrA*'-'*lacZ* reporter constructs (pJH27 (**B**), pJH4 (**C**) or pJH48 (**D**)). The specific β-galactosidase activity [µmol/(min*mg)] was measured after the strains were grown in LB medium supplemented with 0.5% arabinose for 2 h at 25 °C following a shift to 37 °C for 4 h. The data represent the mean +/- the standard deviation of 3 biological and 3 technical replicates. The data were analyzed by an unpaired Student's t-test with * - $P < 0.05$; ** - $P < 0.005$; *** - $P < 0.001$; ns - not significant).

3.8 YopD and CsrA are both required for *csrA* control

Previous data of this work demonstrated that regulation of *csrA* is the result of a complex interplay between YopD and CsrA. First, both proteins bind to similar regions in the 5'-UTR of *csrA* whereby YopD is required for activation and CsrA for a direct translational repression and an indirect transcriptional activation of *csrA* expression (**Fig. 3.7**). Second YopD is required for efficient CsrA synthesis (**Fig. 3.4**) thus also indirectly affecting *csrA* transcription and translation.

As CsrA levels are decreased in absence of *yopD*, increasing CsrA levels might induce its own expression. To analyze whether CsrA is able to induce its own expression in the absence

of *yopD*, a translational *csrA'-'lacZ* reporter gene fusion encompassing either the whole regulatory region (pJH4), a deletion in the primary CsrA binding site and part of the YopD binding site (pJH48), or a third fusion with an even more extended deletion of the YopD binding site (pJH49), were introduced in the *Y. pseudotuberculosis* wild-type strain, in the *yopD* mutant and in the *yopD* mutant containing a plasmid with *csrA* under an inducible promoter (pJH25) (**Fig. 3.8A**).

Deletion of *yopD* resulted in a strongly reduced *csrA'-'lacZ* activity of the wild-type construct (pJH4). Increasing CsrA levels in absence of YopD did not induce the *csrA* expression. The most presumable explanation is CsrA indirectly induces its transcription, but also binds to its repressive site in the P4/5 region of the 5'-UTR, thereby preventing *csrA* translation and compensating the transcriptional activation (**Fig. 3.8B**). Indeed, deletion of CsrA's binding site in pJH48 and pJH49 resulted in a 1.27 and 1.30 fold induction in the *yopD* mutant containing the *csrA* expressing plasmid compared to the *yopD* mutant with the empty vector control (**Fig. 3.8C**). However, as observed previously, *csrA* expression cannot be fully restored (**Fig. 3.7D**).

As CsrA is involved in the translational YopD-dependent control of *csrA* expression, the influence of YopD and CsrA on *csrA* expression was analyzed. To do so, the expression of a translational *csrA'-'lacZ* fusion, containing the YopD and CsrA binding region, under the control of the constitutive *tet* promoter (pJH27, see **chapter 3.7**) was analyzed in presence of a *yopD*$^{+}$ plasmid (pRS16) in the wild-type (YPIII), the *yopD* mutant (YP91), the *csrA* mutant (YP53) and the *yopD*/*csrA* double mutant (YP145) strain.

As observed before, the deletion of *yopD* resulted in a strong reduction of *csrA*'-'*lacZ* activity. The deletion of *csrA* mildly increased the *csrA*'-'*lacZ* activity by removing the autorepression of *csrA*. Although expression of *yopD* could restore the *csrA*'-'*lacZ* activity to wild-type levels in the *yopD* mutant, expression of *yopD* did not affect *csrA*'-'*lacZ* activity in the *csrA* mutant. Interestingly, deletion of *yopD* and *csrA* partially restored *csrA*'-'*lacZ* activity compared to the wild-type, demonstrating that the control of *csrA* by YopD is dependent on CsrA. Notably, YopD can induce *csrA* expression independent of *csrA*, as an expression of YopD in the *yopD*/*csrA* double mutant completely restored *csrA*'-'*lacZ* reporter gene activity to wild-type levels (**Fig. 3.8D**).

In conclusion, both proteins are required for full activation of *csrA* under T3SS-inducing conditions. CsrA is needed for the indirect transcriptional activation, while YopD-mediated activation is achieved by binding to the *csrA* 5'-UTR, which additionally weakens the

translational autorepression of *csrA*. However, too high CsrA level might prevent *csrA* translation by interfering with YopD.

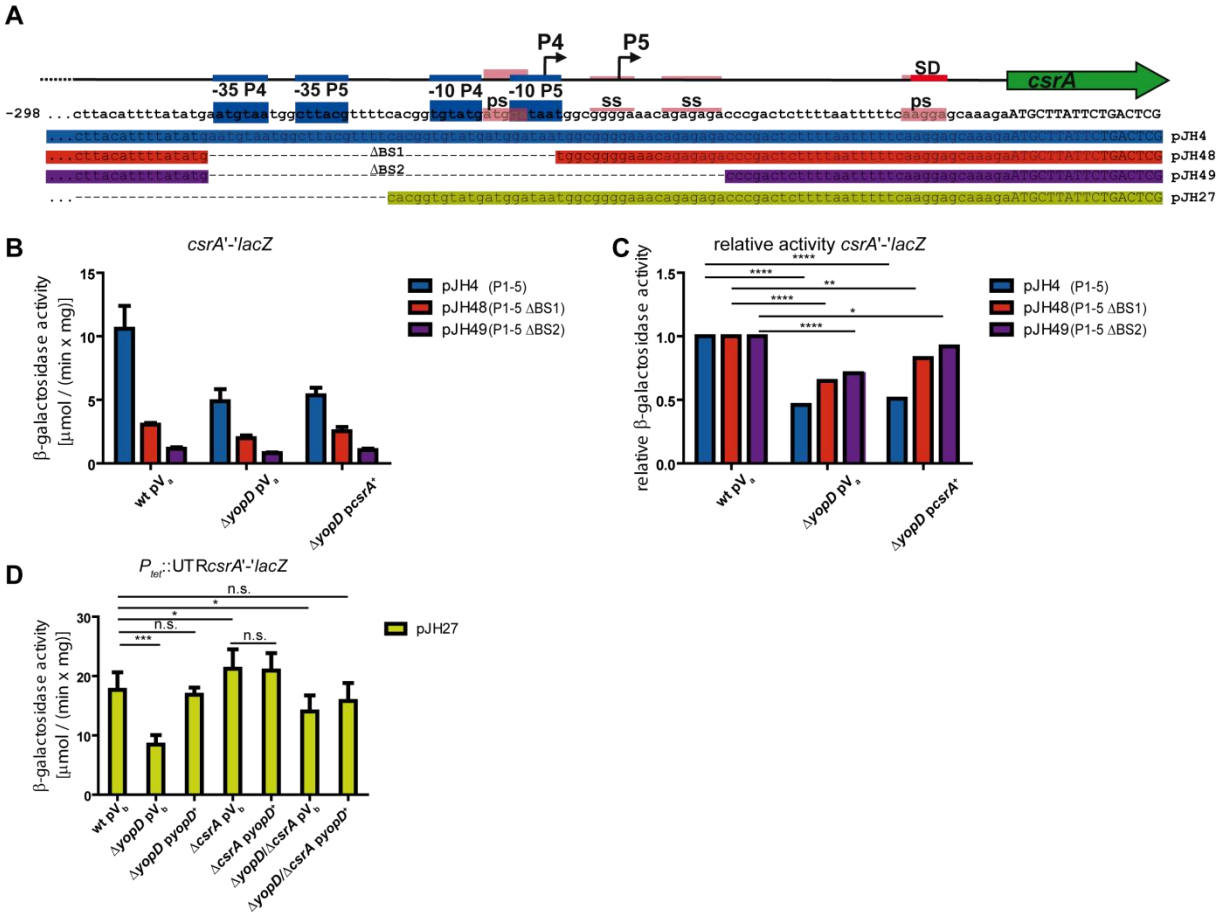

Figure 3.8: YopD and CsrA are both involved in regulation of *csrA*. (**A**) Schematic presentation of the *csrA* gene locus of *Y. pseudotuberculosis* showing the transcriptional start sites (TSS; broken arrows), the -35 and -10 boxes (blue box), CsrA binding sites (light red box; ps - primary high affinity binding site; ss - secondary low affinity binding site), the Shine-Dalgarno sequence (SD; red box) and parts of the *csrA* gene (green arrow). A schematic presentation of the translational *csrA*'-'*lacZ* constructs containing the *csrA* regulatory upstream region (pJH4), reporter constructs (pJH48 and pJH49) with a deletion in the putative YopD binding region (ΔBS1 and ΔBS2) or a translational *csrA*'-'*lacZ* reporter construct encoding the *csrA* upstream region under the control of a constitutive P_{tet} promoter (pJH27) is depicted below. (**B**-**D**) The CsrA- and YopD-dependent expression of translational *csrA*'-'*lacZ* reporter fusions were monitored in *Y. pseudotuberculosis* wild-type (YPIII), the *yopD* mutant (YP91), the *csrA* mutant (YP53) and the *yopD*/*csrA* (YP145) mutant strain. Strains were transformed with the empty vector (pV_a; pBAD33 or pV_b pRS15) or complemented with its derivate pJH25 or pRS16 ($pcsrA^+$ or $pyopD^+$) and different *csrA*'-'*lacZ* reporter constructs (pJH4 (blue), pJH48 (red), pJH49 (purple) or pJH27 (green)). (**B+D**) The specific β-galactosidase activity [µmol/(min*mg)] was measured after the strains were grown in LB medium for 2 h at 25 °C following a shift to 37 °C for 4 h. To induce expression of the pBAD33 plasmid and its derivate, strains were grown in LB medium supplemented with 0.5% arabinose. The data represent the mean +/- the standard deviation of at least 2 biological and 2 technical replicates. (**C**) To compare the overall influence of CsrA on the YopD-dependency of the different *csrA*'-'*lacZ* deletion constructs, the specific β-galactosidase activity of the respective *csrA*'-'*lacZ* fusion was normalized to the corresponding wild-type. The data were analyzed by an unpaired Student's t-test with * - $P < 0.05$; ** - $P < 0.005$; *** - $P < 0.001$; **** - $P < 0.0001$; ns - not significant).

3.9 Transcript stability of *csrA* is not influenced by YopD

As demonstrated previously, YopD binds to the leader region of the *csrA* mRNA. Additionally, deletion of *yopD* causes a reduction in *csrA* mRNA and protein level

(Steinmann, PhD thesis; **Fig. 3.4A**), indicating that YopD affects CsrA synthesis on the posttranscriptional level. Hence, an RNA stability assay was used to analyze the stability of *csrA* mRNA in the wild-type and the *yopD* deficient strains grown under T3SS-inducing conditions. However, the *csrA* transcript stability in the wild-type and the *yopD* mutant were comparable and an RNA half-life of approximately 2.7 min was observed in both strains (**Fig. 3.9A+B**). Interestingly, a second transcript became visible in the *yopD* mutant, indicating the induction of an additional promoter in absence of YopD.

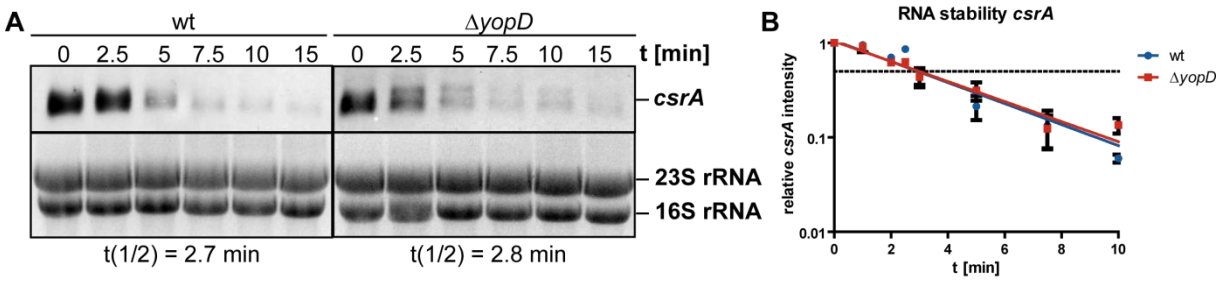

Figure 3.9: The stability of the *csrA* transcript is not affected by YopD. (**A**) RNA stability assay of the wild-type (YPIII) and the *yopD* mutant strain (YP91) to determine the stability of the *csrA* transcript. All strains were grown in LB medium for 2 h at 25 °C following a shift to 37 °C for 4 h and transcription was stopped by addition of rifampicin to a final concentration of 1 mg/mL. Samples were taken before the addition of rifampicin (0) and then 2.5 min, 5 min, 7.5 min, 10 min and 15 min after the transcription stop. The total RNA was isolated, separated and the *csrA* transcript was detected by northern blot analysis using a *csrA* specific DIG-labeled DNA probe. The 16S and 23S ribosomal RNA was stained with ethidium bromide and served as a loading control. (**B**) The northern blot was documented and quantified using the ImageJ software. Data are presented as the relative *csrA* intensity (*csrA* intensity/rRNA intensity) over time on a half-logarithmic scale.

3.10 YopD induces *csrA* only at 37 °C

Translocator YopD is part of the thermo-induced *ysc-yop* regulon and thus mainly expressed at 37 °C. According to this, the question arose if *csrA* is thermo-regulated through the action of YopD. Thus, *csrA* transcript levels and also the CsrA and the YopD protein content were monitored at 25 °C and 37 °C in the wild-type and the *yopD* mutant by northern and western blot analysis. Interestingly, low YopD protein levels were already detectable at 25 °C which dramatically increased at 37 °C, reflecting the thermo-induction of the *ysc-yop* regulon. At both temperatures, no differences in *csrA* transcript level could be recognized in the wild-type, although CsrA protein levels were increased at 37 °C. As described previously, *csrA* transcript and protein levels were decreased in the *yopD* mutant (**Fig. 3.10**). Although high YopD levels are present at 37 °C *csrA* transcript levels were not induced in the wild-type supporting the hypothesis that YopD induces *csrA* post-transcriptionally. Indeed this is reflected by an increase of CsrA protein levels at 37 °C in the wild-type compared to 25 °C.

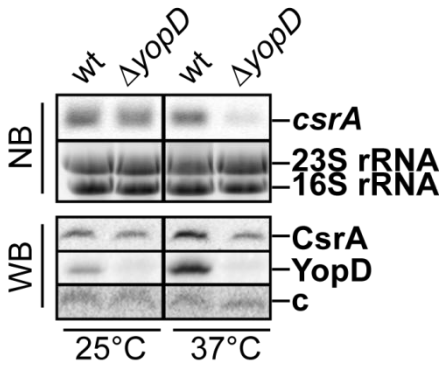

Figure 3.10: YopD is already expressed at 25 °C, but activates *csrA* expression only at 37 °C. The wild-type (YPIII) and the Δ*yopD* (YP91) mutant strain were grown in LB medium for 6 h at 25 °C or for 2 h at 25 °C with a subsequent shift to 37 °C for 4 h (37 °C). *csrA* transcript concentration was monitored by northern blot analysis (NB). The total RNA was isolated, separated and the *csrA* transcript was detected by northern blot analysis using a *csrA* specific DIG-labeled DNA probe. The 16S and 23S ribosomal RNA was stained with ethidium bromide and served as a loading control. The CsrA and YopD protein content were analyzed by western blot analysis (WB). An equivalent of OD_{600} = 1 was prepared for SDS-PAGE and subsequent western blot analysis with polyclonal α-YopD and α-CsrA rabbit sera. An unspecific band served as a loading control (c).

3.11 YopD/LcrH cannot activate *csrA* expression in *E. coli*

YopD is an inducer of *csrA* expression in *Y. pseudotuberculosis*. The YopD-binding region in the *csrA* upstream region is highly conserved in *E. coli* and *Y. pseudotuberculosis* (**Fig. S1**). To test whether heterologous expression of YopD/LcrH could induce *csrA* activation in *E. coli*, *E. coli* DH10β, harboring an empty control vector (pRS1) or a *lcrH/yopD* vector (pRS5), were grown at 37 °C and protein samples were taken during different growth phases for western blot analysis (**Fig. 3.11A**). Plasmid pRS5 encodes the *lcrH-yopBD* operon fused under control of the constitutive P_{lac} promoter. Apparently, YopD protein could only be detected in *E. coli* when expressed from the complementation vector. YopD expression peaked in late exponential phase and during the transition phase reflecting the *yopD* expression pattern in *Y. pseudotuberculosis*. Consistent with Yakhnin and colleagues, *csrA* expression increases over time and peaks in stationary phase in *E. coli* [Yakhnin *et al*., 2011]. Heterologously expressed YopD/LcrH complexes do not regulate *csrA* expression in *E. coli*, as the CsrA protein level is not changed in presence of YopD. This indicates that other *Yersinia*-specific factors are required for YopD/LcrH-mediated CsrA synthesis.

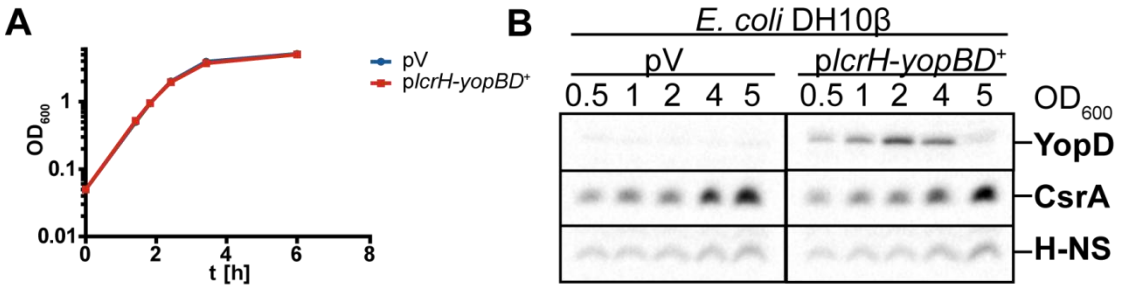

Figure 3.11: *csrA* expression in *E. coli* is not influenced by the heterologous expression of YopD and LcrH. (**A+B**) *The E. coli* DH10β wild-type was transformed with the empty vector (pV; pRS1) or complemented with its derivate pRS5 (p*lcrH-yopBD*$^+$) and grown in LB medium at 37 °C. Samples were taken and the optical density (OD_{600}) was determined to monitor the growth of both strains, additionally, an equivalent of OD_{600} = 1 was prepared for SDS-PAGE and subsequent western blot analysis. (**A**) Influence of *lcrH* and *yopD* on the growth of *E. coli*. Data is represented as the optical density (OD_{600}) over time on a half-logarithmic scale. Sample time points are indicated by square dots. (**B**) Western blot analyses of protein samples taken along the growth curve. Samples were separated by SDS-PAGE following a western blot analysis with polyclonal α-CsrA, α-YopD and α-H-NS rabbit sera. The H-NS band served as a loading control. The OD_{600} of each sample is indicated.

3.12 YopD expression is decoupled from the P_{lcrG} promoter at 25 °C

The *yopD* gene is encoded at the 3'-end of the polycistronic *lcrGVH-yopBD* operon. The transcriptional master activator LcrF activates transcription of this operon at 37 °C. Additionally, Li and colleagues suggested the presence of an unknown promoter located directly upstream of *yopD*, in the *yopB* gene [Li *et al.*, 2014]. To analyze the impact of the two promoters on the temperature-dependent expression of *yopD*, the activity of a translational construct encompassing either the whole operon starting from P_{lcrG} (-327 nt relative to the translational start site of *lcrG*; *lcrGVH-yopBD'-'lacZ*; pJH36) or from the second promoter located in the *yopB* gene, P_{yopD} (-1224 nt relative to the translational start site of *yopD*; *yopD'-'lacZ*; pJH39). In both constructs, the promoter-less *lacZ* gene was fused to the first six codons of the *yopD* gene (**Fig. 3.12A**). The translational reporter gene fusion constructs were introduced into the wild-type strain YPIII and β-galactosidase activity was measured at 25 °C and 37 °C. Expression of both reporter gene constructs was strongly induced at 37 °C compared to 25 °C (**Fig. 3.12B**). Interestingly, the main promoter driving *yopD* expression under environmental temperatures (25 °C) seems to be P_{yopD} (69% compared to 31% of P_{lcrG}). At 37 °C, the percentage of both promoters controlling *yopD* is almost 50% (**Fig. 3.12C)**. This mechanism uncouples expression of *yopD* from the expression of its chaperone LcrH and the major translocator YopB, especially at 25 °C probably resulting in an imbalance in the YopD to LcrH ratio.

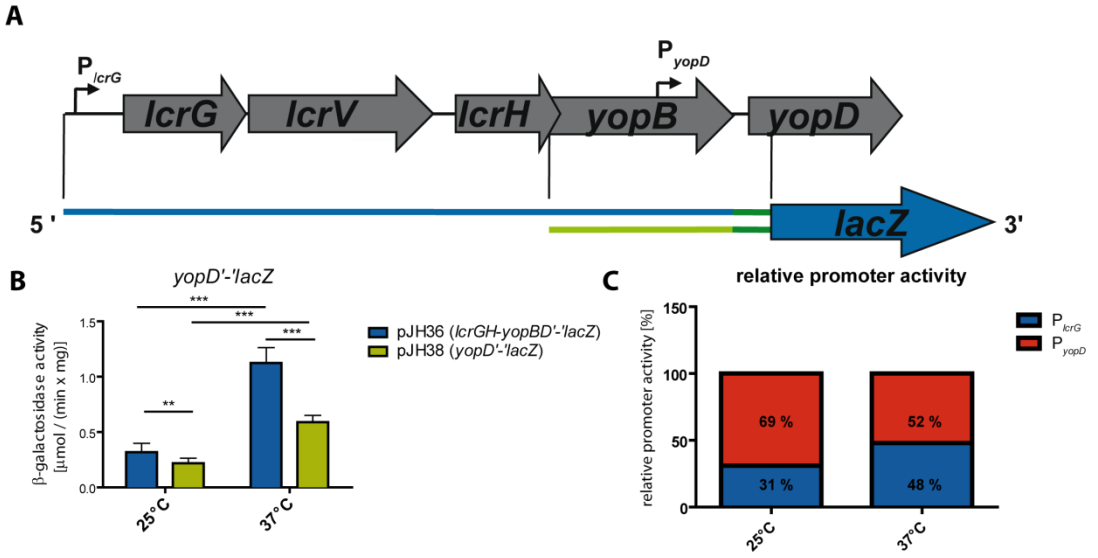

Figure 3.12: YopD-dependent expression at 25 °C is mainly driven by an internal promoter. (**A**) Schematic presentation of the *lcrGVH-yopBD* operon of *Y. pseudotuberculosis* showing the different promoters (broken arrows, P_{lcrG} + P_{yopD}). A schematic presentation of the translational *yopD'-'lacZ* constructs, encoding the whole operon including the P_{lcrG} and P_{yopD} promoters (pJH36) or the *yopB* gene including the P_{yopD} promoter (pJH38), is depicted below. (**B**) The temperature-dependent expression of translational *yopD'-'lacZ* reporter fusions was monitored in the *Y. pseudotuberculosis* wild-type (YPIII). The wild-type strain was transformed with the different *yopD'-'lacZ* constructs (pJH36 (blue) or pJH38 (green)). The specific β-galactosidase activity [µmol/(min*mg)] was measured after the strains were grown in LB medium either for 6 h at 25 °C (25 °C) or 2 h at 25 °C following a shift to 37 °C for 4 h (37 °C). The data represent the mean +/- the standard deviation of 3 biological and 3 technical replicates. The data were analyzed by an unpaired Student's t-test with * - $P < 0.05$; ** - $P < 0.005$; *** - $P < 0.001$; ns - not significant). (**C**) To calculate the relative activity of the 2 promoters, P_{lcrG} and P_{yopD}, to the whole promoter activity, the specific activity of the *yopD'-'lacZ* reporter construct (pJH38) was subtracted from the full-length *lcrGVH-yopBD'-'lacZ* reporter fusion (pJH36) and the percentage of P_{lcrG} and P_{yopD} was calculated.

3.13 Protein stability of YopD is decreased at 25 °C

Expression of *yopD* occurs mainly at 25 °C from its own promoter and is thus uncoupled from the expression of its chaperone LcrH. As YopD requires its chaperone LcrH for stabilization, this would result in less stable YopD protein. For this reason, YopD protein stability was analyzed at 25 °C or 37 °C. To do so, the wild-type strain YPIII was grown for 6 h at 25 °C (25 °C) or 2 h at 25 °C and shifted to 37 °C for 4 h (37 °C). Protein synthesis was stopped by the addition of translation inhibiting antibiotics (chloramphenicol/spectinomycin). As shown in **Fig. 3.13A**, YopD is degraded at 25 °C displaying a half-life of 78 min. In contrast, at 37 °C, YopD is completely stable with a half-life of more than 3 h.

To test whether the reduced stability of YopD at 25 °C is the result of reduced LcrH levels, YopD protein levels were analyzed in the wild-type strain containing either a *lcrH* expression plasmid (pRS17) or the empty vector control (pRS15) by western blot analysis. The analysis demonstrated that low YopD levels could be increased by heterologous expression of *lcrH* at 25 °C and at 37 °C (**Fig. 3.13B**). This indicates, that the reduced stability of YopD is the result of low LcrH levels.

Temperature-dependent protein stability is often caused by regulated proteolysis by ATP-dependent proteases or general proteolysis triggered by unfolded or misfolded proteins. To test whether one or more known proteases are involved in the degradation of YopD at 25 °C, YopD protein levels were analyzed at 25 °C in various ATP-dependent protease mutant strains. For this approach, the major players in regulated proteolysis Lon, ClpP, HslV and FtsH were chosen [Kirstein *et al*, 2009]. ClpP associated proteases are not involved in the destabilization, as deletion of the *clpP* gene did not influence YopD or LcrH level. The loss of *lon*, *ftsH* or *hslV* surprisingly even decreased YopD and LcrH amounts (**Fig. 3.13C**). This might indicate that an ATP-dependent protease targets an upstream regulator of the *lcrVGH-yopBD* operon, as both proteins are affected in these mutants. Due to the down-regulation of YopD and LcrH in these protease mutants, stabilizing effects might be present but cannot be assessed. For this reason, a regulated proteolysis of YopD by these proteases cannot be excluded.

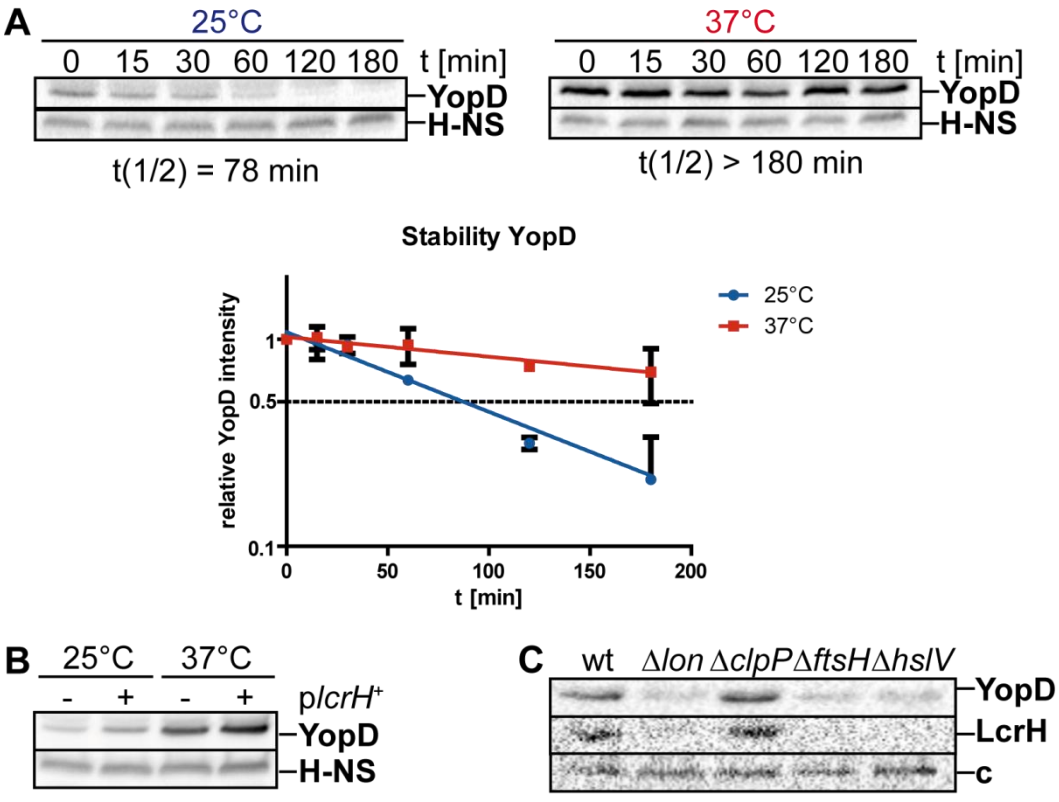

Figure 3.13: Protein stability of YopD is decreased at 25 °C. (**A**) Protein stability assay of the wild-type (YPIII) to determine the stability of the YopD protein. All strains were grown in LB medium either for 6 h at 25 °C (25 °C) or for 2 h following a shift to 37 °C for 4 h (37 °C) and protein synthesis was stopped by addition of spectinomycin and chloramphenicol to a final concentration of 0.5 mg/mL. Samples were taken before (0) and then 15 min, 30 min, 60 min, 120 min and 180 min after the translation stop. The YopD protein and H-NS content were analyzed by western blot analysis. An equivalent of OD_{600} = 1 was prepared for SDS-PAGE and subsequent western blot analysis with polyclonal α-YopD and α-H-NS rabbit sera. The H-NS band served as a loading control. The western blots were documented and quantified using the ImageJ software. Data are presented as the relative YopD intensity (YopD intensity/H-NS intensity) over time on a half-logarithmic scale. (**B**) Expression of *lcrH* increases YopD protein levels. The *Y. pseudotuberculosis* YPIII wild-type was transformed with the empty vector (-; pRS15) or complemented with its derivate p*lcrH* $^{+}$ (+; pRS17). All strains were grown in LB medium either for 6 h at 25 °C (25 °C) or for 2 h at 25 °C following a shift to 37 °C for 4 h (37 °C). Whole cell

extracts were prepared and taken for western blot analysis. An equivalent of OD_{600} = 1 was prepared for SDS-PAGE and subsequent western blot analysis with polyclonal α-YopD and α-H-NS rabbit sera. The H-NS band served as a loading control. (**C**) The influence of ATP-dependent proteases on YopD and LcrH levels was analyzed by western blot analysis. The wild-type (YPIII), the *lon* mutant (YP67), the *clpP* mutant (YP63), the *ftsH* mutant (YP327) and the *hslV* mutant (YP326) strain were grown in LB medium for 2 h at 25 °C with a subsequent shift to 37 °C for 4 h. Samples were taken and an equivalent of OD_{600} = 1 was prepared for SDS-PAGE and subsequent western blot analysis with polyclonal α-YopD and α-LcrH rabbit sera. An unspecific protein band served as a loading control (c).

3.14 YopD interacts with the untranslated leader transcript of the *yscW-lcrF* operon

YopD is an important regulator of the *ysc-yop* regulon and is known to repress the expression of *yop* genes and the virulence master regulator *lcrF* [Steinmann, PhD thesis; Böhme *et al*., 2012]. The *lcrF* gene is the last gene of the bicistronic *yscW-lcrF* operon. Previous experiments demonstrated, *lcrF* expression is controlled by the negative regulators YopD, LcrH and LcrQ by decreasing *lcrF* RNA stability [Steinmann, PhD thesis]. Furthermore, the expression of *yopQ* is post-transcriptionally regulated by YopD and LcrH in *Y. enterocolitica*. Together, both bind the leader transcript and thereby destabilizing the *yopQ* mRNA [Anderson *et al*., 2002]. Additionally, 'AUAAA' motifs are described as putative binding sites for YopD/LcrH [Anderson, 2011]. Such putative binding motifs are located in the 5'-UTR of *yscW* as well as the 5'-UTR of *lcrF* (**Fig. 3.14A**). Therefore, the capability of YopD/LcrH to bind the 5'-UTR of *yscW* and *lcrF* mRNA and thereby destabilizing the whole transcript, were investigate by RNA-EMSAs. To do so, two RNA fragments, encoding either 107 nt upstream of the translational start site including the first three codons of *yscW* (5'-*yscW*) or the entire intergenic region of *yscW-lcrF* and 15 nt of the *lcrF* CDS (5'-*lcrF*) were *in vitro* transcribed and investigated for binding of the YopD/LcrH complex by RNA-EMSA (**Fig. 3.14A**). The RNA-EMSA revealed that both 5'-UTRs were bound by YopD/LcrH, although the 5'-*lcrF* RNA fragment was bound with a slightly higher affinity (67 nM), compared to the 5'-*yscW* RNA fragment (135 nM). A second higher molecular weight complex was recognizable for both transcripts, although these appeared earlier when testing the 5'-*lcrF* transcript (**Fig. 3.14BC**). This indicates that YopD/LcrH is able to specifically and directly interact with the 5'-UTR of *yscW* and *lcrF*.

The intergenic region of *yscW-lcrF* is involved in thermoregulation of *lcrF* expression and contains an RNA thermometer structure. The mRNA folds into a secondary structure, consisting of two hairpins structures required for efficient expression of *lcrF*. Hairpin 1 is involved in the stabilization of the overall architecture of the thermo-responsive element located in hairpin 2. Hairpin 2 contains a 'four U' RNA thermometer element which base-pairs

and sequesters the RBS at moderate temperature. Additionally, a putative YopD binding motif is located upstream of the 'four U' motif ('AUAAA'; **Fig. 3.14D**) [Böhme *et al*., 2012; Steinmann, PhD thesis; Chen & Anderson, 2011].

To further analyze the interaction of YopD/LcrH with the 5'-UTR of *lcrF*, binding of YopD/LcrH complexes to fragments with a deletion of the hairpin 1 or a part of the hairpin 2 sequences was investigated in RNA-EMSAs (**Fig 3.14D**). Both 5'-*lcrF* hairpin mutants were incubated with increasing concentrations of purified YopD/LcrH complexes and binding capabilities were compared to the wild-type 5'-*lcrF* transcript. Interestingly, binding of YopD/LcrH was not completely abolished by the deletion of hairpin 1 or hairpin 2 (**Fig. 3.14EF**). Additionally, deletion of hairpin 1, removed the second high molecular shift, present in the wild-type and Δhairpin 1 RNA fragment (**Fig. 3.14E**). Deletion of the 'AUAAA' motif-containing hairpin 1 did not affect the YopD/LcrH binding pattern. Taken together, this suggests YopD binds to an alternative binding site in the *yscW-lcrF* mRNA apart from the described 'AUAAA' binding motif.

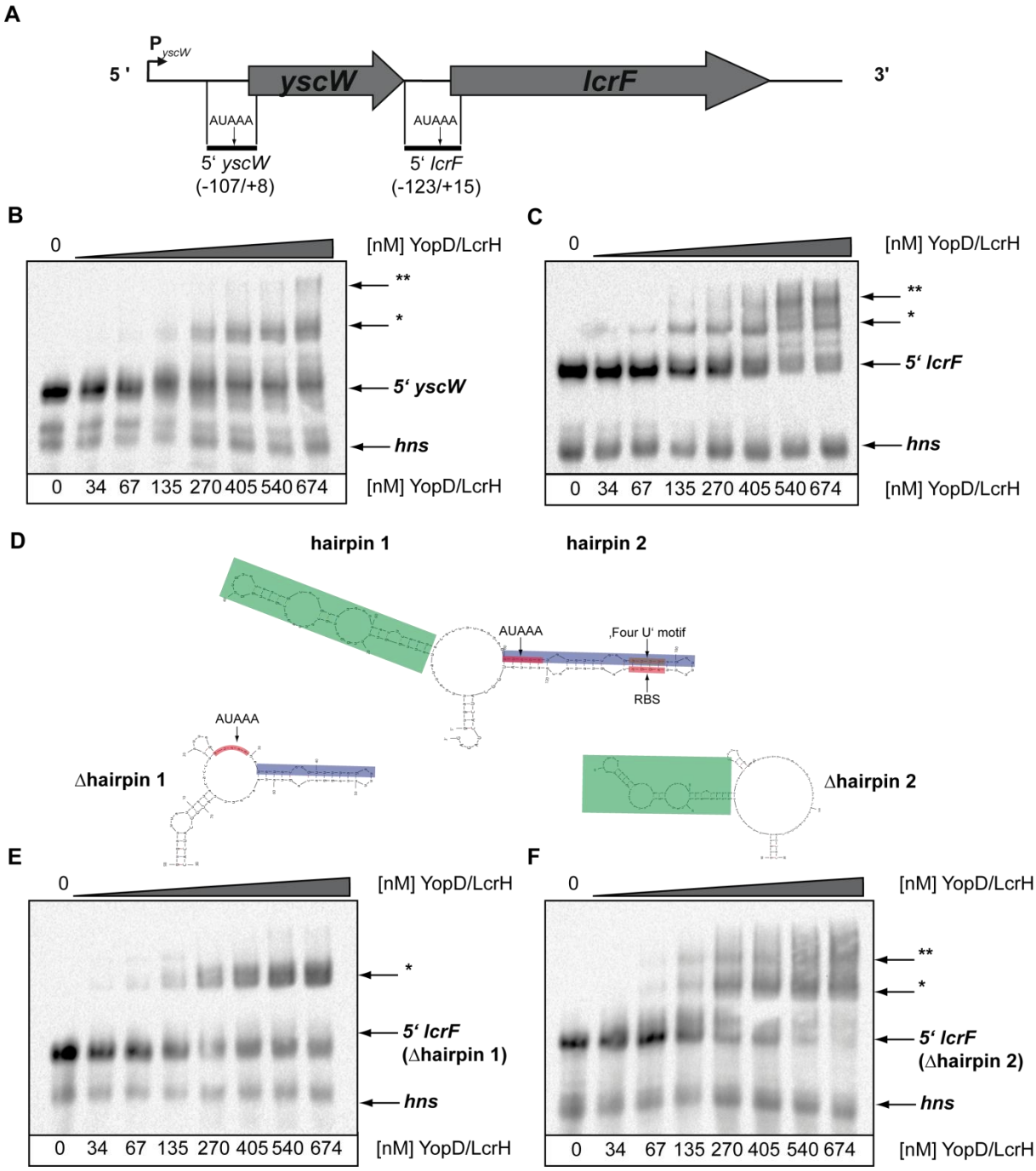

Figure 3.14: YopD/LcrH binds the 5'-UTR of *yscW* and *lcrF*. (**A**) Schematic presentation of the *yscW-lcrF* gene locus of *Y. pseudotuberculosis* showing the P_{yscW} promoter (broken arrows) and the *yscW* and *lcrF* gene (block arrow). The *in vitro* transcribed RNA fragments used in RNA-EMSA are depicted below. Putative YopD binding sites are indicated (vertical arrow). The region of the RNA fragments is indicated relative to the translational start site of the corresponding gene. (**BC+EF**) Binding of YopD/LcrH complexes to the upstream region of *yscW* and *lcrF* was analyzed by RNA-EMSAs. Parts of the *yscW*, *lcrF* 5'-UTR and its hairpin mutants, and the *hns* control fragment were *in vitro* transcribed and biotin-labeled. 2 nM of the resulting *yscW*, *lcrF* and the *hns* control fragment were incubated with increasing concentrations of purified YopD/LcrH complexes, separated onto a native 7% TBE-PAA gel and the biotin-labeled RNAs were visualized after transfer to a nitrocellulose membrane. Higher molecular bands, as a result of YopD/LcrH-RNA binding, are indicated with asterisks. (**D-F**) Hairpin 2 of the *yscW-lcrF* intergenic region is needed for efficient YopD/LcrH binding**.** (**D**) *In silico* prediction of the secondary structure of the *yscW-lcrF* intergenic region of wild-type and hairpin mutants with the lowest free energy (mFold [Zuker, 2003]). Deletions of hairpin 1 (green) and hairpin 2 (blue) are presented below. The position of a putative YopD binding site (AUAAA), the RNA thermometer ('Four U' motif) and the ribosomal binding site (RBS) are marked in red.

3.15 CsrA interacts with multiple regions of the *yscW-lcrF* transcript

Previous studies demonstrated that the RNA binding protein CsrA controls the expression of *lcrF*. CsrA was shown to repress *yscW-lcrF* transcription indirectly but also to stimulate *yscW* and *lcrF* translation by a so far unknown mechanism [Opitz, PhD thesis; Pimenova, Master thesis]. Interestingly, the *yscW-lcrF* operon contains several putative CsrA binding sites (GGA or ANGGA motifs). The *yscW* leader transcript comprises five 'GGA' sequence motifs, whereby two are partially overlapping, high-affinity 'ANGGA' motifs. The 5'-UTR of *lcrF* only harbors one 'GGA' motif (**Fig. 3.15A**). The 5'-UTR of the *yscW* mRNA, as well as the *lcrF* 5'-UTR were *in vitro* transcribed, labeled with biotin and incubated with increasing amounts of purified CsrA protein. The RNA-EMSA demonstrated that the 5'-*yscW* was already bound at low CsrA protein concentrations (5 nM). A second high molecular shift appeared at CsrA concentrations between 40 and 60 nM (**Fig. 3.15B**). CsrA displayed a lower affinity to the intergenic 5'-*lcrF* fragment. Only a single high molecular weight complex appeared at a CsrA concentration of 40-60 nM (**Fig. 3.15D**). Notably, CsrA-bound transcripts possess at least one binding site in the vicinity to the 'GGA' core motif located in the RBS, thereby increasing binding affinity and specificity [Van Assche *et al*., 2015; Mercante *et al*., 2009; Vakulskas *et al*., 2015]. In previous toe print assays it could be demonstrated that besides the high-affinity 'ANGGA' motif, an 'AGAGA' sequence could constitute as such a motif [Baker *et al*., 2005]. This motif could be discovered in the first codons of the *lcrF* gene at position +12 to +16 relative to the translational start site. To test the importance of this secondary binding site with respect to CsrA binding, the intergenic 5'-*lcrF* fragment was prolonged by 60 nt at the 3'-end and binding of this fragment was compared to the shorter 5'-*lcrF* fragment, in which parts of the putative low-affinity binding site were missing (**Fig. 3.15C**). CsrA displayed only a weak affinity to the shorter 5'-*lcrF* fragment, while the prolonged 5'-*lcrF*_long transcript was already bound at lower CsrA concentrations (**Fig. 3.15E**). These results indicate that CsrA specifically interacts with multiple sites of the *yscW-lcrF* mRNA. Especially, the *yscW* 5'-UTR was bound with a somewhat high affinity probably due to multiple high-affinity binding sites (**Fig. 3.15B**). The observation of a secondary, low affinity 'AGAGA' motif, 24 nt apart from the 'AGGA' motif in the RBS, was unexpected as low-affinity motifs were previously only identified in close vicinity (less than 10 nt) to a neighboring high-affinity CsrA binding site.

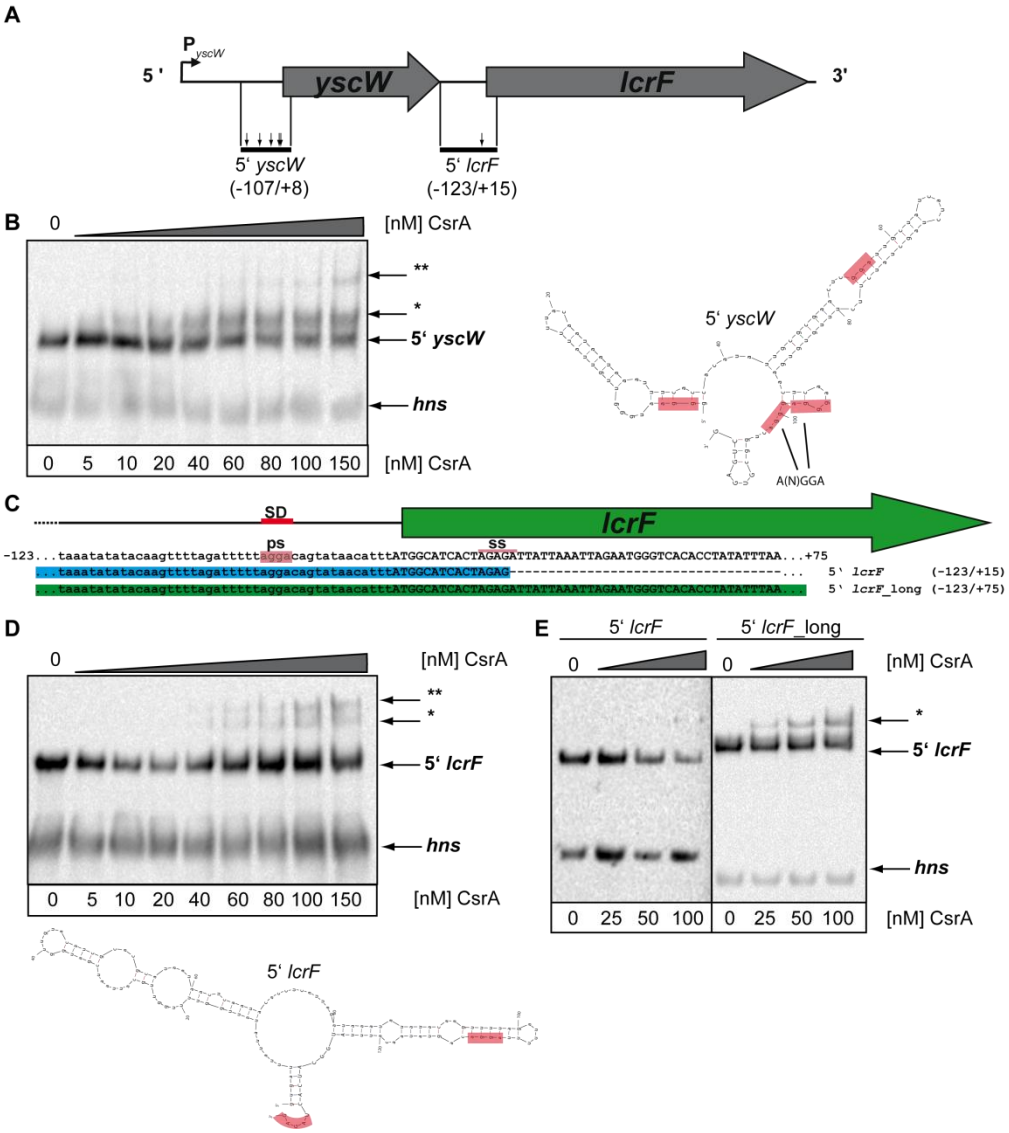

Figure 3.15: CsrA interacts with multiple sites of the *yscW-lcrF* transcripts. (**A**) Schematic presentation of the *yscW-lcrF* gene locus of *Y. pseudotuberculosis* showing the P_{yscW} promoter (broken arrows) and the *yscW* and *lcrF* gene (block arrow). The *in vitro* transcribed RNA fragments used in RNA-EMSA are depicted below. Putative CsrA binding sites are indicated (vertical arrow). The region of the RNA fragments is indicated relative to the translational start site of the corresponding gene. (**B**+**DE**) Binding of CsrA to regions of *yscW* and *lcrF* was analyzed by RNA-EMSAs. Parts of the *yscW* 5'-UTR, *lcrF* 5'-UTR and the *hns* control fragment were *in vitro* transcribed and biotin-labeled. 2 nM of the resulting *yscW*, *lcrF* and the *hns* control fragment were incubated with increasing concentrations of CsrA, separated onto a native 7% TBE-PAA gel and the biotin-labeled RNAs were visualized after transfer to a nitrocellulose membrane. Higher molecular bands, as a result of CsrA-RNA binding, are indicated with asterisks. *In silico* prediction of the secondary structure of the 5'-UTR of *yscW* and *lcrF* with the lowest free energy (mFold [Zuker, 2003]) are presented below. CsrA binding sites are indicated (light red boxes). (**C**-**E**) A secondary low-affinity binding motif is needed for efficient CsrA binding of the *lcrF* 5'-UTR**.** (**C**) Schematic presentation of the *lcrF* gene locus of *Y. pseudotuberculosis* showing the CsrA binding sites (light red box; ps - primary high-affinity binding site; ss - secondary low-affinity binding site), the Shine-Dalgarno sequence (SD; red box) and parts of the *lcrF* gene (green arrow).

3.16 The status of the *lcrF* RNA-thermometer influences binding of CsrA

The CsrA binding site in the intergenic region between the *yscW* and *lcrF* gene directly overlaps with the RBS of *lcrF*. Interestingly, the RBS base pairs with a regulatory 'four U'

motif. Since the RBS is incorporated into the thermosensitive stem-loop structure at low temperature (25 °C), also the access of CsrA to its binding motif is blocked. To investigate whether a 'closed' or 'open' thermo loop influences CsrA binding, a wild-type 5'-*lcrF* RNA fragment (5'-*lcrF*; see **Fig. 3.16**) and fragments containing substitution mutations in the 'four U' motif were *in vitro* transcribed, biotinylated and were compared for CsrA binding in RNA-EMSA. In the 'open' fragment, the 'UUUU' motif was changed to an 'AAAU' sequence that results in an opening of the thermo loop (5'-*lcrF* open). In the second fragment, the 'four U' motif was changed to 'UGGU' resulting in a perfect complementarity to the RBS and a closed thermo loop (5'-*lcrF* closed) [Steinmann, PhD thesis].

When comparing the wild-type 5'-*lcrF* RNA fragment to the one with the open mutation, no difference in the CsrA RNA binding capabilities of CsrA could be observed. In contrast, CsrA binding to the 5'-*lcrF* transcript with the 'closed' mutation was strongly inhibited as no shift appeared (**Fig. 3.16**). This indicates that CsrA binds to the 'AGGA' motif of the RBS and influences its opening state and subsequent translation.

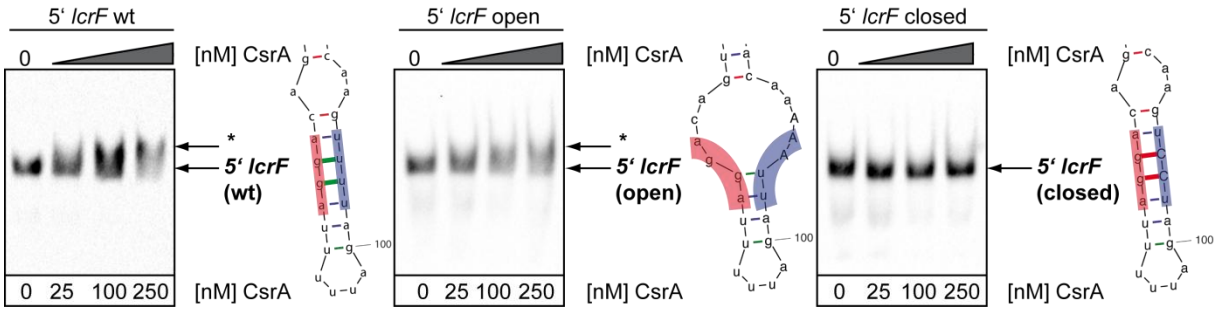

Figure 3.16: CsrA interaction with the *lcrF* 5'-UTR depends on the opening state of the RNA thermometer. Binding of CsrA to the untranslated region of *lcrF* with a wild-type (YPIII) or mutated 'four U' motif (open - YP83; closed - YP84) was analyzed by RNA-EMSAs. The 'four U' motif was either mutated to destabilize (open; *lcrF*(GUU-30/-28AAA)) or to stabilize (closed; *lcrF*(UU-28/-27CC)) base pairing with the ribosomal binding site. Parts of the *lcrF* 5'-UTR was *in vitro* transcribed and biotin-labeled. 2 nM of the resulting *lcrF* was incubated with increasing concentrations of CsrA, separated onto a native 5% TBE-PAA gel and the biotin-labeled RNAs were visualized after transfer to a nitrocellulose membrane. Higher molecular bands, as a result of CsrA-RNA binding, are indicated with asterisks. Cropped *in silico* prediction of the secondary structure of the *lcrF* RNA thermometer of the wild-type and the open and closed 'four U' motif mutants with the lowest free energy (mFold [Zuker, 2003]) are presented next to the corresponding RNA-EMSA. The position of the CsrA binding site (light red) and the 'four U' motif (light blue) are indicated.

3.17 CsrA and YopD influence the stability of the *yscW-lcrF* transcript

Both YopD and CsrA are able to directly bind to the *lcrF* transcript. Previous results indicated that deletion of *csrA* only slightly affected *lcrF* mRNA stability although the overall transcript level was induced [Opitz, PhD thesis]. In contrast, the *lcrF* mRNA stability increased in a *yopD*-deficient mutant strain [Steinmann, PhD thesis]. Considering that YopD is also required

for efficient CsrA synthesis (**Fig. 3.10**), absence of YopD decreases the CsrA-dependent influence on *lcrF* transcript stability. To overcome the combinatory effects of YopD and CsrA on *lcrF* mRNA stability, the *lcrF* half-life was compared between the wild-type strain YPIII, the *yopD* mutant (YP91), the *csrA* mutant (YP53) and the *yopD/csrA* double mutant (YP145) using an RNA stability assay. The strains were grown under T3SS-inducing conditions for 2 h at 25 °C following a shift to 37 °C for 4 h. Transcription was stopped by adding rifampicin and *lcrF* transcript levels were assessed by northern blot analysis (**Fig. 3.17A**). The *lcrF* transcript level was generally very low in the wild-type, while in the *yopD* mutant and the *csrA* mutant high mRNA levels were detectable at time point zero. In the wild-type, a low RNA half-life of approximately 3 min could be detected. In the absence of *yopD*, the *lcrF* transcript is strongly stabilized. In contrast, the *lcrF* transcript was considerably destabilized in the *csrA* deficient mutant in comparison to the wild-type. The absence of both RNA binding proteins (*yopD*/*csrA*) led to an intermediate *lcrF* stability. Quantification of the transcript further showed that the *lcrF* transcript was more stable in the double mutant than in the wild-type, but less stable than in the *yopD* deficient mutant (**Fig. 3.17B**). These results demonstrate, that the transcript stability of *lcrF* is influenced by both RNA-binding proteins. The presence of YopD destabilizes, while CsrA stabilizes the *lcrF* transcript.

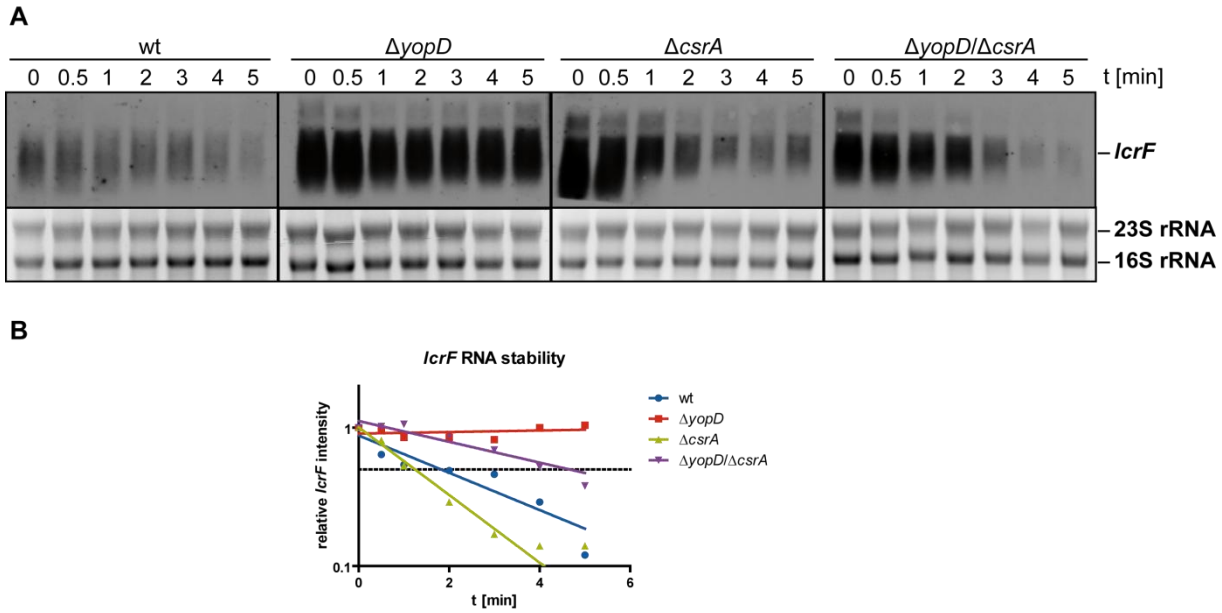

Figure 3.17: Influence of YopD and CsrA on transcript stability of the *yscW-lcrF* operon. (**A**) RNA stability assay of wild-type (YPIII), *yopD* mutant (YP91), *csrA* (YP53) and *yopD*/Δ*csrA* (YP145) mutant to determine the stability of the *lcrF* transcript. All strains were grown in LB medium for 2 h at 25 °C following a shift to 37 °C for 4 h and transcription was stopped by addition of rifampicin to a final concentration of 1 mg/mL. Samples were taken before the addition of rifampicin (0) and then 30 s, 1 min, 2 min, 3 min, 4 min and 5 min after the transcription stop. The total RNA was isolated, 10 µg of total RNA per lane were separated and the *lcrF* transcript was detected by northern blot analysis using a *lcrF* specific DIG-labeled DNA probe. The 16S and 23S ribosomal RNA was stained with ethidium bromide and served as a loading control. (**B**) Northern blots were documented and quantified using the ImageJ software. Data are presented as the relative *lcrF* intensity (*lcrF* intensity/RNA intensity) over time on a half-logarithmic scale (Experiment in cooperation with M. Pimenova).

3.18 YopD and CsrA influence expression of RNA degradosome components

Previously an involvement of RNA degradosome components in the regulation of *Yersinia* virulence and Ysc-Yop expression was demonstrated. In *Y. pestis* RNase E and PNPase were found to be required for the expression of the Ysc-Yop-T3SS and virulence in mouse infection. A *pnp* deficient strain is severely attenuated in a mouse infection model. Furthermore, RNase E is required for optimal function of the T3SS and virulence, as evidenced by reduced virulence in macrophage infection in cell culture and Yop secretion [Lawal *et al*., 2011; Rosenzweig & Schesser, 2007; Yang *et al*., 2008]. Recent results demonstrated that PNPase inhibits synthesis of the virulence master regulator LcrF. Furthermore, *rne* and *pnp* transcript levels are strongly reduced in a *yopD* mutant strain [Steinmann, PhD thesis]. A recent study in *E. coli* indicated CsrA represses *pnp* expression by decreasing transcript stability and protein synthesis [Park *et al*., 2015]. As both YopD and CsrA are regulators of *rne* and *pnp*, their influence on other components of the RNA degradosome was investigated by qRT-PCR analysis in the wild-type strain YPIII, the *yopD* mutant, the *csrA* mutant and the *yopD*/*csrA* double mutant strain. All strains were grown under T3SS-inducing conditions for 2 h at 25 °C and then shifted to 37 °C for 4 h in the presence of Ca^{++} or under Ca^{++}-depletion to induce Yop-secretion. The amount of all degradosome-associated transcripts decreased under secretion conditions in the wild-type. Also, the deletion of *yopD* led to a strong reduction of all degradosome-associated transcripts, irrespective of the secretion status. In the *csrA* mutant strain, the secretion induced downregulation of degradosome transcripts was completely abolished, as no significant changes in transcript levels in comparison to the wild-type could be observed. Only a small reduction of *rne* transcript levels could be detected in the *yopD*/*csrA* mutant under non-secretion conditions while other degradosomal transcript levels were unchanged (**Fig. 3.18**). In summary, levels of multiple degradosomal transcripts are repressed under secretion conditions (calcium depletion). In absence of *yopD*, all tested degradosome transcripts decreased, whereby secretion had no further effect indicating that YopD stabilizes degradosome transcripts. This effect is abolished by secretion of YopD. Additionally, a *csrA* mutant is defective in Yop secretion [Opitz, PhD thesis)] leading to an accumulation of YopD in the cell even under secretion conditions, which in turn increases production of

degradosome components. In absence of *yopD* and *csrA*, degradosomal gene levels were only slightly decreased indicating the effect of CsrA abolishes the YopD effect.

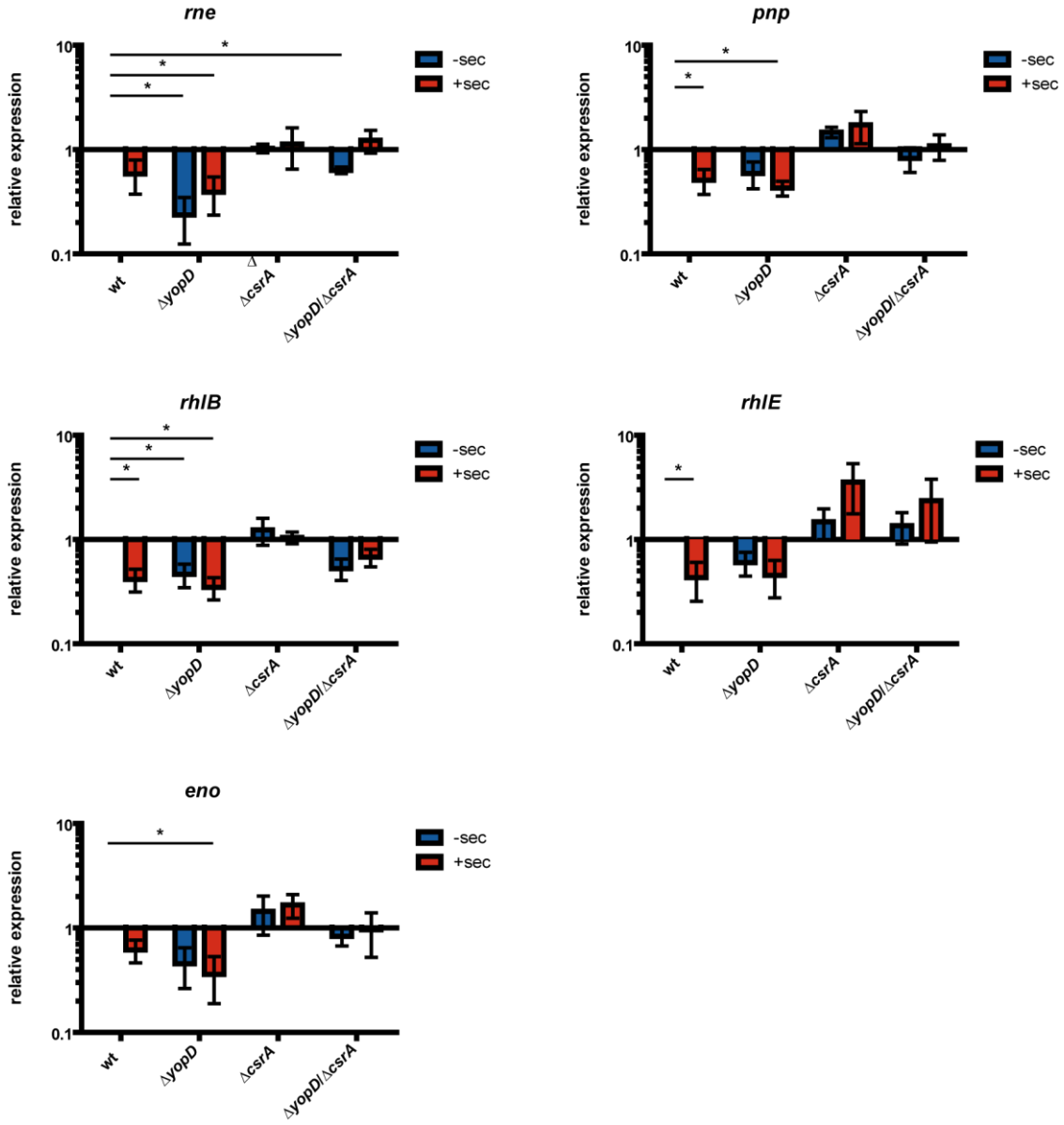

Figure 3.18: Influence of CsrA and YopD on the expression of degradosome components. The one-step real-time qRT-PCR analysis was performed with specific primers for degradosomal core components and associated factors. All strains were grown in LB medium for 2 h at 25 °C. Then secretion was induced by adding NaOx and $MgCl_2$ (+sec) or not (-sec) after a shift to 37 °C for 4 h. The total RNA of the wild-type (YPIII), *yopD* (YP91), *csrA* (YP53) and *yopD/csrA* (YP145) mutant strain was isolated and used for qRT-PCR. The analysis was performed in at least 3 biological and 2 technical replicates. Transcript levels were normalized to the *sopB* reference transcript and are shown as relative expression levels to the wild-type (YPIII) under non-secretion conditions. Data were analyzed by applying a one sample t-test with * ($P < 0.05$).

3.19 CsrA target identification and analysis

The RNA-binding protein CsrA is a global regulator in many bacteria. In *Yersinia*, CsrA has a huge regulon of at least 500 open reading frames as demonstrated in *csrA* microarray and

transcriptome analyses [Bücker *et al*., 2014; Nuss, unpublished data]. As demonstrated in this study, CsrA is an important regulator of virulence-associated genes. The global regulatory role of CsrA has been studied in different Gram-negative bacteria, like *Salmonella typhimurium*, *Pseudomonas aeruginosa* and *E. coli* by differential RNA-Seq analysis [Esquerre *et al*., 2016], interactome studies [Holmqvist *et al*., 2016; Edwards *et al*., 2011] and an *in silico* target prediction [Kulkarni *et al*., 2014]. Recently, the CsrA-dependent regulon in *Y. pseudotuberculosis* at 25 °C and 37 °C has been identified by a comparative RNA-Seq approach [Nuss, unpublished data].

3.19.1 *In silico* prediction of CsrA targets in *Y. pseudotuberculosis*

Most probably not all CsrA-dependent genes are directly targeted by CsrA. To identify directly regulated CsrA target genes, an *in silico* CsrA target prediction was applied, combined with an analysis of the CsrA regulon of *Y. pseudotuberculosis*.

The RNA features that are recognized by CsrA are well characterized and parameters affecting the binding affinity could be identified. The 5'-UTR of high-affinity targets carry multiple high-affinity (ANGGA or AGGA) or low-affinity binding motifs (AGAGA, CTGGA, CGGGA, TGGGA) within a maximal distance of 60 nt. Additionally, at least one of these high-affinity motifs overlaps with the RBS [Dubey *et al*., 2005; Lapouge *et al*., 2013; Duss *et al*., 2014].

By using these parameters, high-affinity targets were predicted by analyzing the upstream region of all annotated coding genes in *Y. pseudotuberculosis* YPIII. Based on an algorithm published by Kulkarni *et al*. to predict CsrA target sequences in *E. coli*, *P. aeruginosa* and *S. typhimurium*, the upstream target regions of all 4306 annotated ORFs encoded on the *Y. pseudotuberculosis* YPIII chromosome (NC_10465) were extracted and analyzed by a self-written Python script (CSRA_TARGET_PREDICTER). Since CsrA is known to especially target the 5'-UTR of target sequences, thereby influencing RNA stability or translation initiation, the region from 150 nt upstream to 60 nt downstream of the translational start site (-150 to +60) of coding genes was isolated and analyzed for CsrA binding sites.

In this algorithm, the most important features for a high-affinity CsrA target RNAs were defined as: (1) The analyzed RNA sequence must have at least one primary binding site present in the vicinity of the ribosomal binding site (-30 to +5 nt relative to the start codon). (2) The RNA sequence harbors at least three CsrA binding sites in total (primary (ps) or secondary (ss) binding sites). (3) The target sequence contains at least three primary binding sites (ps >= 3) or two if at least two additional secondary binding sites (ps = 2 and ss >= 2) are

present in the vicinity of the primary motifs. This is important because low-affinity motifs, which are in the vicinity to a primary binding site, support binding of CsrA to a primary motif [Kulkarni *et al*., 2014]. (4) Finally, as CsrA dimers were demonstrated to bridge two motifs with a spacing of up to 60 nt, all CsrA binding sites neighboring another binding site in a distance of 10 to 60 nt were counted. All genes with at least two of these binding sites were defined as putative CsrA targets.

The analysis led to the identification of 233 putative direct CsrA targets (**Fig. 3.19A**; **table S2)**. Considering that direct CsrA targets are also part of the CsrA regulon, the 233 *in silico* predicted CsrA target genes were compared to the CsrA regulon at stationary phase 25 °C or 37 °C and a genomic distribution analysis was performed to identify genomic regions with CsrA target gene clusters **(Fig. 3.19BC**). Only differentially regulated genes that were at least four times depleted/enriched (-2 >= log2(fc) >= 2) were considered as part of the CsrA regulon.

The analysis revealed 32 *in silico* predicted direct targets that were also differentially regulated at 25 °C and 23 *in silico* predicted CsrA target genes being differentially regulated at 37 °C (**Fig. 3.19D**). Confirming the approach, *csrA* was identified which is known for its direct autoregulation. Interestingly, the genomic distribution analysis highlighted four genes that were highly differentially expressed at 25 °C, *in silico* predicted and clustered closely together on the genome (YPK_0389 - *impG*/*vasA*; YPK_0391 - *impI*/*vasC*; YPK_0393 - *impJ*/*vasE*) (**Fig. 3.19B**). These genes are part of the type six secretion system 1 (T6SS-1) and were at least 8 times (log2(fc) > 3) enriched in a *csrA* negative mutant in comparison to the wild-type [Nuss, unpublished data].

Noteworthy, the T6SS-4 associated gene *rovC*, was also identified as a putative direct CsrA target by this analysis. *rovC* was *in silico* predicted and is highly upregulated at 25 °C in the absence of *csrA*. The *rovC* gene (YPK_3567) encodes a transcriptional regulator of the T6SS-4 and is a known direct target of CsrA [Knittel, Master thesis]. Surprisingly, additional T6SS-4 genes were predicted as direct CsrA targets (YPK_3556, YPK_3552, YPK_3550, YPK_3566, YPK_3564) (**Table S2**), but are not differentially regulated by CsrA at stationary phase 25 °C or 37 °C. Furthermore, the prediction revealed two genes belonging to the T6SS-2 (YPK_1472 (uncharacterized ImpH/VasB protein), YPK_1475 (fimbrial precursor protein)) (**Table S2**). All these T6SS genes are not differentially regulated in absence of *csrA* because they are not expressed by *Y. pseudotuberculosis* when grown in LB medium to stationary phase at 25 °C or 37 °C. Nonetheless, these genes might be regulated and directly targeted by CsrA under other conditions.

Another differentially regulated mRNA and predicted direct target of CsrA was *rovA* (**Fig. 3.19B**). The *rovA* gene encodes an important transcriptional regulator of early virulence genes. Expression of *rovA* was previously shown to be regulated by CsrA. However, this regulation occurred indirectly via CsrA-mediated control of *rovM*, a direct repressor of *rovA* transcription [Heroven *et al*., 2008]. The 5'-UTR of *rovA* contains six GGA motifs (three high-affinity motifs). This might indicate, that CsrA can also directly regulate *rovA* expression. Another virulence-associated gene that was *in silico* predicted and found to be CsrA-dependent regulated at 37 °C was *yadC* that encodes a putative adhesin (**Fig 3.19C**).

In summary, by comparing the list of predicted direct CsrA targets with the set of differentially regulated genes, new possible direct CsrA target genes could be identified. Interestingly, among them are genes of three different T6SSs (T6SS-1, T6SS-2 and T6SS-4). Furthermore, the transcriptional regulator of early virulence *rovA* might be directly targeted by CsrA. Taken together, besides CsrA's role as a regulator of metabolism, these results emphasize the role of CsrA as a direct regulator of virulence systems, especially T6SSs, in *Y. pseudotuberculosis*.

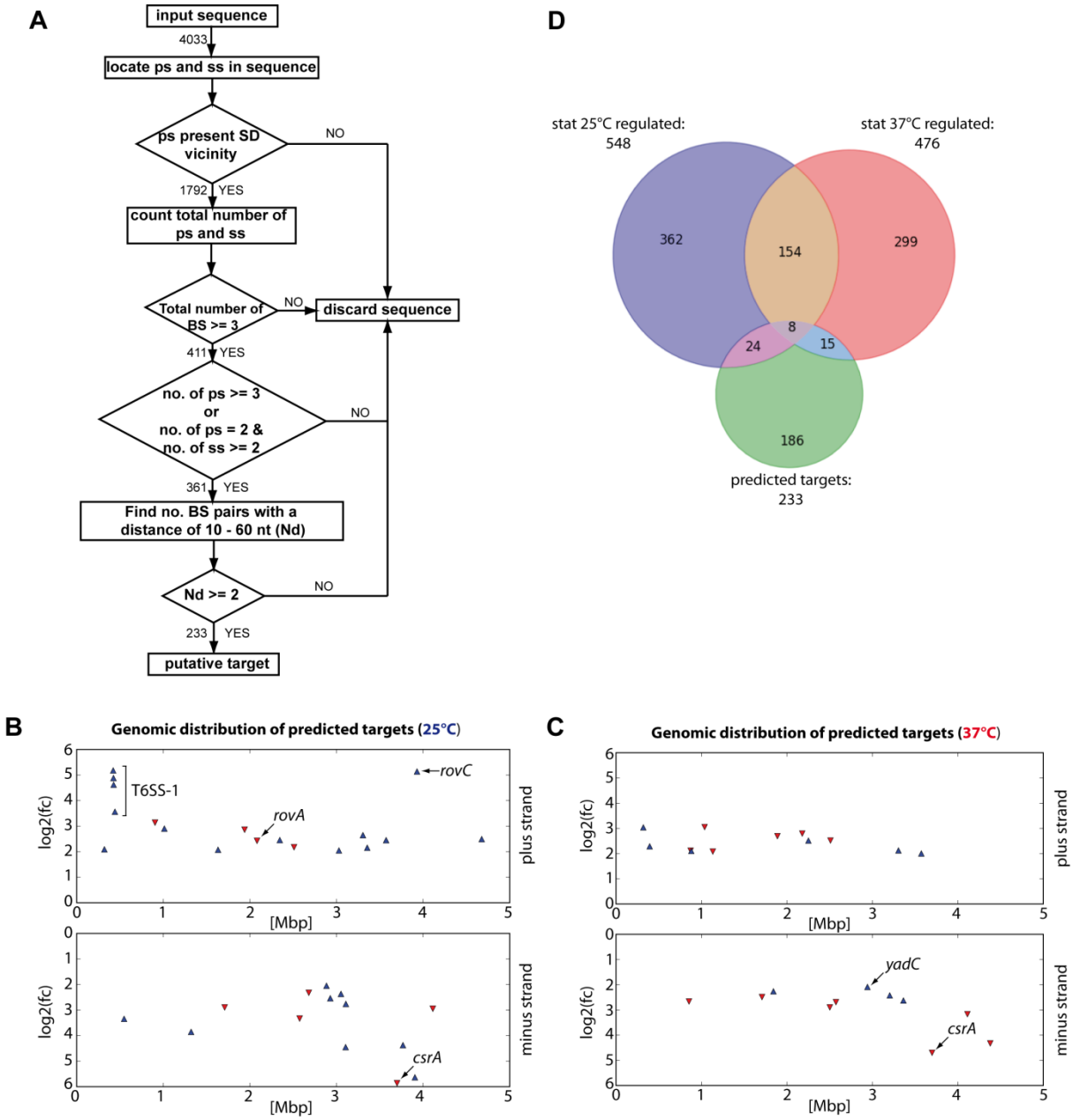

Figure 3.19: CsrA is a direct regulator of multiple T6SS. (**A**) Flowchart of the CsrA target prediction algorithm CSRA-TARGET_PREDICTER of *Y. pseudotuberculosis* YPIII [adopted from Kulkarni *et al*., 2014]. 4033 upstream regions of YPIII chromosomally encoded ORFs were analyzed for CsrA primary sites (ps; A(N)GGA) and secondary sites (ss; AGAGA, CTGGA, CGGGA, TGGGA). The number of analyzed and processed sequences are depicted next to flow line arrows. (**B**+**C**) Genomic distribution of predicted high-affinity CsrA targets, which are differentially regulated by *csrA* in stationary phase at 25 °C (**B**) or 37 °C (**C**). CsrA-dependent regulated, predicted genes are depicted with their log2(fc) versus their localization [Mbp] on the plus (upper panel) or minus strand (lower panel). Upregulated genes in a *csrA* (YP53) mutant are marked with a blue up-pointing triangle and down-regulated genes are marked with a red down-pointing triangle. (**D**) Venn diagram showing the comparison of *in silico* predicted genes and *csrA*-dependent differentially regulated genes at stationary phase 25 °C or 37 ° (regulon: -2 >= log2(fc) >= 2).

3.19.2 CsrA RIP-Seq

The combined analysis of *in silico* predicted, direct CsrA targets and the CsrA regulon already gave the first insight into CsrA's role at 25 °C. CsrA is an important regulator of virulence at body host temperature (37 °C) and influences the expression of the injectisome. To identify

direct targets that are crucial for *Yersinia* virulence under T3SS-inducing conditions (37 °C) an RNA-binding protein immunoprecipitation sequencing (RIP-Seq) analysis was performed. A *Y. pseudotuberculosis* YPIII wild-type strain expressing a plasmid-encoding *csrA*-3xFLAG gene under control of the *csrA* promoter (P_{csrA}::*csrA*-3xFLAG; pJH35; IP sample) or containing a plasmid control (pHSG576; background control sample) were grown under T3SS-inducing conditions. Cells were lysed and CsrA-bound RNAs were extracted by hot phenol RNA extraction after CsrA immunoprecipitation (IP) with anti-FLAG IgG-coupled magnetic beads. Purified RNAs were then analyzed by high throughput RNA-Sequencing. The IP resulted in a very pure CsrA elution fraction (**Fig. 3.20A**). Only the immunoglobulin IgG heavy and light chain were copurified in the control setup, while an additional CsrA-3xFLAG band appeared in the IP sample (**Fig. 3.20A**). Furthermore, in western blot analysis, only wild-type CsrA and an unspecific band could be detected in the control sample, that disappeared in the wash fractions. In the IP sample, CsrA-3xFLAG was detectable in the lysate and eluate fraction. Additionally, a fraction of untagged CsrA was co-immunoprecipitated most probably as part of a CsrA-CsrA-3xFLAG heterodimer (**Fig. 3.20A**). RNA sequencing of cDNA libraries of at least four samples per condition resulted in 18 - 25 million reads per sample (**Table S3**). The global gene expression patterns of control and IP samples were distinct and the related samples clustered together (**Fig. 3.20B**). The mapping analyses also revealed a specific enrichment of RNAs by the IP. 35% of total reads could be uniquely mapped in the IP samples, in comparison to only 4% in the control samples (**Fig. 3.20C**). Other reads (not uniquely mapped) originate from multiple copy genes like ribosomal RNAs, tRNAs and primer dimers. Additionally, reads in the control samples equally mapped to the plus and minus strand, while the IP lead to an enrichment of reads to the minus strand (**Fig. 3.20D)**. This shift corresponded to an enrichment of the small non-coding RNAs *csrB* and *csrC* by CsrA. Both small RNAs represented the most enriched RNAs in all IP samples. Especially, *csrC*, which is encoded on the minus strand and the most abundant ncRNA of the Csr system under T3SS-inducing conditions, was four times more enriched than *csrB*, which is encoded on the plus strand, explaining the shift to the minus strand.

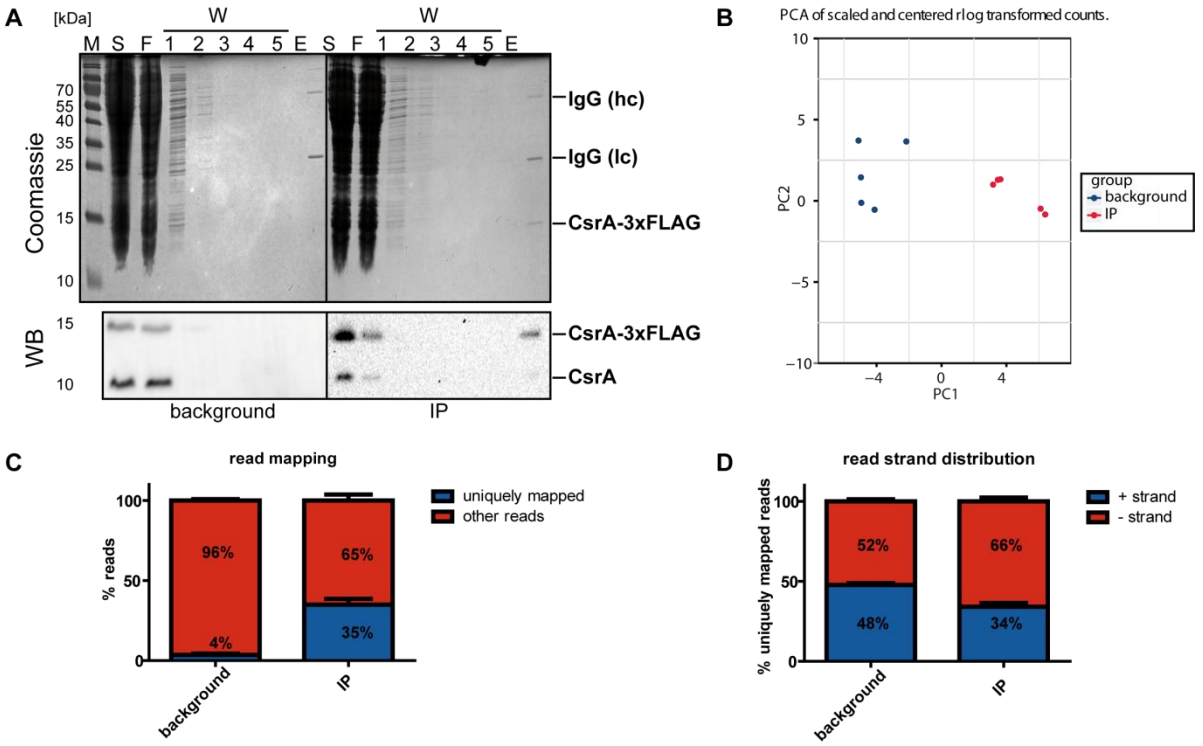

Figure 3.20: Immunoprecipitation of CsrA-enriched RNAs. (**A**) Coomassie blue-stained SDS-PAGE and western blot analysis of CsrA immunoprecipitation by Anti-FLAG affinity chromatography. The *Y. pseudotuberculosis* YPIII wild-type was either transformed with a *csrA*$^{+}$ expressing vector (background; pKB60) or *csrA*-FLAG^{+} expressing vector (pJH35). Strains were grown in LB medium for 2 h at 25 °C and subsequently shifted to 37 °C for 4 h. Following this, cells were harvested, lysed and the resulting lysates were used for CsrA immunoprecipitation using Anti-FLAG dynabeads. Supernatant (S); wash fraction (W1-5); eluate fraction (E1-6). An OD_{600} equivalent of 0.5 was used for SDS-PAGE following a Coomassie blue stain or western blot analysis using a polyclonal α-CsrA rabbit serum. (**B**) Principal component analysis (PCA) plot of IP (red) and the control (blue; background) samples after RNA-Seq. (**C**) Read mapping analysis. Depicted is the mean percentage of uniquely mapped (blue) or other reads (red) relative to all mapped reads. (**D**) Analysis of the mean relative strand distribution of uniquely mapped reads of control or IP samples to the + (blue) or - (red) strand.

3.19.3 Identification of direct CsrA targets in *Y. pseudotuberculosis*

The RIP-Seq analysis revealed a total of 1743 enriched target RNAs with an enrichment of at least 8 fold (log2(fc) > 3) after pull-down of CsrA (**Fig. 3.21A; Table S4)**. From these RNAs, 1248 corresponded to coding mRNAs, 29 trans-, 16 antisense encoded RNAs and 19 tRNAs. Under the 20 most enriched target RNAs, both non-coding RNAs *csrB* (log2(fc) = 6.6) and *csrC* (log2(fc) = 5.8) were identified. This result was expected as these ncRNAs harbor many exposed CsrA binding motifs and function as a molecular sponge to sequester CsrA proteins [Romeo *et al.*, 2012]. Additionally, the *csrA* mRNA could be found under the 20 mostly enriched RNAs (log2(fc) = 6.3). Since CsrA directly interacts with its transcript with a high binding affinity, this indicates a specific enrichment (**Fig. 3.6**) [Yakhnin *et al.*, 2011]. To analyze the genomic distribution of the enriched transcripts, the mean of normalized reads (rpk (reads per kbp gene length)) of the IP or the background (control) samples were plotted corresponding to their genomic location (**Fig. 3.21B**). Although, the 5S, the 6S and the 16S

rRNA were depleted, apparently, almost every RNA was enriched by the CsrA IP. Due to the high sensitivity of the RNA-Seq method, this could point to an overrepresentation of unspecifically bound transcripts in the control sample (**Fig. 3.21B**). Furthermore, the CsrA RIP-Seq enriched three times more potential CsrA target candidates (~1700 targets) than present in the CsrA regulon (~500 targets), corresponding to previously published *csrA* microarray and transcriptome data [Bücker *et al*., 2014; Nuss, unpublished data]. This also indicates enrichment of RNAs that are unspecifically bound by CsrA, probably due to overexpression of CsrA or insufficient washing.

To get an idea of specific CsrA-bound RNAs, enriched transcripts of the interactome analysis (**see chapter 3.19.2**) were compared to the CsrA-transcriptome dataset [Nuss, unpublished data]. For the CsrA regulon data set, only RNAs which were at least four times enriched or depleted (-2 >= log2(fc) >=2) were considered. At 25 °C and 37 °C 548 and 476 genes were differentially regulated, respectively (**Fig. 3.21C**). Of these genes, 292 CsrA-dependently regulated genes overlapped with the interactome (**Fig. 3.21C**; **Table S4)**. This overlap corresponds to 16% of the interactome. These candidates might reflect direct targets of CsrA. As part of the mostly IP-enriched transcripts of the CsrA interactome/regulon overlap, the known direct CsrA target transcripts *csrA*, *csrB* and *csrC* could be identified. Additionally, a high number of tRNAs and the M1 RNA of RNase P were also highly enriched. RNase P is an endoribonuclease that is involved in the maturation process of precursor tRNAs to mature tRNAs [Altman, 1975; Evans *et al*., 2006]. These results highlight the role of CsrA as a modulator of the cellular tRNA landscape.

Finally, the interactome data set was compared with the list of *in silico* predicted, and differentially regulated genes to more specify direct high-affinity targets. This analysis revealed 47 differentially regulated, predicted coding genes (25 °C: 32 genes; 37 °C: 23 genes) and 97 predicted genes that were identified by the RIP-Seq analysis (**Fig. 3.21D; Table S4**). Only 6 genes could be identified as being predicted, differentially regulated at both temperatures and enriched in the RIP-Seq analysis. These genes, besides *csrA* itself, all encoded metabolism-associated regulators enzymes or transporters, like *ulaB* (ascorbate-specific phosphotransferase enzyme subunit IIB component), *ggt* (Gamma-glutamyltranspeptidase) and *miaB* which encodes a tRNA-modifying enzyme. Remarkably, overlapping with the 25 °C regulon, the predicted CsrA target and T6SS-1 gene YPK_0393 and the early virulence regulator gene *rovA* were also enriched in the RIP-Seq, besides *treB* (trehalose-specific PTS enzyme) and the putative chemotaxis protein *yoaH* (methyl-accepting

chemotaxis protein). Although unaffected by CsrA at 37 °C, *rovA* was enriched in the RIP-Seq, this might indicate expression of *rovA* is influenced by CsrA even at 37 °C.

These results are in compliance with CsrA's role as a global regulator of metabolism and virulence. Since CsrA regulates and possibly directly targets tRNA and tRNA-associated genes at 37 °C, it might remodel the tRNA landscape to prepare the bacterial cell for the expression of the Ysc-Yop T3SS and the conditions inside the warm-blooded host. The comparative analysis of CsrA RIP-Seq data with comparative RNA-Seq and *in silico* CsrA target prediction data revealed only a small overlap suggesting that the list of direct CsrA targets in *Y. pseudotuberculosis* still needs to be completed. The *in silico* prediction analysis gave the first overview of putative direct CsrA targets and can support but not replace the experimental validation. For that reason, the *in silico* prediction algorithm still needs to be optimized.

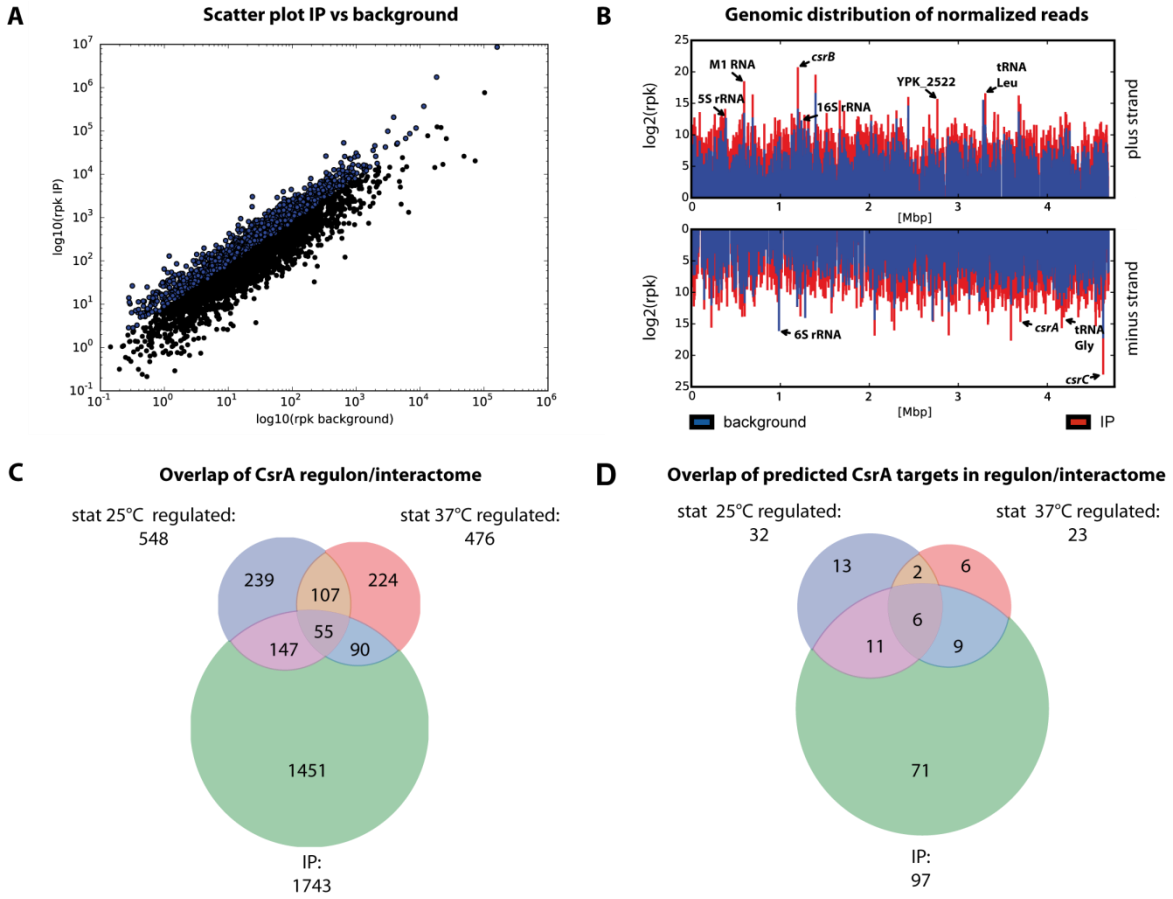

Figure 3.21: Enrichment of putative CsrA interacting RNAs. (**A**) Scatter plot of the $\log_{10}$ mean rpk values of genes from control or IP samples. Genes with a log2(fc)> 3 are represented as blue dots, other genes are depicted in black. (**B**) Genomic distribution of chromosomally encoded genes of control (blue) or IP (red) samples. Depicted are $\log_2$ rpk (reads per gene length [kb]) values versus chromosomal position [Mbp] of all chromosomally encoded genes of YPIII. Genes encoded on the plus strand are shown on the upper panel, while minus strand encoded genes are shown on the lower. (**C**) Venn diagram showing the comparison of genes enriched in CsrA RIP-Seq (interactome: log2(fc) > 3) and the *csrA*-dependent differentially regulated genes at stationary phase 25 °C or 37 ° (regulon: -2 >= log2(fc) >= 2). (**D**) Venn diagram showing the comparison of *in silico* predicted genes enriched in CsrA RIP-Seq (interactome: log2(fc) > 3) and the *csrA*-dependent differentially regulated genes at stationary phase 25 °C or 37 ° (regulon: -2 >= log2(fc) >= 2).

3.19.4 *In silico* prediction of CsrA targets in *Y. pseudotuberculosis* and *E. coli*

A comparative analysis of the *in silico* CsrA target prediction data set by Kulkarni *et al.* of *E. coli*, *S. typhimurium* and *P. aeruginosa* [Kulkarni *et al*., 2014] revealed only a small overlap of predicted CsrA target genes. Apparently, a comparison of CsrA regulons and interactomes of *S. typhimurium*, *E. coli* and *Y. pseudotuberculosis* confirmed this observation (data not shown) [Edwards *et al*., 2011; Holmqvist *et al*., 2016; Esquerre *et al*., 2016; Nuss, unpublished data]. These differences probably originate from the phylogenetic distance of these organisms. Still, CsrA regulates similar cellular processes in all these bacteria (e.g. metabolism, motility, stress responses, information processing) [Heroven *et al*., 2012; Vakulskas *et al*., 2015].

In order to identify the evolutionary mechanism behind the diversification of the CsrA regulon, CsrA targets of *Y. pseudotuberculosis* YPIII and *E. coli* K-12 MG1655 were *in silico* predicted using the CSRA_TARGET_PREDICTER script. The 5'-UTRs of individually predicted targets of *Y. pseudotuberculosis* and *E. coli* were aligned to analyze changes in the CsrA binding site number and distribution. For this purpose, a target prediction in *E. coli* was carried out using the same script and parameters as for the CsrA target prediction in *Y. pseudotuberculosis* (see **chapter 3.19.1**). The upstream region (-150 to +60 nt relative to the translational start site) of all 4147 chromosomally encoded, annotated ORFs in *E. coli* MG1655 (NC_000913) were extracted and putative high-affinity CsrA targets were predicted using the CSRA_TARGET_PREDICTER script. The analysis led to the identification of 275 putative CsrA targets (**Fig. S2**; **Table S2+6)**. This approach was chosen to ensure the comparability of the *E. coli* and *Y. pseudotuberculosis in silico* target prediction data sets (see **chapter 3.19.1**).

Next, the list of predicted CsrA targets in *E. coli* and *Y. pseudotuberculosis* was compared. The predicted CsrA target genes of *E. coli* and *Y. pseudotuberculosis* were assigned by aligning their protein sequences utilizing the blastp command line tool [Camacho *et al*., 2009]. 113 *Y. pseudotuberculosis* ORFs were unassignable to *E. coli*, mostly encoding T6SS-associated and hypothetical genes. This is not surprising as *Y. pseudotuberculosis* YPIII encodes four T6SSs, while the non-pathogenic laboratory *E. coli* strain K12 completely lacks T6SSs [Journet & Cascales, 2015].

Remarkably, only 24 common CsrA target genes were predicted including the *csrA* gene (**Fig. 3.22A**). As the remaining 90% of CsrA target genes were predicted either in *E. coli* or *Y. pseudotuberculosis*, the upstream region of CsrA target genes were further analyzed for differences in the number and distribution of primary and secondary binding site by a ClustalO sequence alignment [Sievers *et al*., 2011]. This analysis demonstrated that CsrA binding motifs in the upstream region are only lowly conserved between *E. coli* and *Y. pseudotuberculosis* explaining the low overlap of targets. Interestingly, the comparison of *in silico* predicted CsrA targets revealed a low conservation of individual target genes, but still genes belonging to the same pathway were identified (see **table 3.1**).

Table 3.1: Selection of predicted CsrA targets in *E. coli* and *Y. pseudotuberculosis* as predicted by the CSRA_TARGET_PREDICTER algorithm

Gene name	Gene description	Pathway
Common targets		
glgB^{R+B}	Glycogen branching protein	Glycogen metabolism
csrA^{R+I}	Carbon storage regulator	Signal transduction
flgG^{R+I}	FtsH protease regulator HflK	Proteolysis
	Flagellar basal body rod protein FlgG	Motility
***E. coli* specific targets**		
glgC^{R+B}	Glucose-1-phosphate adenyltransferase	Glycogen metabolism
aroF^{I}	Phospho-2-dehydro-3-deoxyheptonate aldolase	Amino acid metabolism
ulaD	L-ascorbate utilization protein D	Ascorbate metabolism
fliK^{R+B}	Flagellar hook-length control protein FliK	Motility
fliR^{R}	Flagellar motor switch protein FliN	Motility
***Y. pseudotuberculosis* specific targets**		
glgP-2^{*+I}	Glycogen/starch/alpha-glucan phosphorylase	Glycogen metabolism
glgX*	Glycogen debranching enzyme	Glycogen metabolism
ulaB^{*+I}	Ascorbate-specific PTS system, EIIB component	Ascorbate metabolism
aroE^{I}	Shikimate 5-dehydrogenase	Amino acid metabolism
aroG^{*+I}	Phospho-2-dehydro-3-deoxyheptonate aldolase	Amino acid metabolism
flhB*	Flagellar biosynthesis protein FlhB	Motility
flgC^{*+I}	Flagellar basal body rod protein FlgC	Motility
flgH^{I}	Flagellar L-ring protein FlgH	Motility
motB*	Flagellar motor protein MotB	Motility

^{R} - CsrA-dependent differential regulation in *E. coli* MG1665 [Esquerre *et al*., 2016]
^{B} - Co-purified with CsrA-His_6 in *E. coli* MG1665 [Edwards *et al*., 2011]
* - CsrA-dependent differential regulation on *Y. pseudotuberculosis* YPIII [Bücker *et al*., 2014]
^{I} - Co-purified with CsrA-3xFLAG in RIP-Seq analysis in *Y. pseudotuberculosis* YPIII

Thus, different genes accounted to motility, aromatic amino acid, glycogen and ascorbate metabolism were predicted in both organisms. In more detail, the aromatic amino acid metabolism gene *aroF* was a predicted CsrA target in *E. coli*, while *aroG* was predicted in *Y. pseudotuberculosis*. The *aroF* gene functions upstream of the Shikimate pathway in which *aroE* is involved in. Furthermore, in *Y. pseudotuberculosis*, a component of the ascorbate phosphotransferase system (*ulaB*) was predicted, while in *E. coli* the gene of the ascorbate utilization enzyme UlaD was predicted as a CsrA target, which acts downstream in the ascorbate metabolism. Another example, that showed obvious differences in the number and distribution of CsrA binding sites in both species is the *glgC* gene and other genes of the *glg* operon (**Fig. 3.22BC**). The *glgC* gene encodes the ADP-glucose synthase and is one of the first identified and well-described CsrA-bound target RNAs. For the *glgC* gene are the CsrA binding mechanism as well as the CsrA-bound RNA regions and structures well characterized [Liu *et al*., 1995; Baker *et al*., 2002]. Baker *et al*. demonstrated, that especially the primary binding motif within the ribosomal binding site and the directly upstream located ANGGA motif are involved in the CsrA-dependent *glgC* regulation [Baker *et al*., 2002]. However, only the binding motif within the RBS is present in *Y. pseudotuberculosis*, which indicates a change in the CsrA binding mechanism and might also affect the CsrA binding affinity. Similar observations were made for other genes of *glg* operon (**Fig. 3.22C**). Changes in the CsrA binding site distribution might be the cause for the low comparability of the CsrA regulon in *Enterobacteriaceae*.

The data of this study propose that the CsrA dependency of individual pathways in *Enterobacteriaceae* is conserved rather than individual CsrA target genes. This mechanism might allow a species-specific adaptation.

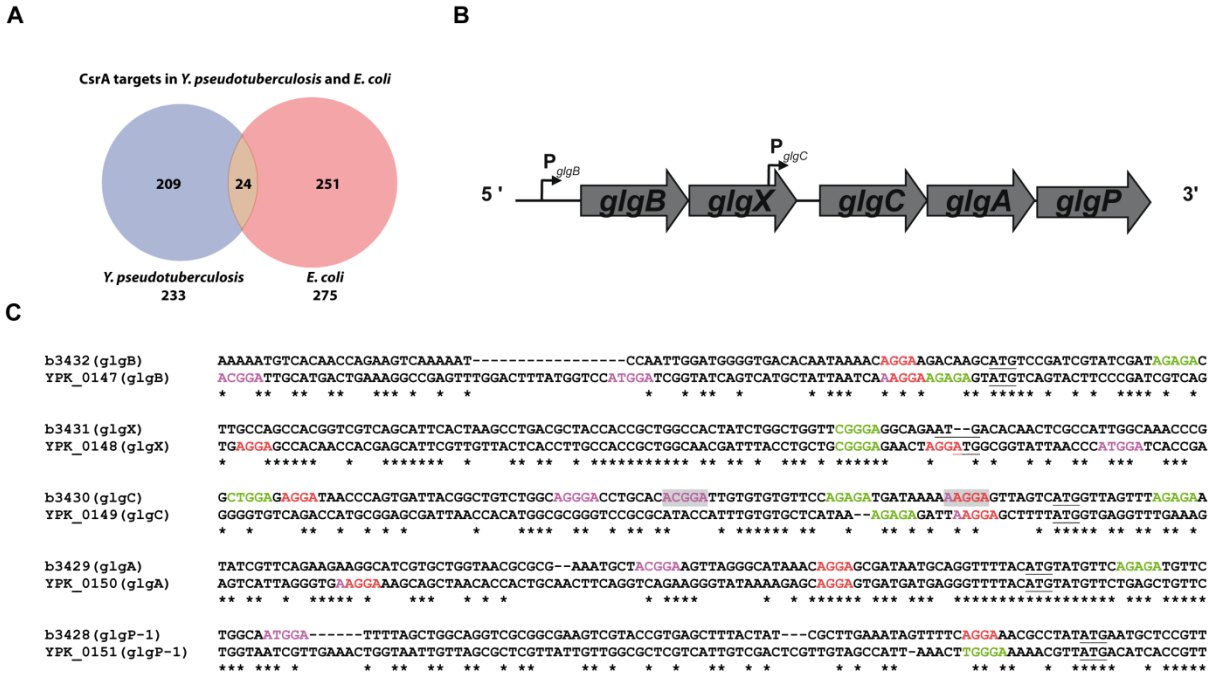

Figure 3.22: Distribution of primary and secondary CsrA binding sites in 5'-UTRs of *glg* genes. (**A**) Venn diagram showing the comparison of chromosomally encoded genes which were *in silico* predicted in *Y. pseudotuberculosis* YPIII and *E. coli* K12. (**B**) Schematic presentation of the *glg* operon of *E. coli* showing the different promoters (broken arrows). (**C**) Sequence alignment of the upstream region of individual *glg* genes from *E. coli* K12 and *Y. pseudotuberculosis* YPIII (ClustalO [Goujon *et al.*, 2010]). High-affinity CsrA binding motifs are marked in violet (ANGGA) or red (AGGA). Low-affinity binding sites are marked in green.

4 Discussion

Y. pseudotuberculosis encodes a vast arsenal of virulence factors, whose expression needs to be timed and coordinated depending on its environment and infection phase. Expression of these virulence factors is resource and energy consuming. Because of this, a complex decision-making system is needed that allows or restricts expression of individual adaptation and virulence systems [Han *et al*., 2016; Somerville & Proctor, 2009; Erhardt & Dersch, 2015]. One of the major virulence factors of *Y. pseudotuberculosis* is the Ysc-Yop T3SS, which is required for colonization of lymphatic tissues and to overcome the host innate immune response. Assembly and maintenance of this nanomolecular machinery are strictly regulated [Portaliou *et al*., 2016]. Thereby, the expression of structural components, as well as, the transcriptional master regulator of the Ysc-Yop T3SS is controlled by the RNA-binding regulators YopD and CsrA in a negative feedback loop. The aim of this study was to analyze the interplay of CsrA and YopD in the regulation of Ysc-Yop T3SS expression.

4.1 Regulation of *csrA* expression in *Y. pseudotuberculosis*

The RNA-binding protein CsrA is the main player in the regulation of a plethora of cellular processes. CsrA is involved in the regulation of metabolism, motility and virulence, such as biofilm formation and the injectisome [Diepold & Armitage, 2015].

In this study, the regulation of *csrA* of *Y. pseudotuberculosis* was examined. Although expression of *csrA* is well-studied in *E. coli*, there is only limited knowledge about *csrA* expression in *Y. pseudotuberculosis*. In *E. coli*, *csrA* is transcribed from five σ^{70} (RpoD)- or σ^{S} (RpoS)-dependent promoters [Yakhnin *et al*., 2011]. In this study, the position of the *csrA* promoters was predicted by a comparative sequence alignment of *Y. pseudotuberculosis* and *E. coli csrA*. Furthermore, *csrA* promoter activity was studied by reporter gene analysis of *csrA'-'lacZ* fusions encoding the different promoters as predicted by sequence alignment of the *csrA* locus. The analysis revealed only promoters P3, P4 and P5 are active at 37 °C during the transition to stationary phase. No activity of the predicted promoters P1 and P2 on the basis of *E. coli* were detectable in *Y. pseudotuberculosis*. Because the region of promoters P1 and P2 is only slightly conserved, these promoters might be *E. coli*-specific and might not be present in *Y. pseudotuberculosis*. Another explanation could be that promoter P1 and P2 of *Yersinia* are not expressed under the tested growth conditions. Indeed, these two promoters

are only and weakly expressed when *E. coli* was grown in minimal medium during stationary phase [Yakhnin *et al*., 2011].

A complex autoregulation of *csrA* and its homolog *rsmA* is described in *E. coli* and *P. aeruginosa*, but in *Y. pseudotuberculosis* and other Gram-negative prokaryotes such an autoregulation was unknown until now [Heroven *et al*., 2012; Syell & Van Melderen, 2013; Jean-Pierre *et al*., 2015]. In this study a direct translational repression of the upstream region and an indirect autoactivation of *csrA*, similar to *E. coli*, was demonstrated by RNA-EMSA binding studies and *csrA'-'lacZ* reporter gene fusions harboring deletions in the autoregulatory regions of *csrA*. Under non-secretory conditions, these opposing autoregulatory effects are nearly compensatory, as a deletion of the *csrA* gene resulted in only a mild repression of a *csrA'-'lacZ* reporter gene fusion encoding the whole regulatory upstream region (Fig. 3.7).

In *Y. pseudotuberculosis* as well as in *E. coli*, the direct negative autoregulation is mediated through two primary CsrA binding motifs (ANGGA motif). The first is located within the RBS of *csrA* and the second in the region of promoters P4 and P5. The 5'-UTR is highly conserved between both species and contains two additional secondary binding motifs, which are bound by CsrA in *E. coli* [Yakhnin *et al*., 2011]. Deletion of the upstream located primary binding motif (ANGGA) obstructed CsrA binding and autorepression, reflecting the importance of this motif (**Fig. 3.6**). Interestingly, CsrA binding was abolished although two neighboring secondary binding motifs were still present. These secondary motifs are essential for CsrA-binding in *E. coli* [Yakhnin *et al*., 2011], but not in *Y. pseudotuberculosis* (**Fig. 3.6**). Binding of CsrA to low-affinity binding motifs, like AGAGA, was found for many of its targets. When in the vicinity of a neighboring high-affinity binding motif (ANGGA), these secondary motifs increase the general CsrA binding affinity, by increasing the local CsrA concentration. Through this mechanism, low-affinity motifs contribute to the cooperative binding of target transcripts [Wang *et al*., 2005; Dubey *et al*., 2002]. Furthermore, secondary motifs need to be in close vicinity to high-affinity binding motifs, either in the primary or the secondary structure [Kulkarni *et al*., 2014; Baker *et al*., 2002]. The closest distance between a secondary binding site and the RBS which contains a primary binding motif had a distance of more than 20 nt and is probably too distant to support effective CsrA binding when the upstream ANGGA motif is missing. Therefore, removal of the primary binding site in the promoter P4/5 region completely abolished binding to the 5'-UTR of *csrA*.

Consistent with data from *E. coli*, the direct autorepression probably functions by inhibition of the translational initiation, because CsrA binds to its ribosomal binding site, [Yakhnin *et al*., 2011].

The direct negative autoregulation of *csrA* in *Y. pseudotuberculosis* and *E. coli* is conserved as well for *rsmA* in *P. aeruginosa*. However, the location of the binding sites differs in *P. aeruginosa*. While *Yersinia* CsrA interacts with binding sites in the 5'-UTR and the RBS, *P. aeruginosa* RsmA binds to two neighboring binding motifs in the RBS and another one located in the coding sequence [Jean-Pierre *et al*., 2015]. The conservation of the direct autorepression demonstrates its importance for *csrA* expression even though the changed binding site distribution might lead to changes in the *csrA* expression strength.

The autoinduction of *csrA* is conferred by a region upstream of the *Yersinia* of promoters P4/5 (**Fig. 3.7**) As no additional CsrA binding sites are present in the autoinducing region, a direct autoactivation of *csrA* transcription can be excluded (**Fig. S1**). Moreover, no DNA-binding capabilities of CsrA have been described to date [Koharudin *et al*., 2013]. Taken together, this indicates an indirect transcriptional autoactivation, as proposed for *E. coli* [Yakhnin *et al*., 2011]. The nature of the transcriptional regulator mediating *csrA* autoactivation is elusive. Apart from the sigma subunits RpoD and RpoS, no direct transcriptional regulators of *csrA* are known in *E. coli* [Yakhnin *et al*., 2011; Vakulska *et al*., 2015]. Recently, in *P. aeruginosa* a transcriptional activation of promoter P3 by sigma subunit AlgU (RpoE) was shown [Stacey & Pritchett, 2016]. AlgU/RpoE is involved in the extracytoplasmic stress, heat shock and oxidative stress response [Potvin *et al*., 2008]. An RpoE-dependent regulation of *Yersinia csrA* has not yet been demonstrated. In *Legionella pneumophila*, *csrA* transcription is directly activated by the PmrA/B two-component system, by binding upstream of the -10 promoter region. *In silico* predictions using a motif model of the PmrA binding site found the PmrA/B two-component system is also a predicted regulator of *csrA* in *Salmonella* spp. and *Yersinia pestis* CO92 [Marchal *et al*., 2004]. As the *csrA* upstream region of *Y. pestis* CO92 and *Y. pseudotuberculosis* YPIII is 100% conserved, a PmrA-dependent regulation of *csrA* can be also expected in YPIII. Although PmrA might be a direct transcriptional activator of *csrA* in *Yersinia*, its involvement in the indirect transcriptional autoactivation of *csrA* is questionable, as a CsrA-dependent regulation of *pmrAB* has not yet been described.

Expression of *csrA* is very sensitive to changes in CsrA protein levels, because of the underlying autoregulatory feedforward loop. Both excessive and very low CsrA protein levels strongly trigger *csrA* autorepression or autoinduction, respectively. Autoregulatory feedforward loops are very robust network motifs, allowing fast adaptation to changing conditions. Moreover, autoregulatory feedforward loops allow precise fine-tuning of protein

levels and protect the system from random noises [Alon, 2007]. Through such an autoregulatory principle, it is possible to strongly induce gene expression through transcriptional autoactivation. Upon reaching a certain threshold, the direct autorepression ensures a rapid shut-down of gene expression and thereby counterbalances the autoactivation and prevents an overshoot of gene expression [Adamson & Lim, 2013; Alon, 2007]. The multileveled autoregulation of *csrA* conferred by the CsrA protein and the ncRNAs CsrB/C allows complex signal integration and very rapid shifts in *csrA* gene expression [Romeo, 1998; Seyel & Van Melderen, 2013; Heroven *et al*., 2012].

4.2 YopD-mediated control of *csrA*

In a recent study, it was shown that the *Y. pseudotuberculosis* translocator protein YopD is an activator of *csrA* expression at host body temperature, as *csrA* expression is repressed in a *yopD* mutant strain and when YopD is secreted [Steinmann, PhD thesis]. YopD is a bifunctional protein that is part of the Ysc-Yop T3SS. Secreted YopD assembles into a pore in the cell membrane of target host cells and functions as a translocator of effector proteins [Montagner *et al*., 2011]. Cytosolic YopD together with its chaperone LcrH was described as a posttranscriptional repressor of many *ysc-yop* genes [Chen & Anderson, 2011]. By limiting the synthesis of injectisome components and associated factors it acts as a feedback regulator for the Ysc-Yop T3SS [Ramamurthi & Schneewind, 2002; Steinmann, PhD thesis]

In this study, binding of YopD/LcrH complexes to the *csrA* leader transcript could be demonstrated. Thereby, a region in close proximity to *csrA* promoters P4 and P5 was identified as being crucial for YopD binding. A shorter transcript with a partial deletion of the YopD binding site bound only weakly at higher protein concentrations. Similarly, the well-studied YopD target *yopQ* is also regulated independently of its promoter region by direct binding of the YopD/LcrH complex to the *yopQ* leader transcript [Anderson *et al*., 2002].

Most 5'-UTRs of characterized YopD target genes, such as *yopK*, *yscN* or *yopE*, contain an AT-rich sequence. This motif is crucial for YopD-dependent regulation, although dispensable for YopD-binding [Chen & Anderson, 2011]. Such an AT-rich stretch is also located directly upstream of the RBS of *csrA*. However, deletion of this region did not affect the binding affinity of YopD/LcrH (**Fig. 3.3**). Furthermore, a *csrA'-'lacZ* reporter fusion missing this element was still YopD-dependent (data not shown). Strikingly, only YopD-repressed *yop* genes contain such a sequence feature [Chen & Anderson, 2011]. This strongly indicates that another sequence feature might be required for YopD-mediated gene activation. Besides this,

the YopD consensus motif, identified in *yop* genes, contains a higher adenine content in comparison to the AT-rich stretch in the 5'-UTR of *csrA*. This suggests that the putative YopD binding site upstream of the RBS of *csrA* might not represent a YopD consensus motif. In contrast to the described AT-rich motif (GC content 0%), the YopD binding region in the *csrA* 5'-UTR has a GC content of ~50% which matches the GC content of the YPIII chromosome (47.5%).

Cytosolic YopD is protected by its chaperone LcrH, which remains in the cytosol even after secretion of YopD. As *csrA* expression is repressed in a *yopD* mutant strain and under calcium depletion when YopD is exported from the cytosol, *csrA* is regulated dependent on the secretion status of the injectisome and the loading status of LcrH. In *B. subtilis* and *Campylobacter jejuni*, *csrA* is also regulated depending on the secretion status of its flagellar T3SS. During flagellum assembly, the flagellin protein Hag gets secreted and its alternative chaperone FliW remains unbound in the cytosol to regulate *csrA* [Mukherjee *et al*., 2011; Dugar *et al*., 2015]. The FliW-dependent *csrA* regulation in *B. subtilis* is the only known example in which a T3SS-associated factor acts as a feedback regulator of CsrA. As demonstrated in this study, the T3SS chaperone LcrH is not directly involved in *csrA* regulation. In accordance with results by other groups, LcrH alone does not confer RNA-binding activity (**Fig. 3.4**) [Chen & Anderson, 2011]. Moreover, the chaperone function of LcrH is needed for YopD-dependent binding [Anderson *et al*., 2002]. The presence of LcrH promotes YopD synthesis as well as functionality by stabilizing YopD. Like other chaperones, LcrH keeps the YopD protein in its native and functional fold and confers protection from aggregation and degradation [Hartl *et al*., 2011; Anderson *et al*., 2002]. For this reason, deletion of *lcrH* leads to a down-regulation of CsrA levels comparable to a *yopD* deficient mutant.

YopD synthesis is induced at 37 °C (**Fig. 3.10**). Strikingly, while CsrA synthesis is also induced at 37 °C, *csrA* mRNA levels are not altered by the induction of YopD synthesis, hinting to a posttranscriptional regulation mechanism. Moreover, both, deletion of the *yopD* gene and secretion of the YopD protein decrease *csrA* transcript levels at 37 °C, although the transcript stability remains unchanged (**Fig. 3.9; Fig. 4.1**). This observation can be explained by a YopD-dependent transcriptional regulation of *csrA* at 37 °C, in addition to the posttranscriptional YopD-dependent thermo-induction. The repression of *csrA* transcription at 37 °C may be mediated by an unknown transcriptional repressor of *csrA*, as DNA-binding of

YopD has not been shown and YopD does not contain any known DNA-binding motifs [Olsson *et al*., 2004; Chen & Anderson, 2011]. The nature of this transcriptional repressor is still elusive. Interestingly, heterologous expression of YopD and LcrH in *E. coli* did not influence CsrA protein level or its growth, even though the YopD binding region in the *csrA* upstream region is highly conserved. This indicates that the unknown transcriptional repressor is *Yersinia*-specific.

Furthermore, the presence of an alternative *csrA* transcript in the *yopD* mutant strain might indicate a YopD-dependent differential transcription of *csrA*, possibly conferred by a transcriptional regulator like RpoS or RpoE (AlgU) (**Fig. 3.9**) [Stacey & Pitchett, 2016].

4.3 YopD- and CsrA-dependent regulation of *csrA* expression

Deletion of the putative YopD binding region close to promoters P4 and P5 only incompletely derepressed *csrA* expression in the *yopD* mutant strain (**Fig. 3.5**). This region also contains a high-affinity binding motif of CsrA crucial for autoregulation as demonstrated by RNA-EMSAs and *csrA'-'lacZ* reporter gene assays, hinting towards a YopD-dependent modulation of *csrA* autoregulation (**Fig. 3.6+7**). This study demonstrated that YopD is a posttranscriptional activator of *csrA* expression. By binding to the *csrA* transcript, YopD most presumably induces *csrA* translation and by interfering with CsrA-mediated autorepression, as demonstrated by a *csrA*'-'*lacZ* reporter gene assay of the *csrA* upstream region containing the YopD and CsrA binding regions under the control of a constitutive promoter (**Fig. 3.8**).

Taken together, this study demonstrated a complex regulation of *csrA* expression by the T3SS translocator YopD and the CsrA protein itself. At environmental temperature (25 °C), CsrA steady-state levels are mainly controlled by its dual autoregulation. CsrA activates its transcription from promoter P3, while at the same time limiting CsrA synthesis by directly binding to its own mRNA when a certain threshold is reached (**Fig. 4.1**). When *Y. pseudotuberculosis* enters its warm-blooded host, expression of the Ysc-Yop-T3SS and thereby of YopD and LcrH is induced, preparing the pathogen for an encounter with the innate immune system. YopD and LcrH start to accumulate in the cytosol and YopD, protected by its chaperone LcrH, binds the *csrA* transcript, thereby occupying the autorepressive CsrA binding site (**Fig. 4.1**). Hence, CsrA synthesis is directly as well as indirectly induced by a YopD-dependent activation and by interfering with CsrA autorepression on the post-transcriptional level. Nevertheless, *csrA* transcript levels are comparable at 37 °C and 25 °C in the absence of secretion. This might be due to the

additional autoregulatory mechanism of the Csr system, conferred by the small non-coding RNAs CsrB/C. A thermo-induction of CsrB/C might reduce CsrA activity by sequestration, thereby preventing the transcriptional autoactivation of *csrA* at 37 °C. Recent results of an RNA-Seq analysis of the *Y. pseudotuberculosis* wild-type at 25 °C and 37 °C hint to a thermo-regulation of CsrB/C expression, although a thermo-induction still needs to be analyzed [Nuss, unpublished data].

Upon host cell contact, YopD is secreted. Now, CsrA autorepression is reactivated, as the CsrA binding site is free. Furthermore, transcription of *csrA* is reduced through an yet unidentified repressor that either is no longer repressed by YopD or by another secretion-dependent factor (**Fig. 4.1**).

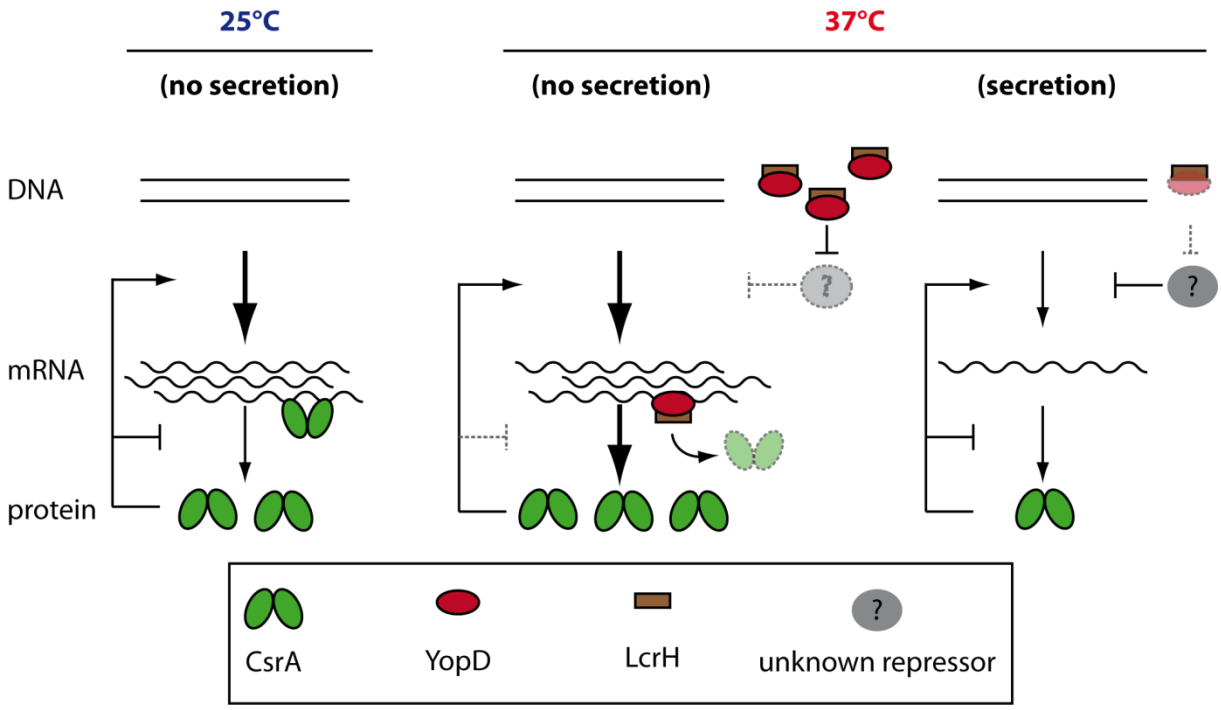

Figure 4.1: Model of the YopD- and CsrA-dependent regulation of *csrA* expression. At 25 °C, the expression of *csrA* is regulated through complex autoregulation, involving an indirect transcriptional activation and a direct translational repression when CsrA dimers (green) bind to its transcript. At 37 °C, YopD (red) and its chaperone LcrH (brown) are synthesized binding to the *csrA* transcript and thereby blocking CsrA autorepression. Through this mechanism, CsrA synthesis is induced. Additionally, expression of an unidentified transcriptional repressor (gray) is blocked by the YopD/LcrH complex. When secretion is triggered, YopD dissociates from LcrH and is exported, while LcrH remains in the cytosol. As a consequence a transcriptional repressor accumulates and represses *csrA* transcription, reducing *csrA* transcript and protein levels.

4.4 Thermoregulation of *yopD*

The *yopD* gene is part of the *ysc-yop* regulon and is regulated in response to temperature and by the transcriptional regulator LcrF. At moderate temperatures (25 °C), the expression of LcrF is repressed and consequently LcrF target genes are not expressed [Schwiesow *et al.*,

2015]. Therefore, it was surprising to find basal YopD protein levels at 25 °C (**Fig. 3.10**). YopD is encoded as the last gene of the polycistronic *lcrGVH-yopBD* operon that is expressed from a LcrF-dependent and temperature-regulated promoter (P_{lcrG}). Being the major promoter of this operon, promoter P_{lcrG} ensures expression at 37 °C. As demonstrated by Li *et al*., *yopD* is additionally transcribed from an upstream promoter located in the *yopB* gene [Li *et al*., 2014]. This study showed that at 25 °C, *yopD* is mainly expressed from its own promoter (P_{yopD}), while promoter P_{lcrG} is almost silent. At 37 °C, this effect is reversed. Through this mechanism, a shift between the shorter *yopD* to the full-length *lcrGVH-yopBD* transcript takes place (**Fig. 3.12**). The role of promoter P_{yopD} is still unclear. In large polycistronic operons, internal promoters amplify transcription of 3'-located genes [Platt, 1986; de Smit *et al*., 2008]. This ensures expression of terminal genes, as with increasing transcript length the probability of premature elongation interruption increases. Due to intracistronic transcriptional polarity, terminal genes would then be transcribed in low amounts [Richardson & Roberts, 1993; Lodish *et al*., 2000; Montero *et al*., 2011]. Besides this, alternative promoters increase the robustness of a regulatory system by enabling a higher number of signal integration possibilities. In this case, the internal promoter enables a LcrF-independent basal expression of *yopD*. As a consequence, the expression of *yopD* is decoupled from the expression of its upstream located chaperone *lcrH*. As demonstrated in this study, LcrH is strictly needed for YopD functionality and stability (see **Fig. 3.4** and **Fig. 3.13).** Thus, it is not surprising that YopD is degraded at 25 °C when P_{lcrG} is repressed. This destabilization seems to be the result of insufficient chaperone levels, as ectopic expression of LcrH can increase YopD protein levels at 25 °C and 37 °C (**Fig. 3.13**). Constant degradation of YopD holds it in standby mode. Interruption of its constant proteolysis allows rapid adaptation to environmental changes, as it results in a fast accumulation of the regulator protein. A similar mechanism is utilized by *E. coli* to ensure a fast activation of its heat shock response. At 37 °C (no heat stress), heat shock sigma factor RpoH (σ^{32}) is constantly synthesized and sequestrated from the RNA polymerase holoenzyme through the action of the small heat shock chaperone DnaK. DnaK-bound RpoH is targeted for the regulated proteolysis by FtsH. Upon heat shock, unfolded cytosolic proteins accumulate and sequester DnaK, thereby freeing and stabilizing RpoH which now rapidly accumulates. Free RpoH associates with the RNA polymerase core enzyme and activates transcription of heat shock genes [Blaszczak *et al*., 1995; Narberhaus *et al*., 2009; Obrist *et al*., 2007]. YopD and LcrH could be involved in a similar mechanism to activate cell-contact induction of the T3SS at moderate temperatures. At 25 °C, the expression of *lcrF*, the master activator of the *ysc-yop* regulon, is repressed. Upon

cell contact, synthesis of the Ysc-Yop T3SS is triggered even at low temperature [Opitz, PhD thesis; Pimenova, Master thesis].

ATP-dependent proteases of the Hsp100/Clp- or AAA+ families are often involved in controlling regulatory processes by ensuring a rapid protein turnover [Kirstein *et al*., 2009]. To identify the protease, involved in YopD degradation at 25 °C, mutant strains of the proteolytic subunit of ATP-dependent proteases were analyzed for YopD expression. A deletion of the protease involved in YopD degradation would cause a stabilization of YopD and increase its steady-state protein level. Apparently, the ClpP-associated proteolytic machinery is not involved in degradation of YopD. Contrary to expectation, inactivation of the individual AAA+ proteases Lon, HslV (ClpQ) or FtsH completely abolished expression of YopD and LcrH (**Fig. 3.13**). As both, LcrH and YopD, are encoded by the same transcriptional unit and are affected by a deletion of all three proteases, it is possible that another protease is upregulated in their absence which degrades YopD and LcrH. Alternatively, a regulatory factor of the *lcrVGH-yopBD* operon could be affected.

The involvement of the Lon protease in the regulation of the Ysc-Yop T3SS master regulator LcrF was already described previously. Lon is required for the thermo-regulated degradation of the LcrF repressor YmoA [Jackson *et al*., 2004]. At moderate temperature, YmoA is stable and represses expression of *lcrF*. At 37 °C, YmoA is degraded by the Lon protease and transcription of the *yscW-lcrF* operon can occur (**Fig. 1.3**) [Jackson *et al*., 2004; Boehme *et al*., 2012]. Thus it is also possible that the decrease of YopD and LcrH protein levels in the corresponding protease mutants are triggered by a reduction of LcrF levels.

4.5 Complex YopD- and CsrA-dependent regulation of *yscW-lcrF*

The *yscW-lcrF* operon encodes the master regulator of the Ysc-Yop T3SS, LcrF. The amount of synthesized LcrF protein is tightly controlled by a negative feedforward loop, which shuts down *lcrF* expression when YopD accumulates in the cytosol. This control is released when secretion is triggered by cell contact and YopD gets exported [Steinmann, PhD thesis; Williams & Straley, 1998; Schiano & Lathem, 2012]. A secretion-dependent feedback control of T3SSs is a reoccurring motif in the regulation of T3SSs. A post-transcriptional control, as present in *Yersinia*, seems to be a unique feature. Most known secretion-dependent feedback loops are conferred by sequestration of transcriptional activators through an anti-sigma factor control system. Such a regulatory system is present in the regulation of the flagellar T3SS of Gram-negative bacteria. The assembly of the flagellum is controlled by the FlgM-FliA sigma-anti-sigma factor system [Katsukake &Iino, 1994; Chilcott & Hughes, 2000]. In *P.*

aeruginosa, the expression of T3SS components and effector gene transcription is regulated by a more complex regulator sequestration mechanism (anti-anti-activator system). This system involves the AraC-like transcriptional activator ExsA and three additional anti-activator proteins (ExsD/C/E). Secretion of the anti-anti-activator ExsE, leads to a partner-switching which frees activator ExsA and allows T3SS gene expression [Dasgupta *et al*., 2004; Diaz *et al*., 2011]. All these systems assure a control step that stops T3SS gene expression until the secretion through the T3SS is activated.

A CsrA-dependent regulation of T3SS master regulators is a common motif in many pathogens. In *E. coli*, CsrA is a post-transcriptional activator of the flagellar T3SS master regulator FlhDC. CsrA binds the 5'-UTR of the *flhDC* gene thereby protects the transcript from RNase E-dependent degradation [Yakhnin *et al*., 2013]. In *Salmonella*, CsrA post-transcriptionally represses expression of the AraC-like transcription factor HilD, which in turn leads to a down regulation of the SPI-1 and SPI-2 T3SSs [Martinez et al., 2011]. In *P. aeruginosa*, the CsrA-homolog RsmA induces expression of the AraC-like regulator and LcrF-homolog *exsA* on a post-transcriptional level [Intile *et al*., 2014; Zhu *et al*., 2016].

In *Yersinia*, expression of the transcriptional activator *lcrF* is precisely controlled through the action of the RNA-binding proteins YopD and CsrA. The global regulator CsrA is a dual regulator of *lcrF*. On the one hand, it indirectly represses transcription of the *yscW-lcrF* operon and on the other hand, it is involved in the posttranscriptional regulation of *yscW* and *lcrF* [Opitz, PhD thesis; Pimenova, Master thesis]. Translocator YopD is a long known repressor of *lcrF* expression. In this study, it could be demonstrated that CsrA and YopD directly influence the LcrF synthesis.

4.5.1 YopD is a direct regulator of the *yscW-lcrF* operon

In this study, a direct interaction of YopD/LcrH with the 5'-UTR of *yscW* and *lcrF* could be shown. Both leader transcripts harbor 'AUAAA' motifs, which are involved in feedback regulation by YopD/LcrH [Cambronne & Schneewind, 2002; Chen & Anderson, 2011]. These motifs only play a minor role in YopD-dependent *lcrF* repression, as deletion of the 'AUAAA' motif-containing region in the 5'-UTR of *lcrF* changed the YopD/LcrH binding pattern, but did not abolish binding (**Fig. 3.14**) or YopD-dependent regulation [Steinmann, PhD thesis]. Until now no alternative binding sequences involved in YopD binding could be identified. This suggests that RNA structural elements (e.g. hairpin structures) could be involved in YopD/LcrH binding.

Interestingly, the 'AUAAA' motif is needed for YopD/LcrH-dependent regulation of *yopH*, but is dispensable for binding [Chen & Anderson, 2011]. Strikingly, the proposed AU-rich sequence motif is also involved in LcrQ-dependent regulation. YopD, LcrH and LcrQ (YscM1/2 in *Y. enterocolitica*) often act synergistically and are involved in the same posttranscriptional repression mechanisms [Cambronne & Schneewind, 2002]. Therefore, the described AU-rich motif is probably not needed for YopD binding but could be important for LcrQ-dependent repression, as deletion of *yopD*, *lcrH* or *lcrQ* derepresses *lcrF* and *yopQ* [Steinmann, PhD thesis; Anderson *et al*., 2002; Cambronne & Schneewind, 2002]. The complex interplay of these proteins is still unknown and needs to be further assessed. Other studies indicate that YopD-dependent gene repression involves additional factors. SycH, the chaperone of YopH, seems to be involved in the same regulatory mechanism. The N-terminus of LcrQ is homologous to parts of YopH and can interact with SycH. An excess of SycH, therefore, mimics a *lcrQ* mutant after secretion of YopD and LcrQ [Wulf-Strobel *et al*., 2002]. Notably, the interaction of SycH and LcrQ seems to be involved in the cell contact-mediated *yop* gene derepression. Repressor LcrQ is in contrast to YopD not secreted by the T3SS [Cambronne *et al*., 2000]. After secretion of the effector protein YopH, its chaperone SycH remains in the cytosol and might bind to LcrQ (YscM1/YscM2) and deactivate its regulatory function [Cambronne *et al*., 2004].

4.5.2 CsrA is a direct regulator of *yscW* and *lcrF*

In this study, binding of CsrA to the 5'-UTR of *yscW* and *lcrF* was demonstrated. The distribution and the type of CsrA binding sites in the tested 5'-UTRs differed significantly, which was reflected in different binding affinities. For efficient CsrA binding, target RNAs need at least two primary binding sites exposed on hairpin structures [Vakulskas *et al*., 2015]. Moreover, in this study the importance of a secondary, low-affinity binding motif (AGAGA) for CsrA binding of 5'-*lcrF* became apparent. The 5'-UTR of *lcrF* is needed for the CsrA-dependent post-transcriptional activation of *lcrF* [Pimenova, unpublished results] and is directly bound by CsrA although it only contains one GGA motif within the RBS. A secondary binding motif was located within the first codons of its coding sequence (**Fig. 3.15D**). Elongation of the 5'-*lcrF* RNA fragment encompassing this low-affinity motif dramatically increased the CsrA binding affinity (**Fig. 3.15F**). This is exceptional, other described CsrA targets usually contain at least two high-affinity binding motifs [Kulkarni *et al*., 2014]. The lowest number of binding motifs of a direct CsrA target are found in the 5'-

UTR of *hfq* [Baker *et al*., 2007]. Notably, AGA motifs are often accompanied by multiple primary binding sites and played only a minor role in direct CsrA binding. In toeprint analyses of *E. coli*, the importance of these AGA motifs was shown for multiple CsrA targets, for example, the *pgaA, glgC, lcrF* or *nhaR* transcripts (**Fig. 3.15**) [Baker *et al*., 2002; Wang *et al*., 2005; Yakhnin *et al*., 2011; Pannuri *et al*., 2012]. AGA motifs support and enhance binding of CsrA to a neighboring primary binding motif, by increasing the local concentration of CsrA molecules [Kulkarni *et al.,* 2014]. However, a recent CsrA interactome study in *S. enterica* serovar Typhimurium identified only [A/C]UGGA motifs as the consensus motif *in vivo*. In addition, CsrA-bound sequences contain at least one minimal GGA and one primary ANGGA motif. Low-affinity (AG)AGA motifs were only enriched in a minor fraction of CLIP peaks whereby most of these motifs were located in close vicinity to a GGA motif [Holmqvist *et al*., 2016].

The intergenic region of the *yscW-lcrF* operon harbors a 'four U' motif, which base pairs with the GGA motif of the *lcrF* ribosomal binding site at low temperature, functioning as an RNA thermometer. This 'four U' motif is crucial for the thermoregulation of *lcrF* and ensures that synthesis of LcrF and thereby expression of the Ysc-Yop T3SS only occurs inside the warm-blooded host. Mutations in the RNA thermometer caused a deregulation of LcrF synthesis and decreased *Yersinia* virulence [Boehme *et al*., 2012; Steinmann, PhD thesis]. Notably, *lcrF* translation is induced in the presence of CsrA by its binding of the GGA motif located within the RBS (**Fig. 3.15**) [Pimenova, Master thesis]. This study demonstrated CsrA binding of the *lcrF* leader transcripts depends on the open state of its RNA thermometer, as demonstrated by RNA-EMSAs of the *lcrF* 5'-UTR containing mutations in the 'four U' motif. These mutations prevent ('open') or promote ('closed' thermometer) base pairing of the 'four U' motif with the RBS, as indicated by RNA fold predictions (**Fig. 3.16**) [Steinmann, PhD thesis]. CsrA binding probably modulates the opening of the thermo loop. *In vivo*, CsrA might bind to the RBS and thereby obstructs closing of the thermo loop. As shown in this study, CsrA has a weak binding affinity to this region and might get easily replaced by ribosomes. A *lcrF'-'lacZ* reporter fusion encoding the intergenic region of *yscW-lcrF* and parts of the *lcrF* CDS is activated in the presence of CsrA. Additionally, the presence of CsrA is needed at moderate temperatures (25 °C) for a cell contact-dependent activation of *lcrF* expression [Pimenova, Master thesis]. At 25 °C, the RBS is inaccessible due to the closed thermometer and *lcrF* translation is restricted. Possibly, CsrA binding to the thermo loop may be needed to open the RNA thermometer and trigger cell contact-dependent *lcrF* induction. Until now, a modulation

of 'four U' RNA thermometer by RNA-binding proteins has not been described. Interestingly, in *Salmonella* the melting temperature of such a thermoresponsive element is modulated by binding of magnesium ions and plays a crucial role in the regulation of heat shock gene *agsA* [Rinnenthal *et al*., 2011]. Since 'four U' RNA-thermometers are often involved in translational regulation through a base pairing mechanism to the 'AGGA' motif of the ribosomal binding site [Waldminghaus *et al*., 2007], CsrA might be a general modulator of this type of RNA thermometers.

4.5.3 CsrA and YopD influence *lcrF* transcript stability and counter-regulate the degradosome

In this study, an antagonistic effect of CsrA and YopD on the stability of the *yscW-lcrF* transcript was observed. At 37 °C under non-secretory conditions, YopD accumulates in the bacterial cytosol and destabilizes the *lcrF* mRNA. High protein levels of CsrA antagonize the YopD effect by stabilizing the *lcrF* transcript. For this reason, in presence of both regulators, the *lcrF* transcript exhibits an intermediate stability. In the *csrA* deficient mutant, the stabilizing effect of CsrA is missing and YopD destabilizes the *lcrF* transcript and a rapid mRNA turnover occurs. In the double mutant, the effect of both regulators is diminished and in comparison to the wild-type, the *lcrF* transcript is stabilized to some extent (**Fig. 3.18**), pointing to a dominant effect of YopD over CsrA on the mRNA stability to a certain degree.

Previous data demonstrated that YopD activates the expression of *rne* encoding the RNase E and *pnp* encoding the PNPase. Both proteins are core components of the RNA degradosome. The involvement of CsrA and YopD in the regulation of degradosomal components was examined by qRT analysis. Transcripts of all integral (RNase E, PNPase) and associated (helicase RhlB/E and enolase) degradosome components were induced in the presence of YopD. Accordingly, all of these genes were downregulated in a *yopD* mutant background and under secretion conditions, where YopD is exported from the cytosol. These results confirm previous microarray data comparing a *csrA* mutant and a *csrA*/*yopD* double mutant [Steinmann, PhD thesis]. In the *csrA/yopD* double mutant, downregulation, as seen in the absence of *yopD* alone, was almost completely diminished, indicating a counter-regulation of the degradosome by both RNA-binding proteins. This is surprising as in absence of *csrA* no significant effects on the transcript levels of degradosomal genes were detectable (**Fig. 3.18**).

A recent RNA-seq analysis comparing the *Y. pseudotuberculosis* wild-type and the *csrA* mutant indicated a mild CsrA-dependent repression of all degradosomal genes [Nuss,

unpublished data]. In *E. coli*, CsrA is a known strong repressor of *pnp* translation. CsrA-dependent regulation of *pnp* is complex and involves RNase III and PNPase which nucleolyticly process the *pnp* 5'-UTR. The action of both RNases frees a CsrA binding site (AGGA) which was priorly sequestered in a secondary RNA structure. The now accessible binding site, as well as the RBS, is bound by CsrA and a translational repression of *pnp* takes place [Park *et al*., 2015]. In *Yersinia*, the CsrA-dependent effect on *pnp* transcript levels is minor in contrast to the strong repression described in *E. coli*. This may be explained by the fact that the *pnp* 5'-UTR of *Yersinia* misses the AGGA binding motif located upstream of its RBS which is crucial for CsrA binding in *E. coli*. This might indicate that the CsrA-dependent *pnp* regulation in *Yersinia* differs from *E. coli*.

Notably, deletion of *yopD* and *csrA*, affect multiple components of the degradosome. Whether this regulation is direct and occurs by targeting every degradosomal gene individually or indirectly by triggering the autoregulation of the whole degradosome is still unclear. Until now, such an intrinsic regulation of the RNA degradosome has not been shown yet but is likely as RNase E is involved in the autoregulation of *pnp* [Carzaniga *et al*., 2009, Park *et al*., 2015].

In summary, YopD and CsrA are opposed regulators of the RNA degradosome: YopD induces the degradosome and enhances the global RNA decay, whereas CsrA antagonizes the YopD effect and probably accelerates down-regulation of the degradosome components after secretion of YopD. Additionally, binding of the *yscW-lcrF* transcript by YopD might tag the transcript for a rapid degradation, while CsrA binding might prevent degradation of the *lcrF* transcript. The YopD-dependent increase of the global RNA decay also explains the large number of genes that are members of the YopD regulon and why YopD is mostly described as a repressor of target genes [Steinmann, PhD thesis].

4.6 Cross-talk between CsrA- and YopD-dependent feedback loops regulating *lcrF* expression - a complex model

The control of the Ysc-Yop T3SS expression in the enteropathogenic bacterium *Y. pseudotuberculosis* is regulated by intertwined CsrA- and YopD-dependent feedback loops. Expression of both RNA-binding proteins is mutually dependent and couples the secretion status of the injectisome (YopD) to the CsrA-mediated control of metabolism, stress adaptation and other virulence systems. Both, CsrA and YopD, interact with the *yscW-lcrF* mRNA and regulate its expression on multiple levels (**Fig. 4.2**).

CsrA indirectly represses transcription from the P_{yscW} promoter and thereby strongly reduces *yscW-lcrF* transcript levels. Additionally, CsrA directly binds the 5'-UTR of *yscW* and *lcrF* and controls protein synthesis. Binding of CsrA to the *lcrF* 5'-UTR induces translation at 37 °C, while CsrA-promoted translational activation of *yscW* occurs only under secretion conditions [Pimenova, Master thesis; Opitz, PhD thesis]. CsrA seems to supports *lcrF*-induction at moderate temperatures by modulating the open state of the RNA thermometer in the 5'-UTR of *lcrF*. Furthermore, in the absence of YopD, CsrA stabilizes the whole *yscW-lcrF* transcript, most likely by repressing the expression of RNA degradosome components.

Under non-secretory conditions, when YopD accumulates in the cytosol, it antagonizes the action of CsrA. YopD binds the *yscW-lcrF* transcript at multiple sites and competes with CsrA binding of the *lcrF* 5'-UTR. On a global level, YopD induces expression of the whole RNA degradosome, thus enhancing *yscW-lcrF* mRNA decay.

Cell contact induces the secretion of effector molecules and the regulators YopD and LcrQ by the Ysc-Yop T3SS. This, in turn, derepresses the production of Yop proteins and LcrF. Expression of the degradosome is down-regulated, probably supported by the action of CsrA. As a result, *lcrF* transcript stability increases. Since the absence of YopD decreases CsrA synthesis (see **Fig. 4.1**), *lcrF* transcription is further induced. Thereby, *lcrF* expression is triggered by an increase in the transcription synthesis rate and a stabilization of the *lcrF* transcript. These complex rearrangements in the global regulatory systems ensure a fast and perfect adaptation to changing conditions during the infection process.

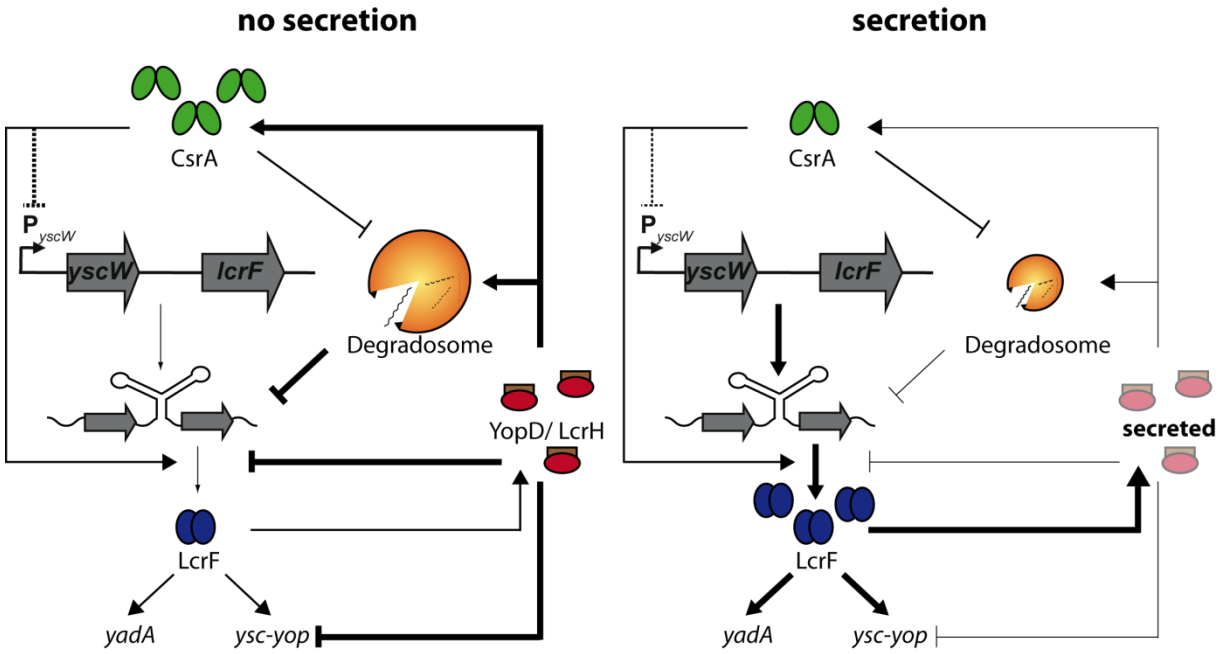

Figure 4.2: Working model of YopD- and CsrA-dependent feedforward regulation of the late virulence gene regulation. The regulatory network controlling the expression of late virulence master regulator *lcrF*. Expression of *lcrF* is

regulated on the transcriptional and post-transcriptional level by YopD, CsrA and the RNA degradosome. Direct and indirect (dashed line) regulatory effects of the involved factors are shown. Arrows symbolize gene activation, while bar-headed lines symbolize gene repression.

4.7 CsrA targets in *Yersinia*

In order to identify direct CsrA targets, a RIP-Seq, and a differential RNA-Seq approach were combined with an *in silico* prediction. The analysis of *in silico* predicted, differentially regulated genes revealed a high number of type six secretion system (T6SS) associated genes. Especially, structural genes of the T6SS-1, the T6SS-2 and the T6SS-4 were predicted. T6SSs form complex macromolecular syringes which function in the interbacterial defense, enhance virulence and pathogenicity [Sana *et al*., 2016; Hachani *et al*., 2016]. Notably, the 5'-UTRs of *impG*/*vasA*, *impI* and *impJ*/*vasE* (YPK_0389, YPK_0391; YPK_0393) harbor a high number of CsrA binding motifs (data not shown) and are strongly repressed by CsrA in *Y .pseudotuberculosis* YPIII [Nuss, unpublished data]. Besides the putative T6SS-4 regulator *rovC* (YPK_3567), which is repressed by CsrA at 25 °C [Knittel, Master thesis] other T6SS-4 genes were predicted, but are not differentially regulated by CsrA at 25 °C or 37 °C (**Fig. 3.21**) [Nuss, unpublished data].

RovC is a *Yersinia*-specific uncharacterized DNA-binding protein with an unknown fold. The *rovC* mRNA is a specifically targeted by CsrA, as demonstrated by RNA-EMSA and reporter gene studies [Knittel, Master thesis; Seekircher, PhD thesis]. Some of the T6SS genes predicted by the algorithm were already positively tested for CsrA-dependency in β-galactosidase reporter gene assays [Kukarcev, Bachelor thesis]. These T6SS-4 genes all harbor a high number of CsrA binding motifs in their upstream regions (data not shown) but are not expressed under the employed conditions of the differential RNA-Seq [Nuss, unpublished data]. In 2009, a direct regulation by the CsrA-homolog RsmA was shown for the structural T6SS genes PA0081 (YPK_0391; T6SS-1) and PA0082 (YPK_3566; T6SS-4) in *P. aeruginosa* [Brencic & Lory, 2009]. When comparing the 5'-UTRs of these genes in *Pseudomonas* and *Yersinia*, a comparably high number of primary binding sites was observed, suggesting a direct CsrA regulation as well in *Y. pseudotuberculosis* YPIII (**Fig. S12+13**). These results extend the list of CsrA targets and highlight the role of CsrA as a central regulator and coordinator of virulence-associated secretion systems in *Yersinia*.

Also, the *rovA* gene encoding the transcriptional regulator of the initial infection phase and an activator of invasin was identified as a possible direct CsrA target. A CsrA-dependent regulation of *rovA* has long been known, although so far it was assumed its influence occurs

solely indirectly via the RovA regulator RovM [Heroven *et al*., 2008]. Results of this study point to a more complex CsrA-dependent regulation of *rovA*. The leader transcript of *rovA* harbors three primary binding sites in the vicinity and overlapping with the RBS. This suggests a CsrA-dependent feedforward regulation of *rovA*, as CsrA is a possible direct as well as an indirect regulator of *rovA*. The complex regulation might be important to precisely adjust *rovA* expression. Precise RovA levels are needed for a successful infection, since changes in the *rovA* expression pattern are disadvantageous for the colonization of the MLNs in the mouse model [Nuss *et al*., 2016; Schuster PhD thesis].

Additionally, the analysis of predicted target genes, which are CsrA dependent and are part of the CsrA interactome, revealed mostly metabolic genes. These results are in agreement with CsrA's role as a regulator of metabolism and virulence [Barnard *et al*., 2004; Heroven *et al*., 2012]. Additionally, tRNAs, the tRNA-modifying enzyme *miaA* and the M1 RNA of RNase P were identified as putative direct CsrA targets at 37 °C. These transcripts were enriched in the RIP-Seq analysis and are part of the CsrA regulon. Interestingly, most of these tRNAs contain only a single or no CsrA binding motif at all. For this reason, these tRNAs seem to be unlikely CsrA targets. Interestingly, mature tRNAs are processed from longer precursor tRNA involving multiple maturation events [Phizicky & Hopper, 2010]. These pre-tRNAs are probably targeted by CsrA. The differential RNA-seq analysis of the YPIII wild-type and the *csrA* mutant gave evidence for a temperature-dependent regulation of tRNA genes. CsrA seems to be involved in this temperature-dependent reorganization of the cellular tRNAs and therefore the cellular codon composition [Nuss, unpublished data]. Genes that need to be expressed at similar levels tend to use the same codons. A remodeling of the cellular tRNA codon availability supports the reorganization of the cellular proteome [Plotkin & Kudla, 2011; Novoa *et al*., 2012]. At body host temperature, mostly proteins of the Ysc-Yop T3SS are synthesized. Hence, the availability of certain tRNAs might lead to a preferential synthesis of Ysc-Yop T3SS genes.

Interactome analysis, differential RNA-Seq and *in silico* target prediction are valuable tools for the identification of direct CsrA targets, however, all these approaches have some drawbacks. A differential RNA-Seq analysis cannot identify target genes those RNA levels are unaffected by CsrA, for example when only translation initiation is changed by CsrA binding, as seen in the CsrA-dependent regulation of *hfq* [Baker *et al*., 2007]. Additionally, not all differentially regulated RNAs are directly targeted by CsrA. A weakness of the RIP-Seq approach can be seen by an absence of the fixation of *in vivo* RNA-protein interactions.

Because of this, interactions can still take place during the *in vitro* IP leading to results that do not necessarily correspond to interactions occurring inside the cell. This can cause an overrepresentation of false-positive RNAs [Mili & Steitz, 2004; Riley & Steitz, 2013]. To overcome some of the disadvantages of RIP-Seq, other IP approaches can be used. For example, UV cross-linking immunoprecipitation coupled with RNA-Seq (CLIP-Seq). The fixation of RNA-RBP interactions allows RNase treatment to isolate binding sites in target RNAs. The applied fixation can cause an overrepresentation of high abundant RNAs that are only bound by CsrA with a low affinity [Holmqvist *et al*., 2016; Zhang *et al*., 2015; Waters *et al*., 2016]. The CsrA core binding motif GGA is also part of the ribosomal binding site and can be found in the leader transcript of a majority of coding genes. These RNAs might only temporarily associate with CsrA due to their low binding affinity. Enriched RNAs are always the sum of binding affinity and abundance of the corresponding transcript, which interferes with the identification of high-affinity targets [Head *et al*., 2014; Riley & Steitz, 2013]. For this reason, CLIP-Seq cannot be used to identify high-affinity targets. To obtain a better understanding of *in vivo* binding dynamics, covalent RNA-tagging can be applied. Here, the RNA-binding protein of choice is fused to a poly(U)-polymerase that adds a growing polyuridine tag dependent on interaction duration and frequency [Lapointe *et al*., 2015].

Interactome approaches are a valuable tool to identify direct RBP target RNAs. Noteworthy, these approaches only reflect RNAs that are expressed under specific conditions and might contain high abundant RNAs with a low-affinity binding affinity. Moreover, *in silico* prediction algorithms can help to identify high-affinity targets and circumvent the drawbacks of *in vivo* approaches that only consider certain growth conditions. A weakness of the employed prediction algorithm of this study is that it only considers the binding motif distribution in the primary RNA sequence and not the secondary structure of putative target RNAs. However, binding motifs need to be exposed on hairpin structures [Vakulskas *et al*., 2015]. To take this into account, *in silico* RNA folding algorithm can be employed, such as mfold or similar tools [Zuker, 2003, Rybarczyck *et al*., 2015]. Such an approach was also tested during this study. Considering only folds with a minimal free energy +/-10% deviation, most 5'-UTRs contained at least one CsrA binding motif exposed on a hairpin (data not shown). Moreover, the fold of a given *in vivo* transcript is not only dependent on the calculated minimal free energy of the fold, but also on additional factors, like the cellular ion concentration, RNA processing, RNA-binding proteins or other molecules. Additionally, crowding in the cytosol causes a deviation between *in silico* and *in vivo* folds [Gao *et al*., 2016; Righetti *et al*., 2016]. Recently, the *in vitro* RNA structurome of *Y. pseudotuberculosis*

was published, which could be combined with *in silico* fold predictions [Righetti *et al*., 2016]. Both methods can be applied to improve results of the target prediction algorithm used in this study.

A comparison of identified CsrA targets in *Y. pseudotuberculosis* by RIP-Seq and *in silico* prediction data of other bacteria revealed only a minor overlap indicating a low phylogenetic conservation of CsrA target genes (data not shown). This observation was also made in a comparison of *in silico* predicted CsrA targets in *Y. pseudotuberculosis* and *E. coli* (see **chapter 3.19.4**) and in prediction dataset of *S. typhimurium* and *P. aeruginosa* by Kulkarni *et al*. [Kulkarni *et al*., 2014]. The number of *in silico* predicted targets in these species was comparable. However, only a fraction of these target genes overlapped between the analyzed species (see **chapter 3.19.4**) [Kulkarni et al., 2014]. A ClustalO alignment of the upstream region of target genes in *E. coli* and *Y. pseudotuberculosis* revealed that, due to mutations, the distribution and number of CsrA binding motifs were drastically changed (see **Fig. S8-11**). According to these results, species-specific differences in the CsrA target gene set can be explained by the phylogenetic distance.

Remarkably, when comparing the list of the CsrA targets of the CLIP-Seq interactome in *S. typhimurium* [Holmqvist *et al*., 2016] to predicted genes in *Y. pseudotuberculosis*, CsrA target genes changed within the same functional enzymatic cascade (data not shown). Such a pattern was also recognizable when comparing the data of predicted CsrA targets between *E. coli*, *S. typhimurium* and *P. aeruginosa* by Kulkarni and colleagues (data not shown) [Kulkarni *et al*., 2014] and predicted targets of *Y. pseudotuberculosis* and *E. coli* (**table 3.1**).

These changes were shown for the extensively studied glycogen (*glg*) operon (see **chapter 3.19.4**). In *E. coli*, the *glgC* gene is regulated and bound by CsrA, due to a high number of binding sites. In *Y. pseudotuberculosis* a CsrA-dependent regulation of this gene was detected neither at 25 °C nor at 37 °C [Nuss, unpublished data] and crucial binding sites are not present. Furthermore, the 5'-UTRs of other *glg* operon genes were analyzed and compared by a ClustalO alignment and analyzed for CsrA binding motifs. The analysis revealed a change in the binding motif composition within the 5'-UTR of individual *glg* genes resulting in an extensive reorganization of the CsrA target gene set within the *glg* operon. Indeed, *glgX* and *glgB* have a low number of binding sites (**Fig. 3.22**) and display no CsrA dependency in *E. coli* [Yang *et al*., 1996]. In contrast, *Y. pseudotuberculosis glgB* and *glgX* have several binding motifs (**Fig. 3.19.4**) and are repressed by CsrA to some extent [Nuss, unpublished

data]. Similar observations were made for motility-specific genes and the tRNA-modifying genes *miaA*/*B* (see **chapter 3.19.4**).

Taken together, this points to a change in the CsrA dependency of individual *glg* genes and other metabolic genes in *E. coli* and *Y. pseudotuberculosis* and a phylogenetic conservation of CsrA-dependent functional modules. Although the glycogen metabolism operon keeps its overall CsrA dependency, individual CsrA targets change or their affinity is weakened.

Similar observation was also made for the small non-coding RNAs *csrB/C*. These RNAs contain a high number of GGA motifs and control the activity of CsrA through a sequestration mechanism. Homologs of *csrB/C* were identified in many Gram-negative bacteria but differ in the number of CsrA binding sites [Babitzke & Romeo, 2007]. These differences might have a major influence on the available amount of CsrA and therefore change the species-specific CsrA regulon.

In conclusion, CsrA target gene sets are only partially conserved between bacteria, but the CsrA dependency of regulated pathways remains (**chapter 3.19.4**). A reason for frequent changes of CsrA binding sites might be the low complexity of the CsrA core binding motif (GGA). Point mutations within this short motif decrease the binding affinity or destroy the binding motif. Additionally, UTRs display only a low degree of evolutionary conservation in comparison to the well-conserved coding sequence. Because of this, CsrA binding motifs in the upstream region of target genes can be easily lost or gained by mutations. While it seems to be crucial for survival to maintain the CsrA-dependent regulation of certain pathways, the CsrA-dependencies can easily switch between genes. This would result in an evolutionary selection of CsrA-dependent pathways rather than of individual CsrA targets. This might also be the reason why CsrA targets dramatically differ with increasing phylogenetic distance and predicted and determined binding sites only lowly overlap between species.

5 Outlook

This study demonstrated the complex regulation of the Ysc-Yop T3SS by the RNA-binding proteins YopD and CsrA. Expression of both regulators is linked in mutually dependent feedback loops. To further investigate the YopD-dependent regulation of *csrA*, the YopD-controlled transcriptional regulator of *csrA* needs to be identified. As this regulator is YopD-dependently regulated and seems to be solely active at 37 °C, a comparative analysis of the YopD regulon at 37 °C under non-secretory and secretion conditions with the YopD interactome might aid to identify the transcriptional regulator of *csrA*.

The RNA-binding domains of YopD as well as the involved RNA binding motifs and folds are still uncharacterized. This study proposed the involvement of different RNA features in the YopD-dependent gene activation and repression. Therefore, YopD/LcrH should be crystallized together with a transcript which is YopD-dependently induced (e.g. *csrA*) and a repressed one (e.g. *yopQ* or *lcrF*). This might help to gain a better understanding of the unknown domain that confers YopD's RNA binding capacity. Additionally, other studies demonstrated that different regions of YopD are needed for pore formation, the translocation, *yop* regulation, secretion and LcrH binding, the crystal structure might help to understand the nature of the dual function of YopD as a translocator and regulator. By CLIP-Seq analysis, direct YopD target genes and RNA binding sites should be isolated on a global scale. Additionally, YopD-dependent repression appears to depend on multiple factors, such as SycH and LcrQ. For this reason, their influence on YopD-dependent RNA binding should be analyzed in RNA-EMSA analysis.

Another important task will be to further characterize CsrA binding parameters, as *in silico* target predictions are still challenging, due to the low complexity of the short CsrA binding motif. CsrA preferentially binds to ANGGA motifs exposed on hairpin loops. To address this parameter, *in silico* fold algorithms should be taken into account. In this study, *in silico* fold prediction could not be utilized as, for a given probability space of RNA folds, most ANGGA motifs will be exposed on hairpin loops in certain folds. As fold algorithms do not consider parameters, such as RNA-binding proteins, ion concentration or cytosolic crowding, an RNA structurome data set can be used instead.

On a larger scale, a combined analysis of RNA-Seq, CLIP-Seq and the RNA structurome datasets can be further used to gain new insights into CsrA binding of high- and low-affinity target RNAs. To classify RNA targets identified by CLIP-Seq into low- and high-affinity RNA targets, the abundance of a given transcript needs to be taken into account and can be

analyzed by differential RNA-Seq. The RNA structurome dataset addresses *in vitro* RNA folds, which help to localize binding sites identified by CLIP-Seq within the secondary structure of a target gene. Moreover, CsrA targets which were identified in this study should be validated for *in vitro* binding by RNA-EMSA.

.

6 Summary

Expression of Ysc-Yop type III secretion system requires a tight regulation, which is conferred by two RNA-binding proteins YopD and CsrA. The underlying study demonstrated that expression of the transcriptional master regulator *lcrF* of the Ysc-Yop T3SS is controlled in intertwined feedback loops by these RNA-binding proteins.

CsrA is a global acting post-transcriptional regulator that coordinates metabolic and virulence gene expression. This study demonstrated that expression of *csrA* is precisely controlled in an autoregulatory feedback loop, indirectly on the transcriptional and directly on the post-transcriptional level. CsrA was found to directly bind to two sites in the 5'-UTR of its transcript, from which one site is located within the ribosomal binding site. By this mechanism, CsrA was shown to block translational initiation and restrict CsrA synthesis when a certain CsrA amount is reached. Under non-secretion conditions, the RNA-binding protein YopD was shown to bind to the *csrA* transcript thereby masking a CsrA binding site and preventing the direct autoinhibition of *csrA*.

Analysis of the mutual role of CsrA and YopD in the regulation of *lcrF* expression demonstrated a direct interaction of both RNA-binding proteins in multiple regions of the *yscW-lcrF* transcript. The 5'-UTR of *lcrF* contains an RNA-thermometer structure, which prevents ribosomal access through a base-pairing mechanism. Furthermore, this study demonstrated, CsrA interacts with the ribosomal binding site of *lcrF* and modulates the opening state of the RNA thermometer.

Interestingly, this work uncovered that both regulators modulate the stability of the *lcrF* transcript. CsrA has a stabilizing and YopD a destabilizing effect on the *lcrF* mRNA. This is caused by the antagonistic YopD- and CsrA-dependent control of the RNA degradosome.

Additionally, this study analyzed the temperature-dependent regulation of *yopD* expression. The *yopD* gene is transcribed from two promoters. This study demonstrated, at 25 °C *yopD* is mainly transcribed from its own promoter P_{yopD}. As a consequence, *yopD* expression is uncoupled from its chaperone *lcrH*. Due to the imbalance of YopD and LcrH protein, YopD is constantly degraded and remains in a stand-by mode as it cannot confer its regulatory role. At 37 °C, *yopD* is mainly transcribed from the P_{lcrG} promoter allowing the translation of YopD, as well as LcrH. Now sufficient amounts of chaperone LcrH are present and the YopD protein is stabilized to confer its regulatory control.

Furthermore, new putative CsrA targets could be identified by an interactome analysis with FLAG-tagged CsrA protein. At body host temperature, CsrA specifically interacts with

tRNAs and transcripts of tRNA processing proteins. Moreover, a comparison of predicted direct CsrA targets in *Escherichia coli* and *Yersinia pseudotuberculosis* demonstrated a low conservation of CsrA target genes between both species and a low conservation of CsrA binding site in the 5'-UTR of these target genes.

In summary, this study revealed the complex interplay of YopD and CsrA in controlling the expression of the T3SS master regulator *lcrF*. Both regulators are in involved in the post-transcriptional control of *lcrF* expression under non-secretion conditions and confer an antagonistic regulation.

7 References

Abby, S. S. & Rocha, E. P. C. The non-flagellar type III secretion system evolved from the bacterial flagellum and diversified into host-cell adapted systems. *PLoS Genet.* **8,** (2012).

Achtman, M. *et al. Yersinia pestis*, the cause of plague, is a recently emerged clone of *Yersinia pseudotuberculosis*. *Proc. Natl. Acad. Sci. U. S. A.* **96,** 14043–8 (1999).

Adamson, D. N. & Lim, H. N. Rapid and robust signaling in the CsrA cascade via RNA-protein interactions and feedback regulation. *Proc. Natl. Acad. Sci. U. S. A.* **110,** 13120–5 (2013).

Aepfelbacher, M., Trasak, C. & Ruckdeschel, K. Effector functions of pathogenic *Yersinia* species. *Thrombosis and Haemostasis* **98,** 521–529 (2007).

Aepfelbacher, M. *et al.* Characterization of YopT effects on Rho GTPases in *Yersinia enterocolitica*-infected cells. *J. Biol. Chem.* **278,** 33217–23 (2003).

Akeda, Y. & Galán, J. E. Chaperone release and unfolding of substrates in type III secretion. *Nature* **437,** 911–5 (2005).

Akopyan, K. *et al.* Translocation of surface-localized effectors in type III secretion. *Proc. Natl. Acad. Sci. U. S. A.* **108,** 1639–44 (2011).

Alon, U. Network motifs: theory and experimental approaches. *Nat. Rev. Genet.* **8,** 450–61 (2007).

Altman, S. Biosynthesis of transfer RNA in *Escherichia coli*. *Cell* **4,** 21–29 (1975).

Alvarez, A. F., Barba-Ostria, C., Silva-Jiménez, H. & Georgellis, D. Organization and mode of action of two component system signaling circuits from the various kingdoms of life. *Environ. Microbiol.* (2016).

Anderson, D. M., Ramamurthi, K. S., Tam, C. & Schneewind, O. YopD and LcrH Regulate Expression of *Yersinia enterocolitica* YopQ by a Posttranscriptional Mechanism and Bind to yopQ RNA. *J. Bacteriol.* **184,** 1287–1295 (2002).

Andrade, J. M., Pobre, V., Silva, I. J., Domingues, S. & Arraiano, C. M. *Molecular Biology of RNA Processing and Decay in Prokaryotes*. *Progress in Molecular Biology and Translational Science* **85,** (Elsevier, 2009).

Andrews S. (2010). FastQC: a quality control tool for high throughput sequence data. Available online at: http://www.bioinformatics.babraham.ac.uk/projects/fastqc

Atkinson, S. & Williams, P. *Yersinia* virulence factors - a sophisticated arsenal for combating host defences. *F1000Research* **5,** (2016).

Autenrieth, I. B., Hantschmann, P., Heymer, B. & Heesemann, J. Immunohistological characterization of the cellular immune response against *Yersinia enterocolitica* in mice: evidence for the involvement of T lymphocytes. *Immunobiology* **187,** 1–16 (1993).

Autenrieth, I. B. & Firsching, R. Penetration of M cells and destruction of Peyer's patches by *Yersinia enterocolitica*: An ultrastructural and histological study. *J. Med. Microbiol.* **44,** 285–294 (1996).

Babitzke, P. & Romeo, T. CsrB sRNA family: sequestration of RNA-binding regulatory proteins. *Curr. Opin. Microbiol.* **10,** 156–63 (2007).

Baker, C. S. *et al.* CsrA Inhibits Translation Initiation of *Escherichia coli* hfq by Binding to a Single Site Overlapping the Shine-Dalgarno Sequence. *J. Bacteriol.* **189,** 5472–5481 (2007).

Baker, C. S., Morozov, I., Suzuki, K., Romeo, T. & Babitzke, P. CsrA regulates glycogen biosynthesis by preventing translation of glgC in *Escherichia coli*. *Mol. Microbiol.* **44,** 1599–1610 (2002).

Balada-Llasat, J.-M. & Mecsas, J. *Yersinia* has a tropism for B and T cell zones of lymph nodes that is independent of the type III secretion system. *PLoS Pathog.* **2,** e86 (2006).

Balsalobre, C. *et al.* Complementation of the hha mutation in *Escherichia coli* by the ymoA gene from *Yersinia enterocolitica*: dependence on the gene dosage. *Microbiology* **142 (Pt 7,** 1841–6 (1996).

Bandyra, K. J., Bouvier, M., Carpousis, A. J. & Luisi, B. F. The social fabric of the RNA degradosome. *Biochim. Biophys. Acta* **1829,** 514–22 (2013).

Barnard, F. M. *et al.* Global regulation of virulence and the stress response by CsrA in the highly adapted human gastric pathogen Helicobacter pylori. *Mol. Microbiol.* **51,** 15–32 (2004).

Barz, C., Abahji, T. N., Trülzsch, K. & Heesemann, J. The *Yersinia* Ser/Thr protein kinase YpkA/YopO directly interacts with the small GTPases RhoA and Rac-1. *FEBS Lett.* **482,** 139–43 (2000).

Bengoechea, J. A., Najdenski, H. & Skurnik, M. Lipopolysaccharide O antigen status of *Yersinia enterocolitica* O:8 is essential for virulence and absence of O antigen affects the expression of other *Yersinia* virulence factors. *Mol. Microbiol.* **52,** 451–69 (2004).

Biedzka-Sarek, M. *et al.* Functional mapping of YadA- and Ail-mediated binding of human factor H to *Yersinia enterocolitica* serotype O:3. *Infect. Immun.* **76,** 5016–27 (2008).

Black, D. S., Marie-Cardine, A., Schraven, B. & Bliska, J. B. The *Yersinia* tyrosine phosphatase YopH targets a novel adhesion-regulated signalling complex in macrophages. *Cell. Microbiol.* **2,** 401–414 (2000).

Blaszczak, A., Zylicz, M., Georgopoulos, C. & Liberek, K. Both ambient temperature and the DnaK chaperone machine modulate the heat shock response in *Escherichia coli* by regulating the switch between sigma 70 and sigma 32 factors assembled with RNA polymerase. *EMBO J.* **14,** 5085–93 (1995).

Böhme, K. *et al.* Concerted actions of a thermo-labile regulator and a unique intergenic RNA thermosensor control *Yersinia* virulence. *PLoS Pathog.* **8,** e1002518 (2012).

Bolin, I., Norlander, L. & Wolf-Watz, H. Temperature-inducible outer membrane protein of *Yersinia pseudotuberculosis* and *Yersinia enterocolitica* is associated with the virulence plasmid. *Infect. Immun.* **37,** 506–512 (1982).

Bottone, E. J. *Yersinia enterocolitica*: the charisma continues. *Clin. Microbiol. Rev.* **10,** 257 (1997).

Bradford, M. A rapid and sensitive method for the quantiWcation of microgram quantities of protein utilizing the principle of protein– dye binding. *Anal. Biochem.* **72,** 248–254 (1976).

Brencic, A. & Lory, S. Determination of the regulon and identification of novel mRNA targets of *Pseudomonas aeruginosa* RsmA. *Mol. Microbiol.* **72,** 612–632 (2009).

Broz, P. *et al.* Function and molecular architecture of the *Yersinia* injectisome tip complex. *Mol. Microbiol.* **65,** 1311–20 (2007).

Brutinel, E. D., Vakulskas, C. A., Brady, K. M. & Yahr, T. L. Characterization of ExsA and of ExsA-dependent promoters required for expression of the *Pseudomonas aeruginosa* type III secretion system. *Mol. Microbiol.* **68,** 657–71 (2008).

Buchmeier, N. *et al.* SlyA, a transcriptional regulator of *Salmonella typhimurium*, is required for resistance to oxidative stress and is expressed in the intracellular environment of macrophages. *Infect. Immun.* **65,** 3725–30 (1997).

Burghout, P. *et al.* Role of the pilot protein YscW in the biogenesis of the YscC secretin in *Yersinia enterocolitica*. *J. Bacteriol.* **186,** 5366–5375 (2004).

Bustin, S. A., Benes, V., Nolan, T. & Pfaffl, M. W. Quantitative real-time RT-PCR--a perspective. *J Mol Endocrinol* **34,** 597–601 (2005).

Callaghan, A. J. *et al.* Structure of *Escherichia coli* RNase E catalytic domain and implications for RNA turnover. *Nature* **437,** 1187–91 (2005).

Camacho, C. *et al.* BLAST+: architecture and applications. *BMC Bioinformatics* **10,** 421 (2009).

Camacho, M. I. *et al.* Effects of the global regulator CsrA on the BarA/UvrY two-component signaling system. *J. Bacteriol.* **197,** 983–91 (2015).

Cambronne, E. D., Cheng, L. W. & Schneewind, O. LcrQ/YscM1, regulators of the *Yersinia* yop virulon, are injected into host cells by a chaperone-dependent mechanism. *Mol. Microbiol.* **37,** 263–273 (2000).

Cambronne, E. D. & Schneewind, O. *Yersinia enterocolitica* type III secretion: yscM1 and yscM2 regulate yop gene expression by a posttranscriptional mechanism that targets the 5' untranslated region of yop mRNA. *J. Bacteriol.* **184,** 5880–93 (2002).

Cambronne, E. D., Sorg, J. A. & Schneewind, O. Binding of SycH chaperone to YscM1 and YscM2 activates effector yop expression in *Yersinia enterocolitica*. *J. Bacteriol.* **186,** 829–41 (2004).

Carpousis, A. J. The RNA degradosome of *Escherichia coli*: an mRNA-degrading machine assembled on RNase E. *Annu. Rev. Microbiol.* **61,** 71–87 (2007).

Caruthers, J. M. & McKay, D. B. Helicase structure and mechanism. *Curr. Opin. Struct. Biol.* **12,** 123–133 (2002).

Carzaniga, T. *et al.* Autogenous Regulation of *Escherichia coli* Polynucleotide Phosphorylase Expression Revisited. *J. Bacteriol.* **191,** 1738–1748 (2009).

Casadaban, M. J. & Cohen, S. N. Analysis of gene control signals by DNA fusion and cloning in *Escherichia coli*. *J. Mol. Biol.* **138,** 179–207 (1980).

Cascales, E. & Journet, L. The Type VI Secretion System in *Escherichia coli* and Related Species. *EcoSal Plus* **7,** (2016).

Casutt-Meyer, S. *et al.* Oligomeric coiled-coil adhesin YadA is a double-edged sword. *PLoS One* **5,** e15159 (2010).

Chandran, V. & Luisi, B. F. Recognition of enolase in the *Escherichia coli* RNA degradosome. *J. Mol. Biol.* **358,** 8–15 (2006).

Chang, A. C. Y. & Cohen, S. N. Construction and characterization of amplifiable multicopy DNA cloning vehicles derived from the P15A cryptic miniplasmid. *J. Bacteriol.* **134,** 1141–1156 (1978).

Chavez, R. G., Alvarez, A. F., Romeo, T. & Georgellis, D. The Physiological Stimulus for the BarA Sensor Kinase. *J. Bacteriol.* **192,** 2009–2012 (2010).

Chen, S., Thompson, K. M. & Francis, M. S. Environmental Regulation of *Yersinia* Pathophysiology. *Front. Cell. Infect. Microbiol.* **6,** 25 (2016).

Chen, Y. & Anderson, D. M. Expression hierarchy in the *Yersinia* type III secretion system established through YopD recognition of RNA. *Mol. Microbiol.* **80,** 966–80 (2011).

Chilcott, G. S. & Hughes, K. T. Coupling of flagellar gene expression to flagellar assembly in *Salmonella enterica* serovar typhimurium and Escherichia coli. *Microbiol. Mol. Biol. Rev.* **64,** 694–708 (2000).

Chouikha, I. & Hinnebusch, B. J. *Yersinia*--flea interactions and the evolution of the arthropod-borne transmission route of plague. *Curr. Opin. Microbiol.* **15,** 239–46 (2012).

Chung, L. K. *et al.* The Yersinia Virulence Factor YopM Hijacks Host Kinases to Inhibit Type III Effector-Triggered Activation of the Pyrin Inflammasome. *Cell Host Microbe* **20,** 296–306 (2016).

Clark, M. A., Hirst, B. H. & Jepson, M. A. M-cell surface beta1 integrin expression and invasin-mediated targeting of *Yersinia pseudotuberculosis* to mouse Peyer's patch M cells. *Infect. Immun.* **66,** 1237–43 (1998).

Condon, C. Airpnp: Auto- and Integrated Regulation of Polynucleotide Phosphorylase. *J. Bacteriol.* **197,** 3748–50 (2015).

Cordin, O., Banroques, J., Tanner, N. K. & Linder, P. The DEAD-box protein family of RNA helicases. *Gene* **367,** 17–37 (2006).

Cornelis, G. R. The type III secretion injectisome. *Nat. Rev. Microbiol.* **4,** 811–25 (2006).

Cornelis, G. R. The *Yersinia* Ysc-Yop 'type III' weaponry. *Nat. Rev. Mol. Cell Biol.* **3,** 742–52 (2002).

Cornelis, G. R. The type III secretion injectisome, a complex nanomachine for intracellular 'toxin' delivery. *Biological Chemistry* **391,** 745–751 (2010).

Cornelis, G. R. & Wolf-Watz, H. The *Yersinia* Yop virulon: a bacterial system for subverting eukaryotic cells. *Mol. Microbiol.* **23,** 861–867 (1997).

Costa, T. R. D., Amer, A. A. A., Fällman, M., Fahlgren, A. & Francis, M. S. Coiled-coils in the YopD translocator family: a predicted structure unique to the YopD N-terminus contributes to full virulence of *Yersinia pseudotuberculosis*. *Infect. Genet. Evol.* **12,** 1729–42 (2012).

Daniels, J. J., Autenrieth, I. B., Ludwig, A. & Goebel, W. The gene *slyA* of *Salmonella typhimurium* is required for destruction of M cells and intracellular survival but not for invasion or colonization of the murine small intestine. *Infect. Immun.* **64,** 5075–84 (1996).

Dasgupta, N., Lykken, G. L., Wolfgang, M. C. & Yahr, T. L. A novel anti-anti-activator mechanism regulates expression of the *Pseudomonas aeruginosa* type III secretion system. *Mol. Microbiol.* **53,** 297–308 (2004).

Davis MW (2016). ApE: a plasmid Editor. Available online at: http://biologylabs.utah.edu/jorgensen/wayned/ape/

de Smit, M. H., Verlaan, P. W. G., van Duin, J. & Pleij, C. W. A. Intracistronic transcriptional polarity enhances translational repression: a new role for Rho. *Mol. Microbiol.* **69,** 1278–1289 (2008).

Deneke, C., Lipowsky, R. & Valleriani, A. Effect of ribosome shielding on mRNA stability. *Phys. Biol.* **10,** 46008 (2013).

Diaz, M. R., King, J. M. & Yahr, T. L. Intrinsic and Extrinsic Regulation of Type III Secretion Gene Expression in *Pseudomonas Aeruginosa*. *Front. Microbiol.* **2,** 89 (2011).

Diepold, A. & Armitage, J. P. Type III secretion systems: the bacterial flagellum and the injectisome. *Philos. Trans. R. Soc. Lond. B. Biol. Sci.* **370,** (2015).

Diepold, A. & Wagner, S. Assembly of the bacterial type III secretion machinery. *FEMS Microbiol. Rev.* **38,** 802–22 (2014).

Dube, P. H., Handley, S. A., Revell, P. A. & Miller, V. L. The *rovA* mutant of *Yersinia enterocolitica* displays differential degrees of virulence depending on the route of infection. *Infect. Immun.* **71,** 3512–20 (2003).

Dubey, A. K., Baker, C. S., Romeo, T. & Babitzke, P. RNA sequence and secondary structure participate in high-affinity CsrA-RNA interaction. *RNA* **11,** 1579–87 (2005).

Dubey, A. K. *et al.* CsrA regulates translation of the *Escherichia coli* carbon starvation gene, cstA, by blocking ribosome access to the cstA transcript. *J. Bacteriol.* **185,** 4450–60 (2003).

Dugar, G. *et al.* The CsrA-FliW network controls polar localization of the dual-function flagellin mRNA in Campylobacter jejuni. *Nat. Commun.* **7,** 11667 (2016).

Edgren, T., Forsberg, A., Rosqvist, R. & Wolf-Watz, H. Type III secretion in *Yersinia*: injectisome or not? *PLoS Pathog.* **8,** e1002669 (2012).

Edwards, A. N. *et al.* Circuitry linking the Csr and stringent response global regulatory systems. *Mol. Microbiol.* **80,** 1561–80 (2011).

Eitel, J. & Dersch, P. The YadA protein of *Yersinia pseudotuberculosis* mediates high-efficiency uptake into human cells under environmental conditions in which invasin is repressed. *Infect. Immun.* **70,** 4880–91 (2002).

El Tahir, Y. & Skurnik, M. YadA, the multifaceted *Yersinia* adhesin. *Int. J. Med. Microbiol.* **291,** 209–18 (2001).

Erhardt, M. & Dersch, P. Regulatory principles governing *Salmonella* and *Yersinia* virulence. *Front. Microbiol.* **6,** 949 (2015).

Esquerré, T. *et al.* The Csr system regulates genome-wide mRNA stability and transcription and thus gene expression in *Escherichia coli*. *Sci. Rep.* **6,** 25057 (2016).

Evans, D., Marquez, S. M. & Pace, N. R. RNase P: interface of the RNA and protein worlds. *Trends Biochem. Sci.* **31,** 333–341 (2006).

Fahlgren, A., Westermark, L., Akopyan, K. & Fällman, M. Cell type-specific effects of *Yersinia pseudotuberculosis* virulence effectors. *Cell. Microbiol.* **11,** 1750–67 (2009).

Fang, F. C., Frawley, E. R., Tapscott, T. & Vázquez-Torres, A. Bacterial Stress Responses during Host Infection. *Cell Host Microbe* **20,** 133–143 (2016).

Feng, Y., Huang, H., Liao, J. & Cohen, S. N. *Escherichia coli* poly(A)-binding proteins that interact with components of degradosomes or impede RNA decay mediated by polynucleotide phosphorylase and RNase E. *J. Biol. Chem.* **276,** 31651–6 (2001).

Fortune, D. R., Suyemoto, M. & Altier, C. Identification of CsrC and characterization of its role in epithelial cell invasion in *Salmonella enterica* serovar Typhimurium. *Infect. Immun.* **74,** 331–9 (2006).

Foster, J. W. When protons attack: microbial strategies of acid adaptation. *Curr. Opin. Microbiol.* **2,** 170–4 (1999).

Francis, M. S., Aili, M., Wiklund, M. L. & Wolf-Watz, H. A study of the YopD-lcrH interaction from *Yersinia pseudotuberculosis* reveals a role for hydrophobic residues within the amphipathic domain of YopD. *Mol. Microbiol.* **38,** 85–102 (2000).

Francis, M. S., Lloyd, S. A. & Wolf-Watz, H. The type III secretion chaperone LcrH co-operates with YopD to establish a negative, regulatory loop for control of Yop synthesis in *Yersinia pseudotuberculosis*. *Mol. Microbiol.* **42,** 1075–1093 (2001).

Fredriksson-Ahomaa, M., Stolle, A. & Korkeala, H. Molecular epidemiology of *Yersinia enterocolitica* infections. *FEMS Immunol. Med. Microbiol.* **47,** (2006).

Frees, D., Thomsen, L. E. & Ingmer, H. Staphylococcus aureus ClpYQ plays a minor role in stress survival. *Arch. Microbiol.* **183,** 286–291 (2005).

Gallegos, M. T., Schleif, R., Bairoch, a, Hofmann, K. & Ramos, J. L. Arac/XylS family of transcriptional regulators. *Microbiol. Mol. Biol. Rev.* **61,** 393–410 (1997).

Gao, M. *et al.* RNA Hairpin Folding in the Crowded Cell. *Angew. Chem. Int. Ed. Engl.* **55,** 3224–8 (2016).

Goujon, M. *et al.* A new bioinformatics analysis tools framework at EMBL-EBI. *Nucleic Acids Res.* **38,** (2010).

Grassl, G. A., Bohn, E., Müller, Y., Bühler, O. T. & Autenrieth, I. B. Interaction of *Yersinia enterocolitica* with epithelial cells: invasin beyond invasion. *Int. J. Med. Microbiol.* **293,** 41–54 (2003).

Grützkau, A., Hanski, C., Hahn, H. & Riecken, E. O. Involvement of M cells in the bacterial invasion of Peyer's patches: a common mechanism shared by *Yersinia enterocolitica* and other enteroinvasive bacteria. *Gut* **31,** 1011–5 (1990).

Gutiérrez, P. *et al.* Solution structure of the carbon storage regulator protein CsrA from *Escherichia coli*. *J. Bacteriol.* **187,** 3496–501 (2005).

Guttenplan, S. B. & Kearns, D. B. Regulation of flagellar motility during biofilm formation. *FEMS Microbiol. Rev.* **37,** 849–71 (2013).

Guzman, L. M., Belin, D., Carson, M. J. & Beckwith, J. Tight regulation, modulation, and high-level expression by vectors containing the arabinose P_{BAD} promoter. *J. Bacteriol.* **177,** 4121–30 (1995).

Hachani, A., Wood, T. E. & Filloux, A. Type VI secretion and anti-host effectors. *Curr. Opin. Microbiol.* **29,** 81–93 (2016).

Hakansson, S., Galyov, E. E., Rosqvist, R. & Wolf-Watz, H. The *Yersinia* YpkA Ser/Thr kinase is translocated and subsequently targeted to the inner surface of the HeLa cell plasma membrane. *Mol. Microbiol.* **20,** 593–603 (1996).

Hamburger, Z. A. Crystal Structure of Invasin: A Bacterial Integrin-Binding Protein. *Science (80-.).* **286,** 291–295 (1999).

Han, Y., Fang, H., Liu, L. & Zhou, D. in *Yersinia pestis: Retrospective and Perspective* (eds. Yang, R. & Anisimov, A.) 223–256 (Springer Netherlands, 2016).

Handley, S. A., Dube, P. H., Revell, P. A. & Miller, V. L. Characterization of oral *Yersinia enterocolitica* infection in three different strains of inbred mice. *Infect. Immun.* **72,** 1645–56 (2004).

Hartl, F. U., Bracher, A. & Hayer-Hartl, M. Molecular chaperones in protein folding and proteostasis. *Nature* **475,** 324–332 (2011).

al-Hazred, A. Al-Azif. (830).

Head, S. R. *et al.* Library construction for next-generation sequencing: overviews and challenges. *Biotechniques* **56,** 61–4, 66, 68, passim (2014).

Heesemann, J., Sing, A. & Trülzsch, K. *Yersinia*'s stratagem: targeting innate and adaptive immune defense. *Curr. Opin. Microbiol.* **9,** 55–61 (2006).

Heise, T. & Dersch, P. Identification of a domain in *Yersinia* virulence factor YadA that is crucial for extracellular matrix-specific cell adhesion and uptake. *Proc. Natl. Acad. Sci. U. S. A.* **103,** 3375–80 (2006).

Hengge-Aronis, R. Signal transduction and regulatory mechanisms involved in control of the sigma(S) (RpoS) subunit of RNA polymerase. *Microbiol. Mol. Biol. Rev.* **66,** 373–95, table of contents (2002).

Heroven, A. K., Böhme, K. & Dersch, P. The Csr/Rsm system of *Yersinia* and related pathogens: a post-transcriptional strategy for managing virulence. *RNA Biol.* **9,** 379–91 (2012).

Heroven, A. K., Böhme, K., Rohde, M. & Dersch, P. A Csr-type regulatory system, including small non-coding RNAs, regulates the global virulence regulator RovA of *Yersinia pseudotuberculosis* through RovM. *Mol. Microbiol.* **68,** 1179–95 (2008).

Heroven, A. K., Böhme, K., Tran-Winkler, H. & Dersch, P. Regulatory elements implicated in the environmental control of invasin expression in enteropathogenic *Yersinia*. *Adv. Exp. Med. Biol.* **603,** 156–66 (2007).

Heroven, A. K. & Dersch, P. RovM, a novel LysR-type regulator of the virulence activator gene *rovA*, controls cell invasion, virulence and motility of *Yersinia pseudotuberculosis*. *Mol. Microbiol.* **62,** 1469–1483 (2006).

Heroven, A. K. & Dersch, P. Coregulation of host-adapted metabolism and virulence by pathogenic yersiniae. *Front. Cell. Infect. Microbiol.* **4,** (2014).

Heroven, A. K. *et al.* Crp induces switching of the CsrB and CsrC RNAs in *Yersinia pseudotuberculosis* and links nutritional status to virulence. *Front. Cell. Infect. Microbiol.* **2,** 158 (2012).

Hoe, N. P. & Goguen, J. D. Temperature sensing in *Yersinia pestis*: translation of the LcrF activator protein is thermally regulated. *J. Bacteriol.* **175,** 7901–9 (1993).

Hoe, N. P., Minion, F. C. & Goguen, J. D. Temperature sensing in *Yersinia pestis*: regulation of *yopE* transcription by lcrF. *J. Bacteriol.* **174,** 4275–86 (1992).

Hoiczyk, E., Roggenkamp, A., Reichenbecher, M., Lupas, A. & Heesemann, J. Structure and sequence analysis of *Yersinia* YadA and Moraxella UspAs reveal a novel class of adhesins. *EMBO J.* **19,** 5989–99 (2000).

Holmqvist, E. *et al.* Global RNA recognition patterns of post-transcriptional regulators Hfq and CsrA revealed by UV crosslinking in vivo. *EMBO J.* **35,** 991–1011 (2016).

Hui, M. P., Foley, P. L. & Belasco, J. G. Messenger RNA degradation in bacterial cells. *Annu. Rev. Genet.* **48,** 537–59 (2014).

Intile, P. J., Diaz, M. R., Urbanowski, M. L., Wolfgang, M. C. & Yahr, T. L. The AlgZR two-component system recalibrates the RsmAYZ posttranscriptional regulatory system to inhibit expression of the *Pseudomonas aeruginosa* type III secretion system. *J. Bacteriol.* **196,** 357–366 (2014).

Iriarte, M., Stainier, I. & Cornelis, G. R. The *rpoS* gene from *Yersinia enterocolitica* and its influence on expression of virulence factors. *Infect. Immun.* **63,** 1840–7 (1995).

Jackson, D. W. *et al.* Biofilm formation and dispersal under the influence of the global regulator CsrA of *Escherichia coli*. *J. Bacteriol.* **184,** 290–301 (2002).

Jackson, M. W., Silva-Herzog, E. & Plano, G. V. The ATP-dependent ClpXP and Lon proteases regulate expression of the *Yersinia pestis* type III secretion system via regulated proteolysis of YmoA, a small histone-like protein. *Mol. Microbiol.* **54,** 1364–1378 (2004).

Jarrige, A. C., Mathy, N. & Portier, C. PNPase autocontrols its expression by degrading a double-stranded structure in the pnp mRNA leader. *EMBO J.* **20,** 6845–55 (2001).

Jean-Pierre, F., Déziel, E. & Perreault, J. Complex autoregulation of the post-transcriptional regulator RsmA in *Pseudomonas aeruginosa*. *Microbiology* **161,** 1889–1896 (2015).

Juris, S. J., Rudolph, A. E., Huddler, D., Orth, K. & Dixon, J. E. A distinctive role for the *Yersinia* protein kinase: actin binding, kinase activation, and cytoskeleton disruption. *Proc. Natl. Acad. Sci. U. S. A.* **97,** 9431–6 (2000).

Kapperud, G. *Yersinia enterocolitica* in food hygiene. *Int. J. Food Microbiol.* **12,** 53–65 (1991).

Kutsukake, K. & Iino, T. Role of the FliA-FlgM regulatory system on the transcriptional control of the flagellar regulon and flagellar formation in Salmonella typhimurium. *J. Bacteriol.* **176,** 3598–3605 (1994).

Khemici, V., Poljak, L., Luisi, B. F. & Carpousis, A. J. The RNase E of *Escherichia coli* is a membrane-binding protein. *Mol. Microbiol.* **70,** 799–813 (2008).

King, J. M., Schesser Bartra, S., Plano, G. & Yahr, T. L. ExsA and LcrF recognize similar consensus binding sites, but differences in their oligomeric state influence interactions with promoter DNA. *J. Bacteriol.* **195,** 5639–50 (2013).

Kirjavainen, V. *et al. Yersinia enterocolitica* serum resistance proteins YadA and ail bind the complement regulator C4b-binding protein. *PLoS Pathog.* **4,** e1000140 (2008).

Kirstein, J., Molière, N., Dougan, D. A. & Turgay, K. Adapting the machine: adaptor proteins for Hsp100/Clp and AAA+ proteases. *Nat. Rev. Microbiol.* **7,** 589–599 (2009).

Knittel, VD. Function and regulation of RovC - a new virulence factor in *Yersina pseudotuberculosis*. (2015).

Koharudin, L. M. I., Boelens, R., Kaptein, R. & Gronenborn, A. M. A NMR guided approach for CsrA–RNA crystallization. *J. Biomol. NMR* **56,** 31–39 (2013).

Kopaskie, K. S., Ligtenberg, K. G. & Schneewind, O. Translational regulation of *Yersinia enterocolitica* mRNA encoding a type III secretion substrate. *J. Biol. Chem.* **288,** 35478–88 (2013).

Koretke, K. K., Szczesny, P., Gruber, M. & Lupas, A. N. Model structure of the prototypical non-fimbrial adhesin YadA of *Yersinia enterocolitica*. *J. Struct. Biol.* **155,** 154–61 (2006).

Kortmann, J. & Narberhaus, F. Bacterial RNA thermometers: molecular zippers and switches. *Nat. Rev. Microbiol.* **10,** 255–65 (2012).

Kulkarni, P. R. *et al.* A sequence-based approach for prediction of CsrA/RsmA targets in bacteria with experimental validation in *Pseudomonas aeruginosa*. *Nucleic Acids Res.* **42,** 6811–25 (2014).

Kukarcev, E. Die Typ VI-Sekretionssysteme von *Yersinia pseudotuberculosis* - Umweltregulation und Transkriptionskontrolle. (2015).

Kwuan, L., Adams, W. & Auerbuch, V. Impact of host membrane pore formation by the *Yersinia pseudotuberculosis* type III secretion system on the macrophage innate immune response. *Infect. Immun.* **81,** 905–14 (2013).

Laemmli, U. K. Cleavage of Structural Proteins during the Assembly of the Head of Bacteriophage T4. *Nature* **227,** 680–685 (1970).

Lapointe, C. P., Wilinski, D., Saunders, H. A. J. & Wickens, M. Protein-RNA networks revealed through covalent RNA marks. *Nat. Methods* **12,** 1163–1170 (2015).

Lapouge, K. *et al.* RNA pentaloop structures as effective targets of regulators belonging to the RsmA/CsrA protein family. *RNA Biol.* **10,** 1031–41 (2013).

Lawal, A., Jejelowo, O., Chopra, A. K. & Rosenzweig, J. A. Ribonucleases and bacterial virulence. *Microb. Biotechnol.* **4,** 558–71 (2011).

LeGrand, K. *et al.* CsrA impacts survival of *Yersinia enterocolitica* by affecting a myriad of physiological activities. *BMC Microbiol.* **15,** 31 (2015).

Leng, Y. *et al.* Regulation of CsrB/C sRNA decay by EIIA ^{Glc} of the phosphoenolpyruvate: carbohydrate phosphotransferase system. *Mol. Microbiol.* **99,** 627–639 (2016).

Leo, J. C. & Skurnik, M. Adhesins of human pathogens from the genus *Yersinia*. *Adv. Exp. Med. Biol.* **715,** 1–15 (2011).

Levy, S. B. & Marshall, B. Antibacterial resistance worldwide: causes, challenges and responses. (2004).

Li, H. *et al.* The Sequence Alignment/Map format and SAMtools. *Bioinformatics* **25,** 2078–9 (2009).

Li, L. *et al.* LcrQ blocks the role of LcrF in regulating the Ysc-Yop type III secretion genes in *Yersinia pseudotuberculosis*. *PLoS One* **9,** e92243 (2014).

Linder, P. *et al.* Birth of the D-E-A-D box. *Nature* **337,** 121–2 (1989).

Liou, G.-G., Chang, H.-Y., Lin, C.-S. & Lin-Chao, S. DEAD box RhlB RNA helicase physically associates with exoribonuclease PNPase to degrade double-stranded RNA independent of the degradosome-assembling region of RNase E. *J. Biol. Chem.* **277,** 41157–62 (2002).

Lithgow, J. K., Ingham, E. & Foster, S. J. Role of the hprT-ftsH locus in Staphylococcus aureus. *Microbiology* **150,** 373–381 (2004).

Liu, M. Y. *et al.* The RNA Molecule CsrB Binds to the Global Regulatory Protein CsrA and Antagonizes Its Activity in *Escherichia coli*. *J. Biol. Chem.* **272,** 17502–17510 (1997).

Mabbott, N. A., Donaldson, D. S., Ohno, H., Williams, I. R. & Mahajan, A. Microfold (M) cells: important immunosurveillance posts in the intestinal epithelium. *Mucosal Immunol.* **6,** 666–77 (2013).

Maciag, A. *et al.* In vitro transcription profiling of the σS subunit of bacterial RNA polymerase: re-definition of the σS regulon and identification of σS-specific promoter sequence elements. *Nucleic Acids Res.* **39,** 5338–55 (2011).

Mackie, G. A. Ribonuclease E is a 5'-end-dependent endonuclease. *Nature* **395,** 720–3 (1998).

Madrid, C., Balsalobre, C., García, J. & Juárez, A. The novel Hha/YmoA family of nucleoid-associated proteins: use of structural mimicry to modulate the activity of the H-NS family of proteins. *Mol. Microbiol.* **63,** 7–14 (2007).

Marceau, M. Transcriptional regulation in *Yersinia*: an update. *Curr. Issues Mol. Biol.* **7,** 151–77 (2005).

Marchal, K. *et al.* In silico identification and experimental validation of PmrAB targets in *Salmonella typhimurium* by regulatory motif detection. *Genome Biol.* **5,** R9 (2004).

Marlovits, T. C. *et al.* Structural insights into the assembly of the type III secretion needle complex. *Science* **306,** 1040–2 (2004).

Martínez-Chavarría, L. C. & Vadyvaloo, V. *Yersinia pestis* and *Yersinia pseudotuberculosis* infection: a regulatory RNA perspective. *Front. Microbiol.* **6,** 956 (2015).

McDowall, K. J. & Cohen, S. N. The N-terminal domain of the rne gene product has RNase E activity and is non-overlapping with the arginine-rich RNA-binding site. *J. Mol. Biol.* **255,** 349–55 (1996).

McNally, A., Thomson, N. R., Reuter, S. & Wren, B. W. 'Add, stir and reduce': *Yersinia* spp. as model bacteria for pathogen evolution. *Nat. Rev. Microbiol.* **14,** 177–190 (2016).

Mercante, J., Edwards, A. N., Dubey, A. K., Babitzke, P. & Romeo, T. Molecular geometry of CsrA (RsmA) binding to RNA and its implications for regulated expression. *J. Mol. Biol.* **392,** 511–28 (2009).

Mercante, J., Suzuki, K., Cheng, X., Babitzke, P. & Romeo, T. Comprehensive alanine-scanning mutagenesis of *Escherichia coli* CsrA defines two subdomains of critical functional importance. *J. Biol. Chem.* **281,** 31832–42 (2006).

Mikula, K. M., Kolodziejczyk, R. & Goldman, A. *Yersinia* infection tools-characterization of structure and function of adhesins. *Front. Cell. Infect. Microbiol.* **2,** 169 (2012).

Mili, S. & Steitz, J. A. Evidence for reassociation of RNA-binding proteins after cell lysis: implications for the interpretation of immunoprecipitation analyses. *RNA* **10,** 1692–4 (2004).

Miller, J. H. *Experiments in molecular genetics. Cold Spring Harbor Laboratory Press, Cold Spring Harbor, NY* **433,** (1972).

Mills, S. D. *et al. Yersinia enterocolitica* induces apoptosis in macrophages by a process requiring functional type III secretion and translocation mechanisms and involving YopP, presumably acting as an effector protein. *Proc. Natl. Acad. Sci.* **94,** 12638–12643 (1997).

Milton, D. L., O'Toole, R., Hörstedt, P. & Wolf-Watz, H. Flagellin A is essential for the virulence of Vibrio anguillarum. *J. Bacteriol.* **178,** 1310–1319 (1996).

Mohanty, B. K. & Kushner, S. R. Polynucleotide phosphorylase functions both as a 3' right-arrow 5' exonuclease and a poly(A) polymerase in *Escherichia coli*. *Proc. Natl. Acad. Sci. U. S. A.* **97,** 11966–71 (2000).

Montagner, C., Arquint, C. & Cornelis, G. R. Translocators YopB and YopD from *Yersinia enterocolitica* form a multimeric integral membrane complex in eukaryotic cell membranes. *J. Bacteriol.* **193,** 6923–8 (2011).

Montagner, C., Arquint, C. & Cornelis, G. R. Translocators YopB and YopD from *Yersinia enterocolitica* form a multimeric integral membrane complex in eukaryotic cell membranes. *J. Bacteriol.* **193,** 6923–8 (2011).

Montero, M. *et al. Escherichia coli* glycogen genes are organized in a single *glgBXCAP* transcriptional unit possessing an alternative suboperonic promoter within *glgC* that directs *glgAP* expression. *Biochem. J.* **433,** 107–17 (2011).

Morita, T., Kawamoto, H., Mizota, T., Inada, T. & Aiba, H. Enolase in the RNA degradosome plays a crucial role in the rapid decay of glucose transporter mRNA in the response to phosphosugar stress in *Escherichia coli*. *Mol. Microbiol.* **54,** 1063–75 (2004).

Morita, T., Maki, K. & Aiba, H. RNase E-based ribonucleoprotein complexes: mechanical basis of mRNA destabilization mediated by bacterial noncoding RNAs. *Genes Dev.* **19,** 2176–86 (2005).

Mota, L. J., Journet, L., Sorg, I., Agrain, C. & Cornelis, G. R. Bacterial injectisomes: needle length does matter. *Science* **307,** 1278 (2005).

Mu Ya Liu, Yang, H. & Romeo, T. The product of the pleiotropic *Escherichia coli* gene csrA modulates glycogen biosynthesis via effects on mRNA stability. *J. Bacteriol.* **177,** 2663–2672 (1995).

Mühlenkamp, M., Oberhettinger, P., Leo, J. C., Linke, D. & Schütz, M. S. *Yersinia* adhesin A (YadA) – Beauty & beast. *Int. J. Med. Microbiol.* **305,** 252–258 (2015).

Mukherjee, S., Oshiro, R. T., Yakhnin, H., Babitzke, P. & Kearns, D. B. FliW antagonizes CsrA RNA binding by a noncompetitive allosteric mechanism. *Proc. Natl. Acad. Sci. U. S. A.* **113,** 9870–5 (2016).

Mukherjee, S. *et al.* CsrA-FliW interaction governs flagellin homeostasis and a checkpoint on flagellar morphogenesis in Bacillus subtilis. *Mol. Microbiol.* **82,** 447–61 (2011).

Naktin, J. & Beavis, K. G. *Yersinia enterocolitica* and *Yersinia pseudotuberculosis*. *Clin. Lab. Med.* **19,** 523–36, vi (1999).

Narberhaus, F., Obrist, M., Führer, F. & Langklotz, S. Degradation of cytoplasmic substrates by FtsH, a membrane-anchored protease with many talents. *Res. Microbiol.* **160,** 652–659 (2009).

Navarro, L., Alto, N. M. & Dixon, J. E. Functions of the *Yersinia* effector proteins in inhibiting host immune responses. *Curr. Opin. Microbiol.* **8,** 21–7 (2005).

Navarro, L. *et al.* Identification of a molecular target for the *Yersinia* protein kinase A. *Mol. Cell* **26,** 465–77 (2007).

Neyt, C. & Cornelis, G. R. Insertion of a Yop translocation pore into the macrophage plasma membrane by *Yersinia enterocolitica*: requirement for translocators YopB and YopD, but not LcrG. *Mol. Microbiol.* **33,** 971–981 (1999).

Nieto, J. M. *et al.* Evidence for direct protein-protein interaction between members of the enterobacterial Hha/YmoA and H-NS families of proteins. *J. Bacteriol.* **184,** 629–35 (2002).

Notti, R. Q. & Stebbins, C. E. The Structure and Function of Type III Secretion Systems. *Microbiol. Spectr.* **4,** (2016).

Novoa, E. M. & Ribas de Pouplana, L. Speeding with control: codon usage, tRNAs, and ribosomes. *Trends Genet.* **28,** 574–581 (2012).

Nuss, A. M. *et al.* Tissue dual RNA-seq allows fast discovery of infection-specific functions and riboregulators shaping host-pathogen transcriptomes. *Proc. Natl. Acad. Sci. U. S. A.* **114,** E791–E800 (2017).

Nuss, A. M. *et al.* Transcriptomic profiling of *Yersinia pseudotuberculosis* reveals reprogramming of the Crp regulon by temperature and uncovers Crp as a master regulator of small RNAs. *PLoS Genet.* **11,** e1005087 (2015).

Nuss, A. M. *et al.* A direct link between the global regulator PhoP and the Csr regulon in Y. pseudotuberculosis through the small regulatory RNA CsrC. *RNA Biol.* **11,** 580–93 (2014).

Nuss, A. M. *et al.* A Precise Temperature-Responsive Bistable Switch Controlling *Yersinia* Virulence. *PLoS Pathog.* **12,** e1006091 (2016).

Obrist, M., Milek, S., Klauck, E., Hengge, R. & Narberhaus, F. Region 2.1 of the *Escherichia coli* heat-shock sigma factor RpoH (32) is necessary but not sufficient for degradation by the FtsH protease. *Microbiology* **153,** 2560–2571 (2007).

Olsson, J. *et al.* The YopD Translocator of *Yersinia pseudotuberculosis* Is a Multifunctional Protein Comprised of Discrete Domains. *J. Bacteriol.* **186,** 4110–4123 (2004).

Opitz, W. Cell contact-dependent virulence gene expression in *Yersinia pseudotuberculosis*. (2013).

Orth, K. Function of the *Yersinia* effector YopJ. *Curr. Opin. Microbiol.* **5,** 38–43 (2002).

Page, A.-L. & Parsot, C. Chaperones of the type III secretion pathway: jacks of all trades. *Mol. Microbiol.* **46,** 1–11 (2002).

Pannuri, A. *et al.* Translational repression of NhaR, a novel pathway for multi-tier regulation of biofilm circuitry by CsrA. *J. Bacteriol.* **194,** 79–89 (2012).

Park, H., Yakhnin, H., Connolly, M., Romeo, T. & Babitzke, P. CsrA participates in a PNPase autoregulatory mechanism by selectively repressing translation of *pnp* transcripts that have been previously processed by RNase III and PNPase. *J. Bacteriol.* **197,** JB.00721-15 (2015).

Pepe, J. C. & Miller, V. L. *Yersinia enterocolitica* invasin: a primary role in the initiation of infection. *Proc. Natl. Acad. Sci. U. S. A.* **90,** 6473–7 (1993).

Perry, R. D. & Fetherston, J. D. *Yersinia pestis*--etiologic agent of plague. *Clin. Microbiol. Rev.* **10,** 35–66 (1997).

Perry, R. D. & Fetherston, J. D. *The Genus Yersinia*. **603,** (Springer New York, 2007).

Pettersson, J. *et al.* Modulation of Virulence Factor Expression by Pathogen Target Cell Contact. *Science (80-.).* **273,** 1231–1233 (1996).

Pfaffl, M. W. A new mathematical model for relative quantification in real-time RT–PCR. *Nucleic Acids Res.* **29,** e45 (2001).

Phizicky, E. M. & Hopper, A. K. tRNA biology charges to the front. *Genes and Development* **24,** 1832–1860 (2010).

Pilar, A. V. C. & Coombes, B. K. A Fresh Look at the Type III Secretion System: Two-Step Model of Effector Translocation in Pathogenic Bacteria. *Front. Microbiol.* **2,** 113 (2011).

Pimenova, M. Regulation of the cell contact-dependent expression of the major virulence activator LcrF in *Yersinia pseudotuberculosis.* (2014).

Plano, G. V, Day, J. B. & Ferracci, F. Type III export: new uses for an old pathway. *Mol. Microbiol.* **40,** 284–93 (2001).

Platt, T. Transcription Termination and the Regulation of Gene Expression. *Annu. Rev. Biochem.* **55,** 339–372 (1986).

Plotkin, J. B. & Kudla, G. Synonymous but not the same: the causes and consequences of codon bias. *Nat. Rev. Genet.* **12,** 32–42 (2011).

Pope, B. & Kent, H. M. High efficiency 5 min transformation of *Escherichia coli*. *Nucleic Acids Res.* **24,** 536–537 (1996).

Potvin, E., Sanschagrin, F. & Levesque, R. C. Sigma factors in *Pseudomonas aeruginosa*. *FEMS Microbiol. Rev.* **32,** (2008).

Prentice, M. B. & Rahalison, L. Plague. *Lancet* **369,** 1196–1207 (2007).

Py, B., Higgins, C. F., Krisch, H. M. & Carpousis, A. J. A DEAD-box RNA helicase in the *Escherichia coli* RNA degradosome. *Nature* **381,** 169–72 (1996).

Quade, N. *et al.* Structural basis for intrinsic thermosensing by the master virulence regulator RovA of *Yersinia*. *J. Biol. Chem.* **287,** 35796–803 (2012).

Radics, J., Königsmaier, L. & Marlovits, T. C. Structure of a pathogenic type 3 secretion system in action. *Nat. Struct. Mol. Biol.* **21,** 82–7 (2014).

Rajanna, C. *et al.* Characterization of pPCP1 plasmids in *Yersinia pestis* strains isolated from the former Soviet Union. *Int. J. Microbiol.* (2010).

Ramamurthi, K. S. & Schneewind, O. Type III Protein Secretion in *Yersinia* Species. *Annu. Rev. Cell Dev. Biol.* **18,** 107–133 (2002).

Ranquet, C. & Gottesman, S. Translational Regulation of the *Escherichia coli* Stress Factor RpoS: a Role for SsrA and Lon. *J. Bacteriol.* **189,** 4872–4879 (2007).

Rasis, M. & Segal, G. The LetA-RsmYZ-CsrA regulatory cascade, together with RpoS and PmrA, post-transcriptionally regulates stationary phase activation of *Legionella pneumophila* Icm/Dot effectors. *Mol. Microbiol.* **72,** 995–1010 (2009).

Reinés, M. *et al.* Molecular basis of *Yersinia enterocolitica* temperature-dependent resistance to antimicrobial peptides. *J. Bacteriol.* **194,** 3173–88 (2012).

Revell, P. A. & Miller, V. L. A chromosomally encoded regulator is required for expression of the *Yersinia enterocolitica* inv gene and for virulence. *Mol. Microbiol.* **35,** 677–685 (2002).

Reyrat, J. M., Pelicic, V., Gicquel, B. & Rappuoli, R. Counterselectable markers: untapped tools for bacterial genetics and pathogenesis. *Infect. Immun.* **66,** 4011–7 (1998).

Richardson, J. P. & Roberts, J. W. Transcription termination. *Crit. Rev. Biochem. Mol. Biol.* **28,** 1–30 (1993).

Rife, C. *et al.* Crystal structure of the global regulatory protein CsrA from *Pseudomonas putida* at 2.05 A resolution reveals a new fold. *Proteins* **61,** 449–53 (2005).

Righetti, F. *et al.* Temperature-responsive in vitro RNA structurome of *Yersinia pseudotuberculosis*. *Proc. Natl. Acad. Sci. U. S. A.* **113,** 7237–42 (2016).

Riley, K. J. & Steitz, J. A. The 'Observer Effect' in genome-wide surveys of protein-RNA interactions. *Mol. Cell* **49,** 601–4 (2013).

Rimpiläinen, M., Forsberg, A. & Wolf-Watz, H. A novel protein, LcrQ, involved in the low-calcium response of *Yersinia pseudotuberculosis* shows extensive homology to YopH. *J. Bacteriol.* **174,** 3355–63 (1992).

Rinnenthal, J., Klinkert, B., Narberhaus, F. & Schwalbe, H. Modulation of the stability of the *Salmonella* fourU-type RNA thermometer. *Nucleic Acids Res.* **39,** 8258 (2011).

Robert-Le Meur, M. & Portier, C. Polynucleotide phosphorylase of *Escherichia coli* induces the degradation of its RNase III processed messenger by preventing its translation. *Nucleic Acids Res.* **22,** 397–403 (1994).

Robert-Le Meur, M. & Portier, C. Polynucleotide phosphorylase of *Escherichia coli* induces the degradation of its RNase III processed messenger by preventing its translation. *Nucleic Acids Res.* **22,** 397–403 (1994).

Romeo, T. Global regulation by the small RNA-binding protein CsrA and the non-coding RNA molecule CsrB. *Mol. Microbiol.* **29,** 1321–1330 (1998).

Romeo, T., Vakulskas, C. A. & Babitzke, P. Post-transcriptional regulation on a global scale: form and function of Csr/Rsm systems. *Environ. Microbiol.* **15,** 313–324 (2013).

Rosenzweig, J. A. & Schesser, K. Polynucleotide phosphorylase independently controls virulence factor expression levels and export in *Yersinia* spp. *FEMS Microbiol. Lett.* **270,** 255–64 (2007).

Rosenzweig, J. A., Weltman, G., Plano, G. V & Schesser, K. Modulation of *Yersinia* type three secretion system by the S1 domain of polynucleotide phosphorylase. *J. Biol. Chem.* **280,** 156–63 (2005).

Ruckdeschel, K. *et al.* Interaction of *Yersinia enterocolitica* with macrophages leads to macrophage cell death through apoptosis. *Infect. Immun.* **65,** 4813–21 (1997).

Rüter, C., Buss, C., Scharnert, J., Heusipp, G. & Schmidt, M. A. A newly identified bacterial cell-penetrating peptide that reduces the transcription of pro-inflammatory cytokines. *J. Cell Sci.* **123,** 2190–8 (2010).

Rybarczyk, A. *et al.* New *in silico* approach to assessing RNA secondary structures with non-canonical base pairs. *BMC Bioinformatics* **16,** 276 (2015).

Saiki, R. K. *et al.* Primer-directed enzymatic amplification of DNA with a thermostable DNA polymerase. *Science* **239,** 487–491 (1988).

Sambrook, J., Fritsch, E. F. & Maniatis, T. Molecular Cloning: A Laboratory Manual. *Cold Spring Harbor laboratory press. New York* (1989).

Sample, A. K., Fowler, J. M. & Brubaker, R. R. Modulation of the low-calcium response in *Yersinia pestis* via plasmid-plasmid interaction. *Microb. Pathog.* **2,** 443–453 (1987).

Sana, T. G., Berni, B. & Bleves, S. The T6SSs of *Pseudomonas aeruginosa* Strain PAO1 and Their Effectors: Beyond Bacterial-Cell Targeting. *Front. Cell. Infect. Microbiol.* **6,** 61 (2016).

Savin, C. *et al.* The *Yersinia pseudotuberculosis* complex: characterization and delineation of a new species, *Yersinia wautersii*. *Int. J. Med. Microbiol.* **304,** 452–63 (2014).

Schägger, H. Tricine-SDS-PAGE. *Nat. Protoc.* **1,** 16–22 (2006).

Schellhorn, H. E., Audia, J. P., Wei, L. I. & Chang, L. Identification of conserved, RpoS-dependent stationary-phase genes of *Escherichia coli*. *J. Bacteriol.* **180,** 6283–91 (1998).

Schiano, C. A. & Lathem, W. W. Post-transcriptional regulation of gene expression in *Yersinia* species. *Front. Cell. Infect. Microbiol.* **2,** 129 (2012).

Schindler, M. K. H. *et al. Yersinia enterocolitica* YadA mediates complement evasion by recruitment and inactivation of C3 products. *J. Immunol.* **189,** 4900–8 (2012).

Schleif, R. AraC protein, regulation of the l-arabinose operon in *Escherichia coli*, and the light switch mechanism of AraC action. *FEMS Microbiology Reviews* **34,** 779–796 (2010).

Schmidt, G. *Yersinia enterocolitica* outer protein T (YopT). *Eur. J. Cell Biol.* **90,** 955–8 (2011).

Schneider, C. a, Rasband, W. S. & Eliceiri, K. W. NIH Image to ImageJ: 25 years of image analysis. *Nat. Methods* **9,** 671–675 (2012).

Schoberle, T. J., Chung, L. K., McPhee, J. B., Bogin, B. & Bliska, J. B. Uncovering an Important Role for YopJ in the Inhibition of Caspase-1 in Activated Macrophages and Promoting *Yersinia pseudotuberculosis* Virulence. *Infect. Immun.* **84,** 1062–72 (2016).

Schotte, P. *et al.* Targeting Rac1 by the *Yersinia* effector protein YopE inhibits caspase-1-mediated maturation and release of interleukin-1beta. *J. Biol. Chem.* **279,** 25134–42 (2004).

Schraidt, O. & Marlovits, T. C. Three-Dimensional Model of *Salmonella*'s Needle Complex at Subnanometer Resolution. *Science (80-.).* **331,** (2011).

Schubert, M. *et al.* Molecular basis of messenger RNA recognition by the specific bacterial repressing clamp RsmA/CsrA. *Nat. Struct. Mol. Biol.* **14,** 807–813 (2007).

Schuster, F. Underlying principles of bistability in the expression of the pivotal virulence regulator RovA of *Yersinia pseudotuberculosis* and its role for virulence. (2015).

Schwiesow, L., Lam, H., Dersch, P. & Auerbuch, V. *Yersinia* Type III Secretion System Master Regulator LcrF. *J. Bacteriol.* **198,** 604–14 (2015).

Seekircher, S.: Identification of regulatory factors that control the synthesis of the small regulatory RNA CsrC in *Yersinia pseudotuberculosis*. (2014).

Seyll, E. & Van Melderen, L. The ribonucleoprotein Csr network. *Int. J. Mol. Sci.* **14,** 22117–31 (2013).

Shao, F. *et al.* Biochemical characterization of the *Yersinia* YopT protease: cleavage site and recognition elements in Rho GTPases. *Proc. Natl. Acad. Sci. U. S. A.* **100,** 904–9 (2003).

Shi, Z., Yang, W.-Z., Lin-Chao, S., Chak, K.-F. & Yuan, H. S. Crystal structure of *Escherichia coli* PNPase: central channel residues are involved in processive RNA degradation. *RNA* **14,** 2361–71 (2008).

Sievers, F. *et al.* Fast, scalable generation of high-quality protein multiple sequence alignments using Clustal Omega. *Mol. Syst. Biol.* **7,** 539 (2011).

Simon, R., Priefer, U. & Pühler, A. A Broad Host Range Mobilization System for In Vivo Genetic Engineering: Transposon Mutagenesis in Gram Negative Bacteria. *Bio/Technology* **1,** 784–791 (1983).

Singh, S. K., Boyle, A. L. & Main, E. R. G. LcrH, a class II chaperone from the type three secretion system, has a highly flexible native structure. *J. Biol. Chem.* **288,** 4048–4055 (2013).

Skurnik, M. & Wolf-Watz, H. Analysis of the yopA gene encoding the Yop1 virulence determinants of *Yersinia* spp. *Mol. Microbiol.* **3,** 517–529 (1989).

Skurnik, M. & Toivanen, P. *Yersinia enterocolitica* lipopolysaccharide: genetics and virulence. *Trends Microbiol.* **1,** 148–152 (1993).

Somerville, G. A. & Proctor, R. A. At the crossroads of bacterial metabolism and virulence factor synthesis in staphylococci. *Microbiol.Mol.Biol.Rev.* **73,** 233–248 (2009).

Spiro, S. & Guest, J. R. FNR and its role in oxygen-regulated gene expression in *Escherichia coli*. *FEMS Microbiol. Lett.* **75,** 399–428 (1990).

Stacey, S. D. & Pritchett, C. L. *Pseudomonas aeruginosa* AlgU Contributes to Posttranscriptional Activity by Increasing rsmA Expression in a mucA22 Strain. *J. Bacteriol.* **198,** 1812–26 (2016).

Stebbins, C. E. & Galán, J. E. Maintenance of an unfolded polypeptide by a cognate chaperone in bacterial type III secretion. *Nature* **414,** 77–81 (2001).

Steinmann S. Characterization of temperature-dependent and feedback-controlled expression of the virulence activator LcrF in *Yersinia pseudotuberculosis*. (2013).

Straley, S. C., Plano, G. V., Skrzypek, E., Haddix, P. L. & Fields, K. A. Regulation by Ca 2+ in the *Yersinia* low-Ca 2+ response. *Mol. Microbiol.* **8,** 1005–1010 (1993).

Studier, F. W. & Moffatt, B. a. Use of bacteriophage T7 RNA polymerase to direct selective high-level expression of cloned genes. *J. Mol. Biol.* **189,** 113–130 (1986).

Suzuki, K., Babitzke, P., Kushner, S. R. & Romeo, T. Identification of a novel regulatory protein (CsrD) that targets the global regulatory RNAs CsrB and CsrC for degradation by RNase E. *Genes Dev.* **20,** 2605–17 (2006).

Symmons, M. F., Jones, G. H. & Luisi, B. F. A Duplicated Fold Is the Structural Basis for Polynucleotide Phosphorylase Catalytic Activity, Processivity, and Regulation. *Structure* **8,** 1215–1226 (2000).

Takeshita, S., Sato, M., Toba, M., Masahashi, W. & Hashimoto-Gotoh, T. High-copy-number and low-copy-number piasmid vectors for *lacZ* alpha-complementation and chloramphenicol- or kanamycin-resistance selection. *Gene* **61,** 63–74 (1987).

Taylor, D. E., Trieber, C. A., Trescher, G. & Bekkering, M. Host mutations (*miaA* and *rpsL*) reduce tetracycline resistance mediated by Tet(O) and Tet(M). *Antimicrob. Agents Chemother.* **42,** 59–64 (1998).

Tengel, T., Sethson, I. & Francis, M. S. Conformational analysis by CD and NMR spectroscopy of a peptide encompassing the amphipathic domain of YopD from *Yersinia*. *Eur. J. Biochem.* **269,** 3659–3668 (2002).

Timmermans, J. & Van Melderen, L. Post-transcriptional global regulation by CsrA in bacteria. *Cell. Mol. Life Sci.* **67,** 2897–908 (2010).

Tomalka, A. G., Zmina, S. E., Stopford, C. M. & Rietsch, A. Dimerization of the *Pseudomonas aeruginosa* translocator chaperone PcrH is required for stability, not function. *J. Bacteriol.* **195,** 4836–43 (2013).

Towbin, H., Staehelin, T. & Gordon, J. Electrophoretic transfer of proteins from polyacrylamide gels to nitrocellulose sheets: procedure and some applications. *Proc. Natl. Acad. Sci. U. S. A.* **76,** 4350–4 (1979).

Tseng, Y.-T., Chiou, N.-T., Gogiraju, R. & Lin-Chao, S. The Protein Interaction of RNA Helicase B (RhlB) and Polynucleotide Phosphorylase (PNPase) Contributes to the Homeostatic Control of Cysteine in *Escherichia coli*. *J. Biol. Chem.* **290,** 29953–63 (2015).

Uliczka, F. *et al.* Unique cell adhesion and invasion properties of *Yersinia enterocolitica* O:3, the most frequent cause of human Yersiniosis. *PLoS Pathog.* **7,** e1002117 (2011).

Vakulskas, C. A. *et al.* Antagonistic control of the turnover pathway for the global regulatory sRNA CsrB by the CsrA and CsrD proteins. *Nucleic Acids Res.* **44,** 7896–910 (2016).

Vakulskas, C. A., Potts, A. H., Babitzke, P., Ahmer, B. M. M. & Romeo, T. Regulation of bacterial virulence by Csr (Rsm) systems. *Microbiol. Mol. Biol. Rev.* **79,** 193–224 (2015).

Vijay-Kumar, M. & Gewirtz, A. T. Flagellin: key target of mucosal innate immunity. *Mucosal Immunol.* **2,** 197–205 (2009).

Waldminghaus, T., Gaubig, L. C. & Narberhaus, F. Genome-wide bioinformatic prediction and experimental evaluation of potential RNA thermometers. *Mol. Genet. Genomics* **278,** 555–64 (2007).

Waldminghaus, T., Heidrich, N., Brantl, S. & Narberhaus, F. FourU: a novel type of RNA thermometer in *Salmonella*. *Mol. Microbiol.* **65,** 413–424 (2007).

Wallace, N., Zani, A., Abrams, E. & Sun, Y. The Impact of Oxygen on Bacterial Enteric Pathogens. *Adv. Appl. Microbiol.* **95,** 179–204 (2016).

Wang, H. *et al.* Increased plasmid copy number is essential for *Yersinia* T3SS function and virulence. *Science* **353,** 492–5 (2016).

Wang, X. *et al.* CsrA post-transcriptionally represses *pgaABCD* , responsible for synthesis of a biofilm polysaccharide adhesin of *Escherichia coli*. *Mol. Microbiol.* **56,** 1648–1663 (2005).

Wang, Y. *et al.* The flhDC gene affects motility and biofilm formation in *Yersinia pseudotuberculosis*. *Sci. China Ser. C Life Sci.* **50,** 814–821 (2007).

Waters, S. A. *et al.* Small RNA interactome of pathogenic *E. coli* revealed through crosslinking of RNase E. *EMBO J.* **130,** 101–112 (2016).

Wattam, A. R. *et al.* PATRIC, the bacterial bioinformatics database and analysis resource. *Nucleic Acids Res.* **42,** (2014).

Wattiau, P. & Cornelis, G. R. Identification of DNA sequences recognized by VirF, the transcriptional activator of the *Yersinia* yop regulon. *J. Bacteriol.* **176,** 3878–3884 (1994).

Weber, G. G., Kortmann, J., Narberhaus, F. & Klose, K. E. RNA thermometer controls temperature-dependent virulence factor expression in Vibrio cholerae. *Proc. Natl. Acad. Sci. U. S. A.* **111,** 14241–6 (2014).

Weilbacher, T. *et al.* A novel sRNA component of the carbon storage regulatory system of *Escherichia coli*. *Mol. Microbiol.* **48,** 657–670 (2003).

Williams, A. W. & Straley, S. C. YopD of *Yersinia pestis* plays a role in negative regulation of the low-calcium response in addition to its role in translocation of Yops. *J. Bacteriol.* **180,** 350–8 (1998).

Wren, B. W. The yersiniae--a model genus to study the rapid evolution of bacterial pathogens. *Nat. Rev. Microbiol.* **1,** 55–64 (2003).

Wulff-Strobel, C. R., Williams, A. W. & Straley, S. C. LcrQ and SycH function together at the Ysc type III secretion system in *Yersinia pestis* to impose a hierarchy of secretion. *Mol. Microbiol.* **43,** 411–423 (2002).

Yakhnin, A. V *et al.* CsrA activates flhDC expression by protecting flhDC mRNA from RNase E-mediated cleavage. *Mol. Microbiol.* **87,** 851–66 (2013).

Yakhnin, H. *et al.* Complex regulation of the global regulatory gene csrA: CsrA-mediated translational repression, transcription from five promoters by $E\sigma^{70}$ and $E\sigma(S)$, and indirect transcriptional activation by CsrA. *Mol. Microbiol.* **81,** 689–704 (2011).

Yang, H., Liu, M. Y. & Romeo, T. Coordinate genetic regulation of glycogen catabolism and biosynthesis in *Escherichia coli* via the CsrA gene product. *J. Bacteriol.* **178,** 1012–1017 (1996).

Yang, J., Jain, C. & Schesser, K. RNase E regulates the *Yersinia* type 3 secretion system. *J. Bacteriol.* **190,** 3774–8 (2008).

Yother, J., Chamness, T. W. & Goguen, J. D. Temperature-controlled plasmid regulon associated with low calcium response in *Yersinia pestis*. *J. Bacteriol.* **165,** 443–7 (1986).

Zhang, Y., Xie, S., Xu, H. & Qu, L. CLIP: viewing the RNA world from an RNA-protein interactome perspective. *Sci. China Life Sci.* **58,** 75–88 (2015).

Zhu, M., Zhao, J., Kang, H., Kong, W. & Liang, H. Modulation of type III secretion system in *Pseudomonas aeruginosa*: Involvement of the PA4857 gene product. *Front. Microbiol.* **7,** (2016).

Zuker, M. Mfold web server for nucleic acid folding and hybridization prediction. *Nucleic Acids Res.* **31,** 3406–3415 (2003).

8 Appendix

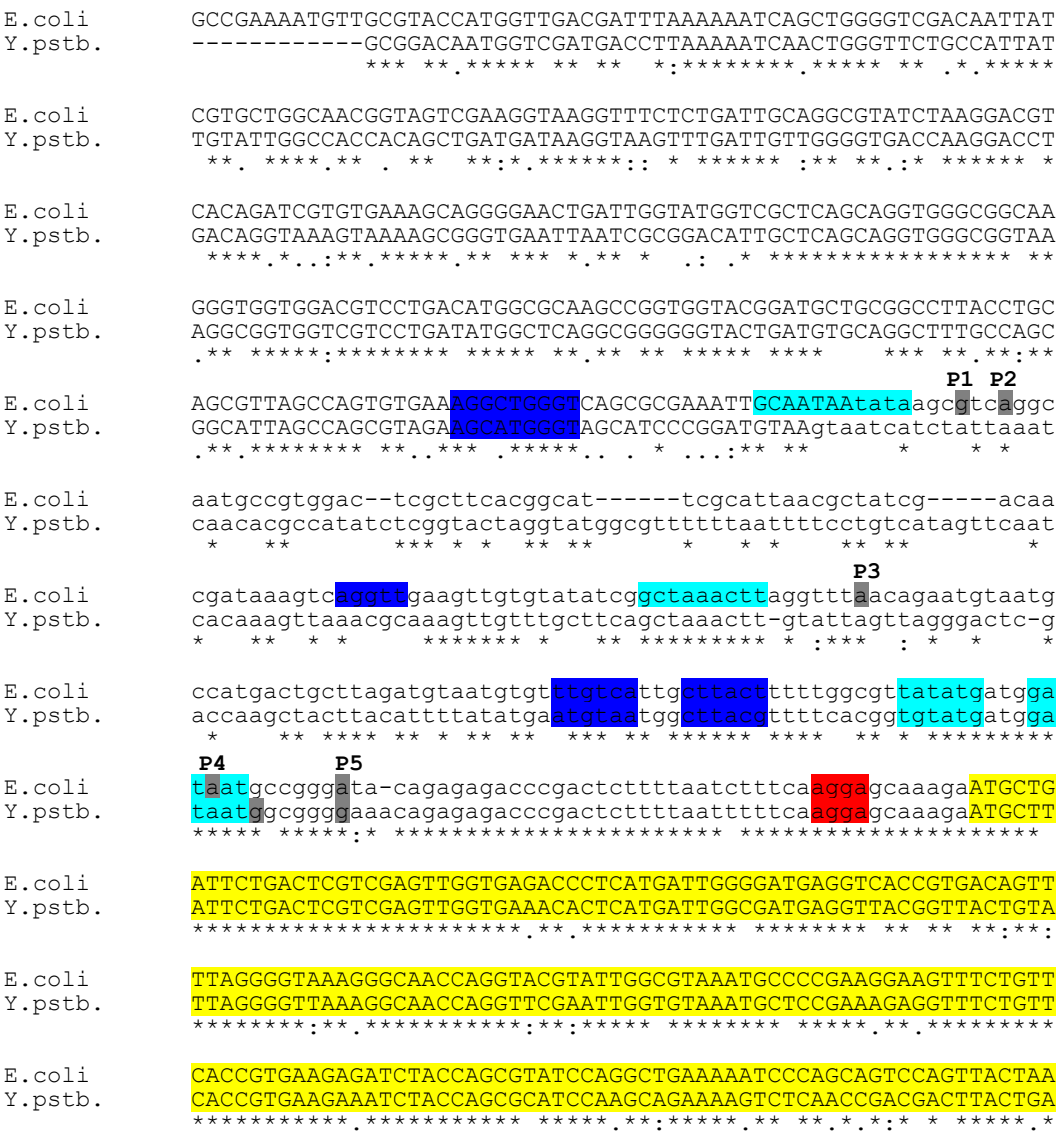

Figure S1: DNA sequence alignment of the *csrA* locus of *Y. pseudotuberculosis* YPIII and *E. coli* K12. ClustalO was used for the alignment of the *csrA* locus (-520 to +186 relative to the translational start site) with default parameters. Nucleotides which were identical in both species are marked with a star below the sequence. The position of the -35 (blue) and -10 boxes (cyan), transcriptional start sites (gray) the ribosomal binding site (red) and the coding sequence (yellow) are indicated. The position of the -35 and -10 boxes, as well as, the transcriptional start site were identified in *E. coli* [Yakhnin *et al.*, 2011]. The position of the transcriptional start site of *Y. pseudotuberculosis* are shown as identified by RNA-Seq [Nuss *et al.*, 2015].

Table S2: CsrA targets in *Y. pseudotuberculosis* YPIII as predicted by the CSRA_TARGET_PREDICTER script. CsrA dependently up or down regulated genes are highlighted with an up or down pointing arrow. CsrA dependently up or down regulated genes are highlighted with an up or down pointing arrow. Highlighted are only genes which were at least 4 times enriched or depleted (-2 >= log2(fc) >= 2) in stationary phase at 25 °C (diff. S25) or 37 °C (diff. S37) in absence of *csrA* [Nuss, unpublished data].

Locus	Gene name	Gene description	diff. S25	diff. S37
YPK_0008	ilvA, tdcB	pyridoxal-phosphate dependent enzyme family protein		
YPK_0013	yidE	Mediator of hyperadherence YidE		
YPK_0043	selB	Selenocysteine-specific translation elongation factor		
YPK_0046		hypothetical protein		
YPK_0063		hypothetical protein		
YPK_0075	cysK-1	Pyridoxal-5'-phosphate-dependent enzyme beta superfamily (fold type II)		
YPK_0088	dppA	Dipeptide-binding ABC transporter, periplasmic substrate-binding component		
YPK_0108		hypothetical protein		
YPK_0121	uspB	Universal stress protein B		
YPK_0126	rbsC-1	ABC transport system, permease protein Z5690		
YPK_0147	glgB	1,4-alpha-glucan (glycogen) branching enzyme		
YPK_0148	glgX	Glycogen debranching enzyme		
YPK_0161	glgP-2	Maltodextrin phosphorylase		
YPK_0162	malQ	4-alpha-glucanotransferase (amylomaltase)		
YPK_0174	pckA	Phosphoenolpyruvate carboxykinase [ATP]		
YPK_0201		hypothetical protein		
YPK_0202		COG4382: Mu-like prophage protein gp16		
YPK_0220	hofM	Type IV pilus biogenesis protein PilM		
YPK_0259	tauB-1	Taurine transport ATP-binding protein TauB		
YPK_0271		YheO-like PAS domain		
YPK_0279	tnp-4	Mobile element protein		
YPK_0284	rplD	LSU ribosomal protein L4p (L1e)		
YPK_0321	aroE-1	Shikimate 5-dehydrogenase I alpha		
YPK_0366	aceK	Isocitrate dehydrogenase phosphatase		↑
YPK_0389	impG-1, vasA-1	Protein ImpG/VasA		
YPK_0391	impI, vasC	Uncharacterized protein ImpI/VasC		
YPK_0393	impJ-1, vasE-1	Uncharacterized protein ImpJ/VasE	↑	
YPK_0402		hypothetical protein		
YPK_0427		Mobile element protein		
YPK_0449		Putative metabolite transport protein		
YPK_0487		Ribonuclease (Barnase), secreted		
YPK_0489	yjgA	FIG138315: Putative alpha helix protein		
YPK_0495	treB	PTS system, trehalose-specific IIB component	↑	
YPK_0512	mlaF	Phospholipid ABC transporter ATP-binding protein MlaF		
YPK_0534	elbB	Sigma cross-reacting protein 27A		

YPK_0538	yraN	Predicted endonuclease distantly related to archaeal Holliday junction resolvase		
YPK_0580		Rhs-family protein		
YPK_0588	lacI-2, galR-2	LacI-family regulatory protein		
YPK_0600		putative membrane protein		
YPK_0670	yghB	DedA family inner membrane protein YghB		
YPK_0732		hypothetical protein		
YPK_0752		Siderophore biosynthesis non-ribosomal peptide synthetase modules		
YPK_0755		Thioesterase in siderophore biosynthesis gene cluster		
YPK_0759		Putative exported protein precursor		↓
YPK_0765		hypothetical protein		
YPK_0769		hypothetical protein		
YPK_0777		putative membrane protein		
YPK_0781		Galactose permease		
YPK_0783	iucD	L-lysine 6-monooxygenase [NADPH]		
YPK_0796		Phage protein		
YPK_0819	yggX	FIG001341: Probable Fe(2+)-trafficking protein YggX		
YPK_0838	gshB	Glutathione synthetase		
YPK_0846		Mobile element protein		
YPK_0848	tnp-4	Mobile element protein		
YPK_0854	mscS	Protein involved in stability of MscS mechanosensitive channel		
YPK_0889		FIG01221547: hypothetical protein		
YPK_0919		hypothetical protein		↓
YPK_0933		hypothetical protein		
YPK_0950		hypothetical protein		
YPK_0978	exuT-2	Putative MFS superfamily hexuronate transporter		
YPK_0984	ydeN, yidJ	N-acetylgalactosamine 6-sulfate sulfatase (GALNS)		
YPK_1006	gspF	General secretion pathway protein F		↓
YPK_1008	gspH	General secretion pathway protein H		
YPK_1009	gspI	General secretion pathway protein I		
YPK_1045	argA	N-acetylglutamate synthase		
YPK_1056	ygdH	Decarboxylase family protein		
YPK_1111	hpxB	Uricase (urate oxidase)		
YPK_1123		hypothetical protein		
YPK_1134	ureE	Urease accessory protein UreE		
YPK_1148	chbG	N,N'-diacetylchitobiose utilization operon protein YdjC		
YPK_1162		FIG143828: Hypothetical protein YbgA		
YPK_1179	srmB	ATP-dependent RNA helicase SrmB		
YPK_1186		putative membrane protein	↑	
YPK_1198		Phage DNA binding protein Roi		
YPK_1299		Uncharacterized protein YfgJ		
YPK_1339		FIG01222552: hypothetical protein		
YPK_1344	ppk	Polyphosphate kinase		

YPK_1357	perM	Putative permease PerM		
YPK_1362	dapA	4-hydroxy-tetrahydrodipicolinate synthase		
YPK_1391	maeB	NADP-dependent malic enzyme		
YPK_1426	crr	PTS system, glucose-specific IIA component		
YPK_1451		putative lipoprotein		
YPK_1459	yhhZ-3	hypothetical protein		
YPK_1472	impH-2, vasB-2	Uncharacterized protein ImpH/VasB		
YPK_1475	fimA-2	Fimbrial protein precursor		
YPK_1532	folC	Dihydrofolate synthase		
YPK_1542	yfcH	Cell division inhibitor Slr1223		
YPK_1547	ulaB, sgaB	Putative sugar phosphotransferase component II B	↓	↓
YPK_1576	idnO	5-keto-D-gluconate 5-reductase		
YPK_1617		putative membrane protein		
YPK_1629		Putative large exoprotein involved in heme utilization		
YPK_1644	cas-1	CRISPR-associated protein Cas1		
YPK_1659		hypothetical protein		↑
YPK_1679		Mobile element protein		
YPK_1703		hypothetical protein		↓
YPK_1718	purB	Adenylosuccinate lyase		
YPK_1719	hflD	Protein of unknown function perhaps involved in purine metabolism		
YPK_1725		hypothetical protein		
YPK_1748	motB-2	Flagellar motor rotation protein MotB		
YPK_1752		putative lipoprotein		
YPK_1773		Sigma-fimbriae tip adhesin		
YPK_1782	proQ	ProQ: influences osmotic activation of compatible solute ProP		
YPK_1807		Mobile element protein		
YPK_1852	sufE-2	Sulfur acceptor protein SufE for iron-sulfur cluster assembly		
YPK_1876	rovA, slyA	Transcriptional regulator SlyA	↓	
YPK_1885		Inner membrane protein YohC		
YPK_1901		putative phosphatase/kinase		
YPK_1932		hypothetical protein		
YPK_1961	rbsA-4	Predicted erythritol ABC transporter 2, ATP-binding component		↓
YPK_1964		hypothetical protein		
YPK_2022	osmB	Osmotically inducible lipoprotein B precursor		
YPK_2064		FIG002901: hypothetical protein co-occurring with Cardiolipin synthetase		
YPK_2114		hypothetical protein		
YPK_2131	mdtJ	Spermidine export protein MdtJ		
YPK_2154	yecM	Protein YecM		
YPK_2195		Putative exported protein precursor		
YPK_2234	tnp-4	Mobile element protein		
YPK_2254	glsA-2	Glutaminase		↓

YPK_2258	nqrE-1	Na(+)-translocating NADH-quinone reductase subunit E		
YPK_2267	ripB, ich-Y	Transcriptional regulator		
YPK_2292		Mobile element protein		
YPK_2304		Phage-related tail protein		
YPK_2338		hypothetical protein	↓	↓
YPK_2351		Phage-related tail protein		
YPK_2373		hypothetical protein		
YPK_2374	yecC	L-cystine ABC transporter (wide substrate range), ATP-binding protein		
YPK_2406		hypothetical protein		
YPK_2409	yphE-2; ytfR-2	ABC-type sugar transport system, ATP-binding protein		
YPK_2419	flgH	Flagellar L-ring protein FlgH		
YPK_2420	flgG	Flagellar basal-body rod protein FlgG		
YPK_2424	flgC-2	Flagellar basal-body rod protein FlgC		
YPK_2432	flhB-2	Flagellar biosynthesis protein FlhB		
YPK_2433		putative membrane protein		
YPK_2448	yoaH	hypothetical protein	↓	
YPK_2465	manY	PTS system, mannose-specific IIC component		
YPK_2509		2,4-diketo-3-deoxy-L-fuconate hydrolase		
YPK_2533		Mobile element protein		
YPK_2538		Siderophore [Alcaligin-like] biosynthesis complex, medium chain		
YPK_2545	ysuH, alcB	Siderophore [Alcaligin-like] biosynthesis complex, short chain		
YPK_2567	yeiB	Uncharacterized protein YeiB		
YPK_2571	frmA, adhC	S-(hydroxymethyl)glutathione dehydrogenase		
YPK_2593		hypothetical protein		
YPK_2601		hypothetical protein		
YPK_2628	tfoX	DNA transformation protein TfoX	↑	
YPK_2631	tnp-4	Mobile element protein		
YPK_2662	cspB-2	Cold shock protein CspI	↑	
YPK_2672	yadC	Putative exported protein precursor		
YPK_2674	ansB	L-asparaginase		
YPK_2678		hypothetical protein		
YPK_2704		hypothetical protein		
YPK_2746		Phosphoserine phosphatase	↑	
YPK_2766	yphD-7, ytfT-7	Xylose ABC transporter, permease protein XylH	↑	
YPK_2801		hypothetical protein		
YPK_2817		hypothetical protein		
YPK_2822		Putative bacteriophage protein		
YPK_2889		Mobile element protein		
YPK_2905		Transcriptional regulator		
YPK_2908	zraS, hydH	Sensor protein of zinc sigma-54-dependent two-component system		
YPK_2927		Probable ATP-binding ABC transporter protein		

YPK_2949	aroG	2-keto-3-deoxy-D-arabino-heptulosonate-7-phosphate synthase I alpha		
YPK_2951	zitB	Cobalt-zinc-cadmium resistance protein CzcD		
YPK_2981		Phage integrase		
YPK_2995		Mobile element protein		
YPK_3005	miaB	tRNA-i(6)A37 methylthiotransferase	↑	↑
YPK_3038		hypothetical protein		
YPK_3053	yfhM	putative membrane protein		
YPK_3055	ner-1, nlp-1	Putative regulatory protein		↑
YPK_3078		putative membrane protein		
YPK_3143		hypothetical protein		
YPK_3146		hypothetical protein		
YPK_3151	ybcJ	FIG002958: hypothetical protein		
YPK_3165	copA	Copper-translocating P-type ATPase		
YPK_3168		hypothetical protein		
YPK_3173		Mobile element protein		
YPK_3209	tnp-4	Mobile element protein		
YPK_3242	cyoB	Cytochrome O ubiquinol oxidase subunit I		
YPK_3260		hypothetical protein		
YPK_3269	ggt	Gamma-glutamyltranspeptidase	↑	↑
YPK_3270		Putative short-chain dehydrogenase		
YPK_3301	nqrE	Na(+)-translocating NADH-quinone reductase subunit E		
YPK_3310		hypothetical protein		
YPK_3367	yfjD	Putative membrane protein YfjD		
YPK_3372	csrA	Carbon storage regulator	↓	↓
YPK_3412	pheC	Prephenate dehydratase		
YPK_3414		hypothetical protein		
YPK_3428	surE	5-nucleotidase SurE		
YPK_3435	cysN	Sulfate adenylyltransferase subunit 1	↑	
YPK_3439		hypothetical protein		
YPK_3473	panC	Pantoate--beta-alanine ligase		
YPK_3488		Mobile element protein		
YPK_3506		Mobile element protein		
YPK_3521	mraY	Phospho-N-acetylmuramoyl-pentapeptide-transferase		
YPK_3526	mraW, rsmH	16S rRNA (cytosine(1402)-N(4))-methyltransferase		
YPK_3530	ilvH	Acetolactate synthase small subunit		
YPK_3542	thiB, tbpA	Thiamin ABC transporter, substrate-binding component		
YPK_3548		hypothetical protein		
YPK_3550	impL-4, vasK-4	Putative membrane protein precursor		
YPK_3552	impJ-4, vasE-4	Uncharacterized protein ImpJ/VasE		
YPK_3556		hypothetical protein		
YPK_3564	impC-4	Uncharacterized protein ImpC		
YPK_3566	impA-2	Uncharacterized protein ImpA		

YPK_3567	rovC	hypothetical protein		
YPK_3593	dnaJ	Chaperone protein DnaJ		
YPK_3645		hypothetical protein		
YPK_3679	pepA	Cytosol aminopeptidase PepA		
YPK_3694	phnG	Alpha-D-ribose 1-methylphosphonate 5-triphosphate synthase subunit PhnG		
YPK_3699	phnL	Alpha-D-ribose 1-methylphosphonate 5-triphosphate synthase subunit PhnL		
YPK_3721		Putative membrane protein	↓	↓
YPK_3725	nlpI	Lipoprotein NlpI		
YPK_3759		hypothetical protein		
YPK_3767	ppa	Inorganic pyrophosphatase		
YPK_3770	ytfM	Outer membrane component of TAM transport system		
YPK_3791	rnr	3'-to-5' exoribonuclease RNase R		
YPK_3796	hflK	HflK protein		
YPK_3808	orn	3'-to-5' oligoribonuclease (orn)		
YPK_3820		hypothetical protein		
YPK_3873	terD	Tellurium resistance protein TerD		
YPK_3878		Carbamoylphosphate synthase large subunit (split gene in MJ)		
YPK_3915		FIG027385: Putative type III secretion apparatus		
YPK_3943	ubiB	Ubiquinone biosynthesis monooxygenase UbiB		
YPK_3969		hypothetical protein		
YPK_4005		hypothetical protein		
YPK_4028	rffH, rfbA	Glucose-1-phosphate thymidylyltransferase		
YPK_4047		Colicin immunity protein		
YPK_4062	comM, yifB	MG(2+) CHELATASE FAMILY PROTEIN/ComM-related protein		
YPK_4068	yphF-6, ytfQ-6	Putative sugar ABC transport system, periplasmic binding protein YtfQ precursor		
YPK_4085	hasA	Hemophore HasA		
YPK_4143	yibQ	Putative periplasmic protein YibQ, distant homology with nucleoside diphosphatase and polysaccharide deacetylase		
YPK_4171		hypothetical protein		
YPK_4173		hypothetical protein		
YPK_4190	glnL, ntrB	Nitrogen regulation protein NtrB		
YPK_4201		Mobile element protein		
YPK_4237		ABC-type amino acid transport/signal transduction systems, periplasmic component/domain	↑	

Table S3: Mapping statistic of RIP-Seq analysis with CsrA-3xFLAG.

#	sample name	sample group	read length	total reads	total mapped	total uniquely mapped	total unique plus strand	total unique minus strand	total mapped to genes	mapped to no features
1	wt_2_ctr	wt_ctr	51	18,191,601	15,445,875	399,514	181,019	218,495	336,462	40,898
2	wt_2_IP	wt_IP	51	20,830,793	18,213,767	6,735,667	2,099,822	4,635,845	6,041,256	418,259
3	wt_3_ctr	wt_ctr	51	20,166,439	16,093,235	419,586	197,477	222,109	347,579	45,152
4	wt_3_IP	wt_IP	51	16,094,846	13,536,810	6,307,911	1,704,938	4,602,973	5,682,617	362,563
5	wt_4_ctr	wt_ctr	51	14,492,392	14,277,487	822,344	389,285	433,059	689,889	103,107
6	wt_4_IP	wt_IP	51	19,984,315	19,721,130	4,689,053	1,848,003	2,841,050	4,111,468	422,499
7	wt_5_ctr	wt_ctr	51	16,838,458	16,659,654	548,752	280,028	268,724	468,459	59,738
8	wt_5_IP	wt_IP	51	25,326,874	25,039,089	8,004,987	3,138,102	4,866,885	7,071,951	704,272
10	wt_6_IP	wt_IP	51	24,016,000	23,716,102	8,268,722	2,811,980	5,456,742	7,369,373	692,316

Table S4: Transcripts enriched by CsrA-3xFLAG in RIP-Seq analysis. Shown are transcripts which were at least 8 times (log2(fc) > 3) enriched in IP samples compared to control samples. RNAs which were predicted by the CSRA_TARGET_PREDICTER script are marked with an X mark. CsrA-dependently up or down regulated genes are highlighted with an up or down pointing arrow. Only genes which were at least 4 times enriched or depleted (-2 >= log2(fc) >= 2) in a comparative CsrA RNA-Seq of bacteria grown to stationary phase at 25 °C (diff. S25) or 37 °C (diff. S37) are shown [Nuss, unpublished data] For the complete dataset see **dataset S4**.

Locus	Gene name	Gene description	Class	mean_ctr (rpk)	mean_IP (rpk)	log2(fc)	pre-dicted	diff. S25	diff. S37
YPK_3372	*csrA*	carbon storage regulator	CDS	336.02	26,261.29	6.29	X	↓	↓
YPK_3721		hypothetical protein	CDS	3.44	92.78	4.75	X	↓	↓
YPK_2338		hypothetical protein	CDS	5.41	129.00	4.58	X	↓	↓
YPK_1547	*ulaB, sgaB*	PTS system lactose/cellobiose-specific transporter subunit IIB	CDS	60.76	1,202.08	4.31	X	↓	↓
YPK_3005	*miaB*	(dimethylallyl)adenosine tRNA methylthiotransferase	CDS	206.70	2,394.25	3.53	X	↑	↑
YPK_3269	*ggt*	gamma-glutamyltransferase	CDS	21.26	180.05	3.08	X	↑	↑
Ysr179	*csrB*	CsrB	transRNA	18,082.02	1,747,479.50	6.59		↓	↓
Ysr200			transRNA	23.58	1,784.91	6.24		↓	↓
Ysr186	*csrC*	CsrC	transRNA	160,013.47	8,631,616.84	5.75		↓	↓
Ysr192			transRNA	58.08	2,913.13	5.65		↓	↓
YPK_3035		hypothetical protein	CDS	661.54	25,749.74	5.28		↓	↓
YPK_1765		hypothetical protein	CDS	14.10	524.10	5.22		↓	↓
YPK_3101		hypothetical protein	CDS	1.21	33.82	4.81		↑	↑
sR009/ryhB	*RyhB*	RyhB	transRNA	7.14	200.00	4.81		↓	↓
YPK_2207		Sel1 domain protein repeat-containing protein	CDS	22.31	621.08	4.80		↑	↓
YPK_R0022	*tRNA-Ser*	tRNA Ser	tRNA	5.56	133.33	4.58		↓	↑
YPK_1440		hypothetical protein	CDS	45.89	1,020.77	4.48		↑	↑
YPK_4108		hypothetical protein	CDS	412.50	8,756.67	4.41		↑	↑
Ysr199			transRNA	93.37	1,871.08	4.32		↓	↓
Ysr280		conserved hypothetical protein	asRNA	2.45	49.02	4.32		↓	↓
YPK_R0068	*tRNA-Ser*	tRNA Ser	tRNA	90.91	1,581.82	4.12		↑	↑
YPK_0445	*pcp-1*	17 kDa surface antigen	CDS	104.70	1,760.68	4.07		↓	↓
YPK_2405		hypothetical protein	CDS	32.74	534.52	4.03		↓	↓
YPK_3421	*ydjJ*	alcohol dehydrogenase	CDS	16.58	269.00	4.02		↑	↓

YPK_0962		hypothetical protein	CDS	62.65	1,004.20	4.00		↓	↓
YPK_1766		hypothetical protein	CDS	2.08	33.33	4.00		↓	↓
YPK_2471		hypothetical protein	CDS	66.31	979.21	3.88		↓	↓
YPK_1607		cation diffusion facilitator family transporter	CDS	6.66	95.63	3.84		↓	↓
YPK_2224	*ompC-1*	porin	CDS	14.08	191.51	3.77		↓	↓
Ysr252	*yecS*	polar amino acid ABC transporter, inner membrane subunit	asRNA	3.38	45.95	3.77		↓	↓
Ysr110/sR065			transRNA	140.43	1,903.09	3.76		↓	↓
YPK_3418	*dhaL*	dihydroxyacetone kinase subunit DhaL	CDS	52.96	713.19	3.75		↑	↓
YPK_2655	*mukB*	cell division protein MukB	CDS	40.26	534.63	3.73		↑	↑
YPK_3020	*rlmH, ybeA*	rRNA large subunit methyltransferase	CDS	43.52	548.62	3.66		↑	↑
YPK_3748		hypothetical protein	CDS	4.66	57.81	3.63		↓	↓
YPK_3158	*ybbA-3*	putative ABC transporter ATP-binding protein YbbA	CDS	5.82	71.91	3.63		↑	↑
YPK_3388	*katG*	catalase/peroxidase HPI	CDS	86.38	959.62	3.47		↓	↓
YPK_R0044	*tRNA-Leu*	tRNA Leu	tRNA	45.98	501.15	3.45		↓	↓
YPK_3028	*tatE*	twin arginine translocase protein A	CDS	464.15	5,046.51	3.44		↑	↑
YPK_0283	*rplC*	50S ribosomal protein L3	CDS	86.11	926.35	3.43		↑	↑
Ysr256		FAD linked oxidase domain protein	asRNA	28.09	296.63	3.40		↓	↓
YPK_3389	*cybC-2*	cytochrome b562	CDS	59.24	616.15	3.38		↓	↓
YPK_2696	*macA-2*	macrolide transporter subunit MacA	CDS	39.98	403.41	3.33		↑	↑
YPK_3656		hypothetical protein	CDS	99.59	983.33	3.30		↑	↑
YPK_3760	*ner-2, nlp-2, sfsB-2*	putative transcriptional regulator Nlp	CDS	781.70	7,659.42	3.29		↓	↓
YPK_2971	*sdhD*	succinate dehydrogenase cytochrome b556 small membrane subunit	CDS	191.09	1,805.75	3.24		↑	↑
YPK_2880		hypothetical protein	CDS	56.16	526.99	3.23		↑	↑
YPK_2641	*rlmL*	23S rRNA m(2)G2445 methyltransferase	CDS	37.95	350.12	3.21		↑	↑
YPK_2360	*ailC*	virulence-related outer membrane protein	CDS	2.72	25.00	3.20		↓	↓
Ysr275	*yjgQ*	permease YjgP/YjgQ family protein	asRNA	9.09	83.64	3.20		↓	↓
YPK_2763	*fruK*	1-phosphofructokinase	CDS	8.79	77.74	3.15		↑	↑

YPK_2611	*fabZ-2*	beta-hydroxyacyl-(acyl-carrier-protein) dehydratase FabA/FabZ	CDS	0.95	8.38	3.14		↓	↓
YPK_3015	*leuS*	leucyl-tRNA synthetase	CDS	85.75	747.66	3.12		↑	↑
YPK_0947		hypothetical protein	CDS	3.27	27.45	3.07		↑	↑
YPK_3671		hypothetical protein	CDS	4.87	40.15	3.04		↓	↓
YPK_1703		hypothetical protein	CDS	15.60	946.38	5.92	X		↓
YPK_3055	*ner-1, nlp-1*	putative transcriptional regulator Nlp	CDS	28.46	756.91	4.73	X		↑
YPK_0759		hypothetical protein	CDS	42.81	809.59	4.24	X		↓
YPK_1006	*gspF*	type II secretion system protein	CDS	1.66	29.59	4.15	X		↓
YPK_0919		hypothetical protein	CDS	8.84	135.35	3.94	X		↓
YPK_1961	*rbsA-4*	ABC transporter related	CDS	5.52	82.39	3.90	X		↓
YPK_2254	*glsA-2*	glutaminase	CDS	27.53	382.94	3.80	X		↓
YPK_1659		hypothetical protein	CDS	1.02	13.82	3.77	X		↑
YPK_0366	*aceK*	bifunctional isocitrate dehydrogenase kinase/phosphatase protein	CDS	8.70	71.89	3.05	X		↑
YPK_0762	*gntP*	gluconate transporter	CDS	11.64	385.29	5.05			↓
Ysr151/sR007	*RNase P*	RNase P (M1 RNA)	transRNA	11,411.61	370,964.64	5.02			↑
YPK_R0027	*tRNA-Pro*	tRNA Pro	tRNA	16.23	516.88	4.99			↓
YPK_3631		hypothetical protein	CDS	23.15	671.60	4.86			↑
YPK_2130	*mdtI*	multidrug efflux system protein MdtI	CDS	25.00	683.03	4.77			↑
Ysr259		hypothetical protein	asRNA	7.14	190.00	4.73			↓
YPK_0949		hypothetical protein	CDS	0.76	18.87	4.63			↓
YPK_R0051	*tRNA-Leu*	tRNA Leu	tRNA	270.11	6,036.78	4.48			↓
YPK_3628	*nupC-2*	nucleoside transporter	CDS	22.60	478.30	4.40			↑
YPK_0533	*arcB*	aerobic respiration control sensor protein ArcB	CDS	343.50	6,392.55	4.22			↓
YPK_3733	*secG*	preprotein translocase subunit SecG	CDS	347.47	6,387.50	4.20			↑
YPK_2135	*hexR*	DNA-binding transcriptional regulator HexR	CDS	91.61	1,640.18	4.16			↓
Ysr194			transRNA	203.39	3,440.68	4.08			↑
Ysr201			transRNA	7.14	120.00	4.07			↓
YPK_3817	*sugE*	small multidrug resistance protein	CDS	3.79	63.64	4.07			↑
YPK_R0049	*tRNA-Gly*	tRNA Gly	tRNA	36.18	597.37	4.05			↑

YPK_0968	*cycB, ganO*	sugar(maltose) ABC transporter substrate-binding protein	CDS	56.43	929.77	4.04			↓
YPK_1573		hypothetical protein	CDS	3.47	56.67	4.03			↓
YPK_3422	*rpiB-1*	ribose-5-phosphate isomerase B	CDS	43.86	692.54	3.98			↓
YPK_R0042	*tRNA-Arg*	tRNA Arg	tRNA	386.36	5,997.40	3.96			↓
YPK_0953		hypothetical protein	CDS	151.52	2,313.13	3.93			↑
YPK_2660	*kdsB*	3-deoxy-manno-octulosonate cytidylyltransferase	CDS	21.58	329.35	3.93			↑
YPK_2413		short chain dehydrogenase	CDS	2.18	33.09	3.93			↓
YPK_1419		hypothetical protein	CDS	3.79	56.57	3.90			↓
YPK_3106		hypothetical protein	CDS	127.64	1,891.98	3.89			↑
YPK_1452		4Fe-4S ferredoxin iron-sulfur binding domain protein	CDS	35.96	532.98	3.89			↓
YPK_2796	*ndpA, yejK*	nucleoid-associated protein NdpA	CDS	76.37	1,127.56	3.88			↑
YPK_1978		hypothetical protein	CDS	67.07	982.93	3.87			↑
YPK_2496	*dctP*	TRAP dicarboxylate transporter subunit DctP	CDS	38.02	529.51	3.80			↓
YPK_1197		hypothetical protein	CDS	0.54	7.47	3.79			↓
YPK_3419	*dhaK*	glycerone kinase	CDS	32.37	442.61	3.77			↓
YPK_3345	*yfiM*	hypothetical protein	CDS	27.05	367.25	3.76			↓
YPK_3362	*trmD*	tRNA (guanine-N(1)-)-methyltransferase	CDS	336.71	4,564.91	3.76			↑
YPK_3420		short chain dehydrogenase	CDS	14.59	197.41	3.76			↓
YPK_3029		hypothetical protein	CDS	116.01	1,541.18	3.73			↑
Ysr243	*cvrA, nhaP2*	sodium/hydrogen exchanger	asRNA	83.33	1,106.25	3.73			↓
YPK_0517		BolA family protein	CDS	62.50	828.79	3.73			↑
YPK_2168		ABC transporter-like protein	CDS	6.09	77.72	3.67			↓
YPK_2962	*ybgT*	cyd operon protein YbgT	CDS	62.96	802.96	3.67			↑
YPK_4154	*rpmB*	50S ribosomal protein L28	CDS	1,314.35	16,322.36	3.63			↑
YPK_2920	*moaD*	molybdopterin synthase small subunit	CDS	12.20	150.41	3.62			↑
YPK_1175	*yplA*	phospholipase A(1)	CDS	8.31	99.27	3.58			↓
YPK_3773	*ytfK*	hypothetical protein	CDS	4,419.01	52,341.78	3.57			↑
YPK_4029	*rffG, rfbB*	dTDP-glucose 4,6-dehydratase	CDS	52.20	602.43	3.53			↑
YPK_0465	*mreB*	rod shape-determining protein MreB	CDS	119.73	1,368.01	3.51			↑

YPK_1544	*yfcE*	phosphodiesterase	CDS	111.87	1,277.90	3.51			↑
YPK_2775	*ykgJ, yeiW*	hypothetical protein	CDS	0.98	10.98	3.49			↑
YPK_R0016	*tRNA-Val*	tRNA Val	tRNA	52.63	584.21	3.47			↑
YPK_1558	*aat, alaA, ybfQ*	aminotransferase class I and II	CDS	28.60	315.88	3.47			↑
YPK_3157	*ybbP-3*	hypothetical protein	CDS	4.53	49.96	3.46			↑
YPK_1355	*arsC, yfgD*	arsenate reductase	CDS	177.87	1,956.86	3.46			↑
YPK_0153		hypothetical protein	CDS	5.33	58.13	3.45			↓
Ysr203			transRNA	46.15	502.31	3.44			↓
YPK_0210		hypothetical protein	CDS	1.79	19.46	3.44			↓
YPK_3723		hypothetical protein	CDS	54.20	582.66	3.43			↓
YPK_1457		hypothetical protein	CDS	5.30	56.07	3.40			↑
YPK_0306	*rpsK*	30S ribosomal protein S11	CDS	696.15	7,337.44	3.40			↑
YPK_R0041	*tRNA-Trp*	tRNA Trp	tRNA	9.87	102.63	3.38			↓
YPK_2915	*betI*	transcriptional regulator BetI	CDS	3.68	38.31	3.38			↑
YPK_0993	*agaS*	AgaS family sugar isomerase	CDS	36.85	377.55	3.36			↓
YPK_4214	*asnA*	asparagine synthetase AsnA	CDS	90.13	906.75	3.33			↓
YPK_2759	*psaA*	pH 6 antigen	CDS	70.23	700.63	3.32			↑
YPK_1767		hypothetical protein	CDS	363.45	3,517.27	3.27			↓
YPK_3069	*rluF*	23S rRNA pseudouridine synthase F	CDS	55.27	529.21	3.26			↑
YPK_0044		hypothetical protein	CDS	59.31	562.16	3.24			↓
YPK_0766		YD repeat protein	CDS	1.87	17.41	3.21			↑
YPK_0750	*fhuA-1, yncD-1*	TonB-dependent O,M, iron siderophore receptor/transporter	CDS	2.05	18.81	3.20			↓
YPK_0832	*yggS*	alanine racemase domain-containing protein	CDS	27.18	244.06	3.17			↑
YPK_2703	*poxB*	pyruvate dehydrogenase	CDS	119.48	1,072.82	3.17			↑
YPK_3040	*iolE*	xylose isomerase domain-containing protein	CDS	11.29	101.17	3.16			↑
YPK_2243	*tehB*	tellurite resistance protein TehB	CDS	31.53	280.63	3.15			↓
YPK_0448	*pcaC-1*	carboxymuconolactone decarboxylase	CDS	22.73	200.51	3.14			↓
YPK_0011	*ibpA*	heat shock protein IbpA	CDS	358.70	3,127.05	3.12			↓
YPK_0003	*recF*	recombination protein F	CDS	36.60	317.86	3.12			↑
YPK_3654	*lsrF*	aldolase	CDS	119.58	1,002.74	3.07			↑
YPK_1733	*lrp-1*	AsnC family transcriptional regulator	CDS	116.11	966.67	3.06			↓

YPK_2699	*ybjD*	hypothetical protein	CDS	15.44	128.18	3.05			↑
YPK_3021	*pbpA, mrdA*	penicillin-binding protein 2	CDS	22.28	182.07	3.03			↑
YPK_0797		hypothetical protein	CDS	16.03	130.77	3.03			↑
YPK_2862	*yehW-1, yehY-1, opuBD-1*	binding-protein-dependent transport systems inner membrane component	CDS	7.47	60.45	3.02			↑
YPK_3677	*lptG, yjgQ*	lipopolysaccharide export system permease protein	CDS	42.71	341.88	3.00			↑
YPK_2746		HAD family hydrolase	CDS	33.56	594.87	4.15	X	↑	
YPK_2628	*tfoX*	competence-specific genes regulator	CDS	47.96	830.50	4.11	X	↑	
YPK_1186		hypothetical protein	CDS	2.63	31.81	3.60	X	↑	
YPK_4237		extracellular solute-binding protein	CDS	13.74	156.49	3.51	X	↑	
YPK_2766	*yphD-7, ytfT-7, yjfF-7*	monosaccharide-transporting ATPase	CDS	1.00	11.21	3.49	X	↑	
YPK_1876	*rovA, slyA*	MarR family transcriptional regulator	CDS	361.69	3,572.22	3.30	X	↓	
YPK_0495	*treB*	PTS system trehalose(maltose)-specific transporter subunit IIBC	CDS	618.47	5,944.49	3.26	X	↑	
YPK_2448	*yoaH*	hypothetical protein	CDS	48.45	462.79	3.26	X	↓	
YPK_3435	*cysN*	sulfate adenylyltransferase subunit 1	CDS	6.42	61.00	3.25	X	↑	
YPK_0393	*impJ-1, vasE-1*	type VI secretion protein, VC_A0114 family	CDS	2.60	23.76	3.19	X	↑	
YPK_2662	*cspB-2*	cold-shock DNA-binding domain-containing protein	CDS	534.52	4,355.24	3.03	X	↑	
YPK_2522		hypothetical protein	CDS	638.02	53,193.75	6.38		↓	
YPK_R0048	*tRNA-Gly*	tRNA Gly	tRNA	72.37	3,968.42	5.78		↓	
YPK_4187	*yihX*	phosphatase	CDS	195.01	7,981.05	5.35		↑	
YPK_1911		hypothetical protein	CDS	3.97	142.86	5.17		↓	
YPK_1496	*ccmA*	heme exporter protein CcmA	CDS	37.29	1,203.35	5.01		↓	
YPK_0900		small terminase subunit	CDS	1.43	44.64	4.96		↑	
Ysr16			transRNA	27.60	857.14	4.96		↓	
YPK_3061		hypothetical protein	CDS	4.96	146.83	4.89		↑	
YPK_1754		pseudogene	CDS	4.46	127.22	4.83		↓	
YPK_3109		DinI family protein	CDS	448.17	12,688.62	4.82		↑	
YPK_2206		hypothetical protein	CDS	26.73	745.91	4.80		↓	
YPK_2023	*yciH*	translation initiation factor SUI1	CDS	948.01	25,051.99	4.72		↓	
YPK_0384		hypothetical protein	CDS	1.14	30.14	4.72		↑	

Ysr223			transRNA	377.91	9,960.47	4.72		↓	
YPK_2744		2OG-Fe(II) oxygenase	CDS	0.47	11.80	4.66		↑	
YPK_2299		hypothetical protein	CDS	13.44	337.63	4.65		↑	
YPK_2458	*hpaD*	3,4-dihydroxyphenylacetate 2,3-dioxygenase	CDS	2.62	62.94	4.58		↑	
YPK_1388	*napB*	citrate reductase cytochrome c-type subunit	CDS	5.34	126.50	4.57		↑	
YPK_R0083	*tRNA-Phe*	tRNA Phe	tRNA	9.87	226.32	4.52		↓	
YPK_3684	*argI*	ornithine carbamoyltransferase subunit I	CDS	4.96	112.70	4.51		↑	
YPK_3297		glycerophosphoryl diester phosphodiesterase	CDS	22.94	480.17	4.39		↑	
YPK_3031	*cspE*	cold shock protein CspE	CDS	1,838.10	35,702.86	4.28		↓	
YPK_4107		hypothetical protein	CDS	10.68	203.76	4.25		↑	
YPK_3271	*malZ-2*	maltodextrin glucosidase	CDS	19.54	371.15	4.25		↑	
YPK_0092	*dppF*	oligopeptide/dipeptide ABC transporter, ATPase subunit	CDS	36.21	684.49	4.24		↓	
YPK_1623		hypothetical protein	CDS	11.90	221.59	4.22		↓	
Ysr211/ryeB	*RyeB*	RyeB	transRNA	13.51	250.00	4.21		↓	
YPK_1130		hypothetical protein	CDS	21.83	396.83	4.18		↓	
YPK_3192	*ddhD, rfbI, ascD*	CDP-6-deoxy-delta-3,4-glucoseen reductase	CDS	27.78	484.44	4.12		↓	
YPK_2895		hypothetical protein	CDS	2.98	51.19	4.10		↑	
Ysr287	*ypkA*	putative targeted effector protein kinase	asRNA	13.33	229.33	4.10		↓	
YPK_2814		Mu P family protein	CDS	2.13	36.55	4.10		↑	
YPK_2434		hypothetical protein	CDS	26.76	455.05	4.09		↓	
YPK_3894	*metC-2*	cystathionine beta-lyase	CDS	30.25	508.29	4.07		↑	
YPK_0793		abortive infection protein	CDS	0.38	6.45	4.07		↓	
YPK_0583	*yapF*	outer membrane autotransporter	CDS	11.59	194.40	4.07		↓	
YPK_2425	*flgB-2*	flagellar basal body rod protein FlgB	CDS	4.83	80.19	4.05		↓	
YPK_3071		hypothetical protein	CDS	20.24	335.22	4.05		↑	
YPK_0392	*vasD-1, lip-1*	putative lipoprotein	CDS	10.07	164.84	4.03		↑	

Ysr279		lysine 2,3-aminomutase, YodO family protein	asRNA	28.48	463.29	4.02		↓	
YPK_2421	*flgF*	flagellar basal body rod protein FlgF	CDS	1.98	32.01	4.01		↓	
Ysr215			transRNA	10.42	166.67	4.00		↓	
YPK_2640	*uup*	ABC transporter ATPase	CDS	50.16	783.39	3.97		↑	
YPK_2382	*fliD*	flagellar capping protein	CDS	2.86	44.11	3.95		↓	
YPK_3123		hypothetical protein	CDS	4.35	66.09	3.93		↑	
Ysr205			transRNA	14.39	212.95	3.89		↓	
YPK_3122		Mu tail sheath family protein	CDS	5.23	76.85	3.88		↑	
YPK_1761	*yadE*	YadA domain-containing protein	CDS	15.11	219.61	3.86		↑	
YPK_2635		hypothetical protein	CDS	31.75	452.91	3.83		↑	
YPK_2205		Sel1 domain protein repeat-containing protein	CDS	67.95	964.20	3.83		↑	
YPK_2767	*yphE-4, ytfR-4*	ABC transporter-like protein	CDS	5.56	78.73	3.82		↑	
Ysr282	*murI*	glutamate racemase	asRNA	27.40	383.56	3.81		↓	
YPK_3167	*ybaK*	hypothetical protein	CDS	40.10	559.58	3.80		↑	
YPK_2441		hypothetical protein	CDS	690.79	9,621.05	3.80		↓	
YPK_3326	*glnQ-2*	ABC transporter-like protein	CDS	110.78	1,516.47	3.77		↓	
YPK_2816		hypothetical protein	CDS	6.69	91.57	3.77		↑	
YPK_1646	*csy-1*	CRISPR-associated Csy1 family protein	CDS	18.93	258.50	3.77		↑	
YPK_4238		polar amino acid ABC transporter inner membrane subunit	CDS	4.07	55.28	3.77		↑	
YPK_1616	*dmlA, ttuC, yeaU*	tartrate dehydrogenase	CDS	4.14	55.99	3.76		↓	
YPK_1375	*afuA, fbpA*	extracellular solute-binding protein	CDS	5.51	73.09	3.73		↑	
YPK_0494	*treC*	trehalose-6-phosphate hydrolase	CDS	470.37	6,192.66	3.72		↑	
YPK_1747	*motA-2*	flagellar motor protein MotA	CDS	50.39	653.38	3.70		↓	
YPK_2953	*nadA*	quinolinate synthetase	CDS	72.50	932.96	3.69		↑	
YPK_1647	*csy-2*	CRISPR-associated Csy2 family protein	CDS	7.36	94.64	3.68		↑	
YPK_2483		hypothetical protein	CDS	2,019.74	25,943.86	3.68		↓	
YPK_2854	*yfaZ*	hypothetical protein	CDS	105.43	1,349.17	3.68		↑	
pYV0091		transposase	CDS	21.87	278.01	3.67		↑	
YPK_1577		hypothetical protein	CDS	9.93	126.01	3.67		↑	
Ysr1			transRNA	110.89	1,401.61	3.66		↓	
YPK_2569	*yjiJ*	hypothetical protein	CDS	7.81	98.61	3.66		↓	

YPK_1645	*cas-3*	CRISPR-associated helicase Cas3 family protein	CDS	10.64	134.06	3.65		↑	
YPK_0631		hypothetical protein	CDS	6,893.20	86,746.28	3.65		↓	
YPK_4088	*argB*	acetylglutamate kinase	CDS	31.85	399.74	3.65		↑	
YPK_3840	*rhaT*	rhamnose-proton symporter	CDS	14.49	179.90	3.63		↓	
YPK_2863	*yehX, opuA*	ABC transporter-like protein	CDS	25.56	316.93	3.63		↑	
YPK_2670	*aroA*	3-phosphoshikimate 1-carboxyvinyltransferase	CDS	222.61	2,714.84	3.61		↑	
YPK_1121		hypothetical protein	CDS	4.46	54.17	3.60		↑	
YPK_0665	*sufI, ftsP*	repressor protein for FtsI	CDS	34.91	416.56	3.58		↑	
YPK_2671	*serC*	phosphoserine aminotransferase	CDS	334.71	3,962.80	3.57		↑	
YPK_2430	*flhE*	flagellar FlhE family protein	CDS	1.77	20.80	3.55		↓	
YPK_4109	*raxA, cvaA*	secretion protein HlyD family protein	CDS	1.35	15.78	3.54		↑	
YPK_1762		hypothetical protein	CDS	4.98	57.65	3.53		↑	
Ysr262		hypothetical protein YPK_3103	asRNA	173.33	2,000.00	3.53		↑	
YPK_0117	*rsmJ*	putative methyltransferase	CDS	3.24	37.09	3.52		↑	
YPK_3549		hypothetical protein	CDS	90.40	1,027.12	3.51		↑	
YPK_1007	*gspG*	general secretion pathway protein G	CDS	4.00	45.21	3.50		↓	
YPK_3371	*yqaB*	fructose-1-phosphatase	CDS	91.71	1,029.28	3.49		↑	
YPK_0513	*mlaE*	putative phospholipid ABC transporter permease protein MlaE	CDS	54.92	608.68	3.47		↑	
YPK_0397		hypothetical protein	CDS	3.28	36.10	3.46		↑	
YPK_3788	*aidB*	isovaleryl CoA dehydrogenase	CDS	270.99	2,982.36	3.46		↓	
YPK_1951		hypothetical protein	CDS	8.18	89.81	3.46		↑	
YPK_1729		hypothetical protein	CDS	169.35	1,821.51	3.43		↓	
YPK_1087		hypothetical protein	CDS	1,334.58	14,298.51	3.42		↓	
YPK_R0078	*tRNA-Ala*	tRNA Ala	tRNA	23.03	242.11	3.39		↓	
YPK_2815		DNA circulation family protein	CDS	2.13	22.17	3.38		↑	
YPK_3079		beta-lactamase fold Zn-dependent hydrolase	CDS	4.98	51.74	3.38		↑	
YPK_1001	*cynT, can*	carbonic anhydrase	CDS	1,022.49	10,620.90	3.38		↓	
YPK_0516	*mlaB*	putative phospholipid ABC transporter-binding protein MlaB	CDS	162.54	1,685.15	3.37		↑	
YPK_2669	*cmk*	cytidylate kinase	CDS	209.96	2,147.19	3.35		↑	

YPK_0390	*impH-1, vasB-1*	type VI secretion protein, VC_A0111 family	CDS	2.80	28.38	3.34		↑	
YPK_1763		hypothetical protein	CDS	7.18	71.26	3.31		↑	
YPK_3072	*bglB*	glycoside hydrolase family 3	CDS	21.31	207.56	3.28		↑	
YPK_2505	*argG*	argininosuccinate synthase	CDS	15.90	153.95	3.28		↑	
YPK_2764	*fruB*	bifunctional PTS system fructose-specific transporter subunit IIA/HPr protein	CDS	6.17	59.61	3.27		↑	
YPK_1753	*cheD, tsr*	methyl-accepting chemotaxis sensory transducer	CDS	3.14	30.11	3.26		↓	
YPK_1741	*dsrB*	hypothetical protein	CDS	145.83	1,398.96	3.26		↓	
YPK_2752	*lysP*	lysine transporter	CDS	15.87	152.25	3.26		↑	
YPK_0867	*gcvT*	glycine cleavage system aminomethyltransferase T	CDS	358.83	3,423.50	3.25		↑	
YPK_1712	*pepT-2*	peptidase T	CDS	338.19	3,223.46	3.25		↓	
YPK_2811		baseplate J family protein	CDS	1.10	10.38	3.24		↑	
Ysr114	*trxB*	thioredoxin reductase	asRNA	18.82	176.10	3.23		↑	
YPK_2381	*fliC*	flagellin	CDS	2.03	18.92	3.22		↓	
YPK_3142		hypothetical protein	CDS	77.59	721.84	3.22		↑	
YPK_0387	*impC-1*	type VI secretion protein, EvpB/VC_A0108 family	CDS	10.29	95.55	3.21		↑	
YPK_0695	*papC*	fimbrial biogenesis outer membrane usher protein	CDS	50.28	463.93	3.21		↓	
YPK_0986		glycosyl hydrolase family protein	CDS	15.58	143.72	3.21		↑	
YPK_2812		GP46 family protein	CDS	5.48	50.44	3.20		↑	
YPK_3865		outer membrane autotransporter	CDS	1.44	13.28	3.20		↓	
YPK_3551		hypothetical protein	CDS	8.22	75.48	3.20		↑	
YPK_3144	*ybjD*	SMC (structural maintenance of chromosomes) family protein	CDS	32.33	293.02	3.18		↑	
YPK_3437	*cysG-2*	uroporphyrin-III C-methyltransferase	CDS	6.17	55.53	3.17		↑	
YPK_0388		type VI secretion system lysozyme-related protein	CDS	2.83	25.40	3.16		↑	
YPK_0395	*vasG-1, clpV-1*	type VI secretion ATPase, ClpV1 family	CDS	2.98	26.65	3.16		↑	

YPK_0515	*mlaC*	putative phospholipid-binding protein MlaC	CDS	217.55	1,943.27	3.16		↑	
YPK_2768	*yphF-4, ytfQ-4*	sugar ABC transporter substrate-binding protein	CDS	9.64	85.03	3.14		↑	
YPK_2638	*pqiB*	paraquat-inducible protein B	CDS	37.36	325.95	3.13		↑	
YPK_3882		hypothetical protein	CDS	23.44	201.67	3.11		↑	
YPK_4210	*rbsD*	D-ribose pyranase	CDS	259.52	2,228.57	3.10		↓	
Ysr229			transRNA	16.90	143.77	3.09		↓	
YPK_0398	*vasJ-1*	type VI secretion-associated protein, VC_A0119 family	CDS	1.80	15.12	3.07		↑	
YPK_0281	*bfr*	bacterioferritin	CDS	168.25	1,404.64	3.06		↓	
YPK_2197		hypothetical protein	CDS	125.55	1,030.46	3.04		↑	
YPK_2470	*atoS1*	PAS/PAC sensor-containing diguanylate cyclase	CDS	6.96	56.77	3.03		↑	
YPK_0697		fimbrial protein	CDS	95.56	775.72	3.02		↓	
YPK_0166		hypothetical protein	CDS	176.85	1,420.00	3.01		↓	
YPK_2932	*bioA*	adenosylmethionine-8-amino-7-oxononanoate aminotransferase	CDS	1.95	15.61	3.00		↓	
YPK_0220	*hofM*	DNA catabolic putative pilus assembly protein	CDS	0.28	14.05	5.66	X		
YPK_3260		hypothetical protein	CDS	1.13	53.60	5.57	X		
YPK_2419	*flgH*	flagellar basal body L-ring protein	CDS	1.45	47.25	5.03	X		
YPK_1629		hypothetical protein	CDS	14.88	462.38	4.96	X		
YPK_1111	*hpxB*	urate catabolism protein	CDS	25.24	772.03	4.94	X		
YPK_3759		MuA-transposase/repressor protein CI DNA-binding	CDS	58.91	1,696.55	4.85	X		
YPK_0933		hypothetical protein	CDS	0.76	19.39	4.68	X		
YPK_1451		hypothetical protein	CDS	7.61	182.65	4.58	X		
YPK_1344	*ppk*	polyphosphate kinase	CDS	68.56	1,604.55	4.55	X		
YPK_0202		hypothetical protein	CDS	22.39	515.92	4.53	X		
YPK_0984	*ydeN, yidJ*	sulfatase	CDS	10.11	219.03	4.44	X		
YPK_2131	*mdtJ*	small multidrug resistance protein	CDS	35.47	749.55	4.40	X		
YPK_0538	*yraN*	putative endonuclease	CDS	117.23	2,222.03	4.24	X		
YPK_2433		hypothetical protein	CDS	16.67	298.06	4.16	X		

YPK_1901		hypothetical protein	CDS	79.98	1,409.84	4.14	X		
YPK_2409	*yphE-2; ytfR-2*	ABC transporter-like protein	CDS	6.02	105.58	4.13	X		
YPK_0854	*mscS*	mechanosensitive ion channel MscS	CDS	52.59	920.46	4.13	X		
YPK_1752		putative lipoprotein	CDS	39.17	655.56	4.06	X		
YPK_3143		hypothetical protein	CDS	24.43	395.18	4.02	X		
YPK_3151	*ybcJ*	hypothetical protein	CDS	602.11	9,683.57	4.01	X		
YPK_0534	*elbB*	isoprenoid biosynthesis protein with amidotransferase-like domain	CDS	718.27	11,504.89	4.00	X		
YPK_4171		hypothetical protein	CDS	148.52	2,293.55	3.95	X		
YPK_1123		hypothetical protein	CDS	46.46	697.94	3.91	X		
YPK_1532	*folC*	bifunctional folylpolyglutamate synthase/dihydrofolate synthase	CDS	49.81	714.94	3.84	X		
YPK_4068	*yphF-6, ytfQ-6*	periplasmic binding protein/LacI transcriptional regulator	CDS	32.13	447.44	3.80	X		
YPK_1725		hypothetical protein	CDS	38.31	532.57	3.80	X		
YPK_1045	*argA*	N-acetylglutamate synthase	CDS	30.17	417.35	3.79	X		
YPK_3168		hypothetical protein	CDS	43.60	596.90	3.77	X		
YPK_1339		hypothetical protein	CDS	1.77	24.11	3.77	X		
YPK_0752		putative siderophore biosysnthesis protein	CDS	9.66	126.84	3.71	X		
YPK_2949	*aroG*	phospho-2-dehydro-3-deoxyheptonate aldolase	CDS	256.65	3,249.19	3.66	X		
YPK_0259	*tauB-1*	taurine transporter ATP-binding subunit	CDS	2.60	32.55	3.64	X		
YPK_3428	*surE*	stationary phase survival protein SurE	CDS	78.76	971.76	3.63	X		
YPK_2420	*flgG*	flagellar basal body rod protein FlgG	CDS	3.19	38.83	3.60	X		
YPK_2593		hypothetical protein	CDS	1.28	15.07	3.56	X		
YPK_0201		hypothetical protein	CDS	162.10	1,909.13	3.56	X		
YPK_1362	*dapA*	dihydrodipicolinate synthase	CDS	147.50	1,718.00	3.54	X		
YPK_1426	*crr*	PTS system glucose-specific transporter	CDS	883.33	10,286.67	3.54	X		
YPK_0174	*pckA*	phosphoenolpyruvate carboxykinase	CDS	4,312.19	49,625.06	3.52	X		
YPK_1056	*ygdH*	hypothetical protein	CDS	176.74	1,990.62	3.49	X		
YPK_0013	*yidE*	YidE/YbjL duplication	CDS	177.37	1,988.79	3.49	X		
YPK_0008	*ilvA, tdcB*	threonine dehydratase	CDS	51.92	579.65	3.48	X		

YPK_3796	*hflK*	FtsH protease regulator HflK	CDS	65.32	713.70	3.45	**X**		
YPK_1773		spore coat U domain-containing protein	CDS	0.51	5.45	3.43	**X**		
YPK_2195		cupin	CDS	6.37	67.09	3.40	**X**		
YPK_3146		hypothetical protein	CDS	74.24	770.91	3.38	**X**		
YPK_2374	*yecC*	putative amino-acid ABC transporter ATP-binding protein YecC	CDS	64.30	666.40	3.37	**X**		
YPK_3564	*impC-4*	type VI secretion protein, EvpB/VC_A0108 family	CDS	15.54	159.26	3.36	**X**		
YPK_1472	*impH-2, vasB-2*	type VI secretion protein, VC_A0111 family	CDS	0.73	7.41	3.34	**X**		
YPK_2905		LysR family transcriptional regulator	CDS	7.68	77.19	3.33	**X**		
YPK_0046		hypothetical protein	CDS	4.03	39.78	3.30	**X**		
YPK_0487		guanine-specific ribonuclease N1 and T1	CDS	260.55	2,567.93	3.30	**X**		
YPK_0108		hypothetical protein	CDS	1.44	14.02	3.29	**X**		
YPK_3310		hypothetical protein	CDS	16.40	159.84	3.28	**X**		
YPK_1299		hypothetical protein	CDS	25.56	248.89	3.28	**X**		
YPK_3808	*orn*	oligoribonuclease	CDS	81.04	788.64	3.28	**X**		
YPK_3078		hypothetical protein	CDS	14.71	142.48	3.28	**X**		
YPK_0043	*selB*	selenocysteinyl-tRNA-specific translation factor	CDS	51.67	500.41	3.28	**X**		
YPK_3770	*ytfM*	surface antigen (D15)	CDS	56.42	545.88	3.27	**X**		
YPK_0512	*mlaF*	putative phospholipid import ATP-binding protein MlaF	CDS	105.62	1,020.02	3.27	**X**		
YPK_0161	*glgP-2*	glycogen/starch/alpha-glucan phosphorylase	CDS	17.87	169.58	3.25	**X**		
YPK_0321	*aroE-1*	shikimate 5-dehydrogenase	CDS	334.55	3,071.29	3.20	**X**		
YPK_3301	*nqrE*	Na(+)-translocating NADH-quinone reductase subunit E	CDS	52.35	458.29	3.13	**X**		
YPK_2154	*yecM*	hypothetical protein	CDS	14.76	122.92	3.06	**X**		
YPK_3270		short chain dehydrogenase	CDS	171.07	1,404.70	3.04	**X**		
YPK_2545	*ysuH, alcB*	putative siderophore biosynthetic enzyme	CDS	2.16	17.62	3.03	**X**		

YPK_1782	*proQ*	putative solute/DNA competence effector	CDS	293.07	2,390.48	3.03	**X**		
YPK_2674	*ansB*	L-asparaginase II	CDS	416.67	3,392.68	3.03	**X**		
YPK_2064		dsDNA-mimic protein	CDS	167.37	1,362.15	3.02	**X**		
YPK_4062	*comM, yifB*	Mg chelatase subunit ChlI	CDS	8.69	70.73	3.02	**X**		
YPK_2704		hypothetical protein	CDS	2.31	18.52	3.00	**X**		
YPK_2678		glycosyl transferase family protein	CDS	56.67	452.15	3.00	**X**		

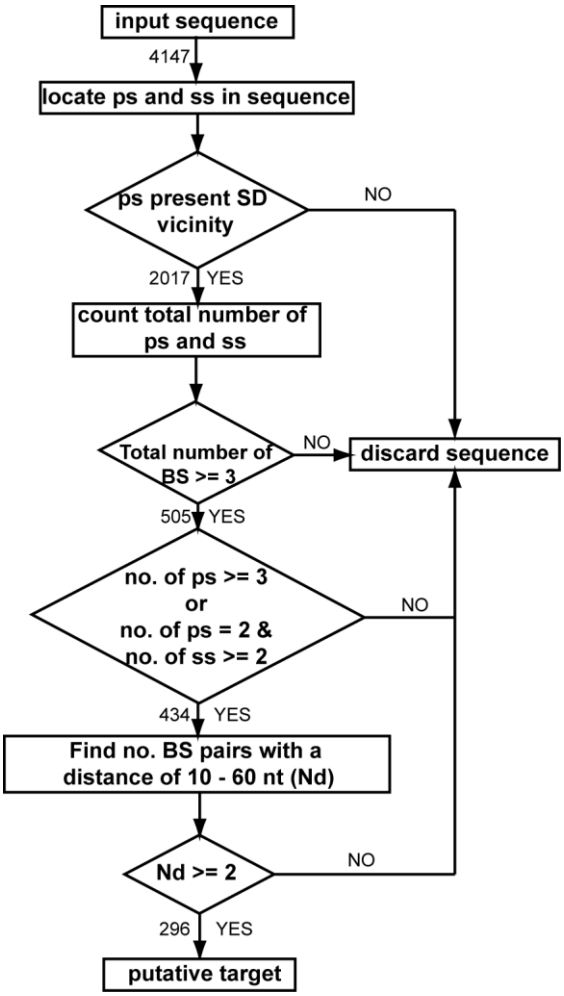

Figure S5: Flowchart of the CsrA target prediction algorithm CSRA-TARGET_PREDICTER of *E. coli* K12. 4147 upstream regions of chromosomally encoded ORFs were analyzed for CsrA primary sites (ps; A(N)GGA) and secondary sites (ss; AGAGA, CTGGA, CGGGA, TGGGA). The number of analyzed and processed sequences are depicted next to flow line arrows.

Table S6: CsrA targets in *E. coli* MG1655 as predicted by the CSRA_TARGET_PREDICTER script. Shown are genes which were predicted by the CSRA_TARGET_PREDICTER script. *In silico* predicted CsrA by Kulkarni *et al*., 2014 are highlighted with an X mark.

Locus	Gene name	Gene description	predicted in Kulkarni *et al*. 2014
b0024	yaaY	hypothetical protein	X
b0037	caiC	Crotonobetaine - CoA ligase	
b0058	rluA	Ribosomal large subunit pseudouridine synthase A	X
b0069	sgrR	SgrR, sugar-phosphate stress, transcriptional activator of SgrS small RNA	
b0076	leuO	LysR family transcriptional activator LeuO	X
b0082	mraW	16S rRNA (cytosine(1402)-N(4))-methyltransferase	X
b0084	ftsI	Cell division protein FtsI [Peptidoglycan synthetase]	
b0129	yadI	Putative PTS system IIA component yadI	
b0176	rseP	Intramembrane protease RasP/YluC, implicated in cell division based on FtsL cleavage	
b0186	ldcC	Lysine decarboxylase 2, constitutive	X
b0187	yaeR	Hypothetical protein YaeR with similarity to glyoxylase family	
b0220	ivy	Inhibitor of vertebrate lysozyme	X
b0225	yafQ	mRNA interferase YafQ	
b0233	yafO	Toxin YafO	X
b0276	yagJ	Putative uncharacterized protein YagJ	X
b0291	yagX	CFA/I fimbrial subunit C usher protein	
b0301	ykgB	Inner membrane protein RclC associated with response to reactive chlorine species	
b0305	ykgD	Reactive-chlorine-species-specific transcriptional activator RclR, AraC family	
b0308	ykgG	Predicted L-lactate dehydrogenase, hypothetical protein subunit YkgG	X
b0312	betB	Betaine aldehyde dehydrogenase	
b0325	yahK	Cinnamyl alcohol dehydrogenase/reductase	
b0328	yahN	Uncharacterized membrane protein YahN	
b0375	yaiV	Uncharacterized protein YaiV	
b0378	yaiW	Uncharacterized outer membrane protein YaiW	
b0412	yajI	Hypothetical lipoprotein yajI	X
b0414	ribD	Diaminohydroxyphosphoribosylaminopyrimidine deaminase	
b0419	yajO	Uncharacterized oxidoreductase, YajO family	
b0425	panE	2-dehydropantoate 2-reductase	X
b0426	yajQ	hypothetical protein YajQ	
b0431	cyoB	Cytochrome O ubiquinol oxidase subunit I	X
b0435	bolA	Cell division protein BolA	X
b0485	ybaS	Glutaminase	
b0490	ybbL	YbbL ABC transporter ATP-binding protein	X
b0493	ybbO	Putative NAD(P)-dependent oxidoreductase EC-YbbO	
b0498	ybbC	Uncharacterized protein YbbC	

b0505	allA	Ureidoglycolate lyase	
b0509	glxR	2-hydroxy-3-oxopropionate reductase	
b0530	sfmA	Uncharacterized fimbrial-like protein SfmA	X
b0592	fepB	Ferric enterobactin-binding periplasmic protein FepB	
b0598	cstA	Carbon starvation protein A	X
b0601	ybdM	Co-activator of prophage gene expression IbrB	
b0607	uspG	Universal stress protein G	
b0645	ybeR	Uncharacterized protein YbeR	
b0648	ybeU	Uncharacterized protein YbeU	
b0662	ubiF	2-octaprenyl-3-methyl-6-methoxy-1,4-benzoquinol hydroxylase	
b0704	ybfC	Uncharacterized protein YbfC	
b0706	ybfD	H repeat-associated protein, YhhI family	X
b0712	ybgK	Allophanate hydrolase 2 subunit 2	
b0717	ybgP	Uncharacterized fimbrial chaperone YbgP	
b0722	sdhD	Succinate dehydrogenase hydrophobic membrane anchor protein	
b0758	galT	Galactose-1-phosphate uridylyltransferase	X
b0770	ybhI	Inner membrane protein YbhI	X
b0787	ybhM	Uncharacterized protein YbhM	
b0794	ybhF	ABC transporter multidrug efflux pump, fused ATP-binding domains	
b0796	ybiH	Transcriptional regulator YbiH, TetR family	
b0800	ybiB	Anthranilate phosphoribosyltransferase like	
b0827	moeA	Molybdopterin molybdenumtransferase	
b0886	cydC	Transport ATP-binding protein CydC	
b0890	ftsK	DNA translocase FtsK	
b0891	lolA	Outer membrane lipoprotein carrier protein LolA	X
b0900	ycaN	LysR family transcriptional regulator YcaN	
b0917	ycaR	Protein YcaR in KDO2-Lipid A biosynthesis cluster	
b0949	uup	ABC transporter ATP-binding protein uup	
b0963	mgsA	Methylglyoxal synthase	X
b0972	hyaA	Uptake hydrogenase small subunit precursor	X
b0976	hyaE	Hydrogenase maturation factor HoxO/HyaE	X
b0978	appC	Cytochrome d ubiquinol oxidase subunit I	
b0989	cspH	Cold shock protein CspH	
b1004	wrbA	NAD(P)H dehydrogenase (quinone)	
b1024	pgaA	Biofilm PGA outer membrane secretin PgaA	X
b1078	flgG	Flagellar basal-body rod protein FlgG	
b1108	ycfP	YcfP protein: probably an esterase that is part of a salvage cluster	
b1122	ymfA	Inner membrane protein YmfA	X
b1127	pepT	Tripeptide aminopeptidase	
b1136	icd	Isocitrate dehydrogenase [NADP]	
b1178	ycgK	Inhibitor of g-type lysozyme	X
b1212	prmC	Peptide chain release factor N(5)-glutamine methyltransferase	X
b1247	oppF	Oligopeptide transport ATP-binding protein OppF	
b1283	osmB	Osmotically inducible lipoprotein B precursor	
b1287	yciW	Uncharacterized protein YciW	X

b1299	puuR	Putrescine utilization regulator	X
b1319	ompG	Outer membrane protein G precursor	X
b1342	ydaN	Zinc transport protein ZntB	
b1394	paaG	1,2-epoxyphenylacetyl-CoA isomerase	
b1407	ydbD	Uncharacterized protein YdbD	X
b1436	yncJ	Uncharacterized protein YncJ	
b1453	ansP	L-asparagine permease	
b1460	ydcC	H repeat-associated protein, YhhI family	
b1477	yddM	Antitoxin HigA	X
b1493	gadB	Glutamate decarboxylase	X
b1511	lsrK	Autoinducer 2 (AI-2) kinase LsrK	X
b1535	ydeH	Diguanylate cyclase YdeH	X
b1558	cspF	Cold shock protein CspF	X
b1561	rem	Uncharacterized protein Rem	X
b1589	ynfG	Anaerobic dimethyl sulfoxide reductase chain B	X
b1606	folM	FolM Alternative dihydrofolate reductase 1	X
b1639	mliC	Membrane-bound lysozyme inhibitor of c-type lysozyme	
b1641	slyB	Outer membrane lipoprotein pcp precursor	X
b1646	sodC	Superoxide dismutase [Cu-Zn] precursor	
b1680	sufS	Cysteine desulfurase	
b1694	ydiF	Acetyl-CoA:acetoacetyl-CoA transferase, alpha subunit	
b1695	ydiO	Acyl-CoA dehydrogenase YdiO	
b1707	ydiV	Putative anti-FlhC(2)FlhD(4) factor YdiV	
b1736	chbA	PTS system, N,N'-diacetylchitobiose-specific IIA component	
b1744	astE	Succinylglutamate desuccinylase	X
b1764	selD	Selenide,water dikinase	
b1797	yeaR	Uncharacterized protein YeaR	
b1800	yeaU	D-malate dehydrogenase [decarboxylating]	
b1809	yoaB	RidA/YER057c/UK114 superfamily	
b1816	yoaE	UPF0053 inner membrane protein YoaE	
b1818	manY	PTS system, mannose-specific IIC component	
b1821	yebN	Probable manganese efflux pump MntP	
b1831	proQ	ProQ: influences osmotic activation of compatible solute ProP	
b1842	holE	DNA polymerase III theta subunit	
b1856	yebA	Murein DD-endopeptidase MepM	
b1872	torZ	Trimethylamine-N-oxide reductase	
b1943	fliK	Flagellar hook-length control protein FliK	X
b1946	fliN	Flagellar motor switch protein FliN	
b1981	shiA	Shikimate transporter	
b1993	cobU	Adenosylcobinamide kinase	
b2001	yeeR	Inner membrane protein YeeR	
b2002	yeeS	UPF0758 protein YeeS	
b2026	hisI	Phosphoribosyl-AMP cyclohydrolase	
b2035	rfc	O-antigen polymerase	
b2083	yegZ	Gene D protein	
b2101	yegW	Uncharacterized HTH-type transcriptional regulator YegW	

b2104	thiM	Hydroxyethylthiazole kinase	X
b2112	yehE	Uncharacterized protein YehE	
b2118	yehI	Uncharacterized protein YehI	
b2125	yehT	Transcriptional regulatory protein YehT	X
b2162	rihB	Pyrimidine-specific ribonucleoside hydrolase RihB	X
b2175	spr	Murein DD-endopeptidase MepS	
b2196	ccmF	Cytochrome c-type biogenesis protein CcmF	X
b2203	napB	Nitrate reductase cytochrome c550-type subunit	
b2247	yfaW	L-rhamnonate dehydratase	X
b2256	arnD	4-deoxy-4-formamido-L-arabinose-phosphoundecaprenol deformylase ArnD	
b2261	menC	O-succinylbenzoate synthase	X
b2265	menF	Isochorismate synthase	
b2270	yfbK	Putative von Willebrand factor	
b2275	yfbP	Uncharacterized protein YfbP	X
b2331	yfcN	UPF0115 protein YfcN	X
b2360	yfdQ	Uncharacterized protein YfdQ	
b2377	yfdY	Uncharacterized protein YfdY	X
b2420	yfeS	Molybdate metabolism regulator	X
b2457	eutM	Ethanolamine utilization polyhedral-body-like protein EutM	
b2463	maeB	NADP-dependent malic enzyme	
b2465	tktB	Transketolase	
b2478	dapA	4-hydroxy-tetrahydrodipicolinate synthase	
b2482	hyfB	Hydrogenase-4 component B	X
b2491	hyfR	Formate hydrogenlyase transcriptional activator	X
b2510	yfgJ	Uncharacterized protein YfgJ	X
b2513	yfgM	Mlr7403 protein	X
b2560	yfhB	Phosphatidylglycerophosphatase C	
b2601	aroF	2-keto-3-deoxy-D-arabino-heptulosonate-7-phosphate synthase I alpha	
b2606	rplS	LSU ribosomal protein L19p	
b2628	yfjL	hypothetical protein	
b2644	yfjY	UPF0758 protein YfjY	
b2696	csrA	Carbon storage regulator	X
b2706	gutM	Glucitol operon activator protein	X
b2714	ascG	AscBF operon repressor	
b2717	hycI	Hydrogenase 3 maturation protease	X
b2748	ftsB	Cell division protein DivIC (FtsB)	
b2752	cysD	Sulfate adenylyltransferase subunit 2	
b2760	casA	CRISPR-associated protein, Cse1 family	
b2769	ygcQ	Putative electron transfer flavoprotein subunit YgcQ	
b2776	ygcE	Uncharacterized sugar kinase YgcE	X
b2781	mazG	Nucleoside triphosphate pyrophosphohydrolase MazG	
b2784	relA	Inactive (p)ppGpp 3'-pyrophosphohydrolase domain	
b2790	yqcA	Hypothetical flavoprotein YqcA	X
b2795	ygdH	Decarboxylase family protein	

b2799	fucO	Lactaldehyde reductase	
b2822	recC	Exodeoxyribonuclease V gamma chain	
b2840	ygeA	Uncharacterized protein YgeA of aspartate/glutamate/hydantoin racemase family	X
b2880	ygfM	Uncharacterized protein YgfM	X
b2881	xdhD	Possible hypoxanthine oxidase XdhD	
b2882	xanQ	Putative purine permease YgfO	
b2883	guaD	Guanine deaminase	X
b2903	gcvP	Glycine dehydrogenase [decarboxylating]	X
b2916	argP	Chromosome initiation inhibitor	
b2917	scpA	Methylmalonyl-CoA mutase	
b2920	scpC	Propionyl-CoA:succinyl-CoA transferase	X
b2921	ygfI	LysR family transcriptional regulator YgfI	X
b2925	fbaA	Fructose-bisphosphate aldolase class II	
b2957	ansB	L-asparaginase	X
b3003	yghA	Putative oxidoreductase	X
b3008	metC	Cystathionine beta-lyase	
b3013	yqhG	Uncharacterized protein yqhG precursor	
b3021	ygiT	Transcriptional regulator, Cro/CI family	
b3032	cpdA	3',5'-cyclic-nucleotide phosphodiesterase	
b3051	yqiK	Inner membrane protein YqiK	
b3052	rfaE	ADP-heptose synthase	
b3074	ygjH	tRNA-binding protein YgjH	X
b3095	yqjA	DedA family inner membrane protein YqjA	
b3096	yqjB	Uncharacterized protein YqjB	X
b3150	yraP	21 kDa hemolysin precursor	
b3157	yhbT	Putative lipid carrier protein	X
b3167	rbfA	Ribosome-binding factor A	
b3188	sfsB	Ner-like regulatory protein	X
b3210	arcB	Aerobic respiration control sensor protein ArcB	
b3220	yhcG	Putative uncharacterized protein YhcG	X
b3251	mreB	Rod shape-determining protein MreB	
b3257	yhdT	Membrane protein	
b3284	smg	Protein of unknown function Smg	X
b3288	fmt	Methionyl-tRNA formyltransferase	
b3291	mscL	Large-conductance mechanosensitive channel	
b3317	rplB	LSU ribosomal protein L2p (L8e)	
b3336	bfr	Bacterioferritin	X
b3350	kefB	Glutathione-regulated potassium-efflux system protein KefB	X
b3393	hofO	Type IV pilus biogenesis protein PilO	X
b3416	malQ	4-alpha-glucanotransferase (amylomaltase)	
b3429	glgA	Glycogen synthase, ADP-glucose transglucosylase	
b3430	glgC	Glucose-1-phosphate adenylyltransferase	X
b3432	glgB	1,4-alpha-glucan (glycogen) branching enzyme	
b3442	yhhZ	Uncharacterized protein YhhZ	
b3483	yhhH	Uncharacterized protein YhhH	

b3484	yhhI	H repeat-associated protein, YhhI family	X
b3487	yhiI	Uncharacterized protein YhiI	X
b3495	uspA	Universal stress protein A	X
b3512	gadE	Transcriptional activator GadE	X
b3517	gadA	Glutamate decarboxylase	X
b3522	yhjD	Inner membrane protein YhjD	
b3524	yhjG	Uncharacterized protein YhjG	X
b3549	tag	DNA-3-methyladenine glycosylase	X
b3552	yiaD	Probable lipoprotein YiaD	X
b3554	yiaF	probable exported protein YPO4070	
b3562	yiaA	Inner membrane protein YiaA	
b3568	xylH	Xylose ABC transporter, permease protein XylH	X
b3573	ysaA	Putative electron transport protein YsaA	
b3574	yiaJ	Hypothetical transcriptional regulator yiaJ	
b3595	yibJ	Protein RhsB	
b3631	rfaG	UDP-glucose:(heptosyl) LPS alpha1,3-glucosyltransferase WaaG	X
b3638	yicR	UPF0758 protein YicR	
b3680	yidL	Hypothetical transcriptional regulator yidL	
b3686	ibpB	16 kDa heat shock protein B	
b3693	dgoK	2-dehydro-3-deoxygalactonokinase	
b3696	yidX	Putative replicase	X
b3697	yidA	Sugar phosphatase YidA	
b3708	tnaA	Tryptophanase	X
b3719	yieL	Putative xylanase	
b3724	phoU	Phosphate transport system regulatory protein PhoU	
b3803	hemX	Homolog of E. coli HemX protein	
b3810	yigA	Protein of unknown function DUF484	
b3817	yigF	hypothetical protein	
b3821	pldA	Phospholipase A1	
b3834	yigP	Protein YigP	
b3856	mobB	Molybdopterin-guanine dinucleotide biosynthesis protein MobB	
b3878	yihQ	Sulpholipid alpha-glucosidase	X
b3892	fdoI	Formate dehydrogenase O gamma subunit	X
b3894	fdoG	Formate dehydrogenase O alpha subunit	
b3899	frvB	PTS system, fructose-specific IIB component	
b3912	cpxR	Copper-sensing two-component system response regulator CpxR	
b3923	uspD	Universal stress protein D	
b3934	cytR	Transcriptional (co)regulator CytR	X
b3945	gldA	Glycerol dehydrogenase	
b3965	trmA	tRNA (uracil(54)-C5)-methyltransferase	
b3987	rpoB	DNA-directed RNA polymerase beta subunit	
b3989	yjaZ	Heat shock protein C	
b3993	thiE	Thiamin-phosphate pyrophosphorylase	
b4002	zraP	Zinc resistance-associated protein	
b4004	zraR	Response regulator of zinc sigma-54-dependent two-component system	X

b4020	yjbB	Sodium-dependent phosphate transporter	
b4040	ubiA	4-hydroxybenzoate polyprenyltransferase	
b4071	nrfB	Cytochrome c-type protein NrfB precursor	
b4080	mdtP	Outer membrane component of tripartite multidrug resistance system	
b4083	yjcS	Putative alkyl/aryl-sulfatase YjcS	
b4119	melA	Alpha-galactosidase	
b4126	yjdI	Uncharacterized protein YjdI	
b4132	cadB	Lysine/cadaverine antiporter membrane protein CadB	
b4135	yjdC	Transcriptional regulator, AcrR family	
b4174	hflK	HflK protein	**X**
b4179	rnr	3'-to-5' exoribonuclease RNase R	**X**
b4185	yjfM	hypothetical protein	
b4196	ulaD	3-keto-L-gulonate-6-phosphate decarboxylase UlaD	
b4206	ytfB	Putative cell envelope opacity-associated protein A	**X**
b4255	rraB	Ribonuclease E inhibitor RraB	
b4279	yjhB	Sialic acid transporter (permease) NanT	
b4298	yjhH	Uncharacterized lyase YjhH	
b4305	sgcX	Putative sgc region protein sgcX	
b4311	nanC	N-acetylneuraminic acid outer membrane channel protein NanC	
b4312	fimB	Type 1 fimbriae regulatory protein FimB	**X**
b4316	fimC	Chaperone protein FimC	**X**
b4326	iraD	YjiD protein	
b4333	yjiK	hypothetical protein	**X**
b4357	yjjM	Regulator of L-galactonate catabolism YjjM	**X**
b4365	yjjQ	Putative regulatory protein	**X**
b4366	bglJ	Transcriptional activator protein bglJ	
b4384	deoD	Purine nucleoside phosphorylase	**X**
b4396	rob	Right origin-binding protein	
b4482	yigE	hypothetical protein	**X**
b4539	yoeB	YoeB toxin protein	**X**
b4543	ypaA	Uncharacterized protein YfaD	
b4547	ypfN	UPF0370 protein YpfN	**X**
b4600	ydfJ	Putative transport protein	
b4683	yqeL	hypothetical protein	
b4684	yqfG	hypothetical protein	
b4694	yagP	LysR family transcriptional regulator YagP	

```
E. coli             AACAAATCATCATCCCCGCCACCCTGTCCTGATCGTTTCCTGAACGATAAATTGTGATCT
Y. pstb             ----CCTGATGAACTGACTCAGTGTCGCCATTTGGGTGAGTGAGCGTCGCGGT------A
                          * ** * *     **   *  **   * * *   *** **      *

E. coli             TCGCTGCGTTTCGGGAACGTTCCCGTTTTTAA-------ATTTTTCCGCGCAATATATTC
Y. pstb             ACACCGAGTAAAAAGGGAATTATAGATTTAATTCGCTGCTGACTTCAGGCAGAGATGGCA
                     * * * **     *    **   * *** *            *** *    * **

E. coli             TGCAGCCAACCAAAAATGTCATCTGCCATGGGGCTTTATGATGAGCAAAATAAACCAAAC
Y. pstb             TCTCATGCGCGCACGTAACCTTTACGGAAAGGACGATAAAATGGGCAAAGTAAAACAGCA
                    *        *  *      * *     *  ** *  **  *** ***** **** **

E. coli             GGATATCGATCGGTTGATTGAACTGGTCGGCGGGCGC---
Y. pstb             GGATATCGATCAACTGATCGTTCTGGTGGGAGGCAGAGAA
                    ***********   **** *  ***** ** **  *
```

Figure S8: DNA sequence alignment of the *treB* gene of *Y. pseudotuberculosis* YPIII and *E. coli* K12. ClustalO was used for the alignment of the *E. coli treB* (b4240) and *Y. pseudotuberculosis treB* (YPK_0495) upstream region (-50 to +20 relative to the translational start site) with default parameters. Nucleotides which were identical in both species are marked with a star below the sequence. The positions of high-affinity (ANGGA - pink), low-affinity CsrA binding motifs (green) and the start codon (underlined) are indicated.

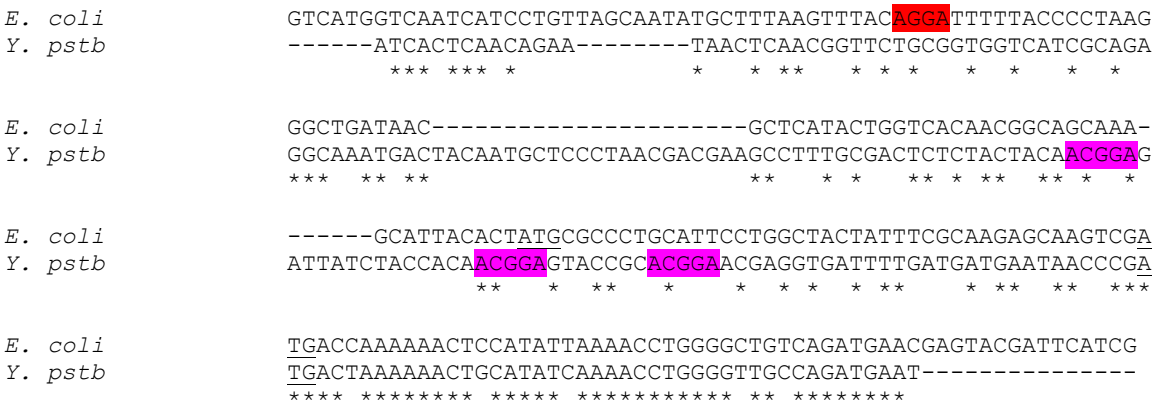

Figure S9: DNA sequence alignment of the *miaB* gene of *Y. pseudotuberculosis* YPIII and *E. coli* K12. ClustalO was used for the alignment of the *E. coli miaB* (b0661) and *Y. pseudotuberculosis miaB* (YPK_3005) upstream region (-50 to +20 relative to the translational start site) with default parameters. Nucleotides which were identical in both species are marked with a star below the sequence. The positions of high-affinity (AGGA - red; ANGGA - pink) and the start codon (underlined) are indicated.

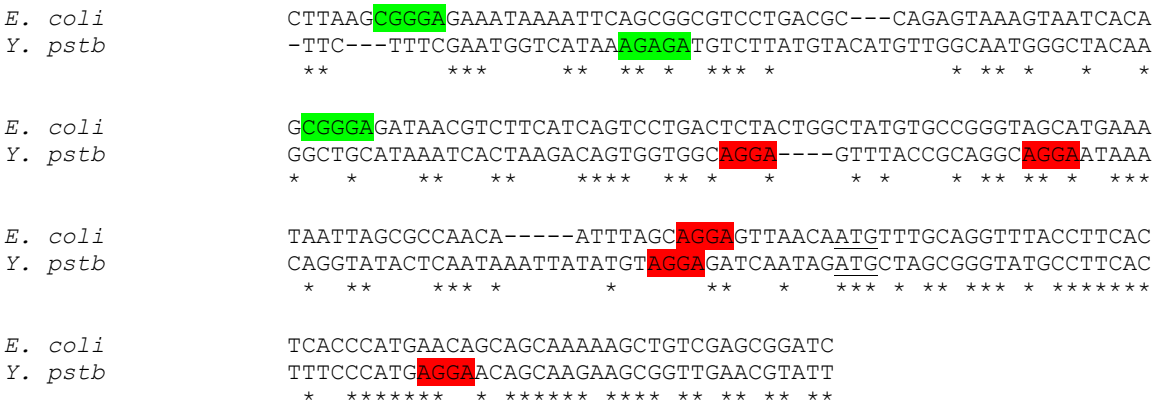

Figure S10: DNA sequence alignment of the *yoaH* gene of *Y. pseudotuberculosis* YPIII and *E. coli* K12. ClustalO was used for the alignment of the *E. coli yoaH* (b1811) and *Y. pseudotuberculosis yoaH* (YPK_2448) upstream region (-50 to +20 relative to the translational start site) with default parameters. Nucleotides which were identical in both species are marked with a star below the sequence. The positions of high-affinity (AGGA - red), low-affinity CsrA binding motifs (green) and the start codon (underlined) are indicated.

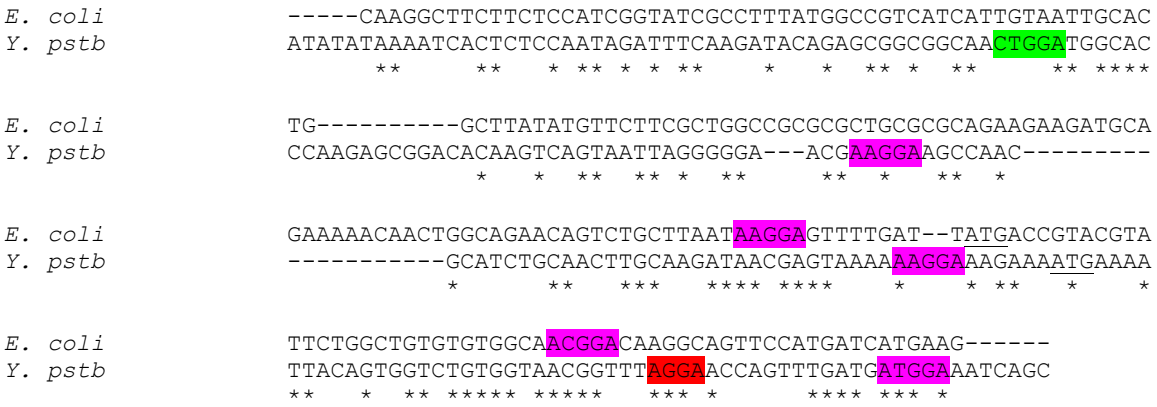

Figure S11: DNA sequence alignment of the *ulaB* gene of *Y. pseudotuberculosis* YPIII and *E. coli* K12. ClustalO was used for the alignment of the *E. coli ulaB* (b4194) and *Y. pseudotuberculosis ulaB* (YPK_1547) upstream region (-50 to +20 relative to the translational start site) with default parameters. Nucleotides which were identical in both species are marked with a star below the sequence. The positions of high-affinity (AGGA - red; ANGGA - pink), low-affinity CsrA binding motifs (green) and the start codon (underlined) are indicated.

```
P. aeruginosa       ------GTCTTTTATAATCCGGTATCACCCGATGTGTCTTCCCGAGGCG-ACGAAACGCC
Y. pstb             CGTAACGATTGGTGTAATGGAATAACGATCGGT--GTAATGGAATAACGGCCGACGCGAT
                           *  *  * ****    ** *   ** *  **  *       **  ***  **

P. aeruginosa       GGAAAGCCGTCGGGCCAGCCTGGATGCGAACCGAAATCCCTCG-GGCACGGGGGTGAGCG
Y. pstb             GGAATAACGGTCGG----CATGATGAAATAACGACCCGCGTTGTGAAATAGCGATCAGCG
                    ****   **   **    * **       * ***    * * * *  *  * * * ****

P. aeruginosa       CCTGGAAGAGCCGGGCGC-------------TGGCAATGCAAGGAGTAGCAATGCCGCTG
Y. pstb             TTATGAAATAAGAATCAGTATTCAGGAAGAGACACCATGGATAAAAAACAACCAACGCTG
                        ***        *                 * *** *   *  *  *    *****

P. aeruginosa       CGATTGACCATCACCAGCTACCACAAGCTGACCCCCGGTCAGTGTTCGGAA
Y. pstb             TCATTGCGGGTCGTCAACAGCGATAAATTAGAGA-------GT--------
                      ****    **  ** *  * * **  *            **
```

Figure S12: DNA sequence alignment of the *fha* gene of *Y. pseudotuberculosis* YPIII and *P. aeruginosa* PAO1. ClustalO was used for the alignment of *P. aeruginosa* (P0081) and *Y. pseudotuberculosis* (YPK_0391) upstream region (-50 to +20 relative to the translational start site) with default parameters. Nucleotides which were identical in both species are marked with a star below the sequence. The positions of high-affinity (ANGGA - pink), low-affinity CsrA binding motifs (green) and the start codon (underlined) are indicated.

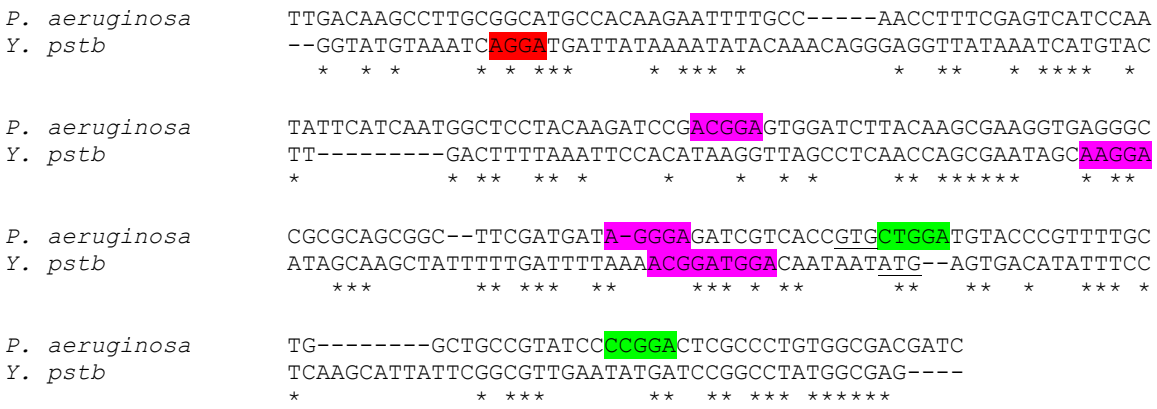

Figure S13: DNA sequence alignment of the *impA* gene of *Y. pseudotuberculosis* YPIII and *P. aeruginosa* PAO1. ClustalO was used for the alignment of the *P. aeruginosa* (P0082) and *Y. pseudotuberculosis rovA* (YPK_3566) upstream region (-50 to +20 relative to the translational start site) with default parameters. Nucleotides which were identical in both species are marked with a star below the sequence. The positions of high-affinity (AGGA - red; ANGGA - pink), low-affinity CsrA binding motifs (green) and the start codon (underlined) are indicated.

Danksagung

An erster Stelle möchte ich meiner Doktormutter Prof. Dr. Petra Dersch dafür danken, dass ich meine Doktorarbeit in ihrer Gruppe anfertigen konnte und für die Überlassung dieses spannenden und facettenreichen Themas. Desweiteren danke ich dir, dafür dass du mir in der Bearbeitung viele Freiheiten gelassen hast, aber mich auch in lebendigen wissenschaftlichen Diskussionen motivierend unterstützt hast. Danke!

Ich möchte Prof. Dr. Michael Steinert ganz herzlich dafür danken, dass er freundlicherweise das Koreferat meiner Doktorarbeit übernommen hat, sowie dieses Projekt im Rahmen des *Thesis Committees* unterstützt hat. Prof. Dr. André Fleißner danke ich für die Übernahme des Prüfungsvorsitz. Vielen Dank, dass ihr bereit wart Zeit und Energie in das Lesen und innerhalb der Prüfungskommision aufzuwenden!

Bei der "Helmholtz International Graduate School for Infection Research" möchte ich mich für die Teilfinanzierung meiner Promotion bedanken. Auch dafür, dass ich im Rahmen eures PhD-Programms die Möglichkeit hatte meine *hard* und *soft skills* auszubauen.

Ein ganz großer Dank geht an die Postdocs (Kathi, Aaron, Sabrina). Schön das man über einer schönen, leckeren, kochend-heißen Tasse Bohnenauszug über Hochs und Tiefs des (Arbeits-)Alltags philosophieren konnte! Insbesondere Kathi 'Dr. Schatz' Heroven für ihre liebevolle Unterstützung und den wissenschaftlichen Diskurs, wenn man doch vor lauter Loops nur noch Fragenzeichen gesehen hat. 'RNA-Seq' Aaron danke ich für die Unterstützung in allen RNA-Seq-Belangen.

Für die schöne Zeit danke ich dem kleinen Labor (Stephi, Rebekka, Vanessa, Maria, Chriselle) und dem späteren großen Labor (Carina, Franzi, Tanja, Karin). Darüber hinaus auch für die tolle Arbeitsatmosphäre, wodurch die Tage nie langweilig wurden. Natürlich danke ich auch unserer uneingeschränkten Administrationskönigin Claudia, die immer sehr hilfreich in jeglichen Belangen der Bürokratie und dem allgemeinen Papierkrieg war. Desweiteren möchte ich auch nicht die IBISse, vorallem Locken-Florian, vergessen: Danke für die schönen Jahre! Unser T3SS ist trotzdem überlegen! Vielen Dank Robert für die vielen fruchtbaren Diskussionen Ich danke auch meinem wichtigsten *partner in crime*, YopD, dafür, dass du tapfer durchgehalten hast und zumeist nicht sofort ausgefallen bist.

Ein ganz großes DANKE an meine Korrekturleser (Kathi, Sabrina, Maria, Florian, Franzi, Carina und Vanessa), die ohne zu klagen ihre Zeit und geistige Gesundheit in dieses Regulationswirrwarr gesteckt haben. ;-)

Ich danke auch meinen Bürogenossen (Franzi, Maik und Wiebke) für die schönen Jahre, die wissenschaftlichen Diskussionen in denen ihr vielleicht nicht immer den Überblick über die ganzen verschachtelten *feedbackloops* und Regulatoren behalten konntet, aber mich doch immer wieder zu neuen Aha! Momenten geleitet habt. Auch danke dafür, dass wir zusammen innerhalb der letzten Jahre die botanischen, entomologischen und crustaceologischen Experimente durchführen konnten. Danke Franzi, dass wir gemeinsam von Anfang bis (Fast-) Ende die Promotion bestreiten durften. '0101001'-Maik - ich danke dir, dass du mir auch im Privaten neue Horizonte eröffnen konntest. Wiebke danke ich vor allem für die schönen Monate in unserem Sekundärbüro in denen wir den Endspurt bestreiten konnten.

Ein sehr großer Dank gilt meiner Mutter und meinem Vater, die mich immer uneingeschränkt in allen Lebenslagen unterstützt und mir immer Kraft gegeben haben. Vielleicht kann ich dir irgendwann einmal erklären was ich überhaupt gemacht habe.

Bei meiner Gretje bedanke ich mich dafür, dass du mich in den 'intensiven' Phasen der Doktorarbeit so tapfer ertragen hast und mir auch in schwierigen Momenten Rückhalt und Kraft und ein gemütliches Zuhause gegeben hast. Danke dass ich immer auf dich zählen kann und konnte! Der kleinen Stine-Eke danke ich weil sie immer so lustig ist und hier schon einmal ein Versprechen an dein Zukunfts-Ich: Zu deinem 18. Geburtstag werde ich dir ein Exemplar dieser Arbeit überreichen, die wir dann zusammen in einträchtiger Qualitätszeit lesen können!

Ph'nglui mglw'nafh Cthulhu R'lyeh wgah'nagl fhtagn

- Abdul al Hazred (730 A.D.)